

2014

Modern Applications of Novel Electroless Plating Techniques

Robert Andrew Petro
University of Windsor

Follow this and additional works at: <http://scholar.uwindsor.ca/etd>

Recommended Citation

Petro, Robert Andrew, "Modern Applications of Novel Electroless Plating Techniques" (2014). *Electronic Theses and Dissertations*. Paper 5095.

This online database contains the full-text of PhD dissertations and Masters' theses of University of Windsor students from 1954 forward. These documents are made available for personal study and research purposes only, in accordance with the Canadian Copyright Act and the Creative Commons license—CC BY-NC-ND (Attribution, Non-Commercial, No Derivative Works). Under this license, works must always be attributed to the copyright holder (original author), cannot be used for any commercial purposes, and may not be altered. Any other use would require the permission of the copyright holder. Students may inquire about withdrawing their dissertation and/or thesis from this database. For additional inquiries, please contact the repository administrator via email (scholarship@uwindsor.ca) or by telephone at 519-253-3000ext. 3208.

Modern Applications of Novel Electroless Plating Techniques

by
Robert Andrew Petro

A Dissertation
Submitted to the Faculty of Graduate Studies
through the Department of Physics
in Partial Fulfillment of the Requirements for
the Degree of Doctor of Philosophy at the
University of Windsor

Windsor, Ontario, Canada

2014

© 2014 Robert Andrew Petro

Modern Applications of Novel Electroless Plating Techniques

by
Robert Petro

APPROVED BY:

S. Mittler, External Examiner
Western University

A. T. Alpas
Department of Mechanical, Automotive & Materials Engineering

C. Rangan
Department of Physics

J. W. McConkey
Department of Physics

M. Schlesinger, Advisor
Department of Physics

16 May 2014

Declaration of Co-Authorship / Previous Publication

I. Co-Authorship Declaration

I hereby declare that this dissertation incorporates material that is result of joint research, as follows:

This dissertation incorporates the outcome of a joint research undertaken with, and under, the supervision of Dr. M. Schlesinger. The collaboration is covered in Chapters 3, 4, and 5 of the dissertation. In all cases, the key ideas, primary contributions, experimental designs, data analysis, and interpretation, were performed by the author.

I am aware of the University of Windsor Senate Policy on Authorship and I certify that I have properly acknowledged the contribution of other researchers to my dissertation, and have obtained written permission from each of the co-author(s) to include the above material(s) in my dissertation.

I certify that, with the above qualification, this dissertation, and the research to which it refers, is the product of my own work.

II. Declaration of Previous Publication

This dissertation includes four (4) original papers and that have been previously published/submitted for publication in peer reviewed journals, as follows:

Dissertation Chapter	Publication Title/Full Citation	Publication Status
Chapter 3	R. Petro and M. Schlesinger, "Direct Electroless Deposition of Nickel Boron Alloys and Copper on Aluminum Containing Magnesium Alloys", <i>Electrochemical and Solid-State Letters</i> , 14, (2011), p.D37-D40	Published
Chapter 3	R. Petro and M. Schlesinger, "Direct Electroless Deposition of Low Phosphorous Ni-P Films on AZ91D Mg Alloy", <i>Journal of The Electrochemical Society</i> , 159, (2012), p.D455-D461	Published
Chapter 3	R. Petro and M. Schlesinger, "Direct Electroless Deposition of Ni-P-Zn Films on AZ91D Mg Alloy", <i>Journal of The Electrochemical Society</i> , 160(9), (2013), p.349-353	Published
Chapter 3	M. Schlesinger and R. Petro, "Process for Electroless Deposition on Magnesium Using a Nickel Hydrate Plating Bath ", Date Filed: February 14 th 2013 Patent #: US 20130216721	Patent Filed

Chapter 3 & Chapter 4	M. Schlesinger and R. Petro, "Process Patent for Electroless Deposition of Metals using Highly Alkaline Plating Bath", International filing date under PCT (Patent Cooperation Treaty): October 12, 2011; Issued: August 15, 2013, Serial number: CA2011/001146, Patent #:US 20130209698	Patent Issued
Chapter 4	M. Schlesinger and R. Petro "Process for Electroless Deposition of Gold and Cu Alloys on Silicon" (2013)*	Patent Filed
Chapter 5	M. Schlesinger and R. Petro "Electro-Electroless Hybrid Multi-layer and Alloy Deposition" (2014)*	Patent Filed
Chapter 5	R. Petro and M. Schlesinger, "Development of Novel Hybrid Electro-Electroless Deposit (HEED) Coatings and Applications", (2014)	Submitted for Publication
Chapter 2.4 & Chapter 3.1	R. Petro and M. Schlesinger, Chapter 1: Applications of Electrochemistry in Medicine, in "Modern Aspects of Electrochemistry Vol:56 - Applications of Electrochemistry in Medicine", p.1-32, ed. M. Schlesinger, (2013), Springer Science+Business Media New York, ISBN 978-1-4614-6148-7	Published
Chapter 2.1 & Chapter 7.4	R. Petro, M. Schlesinger, and G.-L. Song; Chapter 30: Ionic Liquid Treatments for Enhanced Corrosion Resistance of Magnesium-Based Substrates, in "Modern Electroplating, Fifth Edition", p.665-686, eds: M. Schlesinger and M. Paunovic, (2010) John Wiley & Sons, Inc., Hoboken, NJ, USA. doi:10.1002/9780470602638.ch30	Published

*Exact Tiles Unavailable

I certify that I have obtained a written permission from the copyright owner(s) to include the above published material(s) in my dissertation. I certify that the above material describes work completed during my registration as graduate student at the University of Windsor.

I declare that, to the best of my knowledge, my dissertation does not infringe upon anyone's copyright nor violate any proprietary rights and that any ideas, techniques, quotations, or any other material from the work of other people included in my dissertation, published or otherwise, are fully acknowledged in accordance with the standard referencing practices. Furthermore, to the extent that I have included copyrighted material that surpasses the bounds of fair dealing within the meaning of the Canada Copyright Act, I certify that I have obtained a written permission from the copyright owner(s) to include such material(s) in my dissertation.

I declare that this is a true copy of my dissertation, including any final revisions, as approved by my dissertation committee and the Graduate Studies office, and that this dissertation has not been submitted for a higher degree to any other University or Institution.

Abstract

This dissertation is composed of three distinct but closely related topics on the electrochemical metallization of substrates. The first topic solves the longstanding problem of galvanic corrosion in connection with exploiting the advantageous properties of magnesium {Mg} alloys and is of vital interest to the automotive and aerospace sectors. The second topic provides a new approach to the selective electroless metallization of silicon {Si} in connection with solar cells and other electronic devices. The third topic details a novel method of metal thin film formation using wet chemistry techniques which allow for the deposition of alternating metal layers of different and similar nobility from a single electrolyte. Future possible avenues of investigation are suggested for each of the three topics. The resolution of the galvanic corrosion issue, as presented within herein, is based on the direct electroless deposition of metal thin films less active than the Mg alloy substrates. Claddings of copper {Cu}, nickel boron {Ni-B}, and phosphorous {P} alloys including: nickel {Ni-P}, cobalt {Co-P}, nickel-zinc {Ni-Zn-P}, and other ternary alloys, were successfully deposited directly on Mg alloy surfaces. The electroless coating of Mg alloys was accomplished using minimal pre-treatments and made use of the naturally active properties of Mg-based substrates. Qualitative measures of the corrosion resistance of Ni-Zn-P coatings on Mg alloys demonstrated superior resistance to galvanic corrosion compared to uncoated surfaces. The selective electroless metallization of Si is accomplished with the selective removal of the silicon oxide {SiO_x} by means of mechanical scribing thereby exposing Si. The exposure of Si provides a catalytic surface for the electroless deposition of gold {Au}, and silver {Ag}, and other metals. The mechanical scribing provides an inexpensive avenue for the selective metallization of Si for solar cells. The novel method of depositing alternating metal layers of both different and similar nobility is achieved by combining electroplating and electroless deposition within a single electrolyte. The technique, termed here “hybrid electro-electroless deposition” (HEED), provides coatings previously unobtainable using wet electrochemical techniques. The application of HEED is of interest for the provision of sacrificial coatings on Mg alloys for corrosion protection within the transportation sector.

I dedicate this dissertation to my family, especially my mother Emese and my brother Nicholas, for their love and support during the course of my graduate studies.

Acknowledgements

The work contained within this dissertation would not have been possible if not for the help and support of a number of individuals. Most importantly, I would like to thank Dr. Mordechai Schlesinger for accepting me as his Masters level graduate student and encouraging me to pursue my Doctorate degree of which this dissertation is part. Without his guidance none of the work in this dissertation would have been possible, and I am grateful for his trust and belief in my abilities. Additionally, I would also like to thank the folks at GM, especially Dr. Mark Verbrugge, Dr. Jan Herbst, and Dr. Justin Gammage, as well as Jose Costa from the Ontario Centers for Excellence.

I would like to thank the entire Faculty of the Department of Physics for the quality education and guidance provided to me throughout my undergraduate degree and graduate studies. I would like to gratefully acknowledge all University of Windsor staff and in particular specifically thank: Physics Machine Shop Technicians Louis Beaudry and Eric Claussen, for assisting in the production of substrates as well as providing practical insight into the properties of metals; Computer and Electronics Technicians Aldo DiCarlo and Senisa Jedzic, for both help with equipment as well as the procurement thereof; secretaries Qin Tu, Sabina Baraoniciu, Martha Hiuser, and Kimberly Lefebvre, who helped with the paperwork associated with being a graduate student; and SEM Technicians Sharon Lackie and John Robinson for help with SEM and EDS analysis. Additionally I thank the custodians of Essex hall, including Tom Dean and others, who helped keep the lab clean and deal with messes caused by equipment failures.

I thank all graduate and undergraduate students for their friendship over the course of this work. In particular I wish to thank Dr. Michael Sullivan, as well as Nissa Frank and Michael Bolla, who, as graduate students along with me, kept an open door policy to talk about everything from research/academic pursuits to more social topics.

Finally, and most importantly, I would like to thank my mother, Emese, and my brother, Nicholas, both of whom I can never thank enough for their support and love. Without their support I would never have been capable of accomplishing the work within this dissertation. To Jennifer Trymbulak, thank you for your support throughout my research and the process of writing this dissertation; your accompaniment of me during some of those late nights helped complete this work.

Table of Contents

Declaration of Co-Authorship/Previous Publications	iii
Abstract	v
Dedication	vi
Acknowledgements	vii
List of Tables	xii
List of Figures	xv
Chapter 1: Introduction	1
1.1 Overview	2
1.2 Summary of Dissertation	3
1.3 History of Deposition	4
1.4 References	11
Chapter 2: Background	14
2.1 Introduction of Deposition Concepts and Properties	15
2.2 Electroplating & Electrochemistry	17
2.2.1 Electroplating Cell	18
2.2.2 Electroplating Conditions	21
2.2.3 Electroplating Techniques	28
2.2.4 Electroplated Films: Deposition & Structure	32
2.2.5 Selective Deposition	37
2.3 Electroless Deposition	41
2.3.1 Electrolyte Composition	42
2.3.2 Theoretical Considerations	52
2.3.3 Electroless Alloys & Composites	56
2.3.4 Advantages & Applications – Selective Deposition	58

2.4 Single and Multi-layered Thin Film Deposit Properties	62
2.4.1 Diffusion & Deposit Brittleness	63
2.4.2 Multi-Layers	66
2.4.3 Hardness	68
2.4.4 Magnetic Properties & Giant Magneto-Resistance (GMR)	73
2.4.4.1 Magnetization & Coercivity of Thin Films	74
2.4.4.2 Fundamentals of Magneto-Resistance	76
2.4.4.3 Larger Magneto-Resistance Effects	82
2.5 Magnesium & Corrosion	87
2.5.1 Corrosion	89
2.5.2 Galvanic Corrosion	95
2.6 Summary	98
2.7 References	99
Chapter 3: Electroless Cladding of Magnesium {Mg}	106
3.1 Introduction to Applications of Magnesium {Mg}	107
3.2 Current Anti-Corrosion Practises	107
3.3 Materials and Methodology	112
3.3.1 Sample Analysis	113
3.4 Results	114
3.4.1 Early Work	115
3.4.2 Electroless Copper {Cu} and Nickel Boron {Ni-B}	129
3.4.2.1 Surface Treatments	137
3.4.2.2 Immersion Coatings and Electrolyte Modifications	141
3.4.2.3 Metallic, Electroless Cu Coating of AZ91D Mg Alloys	160
3.4.3 Electroless Nickel Phosphorous {Ni-P} and Other Binary Alloys	162
3.4.4 Electroless Nickel-Zinc-Phosphorus {Ni-Zn-P} and Other Ternary Alloys	177
3.5 Summary	195
3.6 References	197

Chapter 4: Selective Electroless Deposition on Silicon {Si}	201
4.1 Introduction to Selective Deposition on Silicon {Si}	202
4.2 Silicon Materials and Applications	202
4.3 Experimental Motivation	209
4.4 Materials and Methods	213
4.5 Experimental Results	214
4.5.1 Electroless Copper {Cu}	216
4.5.2 Electroless Gold {Au}	219
4.5.3 Electroless Nickel {Ni}	222
4.5.4 Role of Ammonium/Ammonia {NH ₄ ⁺ /NH ₃ }	227
4.5.5 Electroless Silver {Ag}	231
4.6 Summary	233
4.7 References	234
Chapter 5: Hybrid Electro-Electroless Deposition	239
5.1 Overview of Electroplating and Electroless Deposition	240
5.2 Theory	242
5.2.1 Multi-layer Deposition	243
5.2.2 Alloy Deposition	246
5.3 Materials and Methodology	246
5.3.1 Electroless Gold {Au} Electrolytes	247
5.3.2 Electrodes and Deposition System	248
5.3.3 Sample Analysis	250
5.4 Ni/Au and Co/Au Results	251
5.5 Application to Coatings on Mg Alloys	259
5.6 Iron Nickel {Fe/Ni} Electrolyte and Ongoing Work	262
5.7 Summary	271
5.8 References	271

Chapter 6: Summary	273
6.1 Overview of Summary	274
6.2 Magnesium {Mg}	274
6.3 Silicon {Si}	275
6.4 Hybrid Electro-Electroless Deposit (HEED) Coatings	276
Chapter 7: Future Work	278
7.1 Introduction of Future Work	279
7.2 Cladding of Magnesium {Mg} Alloys	279
7.3 Electroless Metallization of Silicon {Si}	280
7.4 Hybrid Electro-Electroless Deposition (HEED) Coatings	281
7.5 Ionic Liquids (ILs)	281
Appendix A: Summary of Electroless Electrolytes	283
A.1 Electroless Silver {Ag}	283
A.2 Electroless Gold {Au}	285
A.3 Electroless Copper {Cu}	291
A.4 Electroless Nickel Boron {Ni-B} Alloys	293
A.5 Electroless Nickel Phosphorus {Ni-P} Alloys	294
A.6 Electroless Nickel Zinc Phosphorus {Ni-Zn-P} Alloys	295
A.7 Electroless Cobalt Phosphorus {Co-P} Alloys	296
A.8 Other Electroless Nickel Metal Phosphorus {Ni-Me-P} Alloys	297
A.9 References	298
Appendix B: Nickel/Gold {Ni/Au} Electro-Electroless Layers on a Cobalt {Co} Substrate	300
Vita Auctoris	301

List of Tables

2.1	Selected half-reactions along with their standard electrode potential relative to SHE	22
2.2	Crystal structure of commonly deposited metals.	37
2.3	Chemical dissociation reactions and pKa for select complexing agents.	45
2.4	Denticity and equilibrium constants for select complexing agent anions.	47
2.5	Effective pH range and oxidation potential of some Ni reducing agents.	53
2.6	Comparison of properties of selected Fe, Al, and Mg alloys, as well as common pure Cu and Ni.	87
2.7	Select results of 2.5 year corrosion exposure tests on sheet alloys.	89
2.8	Comparison of spontaneity and stability for the corrosion of Mn in water with, and without, dissolved oxygen.	91
2.9	Type, condition, composition, and tensile strength of select Mg alloys.	92
2.10	Select corrosion potentials of synthetically prepared intermetallic phases a de-aerated, 5 % NaCl, saturated Mg(OH) ₂ , pH 10.5, environment	93
2.11	Anodic Index	96
3.1	Nominal compositions of the AZ91D and AM50 Mg alloys by wt. %	112
3.2a	Pre-treatment process by J. Marton and M. Schlesinger	116
3.2b	Acidic electroless Ni-P electrolyte formulation by J. Marton and M. Schlesinger	116
3.3	Stannate surface conversion treatment for Mg alloys as modified from Huo et al.	117
3.4	Common alkaline Ni-P metallization electrolyte.	118
3.5	Electrolytes for the pre-treatment of AZ91D Mg alloy samples prior to metallization from a Ni-B electrolyte.	119
3.6	Electroless Ni-B electrolyte formulation modified from Gorbunova et al.	120
3.7	Composition and operating conditions for the pre-treatment and subsequent Ni-P and Ni-B metallization of Mg alloys.	122
3.8	Acidic HF and alkaline Zn surface pre-treatments for Mg alloys.	124
3.9	Electroless Cu thin film electrolytes.	129
3.10	Formulation for co-deposition of Co with Ni-B modified from Table 3.5.	133
3.11	Modified electroless Cu thin film electrolytes.	141
3.12	Alkaline Cu electrolytes for immersion deposits on Mg alloys.	143

3.13	Likely half-reactions and associated standard electrode potentials for the formation of Cu immersion coatings on Mg alloys.	153
3.14	Alkaline Cu electrolytes for immersion deposits on Mg alloys	154
3.15	Modified electroless Cu thin film electrolyte	161
3.16	Acidic Ni-P electrolyte, nearly identical to the electrolyte in Table 3.2.	162
3.17	Electroless Ni-P thin film electrolyte for successful deposition on Mg alloys.	163
3.18	Formulations of successful electroless Ni-P thin film electrolytes for deposition on Mg alloys.	165
3.19	Formulations of unsuccessful electroless Ni-P thin film electrolytes for deposition on Mg alloys.	166
3.20	Alkaline electroless Co electrolyte	176
3.21	Alkaline electrolyte for the deposition of electroless Ni-Zn-P alloys on Mg alloys.	177
3.22	Formulations of alkaline electrolytes for the deposition of various electroless Ni-Zn-P alloys on Mg alloys.	180
3.23	Electrolyte for Ni-Zn-P immersion deposit	189
3.24	Alkaline electroless Ni-Co-P electrolyte	190
3.25	Alkaline electroless Ni-Fe-P electrolyte	192
3.26	Alkaline electroless Ni-Re-P and Ni-W-P electrolytes	193
3.27	Electrolyte compositions, and conditions, for electroless Ni-P, Ni-Zn-P, and Ni-Co-P deposits on Mg alloys.	197
4.1	Composition of the electroless Cu electrolyte	216
4.2	Electroless Au electrolyte	219
4.3	Acidic and neutral electroless Ni-P electrolytes.	223
4.4	Electroless Ni-P electrolytes	227
4.5	Electroless Ag electrolyte	232
5.1	Summary of differences between electroplating and electroless plating	241
5.2	Electrolyte for electroless Ni-Fe-P alloy deposition	244
5.3	Electroless Au/Ni and Au/Co electrolytes for electro-electroless deposition	248
5.4	Nominal composition of the Ni, Cu, and Co electrodes	249
5.5	Electroless Ni-Zn-P electrolyte	260

5.6	Hybrid electro-electroless electrolyte, 3:1 Ni:Fe ratio, for Fe/Ni deposition.	262
5.7	Measured voltage, current, and duration of electroplated Fe/Ni deposits with atomic % and weight % EDS results for deposits at various applied voltages.	264
5.8	Standard electrode potentials for Ni and Fe metals	268
A1	Electroless Ag electrolytes	283
A2	Electroless Au electrolyte	285
A3	Electroless Cu thin film electrolytes	291
A4	Electroless Ni-B electrolyte	293
A5.1	Acidic electroless Ni-P electrolyte	294
A5.2	Alkaline electroless Ni-P electrolyte	294
A6	Electroless Ni-Zn-P electrolytes	295
A7	Electroless Co-P and Ni-Co-P electrolytes	296
A8	Electroless Ni-Me-P electrolytes; Me: Fe, Re, W, Mo	297

List of Figures

2.1	Schematic of the basic arrangement of an electroplating cell	17
2.2	Schematic of electroplating cell with reactions for nickel deposition	20
2.3	Typical voltammetric curves for two different metals, M1 & M2.	29
2.4	Ion transfer to a terrace site, surface diffusion, and incorporation at kink site.	34
2.5	Schematic representation of layer growth and the nucleation–coalescence mechanism.	35
2.6	Unit cells of the three crystal lattices of commonly deposited metals.	37
2.7	Insoluble/soluble (positive/negative) photoresists rendered soluble/insoluble to a developer solution after UV light exposure.	38
2.8	Schematic of the Rayleigh Criterion for resolvability.	39
2.9	Evans type mixed potential diagram for the reduction of Cu^{2+} ions, and for oxidation of formaldehyde reducing agent.	55
2.10	Wagner-Traud type mixed potential diagram for electroless Ni-B deposition	56
2.11	Hardness data for electrochemically grown Cu/Ni super-lattice multi-layers	71
2.12	Schematic of hysteresis loops	76
2.13	Schematic magnetization versus applied magnetic field	76
2.14	Spin polarization for paramagnetic and ferromagnetic materials	78
2.15	Schematic of the anisotropic magneto-resistance (AMR) effect	80
2.16	Diagram of the Hall Effect and resulting forces on an electron within a conducting metal	81
2.17	Schematic of the idealized magnetization of the super-lattice in multi-layers producing the GMR effect	83
2.18	Superposition of all contributions toward observed GMR.	84
2.19	Examples of the dependence of spacer layer thickness, Cu, on GMR at magnetic saturation for Ni-Cu and Co-Cu multi-layers.	85
2.20	Die cast AZ91D salt spray performance versus Fe, Ni, and Cu tramp element content.	94
3.1	Incremental and 30 minute immersion deposits of Ni-P deposit from an acidic electrolyte on AZ91D Mg alloy with stannate surface conversion.	118

3.2	Electroless Ni-B “Hulk” coating of an AZ91D Mg alloy substrate.	120
3.3	Comparison of electroless Ni-B coatings on fly-cut AZ91D Mg alloys with 25 °C acidic pre-treatment and alkaline 90 °C stannate conversion treatments	121
3.4	Electroless Ni-P metallization of fly-cut AM50 and AZ91D Mg alloys samples after acidic Mn-cocktail pre-treatment.	123
3.5	Comparison of Ni-P deposits from electrolytes of varying concentrations of thiourea SC(NH ₂) ₂ and HF.	124
3.6	Magnification (10×) of HF and acidic Mn-cocktail pre-treated AZ91D Mg alloy surfaces.	125
3.7	Comparison of Ni-P metallization of fly-cut, acidic Mn-cocktail and HF pre-treated AZ91D Mg alloy samples.	125
3.8	Electroless Ni-P coating on fly-cut AZ91D Mg alloys from HF-containing and HF-free Ni-P electrolytes.	126
3.9	Comparison of electroless Ni-P deposits from an HF-containing electrolyte on Zn treated Mg alloys.	127
3.10	Macroscopic, backscatter SEM, and EDS analysis comparison of electroless deposits formed by alkaline Cu electrolytes on oxidized and polished AZ91D Mg alloy substrates.	131
3.11	Macroscopic scan, backscatter SEM image, and EDS analysis of a Ni-B coated AZ91D substrate.	132
3.12	Macroscopic scan, backscatter SEM image, and EDS analysis of an AZ91D substrate coated with a Co doped Ni-B layer.	133
3.13	Macroscopic scan, backscatter SEM image, and EDS analysis for AM50 and AZ91D samples coated with an initial Ni-B layer and subsequent Cu layer	134
3.14	Macroscopic scanned image accompanied by EDS analysis and backscatter SEM images of an AZ91D sample having initial Ni-B layer and secondary Cu layer deposits.	136
3.15	Macroscopic scanned images of a stannate treated AZ91D samples with and without an electroless Cu deposit.	138
3.16	Macroscopic images of electroless Cu deposits on concentrated HNO ₃ and dilute H ₂ SO ₄ acid pre-treated Mg alloy samples.	138
3.17	Macroscopic images, and negatives, comparing the post-tape test surfaces of Cu deposits on stannate conversion, H ₂ SO ₄ etched, and polished AZ91D Mg alloy samples.	140
3.18	Macroscopic and backscatter SEM image of a Cu immersion deposit formed at pH 11.5.	142

3.19	Macroscopic images of 48 hour Cu immersion deposits on AZ91D Mg alloys within electrolytes of varying NaOH concentration, < 15 g/L.	144-145
3.20	Macroscopic images of 48 hour Cu immersion deposits on AZ91D Mg alloys within electrolytes of varying NaOH concentrations, ≥ 15 g/L.	146-147
3.21	Backscatter SEM images of immersion Cu coatings formed on AZ91D Mg alloys at pH 11.5 and 12.7.	148
3.22	Titration curve for the alkaline Cu electrolyte.	148
3.23	Titration curves for the alkaline Cu electrolytes containing differing concentrations of $\text{CuSO}_4 \cdot 5\text{H}_2\text{O}$.	149
3.24	Titration curve for the alkaline Cu immersion electrolyte showing the pH of the electrolyte after 96 hours.	150
3.25	Macroscopic scanned image of the large faces of a polished AZ91D Mg alloy sample after 40hrs immersion in a pH 11.6 Cu electrolyte.	151
3.26	Compositional EDS analysis of oxide/hydroxide crystallites on the reverse of the Cu film formed on AZ91D Mg from a pH 10.5 Cu electrolyte.	152
3.27	Compositional EDS analysis of the shed Cu thin film produced on AZ91D Mg from a pH 11.5 Cu electrolyte.	153
3.28	Macroscopic image of 14 h Cu immersion deposits on the polished and oxidized sides of AZ91D Mg alloys.	155
3.29	Backscatter SEM images comparing Cu immersion deposits formed on AZ91D Mg alloys within electrolytes containing varying concentrations NH_4OH .	156
3.30	Macroscopic image along with backscatter SEM image of a Cu immersion coatings formed on an AZ91D Mg alloys within an electrolyte containing 83.3 mL/L NH_4OH .	157
3.31	Macroscopic scans of 23 h and 68 h deposits on Sn/Pd treated glass from a Cu immersion electrolyte containing MgSO_4 .	157
3.32	Backscatter SEM images and EDS of a 68 h deposit on Sn/Pd treated glass from a Cu immersion electrolyte containing MgSO_4 .	158
3.33	Macroscopic scanned images of an electroless Cu deposit on a dry polished AZ91D Mg alloy.	160
3.34	Macroscopic image, backscatter SEM images and EDS analyses of an acidic electroless Ni-P coating on an AZ91D Mg alloy.	163
3.35	Macroscopic image, backscatter SEM images, and EDS analyses of an alkaline electroless Ni-P coating on a AZ91D Mg alloy.	164

3.36	Macroscopic scan, backscatter SEM image, and EDS analyses of an alkaline electroless Ni-P deposit from Bath F3, containing Cl ⁻ ions, on a dry polished AZ91D Mg alloy.	167
3.37	Macroscopic scan, backscatter SEM image, and EDS analysis of an alkaline electroless Ni-P deposit, from Bath S2, on dry a polished AZ91D Mg alloy.	168
3.38	Macroscopic scan, backscatter SEM image, and EDS analyses of an alkaline electroless Ni-P deposit, from Bath S4, on a dry polished AZ91D Mg alloy.	168
3.39	Macroscopic scans of failed deposits from Baths F4 and F5 on AZ91D Mg alloys.	169
3.40	Backscatter SEM images and EDS analyses of an oxidized AZ91D Mg alloy sample with No, 2 min, and 5 min deposits from Bath S6.	171
3.41	Macroscopic scans, backscatter SEM images, and EDS analyses, of a Ni immersion deposit formed on a AZ91D Mg alloy.	174
3.42	Macroscopic image, SEM image, and EDS analysis of an electroless Co-P thin film on a polished AZ91D Mg alloy.	176
3.43	Macroscopic scan, backscatter SEM image, and EDS analyses of a Ni-Zn-P on a polished AZ91D Mg alloy.	178
3.44	Macroscopic scan, backscatter SEM image, and EDS analysis of a Ni-Zn-P deposit on an oxidized AZ91D Mg alloy.	179
3.45	Backscatter SEM images and EDS analyses of Ni-Zn-P deposits, on oxidized AZ91D Mg alloys, from electrolytes containing various relative concentration of Ni ²⁺ /Zn ²⁺ .	182
3.46	Macroscopic scans, backscatter SEM images, and EDS analyses of Ni-Zn-P deposits, of different duration, from electrolytes containing 25 % mol Zn on oxidized AZ91D Mg alloys.	184
3.47	Macroscopic scans, and negatives, of pre-, and post-, galvanic coupling of uncoated and Ni-Zn-P coated AZ91D Mg alloys.	186
3.48	Macroscopic scan, SEM image, EDS analysis of a Ni-Zn-P deposit, containing high P, on an AZ91D Mg alloy.	188
3.49	SEM image and EDS results for Ni-Zn-P immersion deposit on AZ91D Mg alloy	189
3.50	Macroscopic scan, SEM image, EDS analysis of a Ni-Co-P deposit on an AZ91D Mg alloy.	191
3.51	Macroscopic scan image of a shedding Ni-Co-P deposit on an oxidized AZ91D Mg alloy.	191

3.52	Backscatter SEM image and associated EDS of a Ni-Fe-P deposit on an AZ91D Mg alloy.	192
3.53	Backscatter SEM images and associated EDS of a Ni-Re-P deposit on an oxidized AZ91D Mg alloy.	194
4.1	Schematic crystal structure of n-type and p-type Si.	203
4.2	Schematics of the band structure of n-type, intrinsic, and p-type semiconductors.	204
4.3	Band structure change within a junction transistor after the application of a potential across the transistor.	206
4.4	Schematic diagram of a solar cell.	207
4.5	SEM images of the micro-textured pattern on p-type and n-type Si wafers used.	213
4.6	Macroscopic image, backscatter SEM images, and EDS analyses of selective electroless deposits of Cu on n-type Si.	217
4.7	Backscatter SEM image and EDS analysis of an attempted electroless deposit of Cu on n-type Si from an electrolyte containing no reducing agent.	218
4.8	Macroscopic, backscatter SEM, and EDS comparison of electroless Au deposits on n-type silicon formed from pH 7 and pH 10 electrolytes not containing $\text{Na}_3\text{C}_6\text{H}_5\text{O}_7$.	220
4.9	Backscatter and secondary emission SEM images, along with associated EDS of electroless Au deposits on n-type and p-type Si formed under differing conditions.	222
4.10	Macroscopic image, backscatter SEM image, and EDS analysis 20min acidic electroless Ni-P deposits on n-type Si.	223
4.11	Macroscopic image, secondary emission SEM images, and backscatter SEM image, with EDS analysis, of a Ni-P cluster on scribed Si.	225
4.12	Comparison of macroscopic images and microscopic optical images of the Ni-P deposits on scribed n-type Si wafers.	226
4.13	Macroscopic scanned images of polished and textured Si surfaces, along with backscatter SEM images, and associated EDS analysis of n-type Si surface post immersion in Ni immersion electrolytes with different pH adjusting chemicals.	228
4.14	Macroscopic scan comparison of the polished and textured sides of control and post- alkaline Ni immersion n-type Si wafers.	229
4.15	Backscatter SEM images of Co precipitates/crystallites formed on n-type Si from an alkaline, pH 10, electrolyte.	231

4.16	Macroscopic image, backscatter SEM image, and EDS analysis of a selective electroless Ag deposit on n-type Si.	232
5.1	Schematic diagram of the electro-electroless plating system.	249
5.2	Macroscopic image of electroless/electro/electroless tri-layer 20 min-Au/60 s-Co/20 min-Au deposit, from a pH 7 electrolyte, on a Ni plate, along with sequential backscatter SEM images and EDS analysis of each layer.	252
5.3	Graph of EDS results for a sequential analysis of the tri-layer deposit presented in Figure 5.2.	253
5.4	Graph of EDS results of a sequential 20 min-Au/60 s-Co/20 min-Au tri-layer deposits on Ni from a pH 10 electrolyte.	254
5.5	Macroscopic image, with backscatter SEM images of a Co/Au tri-layer HEED coating 5 min-Au/60 s-Co/5 min-Au on a Ni substrate, including a graph of sequential EDS analysis of the surface layers.	256
5.6	Macroscopic images, backscatter SEM images, and a graph of EDS analysis electroplated Co on Ni from an 80 °C Co/Au HEED electrolyte for three different applied potentials.	257
5.7	Macroscopic images, backscatter SEM images, and EDS for electroplated Ni on Co from an 80 °C Ni/Au HEED electrolyte for two different applied potentials.	258
5.8	Poor-man (PM) voltammogram for the alkaline Co/Au electrolyte.	259
5.9	Backscatter SEM image and associated EDS analysis of a Ni-Zn-P/Ni-Zn HEED coating on an AZ91D Mg alloy.	261
5.10	Macroscopic image, backscatter SEM image, and EDS analysis of an electroless Ni-P deposit from a 3:1 Ni:Fe electrolyte on Sn/Pd treated glass.	263
5.11	Plot of the measured voltage and current for an applied deposition potential of 2.5 V for the deposition of Fe from a 3:1 Ni:Fe electrolyte.	264
5.12	Plot of the atomic % of Ni, Fe, and P within the electroplated coatings presented in Table 5.7.	265
5.13	Macroscopic scan, backscatter SEM images, and EDS analyses for an electroplated, 5 V applied, Fe/Ni deposit on a Cu substrate from a newer Fe/Ni electrolyte.	266
5.14	Macroscopic scan, backscatter SEM images, and EDS analyses for an electroplated, 4.6 V applied, Fe/Ni deposit on a Cu substrate from a newer Fe/Ni electrolyte.	267

5.15	Macroscopic scan, backscatter SEM images, and EDS analyses for an electroplated, 5 V applied, Fe/Ni deposit on a Cu substrate from an older Fe/Ni electrolyte.	267
5.16	Macroscopic scan, backscatter SEM images, and EDS analysis of a Fe/Ni HEED bi-layer deposit from a newer Fe/Ni electrolyte.	269
5.17	Macroscopic scan, backscatter SEM images, and EDS analysis of a Fe/Ni HEED bi-layer deposit from an older Fe/Ni electrolyte.	270
A1	Macroscopic scanned image, backscatter SEM image, and EDS analysis of an Au deposit on a Cu substrate.	288
A2	Backscatter SEM image with EDS analysis of a Cu containing Au deposit on a Co substrate.	289
B1	Macroscopic image along with a graph of EDS results for a Ni/Au HEED coating of a Co substrate	300

Chapter 1: Introduction	1
1.1 Overview	2
1.2 Summary of Dissertation	3
1.3 History of Deposition	4
1.4 References	11

1.1 Overview

The metallic coating of surfaces is a practise which has evolved over the course of the 20th century from an art to an exact science. Historically, coatings have been achieved by many different means including mechanical application; electrochemical plating techniques such as electroplating and electroless plating; vacuum depositions including chemical vapour deposition (CVD), and physical vapour deposition (PVD)/sputtering techniques; chemical conversion techniques such as anodizing; and spray coatings. Beyond improving the aesthetic appearance of surfaces with the deposition of gold, chrome, or other metals; surface coatings play an integral role in an ever-increasing number of applications in science and engineering.

Electroplating, the most widely used modern method for applying coatings, is a practical branch of electrochemistry, which itself is often classified as a branch of chemistry. Electrochemistry, of which electroplating, electroless plating, and anodizing are parts, is the study of reactions involving electron transfer processes in conductive solutions, known as electrolytes, between ionic species in solution and submerged electron conductors, such as metals or semiconductors. Given the use of solutions in electrochemistry, the term wet chemistry is often used signifying chemistry carried out in the liquid phase. Despite the basis in chemistry, electrochemistry, including electrochemical processes and products such as electrochemical deposition, exists as a multidisciplinary science involving chemistry, engineering, biology, and, most fundamentally, physics.

Electroplating, as well as electroless plating, constitute an essential component for all aspects of electronics, both macro- and microscopic, and play a vital role in key sectors such as transportation, specifically within the automotive industry, where coatings are applied for wear corrosion resistance and aesthetic purposes. Both electro- and electroless methods of depositing metallic thin films have advantages and disadvantages compared to each other with each fulfilling specific purposes. Electroforming, an application of electroplating, is the deposition of a metal film onto a surface such that once the deposit is removed from the surface to form a free standing object which can vary in size and complexity. Notably nickel electroplating, the electrical reduction of nickel ions to metal, is a relatively uncomplicated process which is pursued by many

hobbyists for decorative plating purposes. Electroless plating, the chemical reduction of metal ions to metallic form, is another means of metal film deposition that possesses the often cited advantages of the ability to deposit on non-conducting surfaces of complex shape. Electroplating requires a conductive surface upon which deposition occurs, and uniform deposition using electroplating is not possible as a deposition is dictated by electric field lines in a line of sight manner.

Research into electro- and electroless plating baths and techniques, as well as the properties of resulting coatings is of ongoing interest throughout the academic and industrial settings. This dissertation presents, among a number of topics, new and patented developments in: the application of electrolessly deposited, galvanic corrosion resistant claddings on magnesium alloys, some results of which have been previously published [1-6]; the electroless deposition of conductive metals directly on silicon wafers [4]; as well as a hybridized method for multi-layer and customized thin film alloy deposition using a combination electro/electroless plating technique within a single electrolytic deposition bath [6]. The hybrid deposition technique delineated within this dissertation provides a novel method for the deposition of multi-layers of metal pairs previously unavailable using wet chemistry, and previously only available by means of molecular beam epitaxy [7], sputtering [7, 8], or other vacuum deposition techniques.

1.2 Summary of Dissertation

The remainder of this Chapter, Chapter 1, covers the history of deposition focusing on the historical development of electro- and electroless plating throughout the 19th and 20th centuries. The contents of Chapter 2 provide the scientific background and considerations as well as applications of electro- and electroless plating. The first two sections of Chapter 2 focus on the electrochemistry of electroplating, Section 2.2, and electroless deposition, Section 2.3, while the latter sections focus on more practical applications. Specifically, the deposition and properties of multi-layers, produced primarily by electroplating means, Section 2.4, and properties and corrosion of magnesium alloys, Section 2.5, provide relevant modern applications of electroplating and electroless deposition. Readers interested in the electroless deposition of metals on Mg alloys are encouraged pay close attention to Sections 2.3, 2.4.1, and 2.5. Background

for the understanding of hybrid deposition is covered in Sections 2.2 & 2.3, while readers interested in the specific applications of hybrid multi-layer deposits are encouraged to include Section 2.4.

The experimental sections of Chapter 3 & 4 contain the background, theory, results, and current status of electroless deposition on Mg for the prevention of galvanic corrosion and hybrid deposition, respectively. Chapter 5 provides a number of experiments and avenues to be pursued as future work for both the electroless coating of Mg and hybrid deposition techniques.

1.3 History of Deposition

The application of surface coatings is a practice which dates back thousands of years. The employ of a simple displacement reaction, or electrochemical displacement reaction, to coat surfaces is posited to be the method of silvering lead used in the counterfeit of Roman coins around 3rd and 4th century BC [9, 10]. The application of gold onto surfaces, known as gilding, is probably the best known coating applied to surfaces in the ancient world. Largely for decorative purposes, gilding in the ancient world was most often carried out by means of mechanical application on solid surfaces such as other metals, stone, or even wood. Mechanical gilding was accomplished by means of gluing or hammering gold leaf or powder directly onto the desired object. The ancient Egyptians knew how to hammer gold into leaf as thin as a few dozen nanometers, [11] and descriptions of gilding are included in the Old Testament of the Bible concerning the construction of the Ark of the Covenant; “And thou shalt overlay it with pure gold, within and without shalt thou overlay it...” [12].

The modern gilding of conductive, metal, objects, known as gold electroplating, was first developed by Luigi V. Brugnatelli at the beginning of the 19th century. Brugnatelli, who is credited with the invention of the science of modern electroplating, used the voltaic pile, developed by his friend and colleague Alessandro Volta in 1800, to provide voltaic electricity for the electroplating [13]. The voltaic pile, the first electrochemical battery, was constructed out of a stack of alternating dissimilar metals separated by spacers soaked in salt water. The entirely inorganic cell was constructed in response to the 1780 work of Luigi Galvani, who believed that movement in a frog's leg

when coupled to two dissimilar metals in a closed loop was the result of "animal electricity". Volta correctly held that the electricity was a result of different metals joined together by a moist intermediary and that the organic tissue was simply a medium for the reaction. The terms voltaic and galvanic cells in reference to Volta and Galvani, respectfully, were eventually adopted with both meaning the coupling of two differing metals in the presence of a saline medium producing an electrical current.

In 1803, the first account of gold electroplating, Brugnatelli recounted the reduction of gold ions from a saturated gold solution to metal on the surface of two large silver medals by means of connection to the negative terminal of a voltaic pile [14]. Despite the development, Brugnatelli's work was largely unknown outside his native Italy. Due to the Napoleonic Wars (1803–1815) and an apparent falling out between Brugnatelli and the French Academy of Sciences, the leading scientific body of Europe at the time, little work was conducted on electroplating until the mid-1830s. Aside from enabling electroplating, the voltaic cell enabled many important electrochemical achievements by means of electrolysis, the decomposition of molecules and compounds into their components. These achievements include the decomposition of water {H₂O} into hydrogen {H₂} and oxygen {O₂} by William Nicholson and Anthony Carlisle in 1800 [13]; and the isolation of the chemical elements sodium {Na} and potassium {K} in 1807 as well as calcium {Ca}, boron {B}, barium {Ba}, strontium {Sr}, and magnesium {Mg} in 1808 by Sir Humphry Davy. It should be noted that in response to the voltaic cell, Carlo Matteucci, in 1845, presented a paper to the Royal Society, by means of Michael Faraday, detailing the construction of an entirely organic battery made from the half-thighs of frogs. Though not the first battery of this sort and misguided in the origin of the electricity, the frog battery proved sufficiently powerful to decompose potassium iodide {KI} and Matteucci is credited as one of the fathers of modern electrophysiology [15].

In 1836, Professor John Frederic Daniell of London's King's College described the first constant battery as well as the resulting deposition of metallic copper within the battery [13]. The battery, also known as the Daniell cell, was designed to eliminate the problem of hydrogen bubble formation in the voltaic pile. The battery, consisting of a ceramic container filled with sulfuric acid with a zinc electrode and copper pot filled with

a solution of copper sulfate immersed within, provided a more reliable current source ultimately resulting in “rediscovery” of electroplating and the deposition of thin uniform coatings. In the same year Warren de la Rue experimenting with Daniell’s battery observed that the copper deposited within the cell, when stripped off from the copper electrode, exactly matched every aberration of the surface [13]. In 1837 Moritz Hermann von Jacobi, also known as Boris Semenovich Jacobi, repeating the work of Daniell and drawing on the observations of de la Rue developed the process known as electroforming [13]. Jacobi’s deposit of metal onto an engraved copper plate that had been used to print his visiting cards, when removed from the surface, produced a free standing metal impression of the engraved lines [13]. Electroforming provided the first practical use of electroplating outside of aesthetics and in the production of printing plates, the forming of the two-dimensional object is known as electrotyping, and eventually in the creation of sculptures.

Electroplating gained prominence after 1840 when the first patent for gold and silver electroplating was awarded to Henry and George Elkington. British Patent 8447, titled "Improvements in Coating, Covering, or Plating certain Metals", included work on the suitability of potassium cyanide as electrolyte for gold and silver electroplating which was purchased from surgeon John Wright and included in the patent a few weeks before the patent was finalized [13]. The deposition delineated in the patent was carried out using galvanic current in a cell composed of concentric cylindrical vessels, the outer one made of glazed ceramic and the inner one made of unglazed, porous earthenware vessel. The space between the cylindrical vessels was filled with sodium chloride in which a zinc cylinder was immersed and connected by copper wire to the surface to be plated which was within the earthenware vessel which contained the gold or silver electrolyte [13]. This patent is not to be confused with earlier patents in the late 1830s filed by and issued to George Elkington for "An Improved Method of Gilding Copper, Brass and Other Metals or Alloys of Metals" which involved an immersion/replacement of a thin layer of copper by an equally thin layer of gold [13].

The issuing of the patent on electroplating commercialized what was previously laboratory experiments and spurred many developments throughout Europe. Another development in commercialization was reported by Jacobi on the use of ferrocyanides,

instead of the more readily decomposable potassium gold cyanide, in gold plating. This variation, put forward by a Russian dentist named Briant, was supported by Jacobi as being more suitable for large-scale production. The use of ferrocyanides also provided the capability of depositing gold alloys containing silver as well as changing the color of deposits, making them redder, with the inclusion of copper sulfate.

By 1844 a large plant for electroforming and electroplating opened in St. Petersburg which carried out electroforming of copper statuary and bas-reliefs¹, as well as silver and gold plating from cyanide solutions [13]. The most prominent work carried out that the plant was the 1854 gold plating of the bronze domes, the largest 100 feet in diameter, of the original Church of the Redeemer in Moscow [13], later demolished and since rebuilt. Up until that point, all the many domes of the Moscow churches had been gilt either with gold leaf or by a hot dipping method. The amount of gold deposited on two out of every 100 sheets plated was tested with a specification of 28.44 grams of gold per square meter and required tolerance of 20 per cent. The total weight of gold deposited was slightly less than 500 kilograms was deposited on the domes which were first assembled in the plating shop, each sheet being numbered, and then dismantled for plating [13]. By the 1850's electroplating methods for bright nickel, brass², tin, and zinc were commercialized for engineering and specific commercial applications.

In 1880 John Brashear, an amateur astronomer, developed an improved silvering method for use in telescope mirrors. This method, known today as the Brashear Process [16], used to deposit various other metals including copper, and gold, were deposited from relatively short-lived solutions that contained chemical agents to reduce metal to create films mainly on glass. Though unrelated to electroplating, the chemical reduction of metal was of critical importance in the manufacture of mirrors. The Brashear process in many ways replaced the use of mercury alloys, or amalgams, which were used as far back as the 17th century. Prior to the Brashear process, mirrors were produced mainly using a tin-mercury {Sn-Hg} alloy, or Sn-amalgam. Amalgam deposition consisted of lying flat a thin, ~0.1 mm, tin film on a perfect flat plate of marble, pouring mercury overtop and placing a glass pane over the mercury; within 24 hours the foil completely

¹ Bas-reliefs - shallow-reliefs where figures have less depth than is proportional for wider viewing angles

² Brass - an alloy of zinc and copper

transformed into the amalgam alloy with subsequent hardening of the alloy taking up to a month, depending on the size of the mirror [17]. Despite the replacement of amalgam deposition and allowing for deposition of metals including copper and silver the Brashear process was not well understood.

Throughout most of the late 19th and early 20th century few significant scientific discoveries occurred for metal plating aside from refinements of processes and bath chemistry. Achievements of note within this time period include the advent of electrical power generation in the late 19th century, which obviated the need for batteries, and hard chromium plating in the beginning of the 20th century. The emergence of the electronics industry in the 1940s, more specifically the discovery of transistors in the late 1940s and early 1950s, provided new uses for electroplating and led to the rediscovery of heavy, or thick, gold plating of 100 years earlier for electronic components. In the 1840s and 1850s the Elkington's used heavy, or thick, gold plating for the mass production of electroformed items with the minimum thickness varying [18]; today the definition set out by Title 16 of the U.S. Code of Federal Regulations: Part 23.4c, where heavy gold is defined as not less than 10 karat fineness, 41.6 % gold, with a minimum thickness of at least 100 millionths of an inch, or about 2.5 microns [19].

Equally useful to the electronics industry was the 1946 discovery of electrodeless, also called electroless, plating by Abner Brenner and Grace E. Riddell [20]. Brenner and Riddell accidentally discovered electroless nickel plating when they observed that the additive sodium hypophosphite { NaH_2PO_2 } resulted in apparent cathode efficiencies of more than 100 % in a nickel electroplating bath [21]. The rightful conclusion, explanation, and understanding that some form of chemical reduction was taking place credited Brenner and Riddell with the discovery of electroless deposition. In addition to being little understood, previous baths, such as those used in the Brashear process, were relatively short-lived and subject to homogeneous decomposition allowing for limited ongoing deposition. It is noteworthy that though electroless deposition was not well understood in the 19th century, many of the reducing agents, such as formaldehyde for the reduction of electroless copper, continue to be used in modern formulations.

The term electroless is somewhat misleading, in that other methods, such as chemical displacement and immersion coatings that are self-limiting effectively

depositing only a few layers, also use no external electrodes or electrical source. Given the many “electroless”³ processes, the term autocatalytic was formally adopted to describe the deposition of a metallic coating by a controlled chemical reduction provided by a compound in solution that is catalyzed by the metal or alloy being deposited for sustained deposition, though the term electroless continues to be widely used. The discovery by Brenner and Riddell lead to further research into controlled, stable, electroless deposition processes and development of electroless deposition continued in applications such as the metallization of printed wiring boards among many others. Interpretation of the mechanisms behind electroless deposition occurred in the second half of the 1960s with the work of M. Saito and M. Paunovic in the adaptation of mixed-potential theory for the electroless deposition of copper; mixed potential theory was originally developed by Wagner and Traud in 1938 for the purpose of interpreting metal corrosion processes [22]. Further developments in electroless plating occurred in the early 1970s with the creation of techniques for selective deposition including photo-oxidation of sensitizers for patterning on non-conductive materials [23, 24].

Along with sharing in the discovery of electroless deposition, Brenner was involved in the applications of electroplating and in the production of multi-layered deposits. Early work on the subject by Brenner was conducted in 1939 with the use of two separate electroplating solutions. In 1948 it was observed by Brenner and A. M. Pommer that alloyed multi-layers could be deposited from a single solution where each layer possessed different, alternating, compositions [25]. Work regarding multi-layers continued throughout the 20th century in part due to possibility of magnetic enhancements from the layers which had been experimentally known since the 1960s. Although electrodeposition of multi-layer structures appears to have been described as early as 1921 by W. Blum [26], significant work on multi-layers to make use of the unique/unusual mechanical, electrical, optical, and/or magnetic properties was not carried out until the 1980s [27]. The deposition of pure multi-layers outlined by D. Tench and J. White in 1984 showed that multi-layers possessed higher tensile strength and hardness [27]. In 1986 J. Yahalom and O. Zadok succeeded in producing pure, non-alloyed,

³ The term electroless, though etymologically implying no outside electrodes, wrongly implies no electrical current present within the process. In fact the transfer of electrons within electroless processes provide a current within the system.

electrodeposited copper/nickel multi-layers at a thickness of 8 Å per layer [28]. These layers were found to produce magnetic enhancements, seen for layer thicknesses around 10-30 Å, known as giant magneto-resistance (GMR). Though magnetic enhancement had been sought out since the 1960s, the discovery and understanding of GMR occurred independently by Albert Fert and Peter Grünberg in 1988, for which they shared the 2007 Nobel Prize in physics. Thin films having GMR properties show a significant change in the electrical resistance of the film depending on the layer thicknesses and whether the magnetization of adjacent ferromagnetic layers are in a parallel or an anti-parallel alignment. Altering the magnetic alignment of the layers, and hence changing the resistance of the thin film system, is achieved by the application of an external magnetic field. The application of GMR to computer hard disks was part of the incremental improvement over decades to magneto-resistance based magnetic storage pioneered by David A. Thompson and Lubomyr T. Romankiw in the mid 1970s at IBM's T.J. Watson Research Center [29]. Electroplated multi-layers provided an inexpensive alternative means by which to deposit thin multi-layers without the use of vacuum chambers such as those required for molecular beam epitaxy (MBE) developed in the 1960s.

In addition to advances in plating, the development of more "user friendly" plating baths for large scale commercial applications remains ongoing since beginning in the 1950s with the implementation of deposition solutions based on acid formulae, rather than strongly poisonous baths based on cyanide. The "user friendly" goal has since expanded to include lower operating temperatures and a greater focus on safety. Better environmental practices brought on by continued tightening of regulations concerning waste water since the 1970s have also featured prominently in the ongoing development of new deposition solutions.

Today, the principles of electrochemistry including electroplating and electroless deposition are relatively well understood. Sophisticated plating baths have and continue to be developed and routinely employed throughout academia and industry. Better controls of plating procedures, including development of better current supplies, have led to strict quality controls for performance of deposits and layer thickness far above 20 % tolerances common in the 19th century. While the early days of deposition used constant voltage, potentiostatic, batteries as current sources, modern power supplies offer

precise current control allowing for submicron and nanometre thickness control for deposits under constant current, galvanostatic, as well as potentiostatic conditions. Further developments including bath chemistry and anode shape have enabled greater electroplating speed, more uniform deposits, better plating of irregular shapes, reliable plated finishes, as well as a host of options in metal deposits including platinum {Pt}, osmium {Os}, and ruthenium {Ru}. Electroplating applications in the electronics industry for the fabrication of integrated circuits and deposition multilayer films with GMR for magnetic recording devices have continued to spur development. Equally, focus on coatings for active materials such as magnesium alloys have resulted in a great deal of research in anti-corrosion coatings. Today, electroplating and electroless deposition methods continue to be researched as alternatives to higher cost, conventional fabrication methods.

1.4 References

- [1] R. Petro and M. Schlesinger, "Direct Electroless Deposition of Nickel Boron Alloys and Copper on Aluminum Containing Magnesium Alloys", *Electrochemical and Solid-State Letters*, 14, (2011), p.D37-D40
- [2] R. Petro and M. Schlesinger, "Direct Electroless Deposition of Low Phosphorous Ni-P Films on AZ91D Mg Alloy", *Journal of The Electrochemical Society*, 159, (2012), p.D455-D461
- [3] R. Petro and M. Schlesinger, "Direct Electroless Deposition of Ni-P-Zn Films on AZ91D Mg Alloy", *Journal of The Electrochemical Society*, 160(9), (2013), p.349-353
- [4] M. Schlesinger and R. Petro, "Process Patent for Electroless Deposition of Metal using high Alkaline Plating Bath", International filing date under PCT (Patent Cooperation Treaty): October 12, 2011; Serial number: CA2011/001146
- [5] M. Schlesinger and R. Petro, "Process Patent for Electroless Nickel Phosphorous, and Nickel-Zinc Phosphorous on Magnesium" Provisional patent filing date: February 16th 2012; Provisional patent filing number: 61/599640
- [6] M. Schlesinger and R. Petro, "Process Patent for Hybrid Electro-Electroless Deposition" Provisional patent filing date: (2013)
- [7] M. Gottwald, S. Andrieu, F. Gimbert, E. Shipton, L. Calmels, C. Magen, E. Snoeck, M. Liberati, T. Hauet, E. Arenholz, S. Mangin, E. E. Fullerton, *Physical Review B* 86, Article #014425, (2012)
- [8] M. Haertinger, C. H. Back, S.-H. Yang, S. S. P. Parkin and G. Woltersdorf, "Properties of Ni/Co multilayers as a function of the number of multilayer repetitions", *J. Phys. D: Appl. Phys.* 46 (2013) p.1-4
- [9] G. Giovannelli, S. Natali and B. Bozzini, *Journal of Applied Electrochemistry*, 36, 2006, p.951-956

- [10] G. Giovannelli, S. Natali, B. Bozzini, D. Manno, G. Micocci, A. Serra, G. Sarcinelli, A. Siciliano, R. Vitale, eprint arXiv:cond-mat/0603438, 2006
- [11] P. A. Kohl, Chapter 4: Electrodeposition of Gold, in “Modern Electroplating, Fifth Edition”, p.115-130, eds: M. Schlesinger and M. Paunovic, (2010) John Wiley & Sons, Inc., Hoboken, NJ, USA, DOI: 10.1002/9780470602638.ch4
- [12] The Bible, King James Version, Exodus 25:11
- [13] L. B. Hunt, “The Early History of Gold Plating”, *Gold Bulletin*, 6(1), (1973) p.16-27
- [14] J. B. Van Mons, "Extrait d'une lettre de Brugnatelli" écrit par Luigi Vincenzo Brugnatelli, *Journal de chimie et de physique*, Vol. 5, (1804) p.357-358
- [15] M. Bresadola, Carlo Matteucci and the legacy of Luigi Galvani, *Archives Italiennes de Biologie*, 149 (Suppl.): 3-9, 2011
- [16] J. A. Brashear, A Man Who Loved the Stars, Chapter 6: Making the Twelve-Inch Reflector, p.47-57, 1988, University of Pittsburg Press
- [17] O. Zywitzki, W. Nedon, T. Kopte, T. modes, Characterization of baroque tin amalgam mirrors of the historical Green Vault in Dresden, *Appl. Phys. A*, 92, (2008), p.123-126
- [18] D. Mason, Gold Plating Technology, Chapter 40: Electroforming and heavy deposits, p. 558-572, Electrochemical Publications Ltd., Edited by: F. H. Reid and William Goldie.
- [19] Code of Federal Regulations, Title 16: Commercial practises, Chapter 1 – Federal Trade Commission, Subchapter B – Guides and Trade Practice Rules (Parts 17 to 260), PART 23 – Guides for the Jewelry, Precious metals, and Pewter Industries, Section 4 - Misrepresentation as to gold content, Entry 23.4c including Footnote 4, Current as of July 3rd 2013, (<http://www.ecfr.gov/>)
- [20] A. Brenner and G. Riddell, Nickel plating on steel by chemical reduction, *J. Res. Nat. Bur. Std.*, 37(1), (1946), p.31-34 DOI: <http://dx.doi.org/10.6028/jres.037.019>
- [21] M. Schlesinger, Chapter 18: Electroless Deposition of Nickel, in “Modern Electroplating, Fifth Edition”, p.447-458, eds: M. Schlesinger and M. Paunovic, (2010) John Wiley & Sons, Inc., Hoboken, NJ, USA, DOI: 10.1002/9780470602638.ch18
- [22] M. Paunovic, Chapter 17: Electroless Deposition of Copper, in “Modern Electroplating, Fifth Edition”, p.433-446, eds: M. Schlesinger and M. Paunovic, (2010) John Wiley & Sons, Inc., Hoboken, NJ, USA, DOI: 10.1002/9780470602638.ch17
- [23] J.F. Damico, M.A. Deangelo, J.F. Hendricks, J.T. Kenney, D.J. Sharp, Selective Electroless Metal Deposition Using Patterned Photo-Oxidation of SN(II) Sensitized Substrates, *Journal of the Electrochemical Society*, 118(10), p.1695, 1971
- [24] M. Schlesinger, Ultraviolet Inhibition of Electroless Plating on Glass, *Journal of the Electrochemical Society: Electrochemical Science and Technology*, 121(5), (1974), p.667-668
- [25] “Reference [9] A. Brenner and A. M. Pommer, “Production of a diffraction grating by depositing copper-bismuth alloy”. Unpublished work, National Bureau of Standards, 1948.” in *Electrodeposition of Alloys – Volume II*, A. Brenner, Academic Press, p.589 (1963)
- [26] W. Blum, The structure and properties of alternately deposited metals *Trans. Am. Electrochem. Soc*, 1921

- [27] D. Tench and J. White Enhanced tensile strength for electrodeposited nickel-copper multilayer composites, Metallurgical Transactions A (November 1984), 15 (11), p.2039-2040
- [28] J. Yahalom and O. Zadok, Formation of composition-modulated alloys by electrodeposition, Journal of Material Science, 22(2), (1987).p.499-503
- [29] D. A. Thompson and L. T. Romankiw and A. F. Mayadas, Thin Film Magnetoresistors in Memory, Storage, and Related Applications, IEEE Transactions on Magnetics, 11(4), (1975),p. 1039-1050

Chapter 2: Background	14
2.1 Introduction of Deposition Concepts and Properties	15
2.2 Electroplating & Electrochemistry	17
2.2.1 Electroplating Cell	18
2.2.2 Electroplating Conditions	21
2.2.3 Electroplating Techniques	28
2.2.4 Electroplated Films: Deposition & Structure	32
2.2.5 Selective Deposition	37
2.3 Electroless Deposition	41
2.3.1 Electrolyte Composition	42
2.3.2 Theoretical Considerations	52
2.3.3 Electroless Alloys & Composites	56
2.3.4 Advantages & Applications – Selective Deposition	58
2.4 Single and Multi-layered Thin Film Deposit Properties	62
2.4.1 Diffusion & Deposit Brittleness	63
2.4.2 Multi-Layers	66
2.4.3 Hardness	68
2.4.4 Magnetic Properties & Giant Magneto-Resistance (GMR)	73
2.4.4.1 Magnetization & Coercivity of Thin Films	74
2.4.4.2 Fundamentals of Magneto-Resistance	76
2.4.4.3 Larger Magneto-Resistance Effects	82
2.5 Magnesium & Corrosion	87
2.5.1 Corrosion	89
2.5.2 Galvanic Corrosion	95
2.6 Summary	98
2.7 References	99

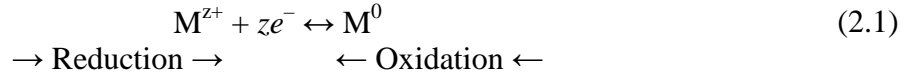
2.1 Introduction of Deposition Concepts and Properties

The purpose of the application of coatings to substrates has evolved much since the discovery of electroplating in the early 19th century. Beyond improving the appearance of surfaces, with the deposition of gold, chrome and other metals, improvements of surfaces characteristics such as corrosion, wear and scratch resistance, conductivity, magnetism, ability to be soldered, have become the focus of modern coatings. Modern methods of surface finishing include, electroplating, electroless plating, vacuum depositions including chemical vapour deposition and sputtering techniques, anodizing, and spray coatings such as cold spray and plasma spray, to name a few. Of these methods, the most common are electro- and electroless plating, both of which make use of an electrolyte a conductive, often liquid, medium containing the necessary ions for deposition.

Depositions of coatings from liquid electrolytes fall under the umbrella of wet chemistry. Metal deposition is achieved by a process known as reduction, a term denoting any reaction that consumes an electron. The deposition of metals from an electrolyte occurs with positively charged metal ions, known as metal cations, reduced to metallic form by the acquisition of electrons. The amount of electrons acquired depends on the oxidation state of the cations in solution which denotes the number of electrons an atom gains in order to be reduced. More generally the oxidation state denotes the number of valence electrons an atom gains, loses, or shares when making bonds with other atoms. Valence electrons are the electrons that form bonds with other atoms and the valence denotes the number of bonds possible. The anti-thesis of the reduction reaction is the liberation of an electron and is known as oxidation. During oxidation processes, the oxidation state of the atom or molecule increases and becomes more positive, while during reduction the oxidation state of the atom or molecule decreases becoming more negative. The surfaces upon which oxidation and reduction occur are known as the anode and cathode, respectively.

Both oxidation and reduction are represented in a single process taken in different directions, Equation 1.1. By convention, reduction is read from left to right, while oxidation is read from right to left. The oxidation/reduction pair has the arrow indicating the reaction may progress in either direction and is termed a redox reaction. This term is

a portmanteau composed of the *red*, for reduction and *ox* for oxidation. Both *red* and *ox* represent the common subscripts for notation dealing with each part of the reaction.



As the name suggests oxidation is also the process by which surfaces become oxidized. As the oxidation state of the metal increases, the electrons liberated aid in the reduction of oxygen gas {O₂} forming negatively charge oxygen species {O₂^{z-}}, oxygen anions. The oxygen anions then attract cations and share electrons ultimately forming, often neutralized, oxygen containing compounds on the surface of the material. It should be noted that oxidation of metals and surfaces is far more complex than the reduction of oxygen alone as many side processes, such as formation of water and subsequent dissociation to hydroxide, often occur; however it does exemplify the process. The process of oxidation is central to corrosion processes as well as the popular metal finishing technique known as anodizing. Anodizing, more a process of growth than deposition, involves the creation of a passive protective surface oxide on certain select metals by means oxidation building up the native oxide layer in an acidic electrolyte. The use of oxidation rather than reduction for the purpose of a protective finish sets anodizing apart from many other techniques. Anodizing is limited to certain metals including aluminum alloys, although processes also exist for titanium {Ti}, zinc {Zn}, magnesium {Mg}, niobium {Nb}, zirconium {Zr}, hafnium {Hf}, tantalum {Ta}, and ferrous metals. The commercial popularity of anodizing is due it being inexpensive and the ability to form porous metal finishes that allow dyeing; though anodizing Ti is able to generate an array of colors without the use of dyes.

Another series of popular metal deposition techniques are under the umbrella of vacuum deposition techniques. Vacuum deposition, a process used to deposit coatings atom-by-atom or molecule-by-molecule on a solid surface. Vacuum deposition techniques are able to deposit pure metals, and non-metals depending on the technique, in layers as thin as a few angstroms up to several millimetres. Due to limitations inherent in the process, such as substrate geometry, vacuum deposition techniques are applied mostly in the electronics and semiconductor industries as part of multi-stepped processes, which include electroplating, in the construction of computer hard disks and processors.

Though anodizing and vacuum deposition techniques are commonly used, electroplating, along with electroless plating, together provide the most robust avenues for the deposition of coatings, hence their continued investigation. Nowadays electrodeposition is used for the fabrication of many important parts of magnetic recording heads, including magnetic shields and poles; Cu coils; and for connecting Cu studs, leads, and pads, Au interconnects, nonmagnetic gaps, and coatings [1].

2.2 Electroplating & Electrochemistry

Electroplating is the electrical reduction of materials, usually metals, from an ionic state onto a surface achieved through the supply of electrons provided by a current. Deposition takes place within an electrolytic cell comprised of an ionic solution, known as an electrolyte, and two electrical conductors, or electrodes, that are immersed within the electrolyte and connected to an electron source, power supply, to complete a circuit, Figure 2.1.

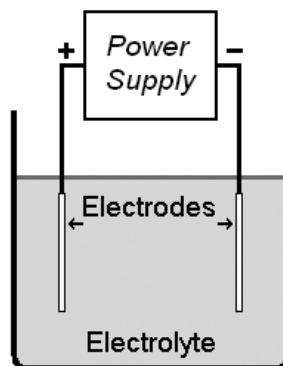


Figure 2.1: Schematic of the basic arrangement of an electroplating cell

The electrolytic environment containing the necessary ions for deposition is commonly supplied by one of three electrolyte types: aqueous solutions; molten salts; or increasingly ionic liquids¹. Each of three electrolyte types utilizes a different solvent for the metal ions, though all exist as liquid for the purpose of deposition. Aqueous solutions are the most common choice of electrolyte and contain dissolved ions in water. Molten salts and ionic liquids nominally contain no water with molten salts produced by increasing the temperature of metal salts to their melting point, and ionic liquids, which

¹ Other common terms for ionic liquids are room temperature ionic liquids, or room temperature molten salts.

are often liquid at, or near, room temperature, composed of ionic organic salts and metal salts providing the needed ions for deposition.

2.2.1 Electroplating Cell

When connected in a circuit with a power supply, a potential difference is achieved between the electrodes and electrons accumulate on the negative electrode. Within the electrolyte, the positively charged species, mainly metal cations², are attracted to the negative electrode while negatively charged species in solution will be attracted to the positive electrode. The applied potential which ultimately results in polarization of the solution is sometimes referred to as the polarization potential. The reduction of metal cations to metal occurs by the acquisition of electrons by the cations on the surface of the electrode supplying the electrons. The electrode upon which reduction occurs is named the cathode. At the other end of the cell, electrons are removed from the electrode by the driving electromotive force, EMF, of the battery or power supply and sent to the cathode resulting in oxidation of the positive electrode. The electrode at which oxidation occurs is known as the anode. It should be noted that it is a common misconception that the anode is always positive and the cathode is always negative such as in electroplating cells; for fuel cells the anode and cathode have opposing polarity as the term anode and cathode are based on the location of oxidation and reduction within the system and not electrical connections. Moreover, in the case of rechargeable batteries, the anode and cathode switch depending on whether the battery is being charged or used. This is because the recharging of a battery resets the system by oxidizing what is the cathode during operation and rebuilding through reduction the operating anode. While both the anode and cathode are electron conductors, the anode within the electroplating cell may be either inert or consumable. Inert anodes, often made of platinum or carbon, require the replenishment of metal ions in solution as they are consumed. Conversely, consumable anodes match the identity metal ion species in solution and replenish the ions in solution as the anode is oxidized and the electrons removed from the metal result in the liberation of metal cations into the electrolyte.

² Hydrogen ions from the deprotonation, removal of H⁺, of acids also present species to be reduced.

In addition to the anode and cathode, electroplating cells often make use of a third, inert, electrode known as a standardized reference electrode, or standard electrode. The purpose of the standard electrode is to provide a stable reference with respect to which the potential between the anode and cathode is measured. The need for the standard electrode is due to the significant difficulty in maintaining a constant potential at an electrode while a current is passed through the electrodes for the purpose of redox reactions. The difficulty originates, in part, from the electrical double layer which is a parallel structure of charges produced when a surface is exposed to a fluid. The electrical double layer, which may be constructed of solid particles or gas bubbles, is caused by the accumulation of charges at the surface of an electrode. The charges at the electrode polarize the electrolyte resulting in the formation of a layer of oppositely charged ions, or polarized molecules, at the interface and another layer of charges, or molecules, attracted by the first layer. The double layer, which behaves like a capacitor storing charge, causes a variation of electrical potential at the surface and is described by several models including the Helmholtz model, the Gouy-Chapman model, and the Gouy-Chapman-Stern model.

The standard electrode provides a known reduction potential, while the other electrode, anode, passes all the current needed to balance the current provided by the cathode. The standard electrode is connected to the cathode with a large resistance placed in the connection between the standard and working electrode to ensure the circuit is not disturbed. The standard, or reference, electrode is itself isolated from the solution by means of a salt bridge or a glass frit so that any minimal electron flow will not result in reduction on the electrode. The salt bridge is constructed by filling a glass tube with a conductive electrolyte such as sodium chloride {NaCl} or potassium chloride {KCl}. The electrolyte is often turned into a conductive gel by mixing it with agar, or may be kept within the tube by sealing an end with glass frit, small glass beads which provide a porous barrier allowing the flow of ions but not the bulk liquid. The standard electrode, isolated by the bridge or frit, is placed as close as possible to the cathode in order to maintain no potential difference between the cathode and standard potential. A summary of the reactions for a consumable anode in a deposition cell containing a standard

electrode for the deposition of nickel {Ni} from aqueous dissociated nickel chloride {NiCl₂} electrolyte is depicted in Figure 2.1.

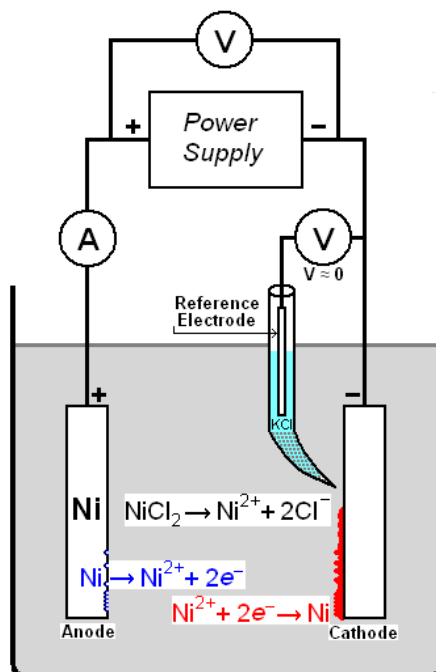


Figure 2.2: Depiction of an electroplating cell using a standard, or reference, electrode, housed within a KCl solution filled salt bridge, for the deposition of Ni from an aqueous NiCl₂ solution onto the cathode. Equations displayed show the dissociation (black), oxidation (blue) and reduction (red) reactions of Ni within the cell.

Standard electrodes are constructed to have a stable equilibrium potential for reversible half-reactions, meaning no current flow is present between electrode and internal electrolyte of the standard electrode. A number of standard electrodes exist, the most common of include the standard hydrogen electrode (SHE), the standard calomel electrode (SCE), and silver-silver chloride electrode (SSCE). The scale of standard electrode potentials is based on the half reaction of hydrogen, $2\text{H}^+(\text{aq}) + 2\text{e}^- \leftrightarrow \text{H}_{2(\text{g})}$, which by convention is defined as having a standard potential of 0.00 V at an effective concentration of 1 M and pressure of 1 atm at 25 °C. Given that half-cell potentials cannot be measured, a relative electrode potential for the reaction is measured against the 0 V potential of the SHE.

Standard hydrogen electrodes are constructed using platinised³ platinum {Pt}, electrode in an acidic solution having a 1.00 M concentration of hydrogen ions {H⁺} [2]. Pure hydrogen gas {H₂} at a pressure of 1 atm is bubbled around the Pt electrode, and equilibrium of the hydrogen in the two phases, aqueous and gaseous, within the system

³ Platinized Pt, also known as black Pt for its black color, is composed of black platinum powder deposit on a shiny platinum surface which results in a highly catalytic surface due to the increased surface area of the micro-structured deposit.

establishes the half-reaction. Due to the difficulty in setting up the SHE, other standard electrodes, such as the silver/silver chloride {Ag/AgCl}, are more commonly used. The SSCE is composed of solid AgCl, usually as a coating on Ag metal, immersed in an aqueous Cl salt solution, often 4 M potassium chloride {KCl}, saturated with AgCl and has a relative electrode, or reduction, potential, E° , of 0.197 V compared to the SHE [2].

The SSCE, along with the SCE, represent electrodes of the second kind in which the equilibrium potential is a function of the concentration of an anion in the solution as it controls the cation concentrations by means of the solubility product of the slightly soluble metal salt [3]. Like electrodes of the second kind, which often are used as standard electrodes, electrodes of the first and third kind both operate on the equilibrium potential determined by the cation in the solution. Electrodes of the first kind consist of a metal salt in solution with the cation in solution matching the metal electrode [3]. Electrodes of the third kind consist of a metal in contact with two slightly soluble salts of differing cations, only one of which matches the electrode, and identical anions immersed in a solution containing a salt of the differing cation [3]. The series of equilibrium within electrodes of the third kind result in instability and hence limited use.

2.2.2 Electroplating Conditions

The measure of the equilibrium electrode potential of a reversible electrode and its ion under standard conditions, effective concentration of 1 M and pressure of 1 atm at 25 °C, relative to the 0 V of the SHE is known as the relative standard electrode potential, or standard electromotive force (EMF), E° . It is often shortened with 'relative' conventionally dropped as E° for hydrogen is 0.00 V by convention. The measure of the electrode potential of a metal is done by coupling the half-cell of an electrode of the first kind, for example copper {Cu} immersed in {CuSO₄}, with a standard electrode, usually hydrogen by means of a salt bridge. If a standard electrode other than hydrogen is used, the standard electrode potential may be related to the hydrogen electrode by adding the reduction potential of the electrode to the potential measured. Converting the measurement to another electrode requires the additional subtraction of the electrode desired for comparison. The standard electrode potentials of the half-reactions provide, among other information, a series for activity of various metals and ultimately their

nobility, or resistance to corrosion. Higher, more positive values of E° indicate an affinity of the material to be reduced resulting in higher resistance to oxidation. Metals such as gold {Au}, which is known to resist oxidation, have a very positive E° . Conversely, highly negative E° metals such as magnesium {Mg} and aluminum {Al} are prone to rapid oxidation and, depending on the environment, corrosion, Table 1.1.

Half-Reaction	E° (V)
$\text{Ag}^{2+} + 2e^- \leftrightarrow \text{Ag}_{(s)}$	+1.98
$\text{Au}^+ + e^- \leftrightarrow \text{Au}_{(s)}$	+1.8
$\text{Au}^{3+} + 3e^- \leftrightarrow \text{Au}_{(s)}$	+1.498
$\text{Pt}^{2+} + 2e^- \leftrightarrow \text{Pt}_{(s)}$	+1.18
$\text{Pd}^{2+} + 2e^- \leftrightarrow \text{Pd}_{(s)}$	+0.915
$\text{Ag}^+ + e^- \leftrightarrow \text{Ag}_{(s)}$	+0.7996
$\text{Cu}^+ + e^- \leftrightarrow \text{Cu}_{(s)}$	+0.521
$\text{Cu}^{2+} + 2e^- \leftrightarrow \text{Cu}_{(s)}$	+0.3419
$2\text{H}^+ + 2e^- \leftrightarrow \text{H}_{2(g)}$	0.0000

Half-Reaction	E° (V)
$\text{Mg}^+ + e^- \leftrightarrow \text{Mg}_{(s)}$	-2.70
$\text{Mg}^{2+} + 2e^- \leftrightarrow \text{Mg}_{(s)}$	-2.372
$\text{Al}^{3+} + 3e^- \leftrightarrow \text{Al}_{(s)}$	-1.662
$\text{Ti}^{2+} + 2e^- \leftrightarrow \text{Ti}_{(s)}$	-1.630
$2\text{H}_2\text{O} + 2e^- \leftrightarrow \text{H}_{2(g)} + 2\text{OH}^-$	-0.8277
$\text{Zn}^{2+} + 2e^- \leftrightarrow \text{Zn}_{(s)}$	-0.7618
$\text{Cr}^{3+} + 3e^- \leftrightarrow \text{Cr}_{(s)}$	-0.744
$\text{Fe}^{2+} + 2e^- \leftrightarrow \text{Fe}_{(s)}$	-0.447
$\text{Co}^{2+} + 2e^- \leftrightarrow \text{Co}_{(s)}$	-0.28
$\text{Ni}^{2+} + 2e^- \leftrightarrow \text{Ni}_{(s)}$	-0.257
$\text{Sn}^{2+} + 2e^- \leftrightarrow \text{Sn}_{(s)}$	-0.1375
$\text{Fe}^{3+} + 3e^- \leftrightarrow \text{Fe}_{(s)}$	-0.037
$2\text{H}^+ + 2e^- \leftrightarrow \text{H}_{2(g)}$	0.0000

Table 2.1: Selected half-reactions along with their standard electrode potential relative to SHE. [4]

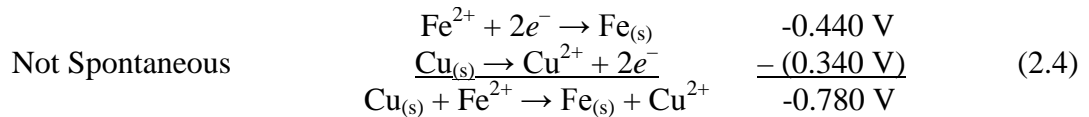
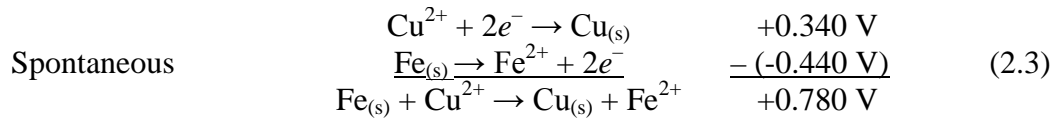
The table of standard electrode potentials, while giving insight into the relative deposition potential, does not provide the true deposition potential of a metal ion in solution. The arrangement of the ions in an electrolyte is generally not simply as charged species but rather as coordinated complexes. Coordinated complexes consist of metal ions surrounded by a shell of bound atoms or molecules known as ligands⁴. The bond between the ion and ligand can range from ionic, electrostatic attraction between two oppositely charged ions, to covalent sharing of electrons between atoms and depends on the identity of the species present in the electrolyte. Water {H₂O}, a common ligand in aqueous solutions forming hydrate coordination complexes, can be displaced by other ligands such as ammonia {NH₃}. Common coordination complexes include {[Cu(H₂O)₆]²⁺} for copper(II) ions {Cu²⁺}; {[Ni(H₂O)₆]²⁺} and {[Ni(NH₃)₆]²⁺} for nickel(II) {Ni²⁺} in the presence of H₂O and ammonia NH₃ respectively; and {[Au(CN)₂]⁻} for gold(III) {Au³⁺} in the presence of cyanide {CN⁻}. The presence, and

⁴ Ligands are also known as complexing agents and are used interchangeably.

identity, of coordinated complexes influence the reduction of the metal ions and ultimately the structure of the deposit. Coordination complexes, or complex metal ions, are critical for the stability of electroless deposition electrolytes and are further discussed in Section 2.3.1.

The table of standard electrode potentials also provides information on the occurrence of displacement reactions. Displacement reactions occur between two metals when a less noble metal is placed in a solution containing metal ions of a more noble metal, the less noble metal will enter solution while the more noble metal will precipitate, most often on the surface of the more noble metal. Whether the reaction will occur or not is calculated by determining the potential of the cell, E°_{cell} , which is defined as the difference between the standard electrode potential half-reactions of the cathode, E°_{cathode} or E°_{red} , and the anode, E°_{anode} or E°_{ox} , Equation 2.2. When E°_{cell} positive the reaction is spontaneous and will occur, Equation 2.3. In cases where E°_{cell} is negative, the reaction will not occur spontaneously, Equation 2.4. The utility of electroplating is that the provision of a potential difference between the anode and cathode can drive the reduction of what does not occur naturally/spontaneously.

$$E^\circ_{\text{cell}} = E^\circ_{\text{red}} - E^\circ_{\text{ox}} \quad (2.2)^5$$



The determination of E°_{cell} as presented in Equation 2.2 is correct only under standard conditions of concentration, temperature, and pressure⁶. Determination of equilibrium potential for a cell outside of standard conditions is achieved by means of the Nernst equation. The Nernst equation, Equation 2.5, named for German physical chemist Walther Nernst, relates E°_{cell} , the temperature and activity of the system to the equilibrium cell voltage, E_{cell} . The equation may be framed to either take into account

⁵ E°_{ox} is the potential of the oxidation half reaction, Equation 2.2 can equivalently be written as:

$E^\circ_{\text{cell}} = E^\circ_{\text{red1}} + (-E^\circ_{\text{red2}})$, where red1 represents reduction and red2 represents oxidation.

⁶ The determination of the displacement reaction does not take into account the formation of a complex. In cases of coordination complexes or more complicated reactions, the reactants and products must be determined and spontaneity is determined using the appropriate standard potentials for reactions present.

the equilibrium reduction potential, E_{red} , of a single species, or the equilibrium cell potential, E_{cell} , of the entire cell, used to determine the potential of a voltaic cell. In the case of E_{cell} , the activity is often replaced by the reaction quotient, Q_r , which is defined as the product of the initial concentrations of the products of the reaction divided by the product of the initial concentration of the reactants with each concentration raised to the power of its stoichiometric number, Equation 2.6. Replacement of the activity of the ion is possible as the activity is proportional to the ion concentration in the solution as long as the concentration of the ion in the electrolyte is moderate, a few fractions of a mole⁷. As concentration increases, accurate calculation requires a complicated function of all the units in the solution [5], with calculation based on concentrations providing only a relative approximation. In addition to deriving the equilibrium electrode potential for metal/metal-ion and hence the deposition potential of ions from an electrolyte, the Nernst equation is also used for the measurement of half-cell potentials for each of the three kinds of electrodes. The Nernst equation applies only in cases where no net current flow through the electrode is present as additional resistance or over-potential alters the equilibrium.

$$E_{\text{red}} = E_{\text{red}}^{\circ} - \frac{RT}{zF} \ln \left(\frac{a_{\text{red}}}{a_{\text{ox}}} \right) \quad (2.5)$$

or

$$E_{\text{cell}} = E_{\text{cell}}^{\circ} - \frac{RT}{zF} \ln(Q_r)$$

where:

- E_{red} = Half-cell reduction potential at the temperature of interest
- E_{red}° = Standard electrode potential of the half-cell
- E_{cell} = Cell potential at the temperature of interest
- E_{cell}° = Standard electrode potential of the cell
- R = Universal gas constant, $8.314472(15) \text{ J} \cdot \text{K}^{-1} \cdot \text{mol}^{-1}$
- T = Absolute Temperature, Kelvin
- z = Number of moles of electrons transferred in the cell or half-reaction
- F = Faraday constant, $9.64853399(24) \times 10^4 \text{ C} \cdot \text{mol}^{-1}$
- a_{red} = Chemical activity for the reductant, electron donator
- a_{ox} = Chemical activity for the oxidant, electron acceptor
- Q_r = Reaction quotient

⁷ Generally the case for most aqueous solutions.

$$Q_r = \frac{[C]^c [D]^d}{[A]^a [B]^b} \quad (2.6)$$



The establishment of the correct deposition potential is essential to ensure electrolysis deposits the desired material rather than decompose chemicals within the bath into their elements. For example, if too negative a potential is provided to a deposition cell containing an aqueous electrolyte, the applied potential break down the water within the cell to hydrogen {H₂} and oxygen {O₂} gases rather than deposit the desired metals. The difference in potential between the reduction potential, the potential of the electrode through which an external current I is flowing, E(I), and the equilibrium potential of the electrode, or potential in the absence of an external current, E, is known as the over-potential, η . The practical relationship between the current density, i, and the over-potential, η , is given by the Tafel equation [5], Equation 2.7.

$$\begin{aligned} \eta &= E(I) - E \\ \eta &= a \pm b \log|i| \end{aligned} \quad (2.7)$$

where: η = Over-Potential
i = Current density
 \pm = sign indicates anodic and cathodic processes, respectively
a & *b* = Constants defined, for the cathodic reaction, by:

$$a_c = \frac{2.303RT}{\alpha zF} \log(i_0) \qquad b_c = \frac{2.303RT}{\alpha zF}$$

where: *i*₀ = exchange current density (*i*₀ = *i* when $\eta = 0$),
 α = Transfer coefficient
F = Faraday constant,
R = gas constant
T = absolute temperature, Kelvin
z = charge of the metallic species, M^{z+}

Key features of the Tafel equation are that small changes in η produce large changes in the current density, *i*, and for large values of η , ($\eta > 100$ mV) the function $\eta = f(\log i)$ is linear; extrapolation from which gives the exchange current density, *i*₀ [5]. It should be noted that the Tafel equation is applied to each electrode separately and assumes that the reverse reaction rate is negligible compared to the forward reaction rate. While the Tafel equation provides information on the relationship between the potential and current density for a reaction, the determination of the potential at which chemical species will be reduced is determined using voltammetry.

Voltammetry, an analytical chemistry technique, is a process where either the potential, or current, between two electrodes is varied with respect to time and the resulting current, or potential, is measured. The electrochemical cell used for voltammetry is effectively the same as is used for electroplating, Figure 2.2. As in electroplating, a standard electrode is desired for voltammetry so that one electrode need not both supply electrons and provide the reference potential. For the purpose of electroplating, voltammetry is conducted such that the cathode is taken as the working electrode, the electrode at which the reaction of interest, reduction, is occurring [6]. The working electrode is frequently cleaned to avoid build up from materials. The anode, or more generally auxiliary electrode, is inert so as to not interfere with the measurement [6]. In cases where by-products generated at the anode could interfere with the reaction, the anode is isolated by means of a salt bridge or glass frit in the same way as a standard electrode. Common voltammetric techniques include the galvanostatic transient technique, the potentiostatic transient technique, and the potential sweep method [6]. In the galvanostatic technique the current between the test and auxiliary electrodes is held constant and the potential between the test and reference electrodes is measured as a function of time [6]. When a constant current is applied to the system, the current is used for charging the double-layer capacitance from the reversible potential up to the potential at which the electrode reaction can proceed with a measurable velocity⁸, and electrode reaction, or charge transfer [6]. From a series of galvanostatic measurements of the over-potential for a set of differing current values, a current–potential relationship for an electrochemical process may be constructed [6]. Determination of the current potential relationship is important in the determination of cathodic and anodic processes and is most useful in the construction of an Evans diagram for electroless deposition, see Chapter 2.3.2. For the potentiostatic technique, the potential of the test electrode is held constant, while the current, the dependent variable, is measured as a function of time [6]. Potentiostatic measurements provide information on the charging of the electrical double layer as the current will decay with time to a steady state. For the potential sweep

⁸ Recall, that the difference between the reversible potential and the potential at which the electrode reaction can proceed is the over-potential.

method, the more commonly used technique for electroplating, curves of the current as a function of the potential, $i = f(E)$ are recorded directly in a single experiment [6].

The potentiodynamic sweep may be conducted either linearly or cyclically at a rate typically between 1 mV/s and 1000 mV/s, depending on the system [6]. Linear sweeps are conducted going from one potential to another, either higher or lower, while cyclic sweeps, of which there may be multiple, are taken from one potential to another, then back to the starting potential. The resulting plot of the current against the potential applied is known as a voltammogram. A peak or trough, $\frac{d}{dx} f(E)|_E = 0$, in the curve of the current associated with a given potential indicates the presence of a redox process. For a reversible process, current peaks at a given voltage indicate reduction for scans of increasing potential and oxidation for decreasing potential. Similarly, troughs indicate oxidation for scans of increasing potential and reduction for scans of decreasing potential. The relative position of reduction peaks coincide with the order of activity provided by the series of standard electrode potentials with more noble elements requiring lower reduction potential. The shape of the voltammogram, including the sharpness of the peaks is dependent on the rate of the potential sweep compared to the rate of the reaction. Rapid scan rates yield more pronounced peaks as rapid scans limit the growth of the diffusion layer on the electrode. The diffusion layer is produced in the vicinity of an electrode where the concentration differs, drops in the case of reduction, compared to the bulk electrolyte. The diffusion layer is not to be confused with the electrical double layer which is due to accumulation of a charged layer due to surface charges on the electrode.

The establishment of a peak and subsequent drop in current on a forward scan is due to the diffusion layer having grown to a point so that the rate of reduction is not sufficient to balance the equilibrium potential set forth by the Nernst equation; more simply, no more reduction can occur. In cyclic voltammetry, the diffusion layer has a lesser impact on the resulting scan as the sweep occurs in both directions minimizing and limiting build-up of the layer. Another important feature of the cyclic voltammogram is that it shows a peak in current during the forward scan and a dip in current on the reverse scan representing the peak cathodic and anodic currents of a reversible reaction. These peaks provide the most efficient potentials at which all of the substrate at the surface has been reduced, cathodic peak, or oxidized, anodic peak.

2.2.3 Electroplating Techniques

The information acquired from voltammetry not only provides the potential difference between the anode and cathode for most efficient deposition, it also allows for deposits to be conducted using either constant voltage or constant current. Historically, until the advent of modern electrical generation, electroplating was conducted under potentiostatic, constant voltage, conditions. Potentiostatic deposition is typically used in cases where the thickness of the deposition layer is not subject to a strict tolerance, or when selection is needed due to more than one candidate for reduction present in solution. In cases where more than one metallic ion exists in an electrolyte as a candidate for reduction, selection may be used to provide a pure or alloyed deposit depending on the construction of the electrolyte.

The benefits of an alloyed film compared to a pure film depend largely on the alloy deposited. Some alloys have superior qualities including: density, hardness, corrosion resistance, wear resistance, or different magnetic properties, which are not available for a single metal metallic film. By definition, the electrodeposition of an alloy requires the co-deposition of two or more metals, meaning that a rapprochement between differing deposition potentials of at least two metals is needed within the electrolyte solution. Ultimately successful alloy deposition relies on the deposition potentials of the metals becoming close, or even identical. The deposition potential, E , of metal ions within a single electrolyte, as provided by the Nernst equation, Equation 2.5, is dependent on the standard electrode potential, E° , of the metal as well as the activity of the ion in the electrolyte, which is controlled by the concentration of ions in solution; the temperature of the electrolyte is moot as both ions share a single electrolyte. For the co-deposition of metals of greatly different E°_{red} the rapprochement of E_{red} is achieved by changing the concentration of the respective ions in solution. Altering the activities by changing the concentration is exemplified in the alloyed co-deposition of Zn and Cu from a bath containing cyanide complexes of both metals. Maintaining the concentration of Cu^+ ions to the order of $10^{-18} \text{ mol}\cdot\text{L}^{-1}$ [5], or equivalently $63.5\cdot 10^{-18} \text{ g}\cdot\text{L}^{-1}$, results in a high concentration ratio of the Zn ions relative to the Cu ions and brings the two deposition potentials closer to one another overcoming the approximately 1.284 V vs. SHE

difference between Cu and Zn; $E^\circ_{\text{Zn}^{2+}} = -0.763 \text{ V}$ and $E^\circ_{\text{Cu}^+} = 0.521 \text{ V}$. The degree of alloying may be determined to some degree by the ratio of the current densities of individual metals at a given potential as seen in the superposition of voltammetry curves, Figure 2.3.

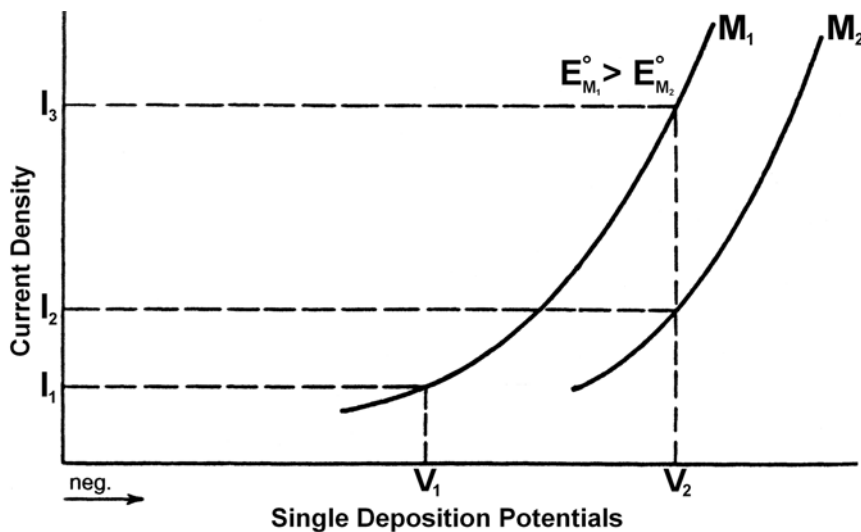


Figure 2.3: Typical voltammetric curves for two different metals, M_1 & M_2 ; at potential V_1 the more noble metal, M_1 , is deposited, at potential V_2 metal M_1 and M_2 are deposited in a ratio of approximately I_3/I_2 [5]. [Image modified from Figure 1.22 “Modern Electroplating, 5th Edition”, with kind permission from John Wiley & Sons, Inc. (2010).]

In addition to the option of alloying, metals of greatly different E° may be deposited individually from the same solution as multiple sequential layers, or multi-layers, provided their deposition potential within the electrolyte is sufficiently different. The electrodeposition of modern multi-layers is achieved by periodically alternating the potential in pulses allowing for the deposition of alternating layers of metals. As shown in Figure 2.3, the metal with the least negative E° , M_1 , may be deposited as a pure metal at potential V_1 , while the metal ions of M_2 will have some contamination of metal M_1 when deposited at potential V_2 . Much as in the case of alloying, the concentrations may be modified to make the voltammetric curves more distinct. Increasing the concentration of the metal with more negative E° will increase the ratio of metal M_2 deposited. In order to ensure uniform layer thickness between each compositionally unique layer, the deposition time, or ‘pulse’, at the less negative deposition potential is longer than the ‘pulse’ at the more negative potential. The difference in pulse lengths accounts for higher current density, and hence deposition rate, at the more negative deposition potential. The limitation of layered deposits of this type is that the maximum difference

between the deposition potentials of differing metals is E_{red}° . Attempting to electroplate alternating layer of metals of similar E_{red}° such as Co, -0.28 V vs. SHE, and Ni, -0.25 V vs. SHE will result, at best, in the formation of Co-Ni alloys of differing Co-Ni ratio. Further details regarding the deposition of multi-layers are discussed in Section 2.3.3 of this chapter.

In addition to the co-deposition of conductive materials and metals, inert materials may also be co-deposited via electroplating. The purpose of co-depositing inert materials is often to increase the wear resistance of surfaces. The inclusion of mixed carbon materials such as silicon carbide {SiC}, tungsten carbide {WC}, or diamond particles, can be achieved by using low current densities allowing for the natural inclusion, trapping, of particles and other impurities within the deposit. One documented application is the inclusion of 100 ppm of carbon in a sulfamate { H_2NSO_3^- } nickel bath which has been shown to increase the tensile strength of the deposit from 500 MPa to approximately 900 MPa [7].

Galvanostatic deposition, deposition at constant current or more specifically using a constant current density, is used when the electrolyte is well defined and a voltammetric curve has been established. Given a voltammetric curve providing the peak current for a system and the size of the cathode, it is possible to determine the current per area, or current density. Application of the optimum density establishes the optimum deposition potential just as establishing the optimum potential results in the peak current density. This method is most convenient when the deposition thickness requires precise control as it is the electrons that reduce the metal ions. The method in which the amount of material deposited and deposition thickness may be calculated is Faraday's law. Faraday's law states that the amount of electrochemical reaction that occurs at an electrode is proportional to the quantity of electric charge, q , passed through an electrochemical cell [5]. The weight, or more correctly the mass, of the deposited materials, Equation 2.8, can be expressed as the product of the electrochemical equivalent, Z , and the amount of charge, q ; more practically q can be replaced by the product of the current, I , and the duration of the deposit, t . The electrochemical equivalent, Z , denotes the atomic weight of the element to be deposited per the number of electrons for the deposition of a single

ion per number of particles per electron charge A_{wt}/nN_ae ; N_ae is known as Faraday's constant, F .

$$w = ZIt = \frac{A_{wt}It}{nN_ae} = \frac{A_{wt}It}{nF} \quad (2.8)$$

where: w = Mass, sometimes referred to as weight, of material deposited (g)
 Z = Electrochemical equivalent
 I = Applied current (A)
 t = Duration of the deposition (s)
 A_{wt} = Atomic weight of the deposited species ($\text{g}\cdot\text{mol}^{-1}$)
 n = number of electrons involved in the deposition reaction
 N_a = Avogadro's Number, $6.022\times 10^{23} \text{ mol}^{-1}$
 e = Electron charge $1.6021\times 10^{-19} \text{ C}$
 F = Faraday constant, $9.6485\times 10^4 \text{ C}\cdot\text{mol}^{-1}$

The thickness of the resulting deposit, h , is determined as the volume of material deposited, V , over the area, a . Given that the density, d , may be expressed as the mass, w , of the deposit over its volume, V , useful relationships may be drawn between the deposition time, current, and desired thickness of the deposit, Equation 2.9.

$$h = V / a = w / ad = \left(\frac{A_{wt}I}{nFad} \right) t \quad (2.9)$$

where: h = Thickness of the deposit (mm)
 V = Volume of material deposited (mm^3)
 a = Area of the deposit (mm^2)
 d = Density of the deposit (g/mm^3)

Though the thickness of the deposit is dependent on the duration of the provided current, the presence of other ionic species in solution provides other candidates for reduction by the supplied electrons. Even at the most efficient current density as set out by voltammetry, the efficiency of the metal deposition is typically less than 100 %. For example, during deposition of Cu from a solution of cupric nitrate $\{\text{Cu}(\text{NO}_3)_2\}$ in dilute nitric acid $\{\text{HNO}_3\}$, three cathodic reactions occur: the deposition of Cu (the reduction of cupric, Cu^{2+} , ions) and the reduction of both nitrate and hydrogen ions [5]. The efficiency of the deposit, known as the current efficiency, CE, is calculated by the amount of charge used to reduce the desired species, q_i , per total charge available, q_{total} ; or alternatively the mass of the reduced species desired, w_i , per total mass reduced, w_{total} , Equation 2.10.

$$CE = q_i/q_{total} \quad (2.10)$$

or

$$CE = w_i/w_{total}$$

where: CE = Current Efficiency
 q_i = Charge used to reduce the desired species
 q_{total} = Total charge available
 w_i = Mass of desired reduced material
 w_{total} = Total mass of reduced materials

Though current efficiency is typically below 100 %, the deposition of Au from alkaline baths, with sufficient agitation, have produced cathodic current efficiencies as high as 90–100 %. The concentrations of ions within the electrolyte, in addition to conditions during deposition and bath composition, have a large influence on the efficiency of the deposit. Current efficiency of 100 % has been obtained for deposition of Au from a $12 \text{ g}\cdot\text{L}^{-1}$ $\text{KAu}(\text{CN})_2$ solution under mild agitation at a current density of $10 \text{ mA}\cdot\text{cm}^{-2}$, while a current efficiency only about 50 % is obtained from a $4 \text{ g}\cdot\text{L}^{-1}$ $\text{KAu}(\text{CN})_2$ solution in otherwise similar conditions [8]. The inclusion of some additives can result in deposition rates of over 100 %. In these cases a chemical reduction of ions, termed electroless deposition, occurs in consort with the electroplating resulting in efficiencies of over 100 %. The chemical reduction of ions without the use of any outside current, known as electroless plating, is discussed in Section 2.3 of this chapter. It should also be noted that when deposition occurs in a magnetic field, the structure, texture, and throwing power⁹ of both magnetic and nonmagnetic materials can be negatively affected [5].

2.2.4 Electroplated Films: Deposition & Structure

The presence of an electrical double layer and diffusion layer on the surface of an electrode complicate the process of electroplating beyond the straightforward reduction of metal ions alone. The cathodic deposition of metals, whether alloyed or pure, can be broken down into three main stages, 1) ionic migration, 2) electron transfer, and 3) incorporation [5]. During the ionic migration phase, hydrated ions in the electrolyte migrate toward the cathode under the influence of the applied potential. The beginning

⁹ Throwing power is a measure of the ability of an electrolyte to plate to a uniform thickness over a cathode of irregular shape. Throwing power may be improved with use of an anode which conforms to the irregular shape of the surface.

of the electron transfer stage is characterized by the hydrated metal ions entering the diffusion/double layer on the surface of the cathode. As the hydrated ions approach the cathode, water molecules of the hydrated ions are aligned by the field present in the double layer and ultimately the hydrated shell around the metal ion is lost due to the high electrical field present in the layer [5]. The electrons present on the cathode then neutralize the metal ion as it is adsorbed onto the surface. The final stage of incorporation is the migration of the adsorbed atom along the cathode to a region of lower energy and finally incorporation of the atom into the growing three-dimensional, regular periodic geometric order of atoms, or unit cells, which define the lattice. The three dimensional constant distance between the beginning of set of atoms and the same pattern as set out by a translation define the lattice constants for the unit cell¹⁰ of a crystal lattice.

The initial layers, up to a few microns, of a continuous deposit are typically referred to as the thin film deposits while further thickening of the deposit is known as bulk deposition. In practise the only difference between the stages is the thin film is deposited on the substrate, often different material than the deposit, while the bulk deposit occurs upon the thin film made of the same material as the deposit. During both these stages, deposition occurs wherever electrons are present to reduce the metal from ionic form. The path the ions take to the substrate is defined in part by electrical field lined established by the charge present on the anode and cathode. Due to the dependence of the deposit on field lines, deposits are most even where the electric field lines are perpendicular to the surface. Fringing fields from the edge of a substrate result in uneven deposition as the aggregation of field lines at the edge produce a thicker deposit at the edges of the substrate compared to the middle. The effect of the fringing fields is commonly known as the “dog-bone” effect as the resulting deposit is shaped like a stereotypical bone one would give to a dog. Additionally, the line of sight limitation brought about by the electric field lines often results in non-existent or extremely poor quality deposits within recessed areas. Both the dog-bone effect and difficulties plating recessed areas can be mitigated by using anodes customized for the substrate.

¹⁰ A unit cell is the smallest repetition of atoms within a crystal lattice, the translational repetition of which produces the entire crystal lattice.

The atomistic perspective of lattice growth provides explanation as to the process of migration of the neutralized atom within the incorporation stage. This approach treats the metal as a fixed lattice of positively charged atoms with the electrons permeating between the atoms moving nearly unimpeded as a gas of free valence electrons [5]. Interactions between the free electrons and the metal ions are largely responsible for the metallic bond [5]. The lattice formed by the deposited metal ions, especially electroplating, is not a perfect, ideal, atomically smooth crystalline structure¹¹ as it contains a variety of defects including vacancies, missing atoms; dislocations, atoms shifted from the periodic geometric ordering; mono-atomic steps in the lattice; clusters of adsorbed atoms, or adatoms; and non-periodic impurities. For example, the density of metal surface atoms is about 10^{15} cm^{-2} , while the density of dislocations on a non-ideal surface is of the order of 10^8 cm^{-2} [5]. The presence of defects in an electroplated deposit are principally the result of coordination chemistry and diffusion layer effects on the migration of reduced atoms/ions along the surface to the position of lowest energy, typically a kink site, Figure 2.4.

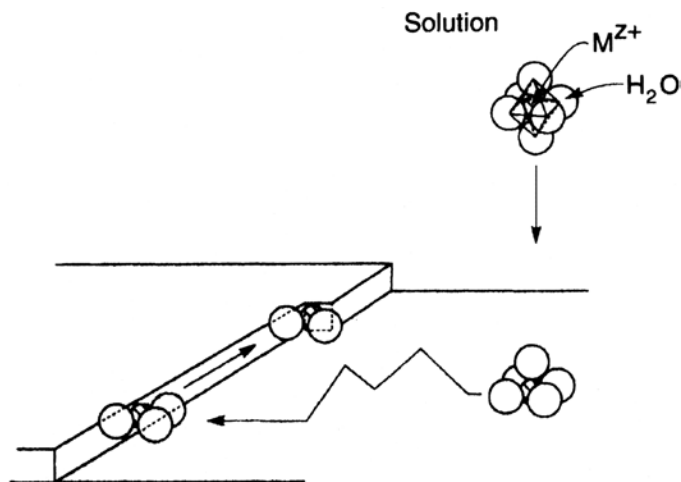


Figure 2.4: Ion transfer to a terrace site, surface diffusion, and incorporation at kink site [5].

Note: The hydrated shell is lost in stages as the ion is transferred to the surface.

[Image reproduced from Figure 1.13 in "Modern Electroplating 5th Edition", with kind permission from John Wiley & Sons, Inc. (2010).]

One unmentioned mechanism of note is Ostwald ripening, which is a thermodynamically-driven, spontaneous process that occurs due to greater stability and lower energy configuration of larger particles compared smaller particles [9]. Compared

¹¹ The inclusion of non-metals within electroplated deposits can provide the freshly deposited films with an amorphous quality. Over time, or with heat treatment, the quasi-amorphous film will crystallize.

to the nucleation of the deposit by electroplating, the role of Ostwald Ripening is effectively non-existent. By definition, the phenomenon of Ostwald ripening can play a more significant role in incorporation of adsorbed molecules, especially the formation of immersion deposits where the rate for crystallite formation is significantly slower. In the case of immersion deposits, the mass transport of material away from smaller particles towards larger particles in a supersaturated environment, Ostwald ripening, is more likely to occur. The theoretical treatment of the deposition mechanisms has been conducted in work by others [6, 10-13] and information beyond the overview presented is not covered within this work.

Beyond the atomistic perspective, the growth of electroplated deposits resulting from the reduction of metal onto the surface of an electrode by the acquisition of electrons can be characterized as a combination of two processes or mechanisms; layer growth and nucleation-coalescence growth, or three-dimensional (3D) crystallite growth, Figure 2.5.

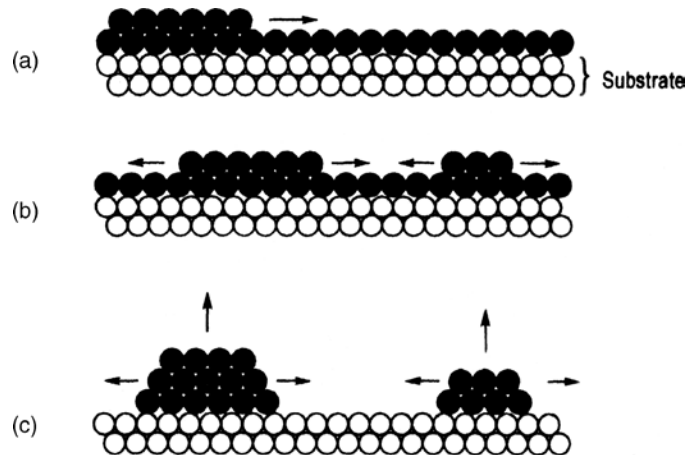


Figure 2.5: Schematic representation of (a, b) layer growth and (c) the nucleation-coalescence mechanism [5]. [Image reproduced from Figure 1.16 in “Modern Electroplating 5th Edition”, with kind permission from John Wiley & Sons, Inc. (2010).]

The ideal layered growth mechanism occurs when single, discrete layers are deposited across the surface with the next layer growing upon completion of the previous layer. The nucleation-coalescence growth of 3D crystallites is characterized by four stages, namely, 1) the formation of isolated nuclei and their growth to 3D crystallites, 2) the coalescence of the crystallites, 3) formation of a linked network, and 4) formation of a continuous deposit [5]. While in practice both growth mechanisms occur during electroplating, control over the deposition conditions may be used in order to favour one

mechanism over another. Such modifications include changing the deposition rate by changing the concentration of ions or bath temperature, as well as the incorporating additives to make the deposit more compact, smoother, or change other qualities associated with crystallite size. Additives adsorbed onto the surface are able to affect the kinetics of electroplating as well as the growth mechanism by changing the concentration of growth sites on a surface, the concentration of adions¹², or the diffusion coefficient of the diffusion layer.

The influencing deposition conditions by means of the inclusion of additives, ion concentration, and deposition conditions ultimately influence the quality of the thin film coating by means of the crystal structure of the deposit. The arrangement of crystallites that form a deposit may be considered as either highly crystalline, meaning the charged atoms/ions are arranged in large, ongoing periodic structures, or amorphous, meaning that the size of the crystallites are of the order of the periodic pattern itself [5]. The higher the degree of crystallinity, the longer the scale upon which the periodic structure is retained up to the formation of a single crystal. Interruptions in the periodicity of the lattice are called grain boundaries with the individual crystallites known as grains [5]. Within a polycrystalline coating, grains typically share periodicity, though the size of individual grains varies. The degree of crystallinity of electroplated structures depends on the competing formation of new crystals and the growth of those existing. A large number of variables during electroplating including metal ion concentration, additives, current density, temperature, agitation, and polarization affect the structure and size of the crystallites as well as the formation of defects within [5]. There is some variation of the term ‘grain’ with some authors attributing the term to groupings or clumps of crystallites which some authors refer to as ‘islands’ [5]; within the context of this work the term grain will refer only to individual crystallites having crystal lattice planes of the same direction. The structures of lattices that make up the crystallites of commonly deposited metals, Table 1.2, fall under one of three different crystal structures, Figure 2.6.

¹² Adions is a term used for adsorbed ions much as adsorbed atoms are known as adatoms.

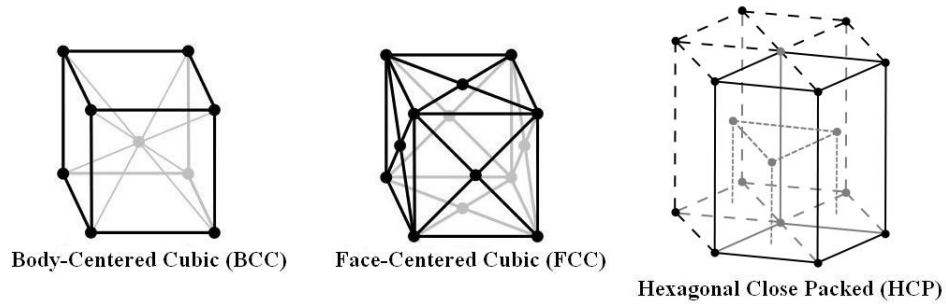


Figure 2.6: Unit cells of the three crystal lattices of commonly deposited metals.
 (Figure assembled from individual original images by Bob Mellish; reprinted under GNU Free Documentation License.)

Crystal Structure	Commonly Deposited Elements
BCC	Cr, Fe, W
FCC	Al, Ni, Cu, Ag, Au
HCP	Co, Zn

Table 2.2: Crystal structure of commonly deposited metals.

As illustrated in Figure 2.6, body-centered cubic (BCC) lattices have unit cells with an atom at each corner as well as the center of the body of the cube with each atom in contact with 8 other adjacent atoms within the lattice, also known as having a coordination number of 8. The more commonly deposited face-centered cubic (FCC) lattices have unit cells of an atom in each corner as well as the center of each face of the cube and have a coordination number of 12. Hexagonal close packed (HCP) lattices are made up from planes of hexagonal lattices with an atom at the center of each hexagon and each plane offset within the tetrahedral hole of the previous plane. Each atom has a coordination number of 12 and the unit cell of the HCP lattice is outlined with bold lines within the figure. The voids between atoms in the FCC and HCP structures account for 25.96 % of the total volume while the BCC structure has voids accounting for 31.98 % of its total volume. The reason for similarities between the voids and coordination number of the HCP and FCC lattices is that the FCC lattice can be constructed from an HCP-like lattice where the tetrahedral holes of a hexagonal plane are not filled symmetrically by atoms above and below the plane; this packing is known as cubic-close packed (CCP) and contains the FCC lattice.

2.2.5 Selective Deposition

Equally important to the creation of thin film and bulk deposits is the limitation and control over the regions upon which deposition occurs. The limitation of the deposit

to certain areas of a surface is known as selective deposition. Selective deposition is typically accomplished by some sort of lithographic technique to form a three-dimensional image on a substrate for subsequent transfer of a pattern to the substrate, in this case, by means of electroplating. Selective deposition may be applied for aesthetic or practical purposes. The most widely used and essential practical purpose is the deposition of conductive pathways for the creation of microelectronics within the electronics industry.

The creation of microchips involves a multi-stepped process which includes multiple selective imaging; deposition; and etching processes. The selectivity of the deposition and etching processes are most commonly enabled by means of photolithography, a printing technique where patterns are written onto a light, typically ultraviolet (UV), sensitive polymer coating called a photoresist. The photoresist applied to the surface is selectively exposed to light, or in some cases an electron beam, which deposits the energy via photon, or electron, into the exposed region. The exposure of the photoresist results in a chemical change, typically the breaking or creation of bonds, which renders the photoresist either soluble or insoluble, depending on the photoresist, to a developer solution, Figure 2.7. Photoresists that become soluble after exposure are termed positive photoresists while photoresists that become insoluble after exposure are termed negative photoresists. While negative resists were popular in the early history of integrated circuit processing, due to increasingly smaller feature sizes and better control over patterns, positive resists have gradually become more widely used [14].

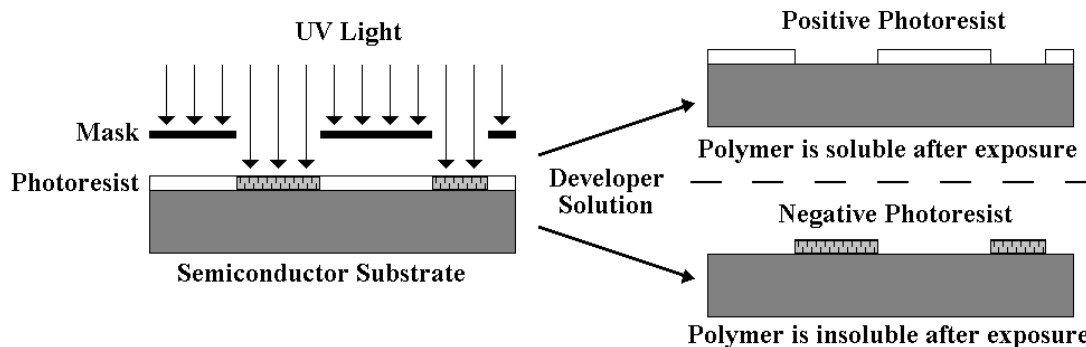


Figure 2.7: Insoluble/soluble (positive/negative) photoresists rendered soluble/insoluble to a developer solution after UV light exposure.

The technological advancement of integrated circuit design has evolved beyond proximity lithography, pictured in Figure 2.7, to projection lithography which employs a

system of lenses between the mask and substrate for miniaturization of the circuit [14]. The resolution achieved using photoresists is dependent on the wavelength, λ , of the photons and numerical aperture, NA, of the mask in the case of UV light. In this context the NA is a dimensionless number ranging from zero to one and characterizes the range of angles over which the system of lenses can emit light, Equation 2.12. Combining the two variables along with the Rayleigh factor, κ_0 , provides the Rayleigh criterion for resolvability which defines the diffraction limit of the optics, Equation 2.13 [14].

$$NA = n \sin \theta \quad (2.12)$$

$$CD = \kappa_0(\lambda/NA) > \kappa_1(\lambda/NA) \quad (2.13)$$

where: NA = Numerical Aperture
 n = Index of refraction, $n = 1$ in vacuum
 θ = Half-angle of the maximum cone of light
 CD = Critical dimension
 κ_0 = Rayleigh factor, 0.61 for incoherent light
 κ_1 = Technological factor, replaces κ_0
 λ = Wavelength of the photon

The Rayleigh criterion is the minimum resolution obtainable where the central maximum of a diffraction pattern of one source is centered on the first minimum of the diffraction pattern of another, Figure 2.8, and defines the minimum projectable feature size, or critical dimension, CD. Further minimization of CD is possible by means of state-of-the-art optical photolithography which effectively replaces κ_0 by a technological factor, κ_1 , which can be made as small as 0.2 [14].

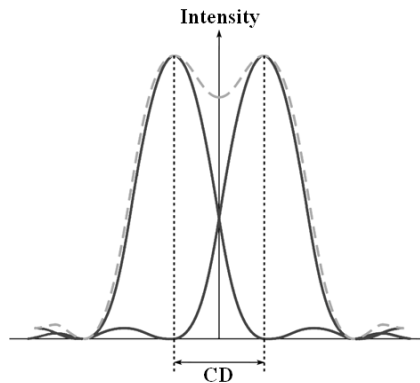


Figure 2.8: Condition of the Rayleigh Criterion for resolvability [14].

[Figure 4c reproduced from R. P. Seisyan, "Nanolithography in Microelectronics: A Review" [14] with kind permission from Springer Science and Business Media"]

Using optical techniques, the resolution of features using photolithography has surpassed the Rayleigh diffraction limit and lead to the ongoing use of photolithography. The four main ways of overcoming the diffraction limit are: (i) optical proximity

correction¹³, by changing the features of the photomask; (ii) introduction of an artificial phase shift¹⁴ to provide destructive interference; (iii) immersion¹⁵; and (iv) double exposure and double patterning, using two photomasks with complementary micropatterns when exposing the same photoresist layer [14]. While electron beam lithography is almost always capable of higher resolution than photolithography, the use of photolithography has continued to dominate due to concurrent writing/printing of the circuit compared to longer writing times with electron beam lithography. Another limiting factor for electron-beam lithography is the scattering of incident electrons over long distances or the production of secondary emission electrons introducing a small uncertainty in the resolution.

Current generation microchips utilize 193 nm wavelength light put out by argon-fluoride {ArF} excimer lasers, a laser using a combination of noble and reactive gas to produce UV light [15]. Photoresists exposed to electron beams produce similar results as exposure to UV light; however unlike photons, which are absorbed by the photoresist depositing all their energy at once, Equation 2.14, electrons deposit energy gradually, scattering within the photoresist.

$$E = h\nu = hc/\lambda \quad (2.14)$$

where: E = Energy of the photon
h = Plank's Constant, 6.626×10^{-34} J·s or 4.136×10^{-15} eV·s
ν = Frequency of the photon
c = Speed of light, 2.998×10^8 m·s⁻²
λ = Wavelength of the photon

Note: 1 electron volt (eV) = energy required to raise an electron through 1 volt = 1.602×10^{-19} J

After the photoresist has been placed over the surface, the transfer of the pattern into the substrate is commonly achieved either by subtractive transfer, also known as etching; additive transfer, also known as selective deposition; or impurity doping, also known as ion implantation. Electroplating is often used as part of selective deposition but may also be utilized in conjunction with etching processes. In the case of etching processes, the photoresist prevents the etchant, usually an acid, from removing masked

¹³ Optical proximity correction utilizes serifs, small lines attached to the end of pattern, and mouse-bites, small areas removed from the pattern, features on the photomask to reduce corner rounding on the outside and inside of a corner, respectively. [13]

¹⁴ Introduction of an artificial phase shift consists of adding extra features to a mask that shift the phase of transmitted light by 180° causing destructive interference and producing sharp demarcation lines. [13]

¹⁵ Immersion of the photoresist in liquid, such as water, incorporates a refractive index into the resolution reducing the λ of the radiation and increasing the NA; e.g. $NA = nNA_0$ [13]

electroplated material. Selective deposition is used whenever workable etching processes are not available, such as the creation of Cu interconnects. Interconnects are created using photoresists to provide regions where deposition is desired with physical vapour deposition providing a seed layer for subsequent Cu electroplating [16]. As of 2013, the feature size on commercially available chips is 22 nm created by 193 nm wavelength light [15, 17]. Due to the ability to project a clear image of a small feature being limited by the wavelength of light used for the lithography, further reduction in feature size requires the use of extreme UV light, 10 nm-124 nm, photolithography, or electron beam or x-ray lithography [15, 18]. Documents put out by the International Technology Roadmap for Semiconductors: 2011 predict feature sizes < 10 nm in NAND flash memory, used in the core of removable USB storage devices, by 2020 [17, 18].

2.3 Electroless Deposition

Electroless deposition, also known as electroless plating, is traditionally defined as an autocatalytic deposition process in which metallic ions are reduced from an electrolyte to metallic form by electrons provided by a chemical agent [19, 20]. The reduction of metal ions occurs initially on a catalytic surface¹⁶, not necessarily a conductor, with further layers also being catalytic for sustained deposition. Like electroplating, electroless deposition is an electrochemical deposition processes that operates based on oxidation and reduction, or redox, reactions¹⁷ within the electrolyte. The difference between the deposition techniques originates from the source of reduction electrons; a chemical reducing agent provides electrons for electroless plating, while an external electrical source provides electrons for electroplating. In recent years, the term electroless deposition has been expanded by some to include reduction originating from any electricity/current free processes including galvanic displacement/immersion plating, or any process where the substrate is catalyzed for plating, in addition to the traditional autocatalytic definition [5]. As it appears here, electroless deposition will refer to autocatalytic deposition with other simultaneous processes specified. The process of

¹⁶ Catalytic surface – a surface which acts as a catalyst that is not consumed by the reaction itself, though the catalyst may form intermediaries within the reaction.

¹⁷ The oxidation and reduction reactions are each partial reactions of the deposition process; deposition cannot occur in a sustained way unless both reactions occur.

electroless deposition is characterized by the oxidation of the reducing agent {R}, Equation 2.15, supplying electrons for the reduction of metal ions {M}, Equation 2.1.



While technically correct, the above stoichiometric equations do not account for all phenomena observed during, or experimental results obtained by, electroless plating. Consequently, a universal mechanism for electroless metal deposition, where each process can be divided into a series of elementary anodic and cathodic reactions, is not feasible given experimentally observed characteristics of the plating reaction [20]. Ostensibly, electroless deposition systems depend on their constituents which are nominally, a metal salt; a reducing agent; a stabilizer for the electrolyte, which stabilizes and/or modifies the pH; a complexing agent for the metal salt; and energy, in the form of heat, for the reaction to occur [20]. Other additives such as brighteners, which provide a smooth surface better able to reflect light, or additives that modify the crystal structure or density of the deposit may be used, but are not essential for electroless deposition [5].

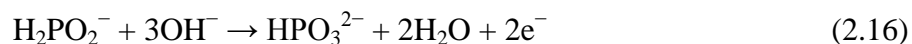
2.3.1 Electrolyte Composition

Keeping with the definition, only metals capable of sustained autocatalytic deposition are candidates for electroless deposition. Autocatalytic metals include nickel {Ni}, cobalt {Co}, copper {Cu}, palladium {Pd}, silver {Ag}, and gold {Au}, and claims have been made regarding chromium {Cr} [21]. Sustained electroless deposition of aluminum {Al} is not possible within aqueous solutions, as Al deposition requires the use of aprotic solvents, solvents unable to donate protons {H⁺} to reagents. Within aprotic solvents, such as ionic liquids which contain only ions, several claims of successful electroless Al deposition do exist [22]. Autocatalytic metals typically have unsatisfied coordinate valences¹⁸ in a direction perpendicular to the interior of the deposit, at the interface with the electrolyte, that allow the adsorption of various electron donor species, such as reducing agents and stabilizers [20]. Metal substrates which possess autocatalytic behaviour may be made less, or 'non'-catalytic if there are species,

¹⁸ Coordinate Valence – Chemical bond between two atoms where one atom supplies an electron pair to form the bond.

such as oxides, which satisfy the coordinate valences at the surface of the metal. Replenishment of the metal salt is achieved by adding either the salt directly into the bath or using an external loop with an anode of the corresponding metal that has higher efficiency than a cathode [21].

Equally important to the autocatalytic metal is the reducing agent, the sustained oxidation of which provides the electrons for sustained reduction. The oxidation of the reducing agent occurs while it is adsorbed onto the surface of the substrate at anodic sites. One of the most ubiquitous reducing agents is the hypophosphite anion $\{\text{H}_2\text{PO}_2^-\}$, the oxidation of which is shown in Equation 2.16.



Whereas oxidation occurs on the anode and deposition on the cathode of an electroplating cell, both the anodic and cathodic reactions occur simultaneously at localized sites on a single catalytic substrate within an electroless plating cell. Though polarization of the solution of the electroplating type does not exist, a dwell time, where the reducing agent is adsorbed onto the surface of a catalyst, does occur before reduction of metal ions takes place. The interspacing of anodic and cathodic sites during electroless plating often results in the inclusion of elements sourced from the reducing agents as a result of the anodic process. These elements are most commonly metalloids such as boron {B}, or non-metals such as phosphorous {P} and sulphur {S}, and their inclusion in the deposit is dependant on the acidity of the electrolyte [23, 24]. While common, and often beneficial, the inclusion of elements from anodic contamination of the deposit does not occur for all system; one such example is the reduction of Cu using formaldehyde-type reducing agents. Oxidation of the reducing agent throughout the electrolyte causes mass reduction of the metal salt within the electrolyte in what is commonly referred to as “plate-out” or “cave-in” of the solution. Prevention of plate-out is achieved by using complexing agents and stabilizers within the electrolyte.

Complexing agents, or ligands, provide the first line of defence against plate-out of electroless deposition solutions and constitute any ion, molecule, or functional group that replace water molecules coordinated to a metal ion, forming what is known as a metal complex [20]. The purposes fulfilled by complexing agents can include: 1) acting as a buffer to prevent the pH of the electrolyte from decreasing; 2) controlling the

concentration of free metal ions in solution; and 3) preventing the precipitation, or allowing better solubility, of metal salts; in addition to affecting the deposition reaction and resultant metal deposit [20]. Aside from a few exceptions, ligands act as Lewis bases¹⁹ donating a pair of electrons to Lewis acids²⁰ forming a single reaction product containing all atoms of all components, known as a Lewis adduct. Complexing agents for electroless nickel plating include any organic acid or its salts as well as the inorganic pyrophosphate anion, which is used exclusively in alkaline electroless Ni solutions, and the ammonium ion, which is usually added to the plating bath for maintaining and/or controlling the pH [20]. Common complexing agents for electroless Ni deposition can be identified by colour; H₂O and succinate {C₃H₄O₄²⁻} complexes provide green solution; citrate {C₆H₅O₇³⁻} complexes provide a teal, or bluish-green, coloured solution; and ammonia {NH₃} complexes result in a blue solution. The reason for the color change is due to effects of the coordinating ligands on electrons in the d orbital of the metal ion when in a complex. The colour change resulting from complex formation along with magnetic properties of complex ions are treated within crystal field theory [25], which is not covered within the context of this work.

Acting as buffers, complexing agents, which similar to reducing agents are electron donors, have a considerable affinity for hydrogen ions {H⁺} resulting in the formation of weak acids in solution [20, 21]. The multiple reactions taking place at the interface also results in the reduction of H⁺ to hydrogen gas {H₂}, Equation 2.17, due to the abundance of free electrons.

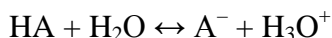


The equilibrium between the complexing agent and its conjugate dissociated products allows for the complexing agent to act as a buffer, resisting limited changes in the acidity, pH, of an electrolyte. Buffers are created by the dissolution of a weak acid with its conjugate base or weak base with its conjugate acid. Specifically, the conjugate base {A⁻} of a weak acid {HA} is the acid less a proton {H⁺} and the conjugate acid {HA⁺} of a weak base {A} is the base plus a proton. The buffering capacity of a complexing agent depends on the ionization constant, K_a for acids and K_b for bases, of

¹⁹ Lewis base - any species that donates a lone electron pair to a Lewis acid; OH⁻ & NH₃

²⁰ Lewis acid - any species that accepts a lone electron pair from a Lewis base; H₃O⁺ & NH₄⁺

the complexing agent which denotes the equilibrium between a chemical and its dissociated products. Keeping with the typical pH scale for the concentration of hydrogen ions $\{H^+\}$, or more specifically hydronium ions²¹ $\{H_3O^+\}$, in solution, the acidic ionization constant²², K_a , Equation 2.18, provides a measure of the acidic equilibrium. As in the case of pH, a scale of acidity defined by taking the negative logarithm of the concentration of H_3O^+ in solution, a pK_a can be similarly defined by doing the same to the K_a , Equation 2.19.



$$K_a = \frac{[A^-][H_3O^+]}{[HA]} \quad (2.18)$$

$$pK_a = -\log K_a \quad (2.19)$$

Complexing agents act as effective buffers within a tolerance of about only ± 1 of the pK_a value, Table 2.3. Polyprotic acids, acids with more than one proton to lose, possess multiple pK_a values and are adequate buffers within that range. Instances where the difference between K_a values is small, less than four orders of magnitude, overlap of the equilibrium reactions becomes greater, increasing the range of the buffer.

Anion	Chemical Reaction	pK_a
Succinate	$H_2C_3H_4O_4 \leftrightarrow HC_3H_4O_4^- + H^+$	4.21
	$HC_3H_4O_4^- \leftrightarrow HC_3H_4O_4^{2-} + H^+$	5.64
Lactate	$HC_3H_5O_3 \leftrightarrow C_3H_5O_3^- + H^+$	3.86
Tartrate ²³ (L+-tartaric acid)	$H_2C_4H_4O_6 \leftrightarrow C_4H_4O_6^- + H^+$	2.98
	$HC_4H_4O_6^- \leftrightarrow C_4H_4O_6^{2-} + H^+$	4.34
Citrate	$H_3C_6H_5O_7 \leftrightarrow H_2C_6H_5O_7^- + H^+$	3.13
	$H_2C_6H_5O_7^- \leftrightarrow HC_6H_5O_7^{2-} + H^+$	4.76
	$HC_6H_5O_7^{2-} \leftrightarrow C_6H_5O_7^{3-} + H^+$	6.40
Ammonia*	$NH_3 + H_2O \leftrightarrow NH_4^+ + OH^-$	9.25
Ethylenediamine*	$N_2C_2H_8 + H_2O \leftrightarrow N_2C_2H_9^+ + OH^-$	9.92
	$N_2C_2H_9^+ + H_2O \leftrightarrow N_2C_2H_{10}^{2+} + OH^-$	6.86

*Reciprocal pK_b used to determine the pK_a , See Equation 2.21.

**L+-tartaric acid

Table 2.3: Chemical dissociation reactions and pK_a for select complexing agents [26, 27]

²¹ H_3O^+ provides a more correct way of expressing the presence of H^+ in solution; both are effectively equivalent $H^+ + H_2O \rightarrow H_3O^+$

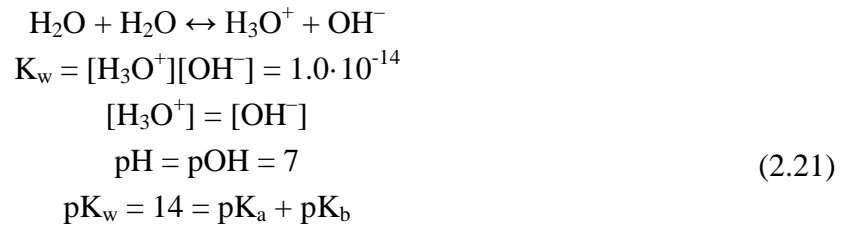
²² K_b is the alkaline ionization constant defined by:
$$K_b = \frac{[HA^+][OH^-]}{[A]}$$

²³ Common source of tartrate as a complexing agent is potassium sodium tartrate tetrahydrate $\{KNaC_4H_4O_6\}$, also known as: L(+)-tartaric acid potassium sodium salt, Rochelle salt, Seignette salt.

The relationship between the pH of a buffer solution and the concentration of weak acid/base and its conjugate base/acid can be determined by means of the Henderson–Hasselbalch equation, Equation 2.20.

$$\text{pH} = \text{pK}_a + \log \frac{[\text{A}^-]}{[\text{HA}]} \quad (2.20)$$

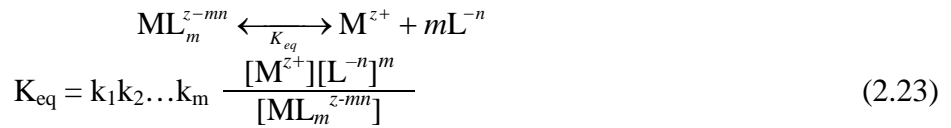
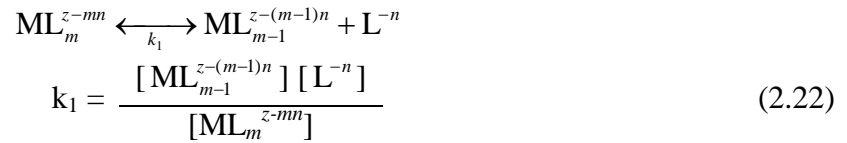
In cases where the ion complexing agent is a weak base, the weak acid, HA, and its conjugate base, A⁻, are replaced by the weak base, A, and its conjugate acid, HA⁺, while the pH and pK_a are replaced by the pK_b and pOH, respectively. The resulting pK_b is then converted to a pK_a using the relationship between pK_a and pK_b as defined by H₂O, which naturally has equal concentrations of acidic protons and alkaline hydroxyls, Equation 2.21.



Ammonium hydroxide {NH₄OH} solutions are efficient buffers as around 30 % exists as NH₃. Complexing agents such as citrate, which are included in solution as dissociated trisodium citrate {Na₃C₆H₅O₇}, form weak acids to their conjugate base by taking up free and excess H⁺ within the solution. The free H⁺ originates from the dissociation of H₂O, while excess H⁺ is created by reactions such as oxidation of the reducing agent that either produces H⁺ directly or consumes OH⁻, Equation 2.16. The use of sodium citrate starts as the triply negatively charged anion buffering best in the range of the first equilibrium from pH 5.4 to 7.4.

Controlling the concentration of free metal ions is essential to maintain control over electroless deposition. Excessive amounts of free metal ions can result in plate-out of the electrolyte, while a scarcity of free metal ions results in lack of plating. Control over the concentration of free metal ions is achieved by complexing agents as chemical reactions with metal ions take place at coordination sites that are weakly bound to coordinated water molecules [20]. At equilibrium, the metal complex dissociates forming a small equilibrium of free metal ions which are used for deposition. Regulation of the free ion concentration, or activity of the solution, is dependent on the complexing

agent. The activity of a free metal ion decreases as the number of ligand molecules bound to the metal ion approaches a maximum; 6 for monodentate²⁴ ligands or 3 bidentate ligands for metals such as Ni [20]. The equilibrium response of the system is consistent with Le Châtelier's principle with the system responding to a change in the equilibrium of the system by attaining a new equilibrium that partially offsets the impact of the change. The overall thermodynamic equilibrium constant, K_{eq} ²⁵, or “instability” constant, for the independent equilibriums of a metal ion {M} with a ligand {L} can be determined for independent equilibriums, the first equilibrium represented by Equation 2.22, or as an overall equilibrium for the total system, Equation 2.23 [20].



The stability constant of the metal complex, the reciprocal of the instability constant, also provides an indication as to the kinetics of the electroless deposition as the plating rate. The deposition rate of a metal is proportional to the rate at which the complex dissociates and provides free ions to the system and is proportional to the stability constant [20]. Larger stability constants indicate a lower rate of complex dissociation and a lower the rate of deposition [20]. In the case of Ni deposition, the Ni-citrate complex is more stable than the Ni-lactate complex and results in a relative drop in Ni plating under similar conditions [20], Table 2.4.

Anion	Chemical Formula		Denticity	pK _{eq}
Succinate	⁻ OOCCH ₂ CH ₂ OO ⁻	C ₃ H ₄ O ₄ ²⁻	monodentate	2.2
Lactate	CH ₃ CH(OH)COO ⁻	C ₃ H ₅ O ₃	bidentate	2.5
Ethylenediamine	H ₂ NCH ₂ CH ₂ NH ₂	N ₂ C ₂ H ₈	bidentate	13.5
Citrate	⁻ OOCCH ₂ (HO)C(COO ⁻)CH ₂ COO ⁻	C ₆ H ₅ O ₇ ³⁻	quadridentate	6.9

Table 2.4: Denticity and equilibrium constants for select complexing agent anions [20]

²⁴ The number of atoms in a single ligand that bind to a central atom in a coordinated complex is known as the denticity of a ligand and is qualified as terms monodentate for a single bond, bidentate for 2 bonds, etc.

²⁵ Equilibrium constants, K_n , are unit-less and the concentration of H₂O is omitted from the reaction as it has unitary activity being a pure liquid in excess of other constituents.

The role of the complexing agent in the control of the acidity and free metal ions in solution may be summarized by considering the involvement of the complexing agent, L, in both the hydrogen ion buffering, Equation 2.24, and metal ion buffering, Equation 2.25, reactions. The combination of expressions for both yields the concentration of the metal ion in a manner analogous to the concentration of hydrogen, or pH, Equation 2.26, [20].

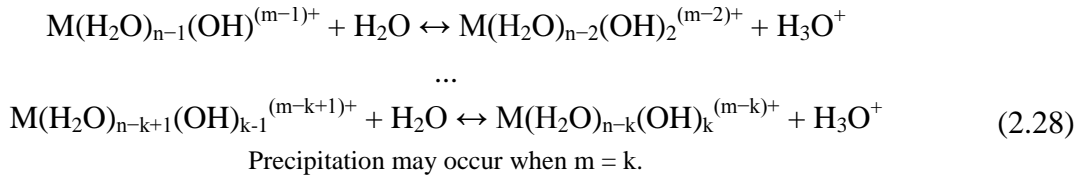
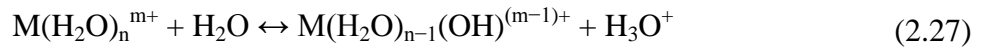
$$\begin{aligned}
 & \text{H}^+ + \text{L}^{-n} \xrightleftharpoons{K_{eq}} \text{HL}^{-(n-1)} \\
 K_{\text{HL}} &= \frac{[\text{HL}^{-(n-1)}]}{[\text{H}^+][\text{L}^{-n}]} \quad (2.24) \\
 [\text{L}^{-n}] &= \left(\frac{1}{K_{\text{HL}}} \right) \frac{[\text{HL}^{-(n-1)}]}{[\text{H}^+]}
 \end{aligned}$$

$$\begin{aligned}
 & \text{M}^{z+} + m\text{L}^{-n} \xrightleftharpoons{K_{eq}} \text{ML}_m^{z-n} \\
 K_{\text{ML}} &= \frac{[\text{ML}_m^{z-n}]}{[\text{M}^{z+}][\text{mL}^{-n}]} \quad (2.25) \\
 \text{p}[\text{M}^{z+}] &= -\log \left(\left(\frac{1}{K_{\text{ML}}} \right) \frac{[\text{ML}_m^{z-n}]}{[\text{L}^{-n}]^m} \right) \\
 \text{p}[\text{M}^{z+}] &= -\log \left(\left(\frac{K_{\text{HL}}^m}{K_{\text{ML}}} \right) \frac{[\text{ML}_m^{z-n}][\text{H}^+]^m}{[\text{HL}^{-(n-1)}]^m} \right) \\
 \text{pM} &= mpK_{\text{HL}} - \text{p}K_{\text{ML}} + mp\text{H} - \log \left(\frac{[\text{ML}_m^{z-n}]}{[\text{HL}^{-(n-1)}]^m} \right) \quad (2.26)
 \end{aligned}$$

Analogous to pH, an increasing value for pM results in a decrease in the concentration of the metal ion in solution and vice versa. Similarly, an increasing pH results in an increasing pM, decreasing amount of free metal ions in solution [20]. While decreasing the amount of free metal ion in solution can aid in preventing the formation of precipitates in solution, hydrolysis of water molecules about a metal ion can result in the formation of precipitates.

The prevention of precipitates, and/or allowing better solubility, of metal salts, is accomplished by the ligand structure of the complexing agents in a manner similar to the control of free metal ions. The specific manner in which the ligand structure prevents precipitation is by the prevention of hydrolysis of coordinated H₂O about a metal atom by replacing coordinated H₂O molecules. The hydrolysis of metal ions within the bulk electrolyte rather than at the catalytic surface for deposition results in decomposition of

the deposition bath. In aqueous solutions, the hydrated metal ions can act as Brønsted acids, proton donors. The formation of a coordinated covalent bond between the metal ion and oxygen atom allows for hydrolysis of the hydrated metal ions when the electron density is drawn towards the metal-oxygen bond and away from the OH bond. The weakening of the bond due to the polarization of the water molecule donates a proton $\{H^+\}$ reducing the charge of the metal complex. The hydrolysis of the aqua-metal, or aquometal²⁶, ion, which contributes to the formation of an acidic environment, Equation 2.27, can result in precipitation of metal complexes, Equation 2.28, which in turn result in decomposition of the electrolyte [20].



Maximum stability against hydrolysis can be achieved by complete coordination of the metal ion; more specifically by means of chelation. Chelation, or the formation of chelates, involves the simultaneous attachment of a polydentate ligand, or chelating agent, to a single central atom at two or more separate coordinate sites forming at least one heterocyclic ring²⁷ [20]. Common chelating ligands for electroless deposition include ethylenediamine $\{N_2C_2H_8\}$, and anions including citrate $\{C_6H_5O_7^{-3}\}$ sourced from trisodium citrate $\{Na_3C_6H_5O_7\}$, and tartrate $\{C_4H_4O_6^{2-}\}$ sourced from potassium sodium tartrate $\{KNaC_4H_4O_6\}$. Though succinate anion $\{C_3H_4O_4^{2-}\}$, generally sourced from sodium succinate $\{Na_2C_3H_4O_4\}$, has two donor atoms per ligand molecule, it is considered monodentate as it is more likely that one end of the ligand molecule will coordinate to another metal ion rather than form a heptagonal, 7-membered, or more chelate ring [20]. Similarly, $C_6H_5O_7^{-3}$, although tetradentate, is assumed to coordinate to the nickel ion with the formation of two chelate rings, a pentagonal and a hexagonal ring, utilizing three of the possible four bonds [20]. Polydentate ligands may not necessarily utilize all possible donor atoms when coordinating to a metal nickel ion due to the ensemble of spatial arrangement/occupation, effective size, and the repulsion between

²⁶ Aquometal ions are metal ions with water as the only ligand, also known as hydrated metal ions.

²⁷ A heterocyclic ring is a chemical ring which contains atoms of at least two different elements.

electron clouds of the atoms, molecules, or group of atoms, known as steric hindrances²⁸ [20]. Complexing agents that do not have a sufficient number of donor atoms to satisfy the coordination number of the metal ion may have the remaining sites occupied by other ligands and/or water molecules [20].

The chelation of an aquometal ion occurs only when the ligand is a much stronger Lewis base than H₂O. Given that H₂O is both a Lewis acid and a Lewis base, as depending on the reaction it can either accept a pair of electrons or donate a pair of electrons, any Lewis base which is either a base itself, such as NH₃ or OH⁻, or a conjugate base of a weak acid, an acid having high pK_a, such as the citrate anion, act as strong chelating agents [20]. For ligands with multiple acidic equilibria, such as citrate, environments equal or more alkaline than the pK_a of maximum dissociation, largest pK_a, ensure the anion acts as a stronger Lewis base by providing the maximum amount of unpaired electrons on the oxygen atoms. The strength of Lewis acidity of a metal ion increases with increasing charge and decreasing radius with the Lewis adduct of strong Lewis acids, such as titanium ion Ti⁴⁺, with strong Lewis bases, such as O²⁻, very resistant to dissolution [20]. The hydrolysis of a metal ion, Equation 2.27, can be viewed as the equilibrium between the hydrated metal ion, a Lewis acid, and the hydroxylated metal ion which is formed by the displacement of the weak Lewis base, H₂O molecule, by the strongly coordinating hydroxyl ion [20].

By preventing precipitation of metal salts, complexing agents can also help make metal salts soluble; a notable example is ethylenediamine {N₂C₂H₈} which complexes Ni within Ni-B deposition baths allowing solubility above pH 13.5. The increase in solubility is a direct result of an increase in the resistance of the ions to hydrolysis. Partial chelation of Ni ions also increases its resistance to hydrolysis, making it possible to keep the nickel ion in solution at a higher pH than would otherwise be possible [20]. The increased solubility is limited by the disassociation of protons from the remaining coordinated water molecules which occurs more frequently as pH increases ultimately resulting in further hydrolysis of the ion [20]. While complexing agents can increase the stability of a deposition bath by controlling metal ion concentration, preventing metal

²⁸ Steric hindrance is the impediment of chemical reactions associated with the size of an atom, molecule, or group of atoms within a molecule resulting from the space taken up by the construct and associated repulsion the electron clouds.

complex precipitation, and buffering the solution; specific chemicals are often added to prevent spontaneous plate-out or precipitation of the electrolyte.

Stabilizers are chemicals added to the deposition bath that prevent homogeneous reactions that trigger the subsequent random decomposition of plating bath [20]. Due to the method of reduction in electroless plating, namely a chemical reducing agent, it is possible for the creation of particles within the electrolyte which result in spontaneous decomposition. Bath decomposition is typically characterized by an increase in the volume of evolved hydrogen gas {H₂} and the appearance of an often finely-divided precipitate throughout the bulk of the solution. In the case of nickel the precipitate is black and consists of nickel particles, nickel phosphide or nickel boride, the latter two in the case of phosphorous and boron containing reducing agents, respectively [20]. The most effective stabilizers can be divided into the four classes: (I) compounds of Group VI elements such as sulphur {S}, selenium {Se} and tellurium {Te}; (II) compounds containing oxygen such as meta-arsenite {AsO₂⁻}, iodate {IO₃⁻}, molybdate {MoO₄²⁻}; (III) heavy metal cations such as tin {Sn²⁺}, lead {Pb²⁺}, mercury {Hg⁺} and Sb³⁺; and (IV) unsaturated organic acids, such as maleic {C₄H₄O₄}, and itaconic {C₅H₆O₄} [20]. Class I or Class II stabilizers can function effectively at concentrations as low as 0.10 ppm²⁹ and can inhibit plating completely beyond 2 ppm; however, at optimum concentration certain Class I stabilizers, such as thiourea {CH₄N₂S}, will increase the rate of deposition substantially over that of a bath without any stabilizer [20]. The concentration range of Class III stabilizers is usually 10⁻⁵ M to 10⁻³ M, whereas Class IV stabilizers are used within the range of 10⁻³ M to 10⁻¹ M [20]. Stabilizers must be targeted to resolve specific issues with an electrolyte taking into account the compatibility and synergy of the stabilizer and other constituents of the electrolyte in order to avoid any adverse loss in catalytic activity. Stabilizers within Ni plating solutions using hypophosphite {H₂PO₂⁻} reducing agent are used for the prevention of localized homogeneous reduction of Ni ions to metal by hydroxyl ions within the bulk solution. In addition to the formation of precipitates within the solution, hydroxyl ions can attach to other contaminant surfaces, including any foreign solid particles at, or near, colloidal dimensions, introduced into the deposition bath by simple displacement reaction or

²⁹ ppm – parts per million, one-millionth of a gram per gram of sample solution, 1/1,000,000 or 0.0001%.

simple particulate contamination [20]. In each case, stabilizers are required to prevent the attachment of hydroxyl ions and hence prevent decomposition.

The stability of an electrolyte can be measured by adding 1 mL to 2 mL of a 100 ppm palladium chloride {PdCl₂} solution to a sample of the warm electrolyte and measuring the time before precipitation begins [20]. A plating bath is considered stable if the time required for precipitate to form is in excess of 60 seconds [20]. Finally, in addition to chemical stabilizers, techniques such as pure oxygen agitation of electroless Ni solutions have been reported to significantly enhance the stability of the plating bath compared to no agitation or argon agitation [20]. Pure oxygen agitation has been shown to shift the mixed (deposition) potential from -625 mV vs. SCE to the nobler potential of -550 mV vs. SCE within a stabilizer-free electroless Ni deposition bath [20].

The final essential component for electroless deposition, along with the metal salt and reducing agent, is energy. Energy is supplied to the electroless deposition system by means of heat, which is measured by the temperature of the deposition bath. The amount of heat added to the reaction increases the kinetics of the redox reaction thereby increasing the deposition rate. The deposition rate for electroless deposition is typically exponentially related to increased heat and hence increasing temperature by a rate constant, K_d, Equation 2.29 [20]. While some deposition baths have efficient deposition rate at room temperature, other requires temperatures up to 100 °C, which are still considered 'near' room temperature.

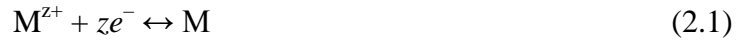
$$K_d = A \exp\left(-\frac{E_a}{RT}\right) \quad (2.29)$$

where: K_d = Deposition rate constant
 A = Frequency factor
 E_a = Activation energy of the reaction
 R = Gas constant
 T = Temperature

2.3.2 Theoretical Considerations

As stated previously, electroless deposition can be considered as the combined result of the anodic and cathodic partial reactions. The theoretical framework for electroless deposition is known as mixed-potential theory which predicts electroless deposition processes from the polarization curves of the partial anodic and cathodic

processes which are obtained using voltammetry. In order that the overall electroless deposition reaction may proceed, the equilibrium rest, or reversible, potential of the reducing agent, $E_{\text{eq,Red}}$, Equation 2.15, must be more negative than that of the metal electrode, $E_{\text{eq,M}}$, Equation 2.16, so that the reducing agent can function as an electron donor and the metal as an electron acceptor [5].



Deposition occurs when a catalytic surface is introduced into the electrolyte containing the metal ions and reducing agent. Each of the partial reactions strives to establish its own equilibrium potential resulting in a compromised potential called the steady-state mixed potential, or deposition potential, E_{mp} . The compromise potential is established by cathodic depression of $E_{\text{eq,M}}$, and anodic raising of $E_{\text{eq,Red}}$ [21]. Additionally, the selection of reducing agent for electroless deposition depends on the acidity of the deposition bath as well as the reduction potential of metal complexes within the deposition bath from which the metal is to be deposited. Reducing agents are effective only within specific ranges of acidity, or pH, with the oxidation of each having different associated standard electrode potential, Table 2.5.

Reducing agent		pH range	Oxidation Potential, E° (V)
Name	Formula		
Sodium Hypophosphite Hydrate	NaH_2PO_2	4-6	0.499
	$\cdot \text{H}_2\text{O}$	7-10	1.57
Sodium Borohydride	NaBH_4	12-14	1.24
Dimethylamine Borane (DMAB)	$(\text{CH}_3)_2\text{NHBH}_3$	6-10	–
Hydrazine	H_2NNH_2	8-11	1.16

Table 2.5: Effective pH range and oxidation potential of some Ni reducing agents [20].

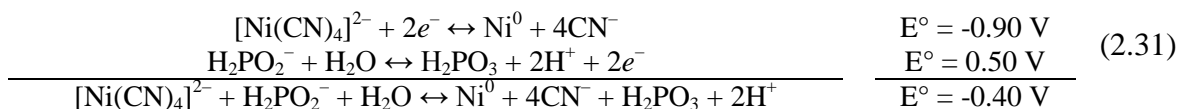
Electrochemical considerations akin to those for displacement deposition, Section 2.2.2, can provide the spontaneity of the electroless deposition reaction, where a reaction is spontaneous where $E^\circ > 0$. Within the language of thermodynamics, the spontaneity of the deposition is indicated by the change in Gibbs free energy³⁰ of a system, Equation 2.30, which is proportional to the standard electrode potential of the deposition reaction.

³⁰ Free energy – amount of work that a thermodynamic system can perform

$$\Delta G^\circ = -nFE^\circ \quad (2.30)$$

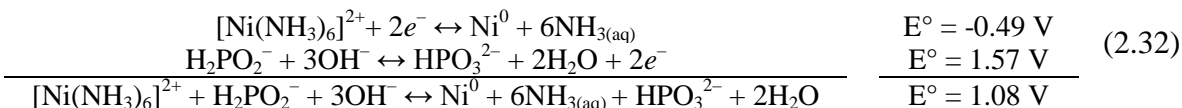
where: ΔG° = Change in standard free energy
 n = number of electrons transferred in the reaction
 F = Faraday constant, $96\,485\text{ C}\cdot\text{mol}^{-1}$, or $23.061\text{ kcal}\cdot\text{V}^{-1}\cdot\text{g}_{\text{eq}}^{-1}$
 E° = Standard electrode potential of the reaction

The thermodynamic formalism indicates a spontaneous reaction, here electroless deposition, takes place when $\Delta G^\circ < 0$, or $E^\circ > 0$, and no deposition occurs when $\Delta G^\circ > 0$, or $E^\circ < 0$. The thermodynamic formalism is most useful in the determination of whether a metal can be reduced by a metal complex by a specific reducing agent. Comparing the reduction of Ni by a hypophosphite $\{\text{H}_2\text{PO}_2^-\}$ reducing agent from a Ni-tetracyanide $\{[\text{Ni}(\text{CN})_4]^{2-}\}$ complex, Equation 2.31, with the reduction of Ni from a Ni-hexamine $\{[\text{Ni}(\text{NH}_3)_6]^{2+}\}$ complex using the same reducing agent, Equation 2.32, demonstrates the interplay between reducing agent and metal complex [20].



$$\Delta G^\circ = -nFE^\circ = -(2)(23601\text{ cal})(-0.40\text{ V}) = 18.88\text{ Kcal} > 0$$

$E^\circ < 0$, $\Delta G^\circ > 0$, No Reaction Occurs



$$\Delta G^\circ = -nFE^\circ = -(2)(23601\text{ cal})(1.08\text{ V}) = -50.978\text{ Kcal} < 0$$

$E^\circ > 0$, $\Delta G^\circ < 0$, Reaction Occurs

The measure of the potential of each half-reaction is known as mixed potential theory and serves as an interpretation for the electroless deposition of metals. Mixed-potential theory, originally developed by Wagner and Traud for the purpose of interpreting corrosion processes, was first applied to electroless deposition, specifically the electroless deposition of Cu, by M. Paunovic and M. Saito [28]. The application of mixed potential theory to a system is most easily achieved using an Evans, Figure 2.9, or Wagner-Traud, Figure 2.10, diagram plotting the current–potential functions, for the individual cathodic and anodic processes [28]. Both diagrams effectively demonstrate the potential at which electroless deposition occurs and are useful in determining the deposition rate by means of the deposition current.

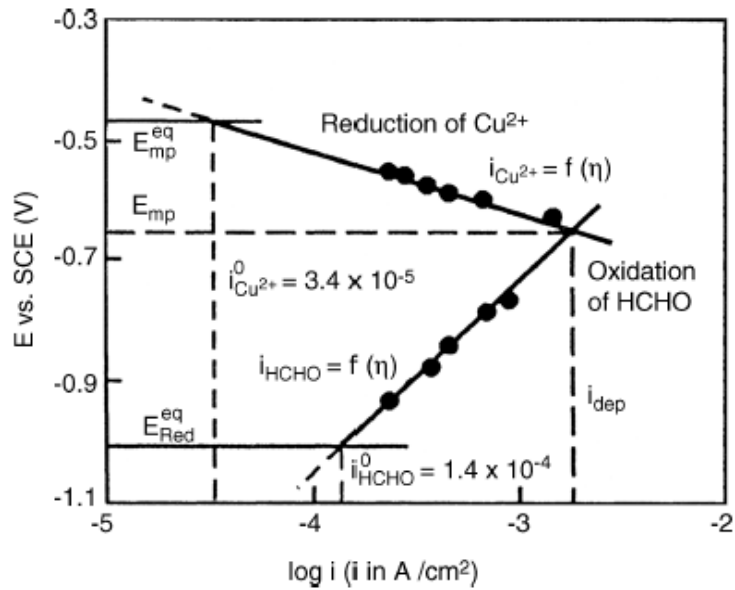


Figure 2.9: Evans type mixed potential diagram for the reduction of Cu^{2+} ions, and for oxidation of formaldehyde reducing agent [29].³¹ [Figure reproduced from M. Paunovic (1968) [29] courtesy of the National Association for Surface Finishing]

The more commonly used Evans diagram plots the potential against the current and the intersection of the anodic and cathodic polarization curves indicating deposition potential and deposition current of the system at the point where the curves intersect. Specifically, point at which the two curves intersect provides the rate of electroless deposition in terms of mA/cm^2 as the electrons provided by the oxidation of the reducing agent are consumed by the reduction of the metal ions.

The Wagner-Traud diagram plots the current density of each reaction against the potential. The current–potential curve for the reduction of the metal ions is recorded from the rest potential, $E_{\text{eq},\text{M}}$, which is located at the point at which the current is at zero. Similarly, a current potential curve is also taken for the oxidation of the reducing agent, the rest potential of which, $E_{\text{eq},\text{Red}}$ is located along the line of zero current. The point at which the sum of both curves is equal to zero, $i_a = i_c$, provides the deposition potential known as the steady-state mixed potential, E_{mp} . The summation of both curves produces a total current, i_{total} , which indicates E_{mp} at the point it crosses the x-axis.

³¹ The 25 °C solutions were used at pH = 12.50. The solution to obtain the Tafel line for the reduction of Cu^{2+} ions was 0.1 M CuSO_4 and 0.175 M ethylene-diamine-tetra-acetic acid (EDTA); the oxidation of formaldehyde was obtained from 0.05 M HCHO and 0.075 M EDTA.
Note: $E_{\text{eq}}(\text{Cu}/\text{Cu}^{2+}) = 0.47 \text{ V vs. SCE}$, $E_{\text{eq}}(\text{HCHO}) = 1.0 \text{ V vs. SCE}$.

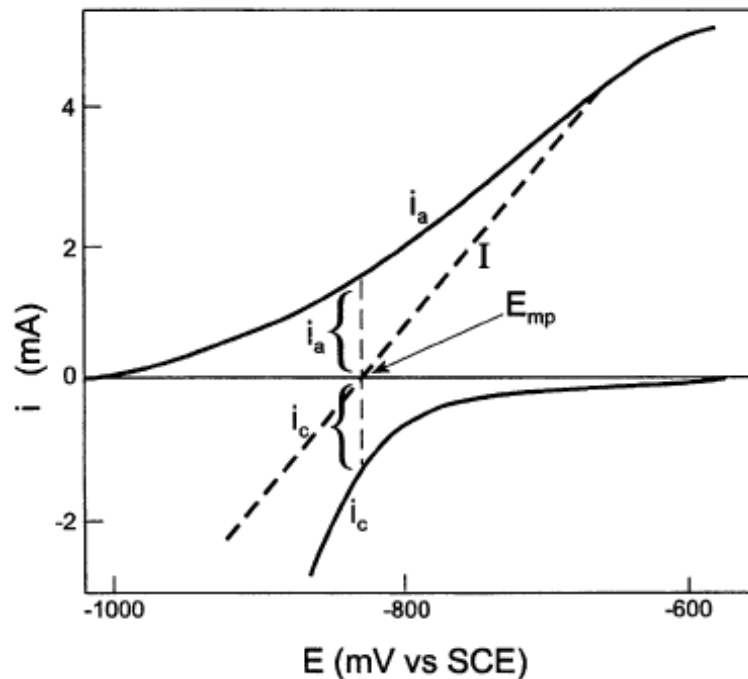


Figure 2.10: Wagner–Traud type mixed potential diagram for electroless Ni(B) deposition: $E_{mp} = 840$ mV versus SCE, electrode area 0.68 cm^2 . Features of the diagram include the component current curves for the overall reaction, i_a and i_c , as well as the resulting current total, i_{total} , for the electroless system [30].

[Figure reproduced from M. Paunovic (1983) [30] courtesy of the National Association for Surface Finishing]

Measuring the polarization curves for the half-reactions is achieved by using two symmetric solutions matching the composition of the deposition bath with the cathodic solution containing no reducing agent and the anodic solution containing no metal ions. Obtaining the accurate polarization curves for mixed potential theory requires the addition of additives to the solutions used for testing the cathodic and anodic processes in order to determine the influence on the deposition potential. This technique of graphical analysis is also used to determine the corrosion of a material within a saline environment. In the case of corrosion, the intersection of the two polarization curves provides the corrosion potential and current.

2.3.3 Electroless Alloys & Composites

As in the case of electroplating, the deposition of alloys by means of electroless deposition requires the rapprochement of the deposition potentials of individual metals.

The electroless deposition of alloys³² provides a practical and effective means by which to increase the number of applications for which electroless deposits are suitable. Deposition of alloys involves several partial reactions, both cathodic deposition of the respective alloy components and anodic oxidation of the reducing agent, which may not be independent from one another [31]. The addition of a second metal, N, for cathodic alloy deposition shifts the natural deposition potential, E_M , of the constituent metal, M, in the M-N metal alloy, which itself is nobler than the oxidation potential of the reducing agent, to a nobler potential, E_M^* , relative to E_M , by virtue of the negative Gibbs energy of the alloy formation, ΔG_M , Equation 2.33 [31].

$$\Delta E_M^* = E_M^* - E_M = \frac{-\Delta G_M}{nF} > 0 \quad (2.33)$$

where: ΔE_M^* = Shift in the potential energy
 E_M^* = Deposition potential of the constituent metal, M
 E_M = Normal deposition potential of the metal, M
 ΔG_M = Gibbs energy of the alloy formation
 n = Number of electrons in the reaction
 F = Faraday constant

The potential shift ΔE_M is typically of the order of 10^{-2} V for solid–solution alloys, but can sometimes reach up to 1 V in case of compound, or intermetallic, alloys. The potential shift allows for the co-deposition of a metal, such as zinc {Zn}, which cannot be electrolessly deposited otherwise as a pure metal [31]. Another difference between alloy deposition and normal electroless deposition is the requirement of the metal having catalytic activity for the anodic oxidation of the reducing agent depends on the composition of the depositing alloy rather than the singular metal [31]. Increasing the content of non-catalytic metals in the alloy can reduce the deposition rate by inhibiting the catalytic properties needed of the surface for ongoing deposition. Both the shift in potential energy and catalytic activity resulting from the presence of the alloying metal can result in lower deposition rates as in the case of Ni-Zn-P and Ni-Fe-B alloys [31]. Commonly deposited alloying metals include, iron {Fe}, rhenium {Re}, molybdenum {Mo}, tungsten {W}, zinc {Zn}, tin {Sn}, and copper {Cu} for Ni-P; W, and Fe for Ni-B; Ni, Fe, Re, W, Zn, and silver {Ag} for Co-P and Co-B [31]. Other common electrolessly deposited alloys include alloys of gold {Au}, such as Au-Cu or Au-Ag, and

³² Strictly speaking, most electroless deposits are alloyed and hence the electroless alloy deposition refers to the cathodic deposition of an alloying element and not the anodic inclusion.

alloys of Cu, such as Cu-selenium {Se} [31]. Other alloys such as zinc-arsenic {Zn-As}, silver-tungsten {Ag-W}, indium-antimony {In-Sb} and iron-tin {Fe-Sn} can also be produced using electroless deposition [31].

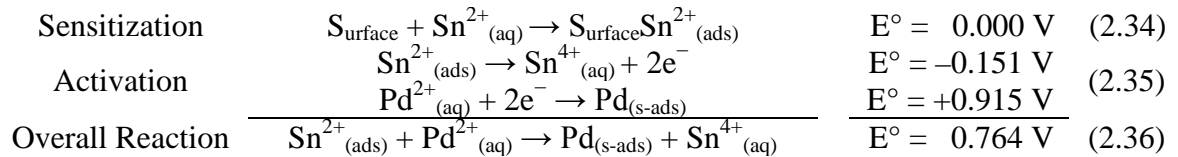
In addition to alloying, as in the case of electroplating, the co-deposition of electrically inert materials, such as carbon{C}, silicon carbide {SiC}, tungsten carbide {WC}, or diamond particles, is an avenue for increasing the wear resistance of electrolessly deposited films. Rather than slowing the deposition rate, as is done for electroplating, successful electroless co-deposition is dependent on various factors including the catalytic inertness and charge of the particle along with electroless bath composition, bath reactivity, compatibility of the particles with the metallic matrix, plating rate, and particle size distribution [32]. Electroless co-deposition of such inert particles often requires agitation and proper complexing agents within the deposition bath to prevent aggregation of the introduced particulate or plate-out of the deposition bath. The resulting wear resistance of the deposited film is related to both particle size and volume percent (loading) of the co-deposited particulate matter in the deposited matrix. Specifically increasing particle size yields an optimum point, around 9 μm , where the wear resistance of the composite is maximized; beyond which there does not appear to be any discernable gain in wear resistance [32]. An example of increased wear resistance is the inclusion of natural diamond particles in the range of 9 μm decreases the wear rate, measured in microns per hour ($\mu\text{m}\cdot\text{h}^{-1}$), of a Ni-B surface by over 2000 fold [32]. Similarly, the inclusion of 8 μm alumina {Al₂O₃} particles reduced the wear rate by approximately 200 fold, while 10 μm silicon carbide {SiC} particles decreased the wear rate by approximately 80 fold [32].

2.3.4 Advantages & Applications – Selective Deposition

The principle advantages of electroless deposition over other metal deposition techniques are twofold; first, deposition is independent of line of sight, such as electric field lines for electroplating; and second, unlike electroplating, deposition is possible on non-conductive surfaces. Freedom from line of sight deposition, possible with electroless deposition, stems from the simultaneity of the anodic and cathodic reactions allowing deposition to occur wherever the substrate and electrolyte are in contact, including

recessed areas. The one caveat to the ability to deposit metal within recessed areas is that trapped H₂ gas produced during the deposition process can create pockets where deposition does not occur. The ability for electroless deposition to deposit on non-conductive surfaces requires the surface be catalytic in nature. Given that most plastics and glasses are not catalytic, surfaces must be catalyzed to allow electroless deposition.

While many methods exist to catalyze non-catalytic surface, including photochemical activation³³, displacement deposition activation,³⁴ and thermal decomposition of metal oxides³⁵, the simplest and most versatile is electrochemical activation [28]. The most common electrochemical activation technique is a two stepped sensitization/activation pre-treatment using aqueous baths containing ions of tin(II) {Sn²⁺}, typically from tin(II) chloride {SnCl₂}, and palladium(II) {Pd²⁺}, typically from palladium(II) chloride {PdCl₂} [28, 33]. The fundamental process for the electrochemical activation begins with sensitization of the surface by the adsorption of Sn²⁺ ions onto the surface of the prospective substrate, Equation 2.34. After sensitization, the substrate is placed within a bath containing Pd²⁺ ions which result in the oxidation of the Sn²⁺ ions and reduction of the Pd²⁺ ions to metallic Pd on the substrate surface, Equation 2.35.



The overall reaction, Equation 2.36, provides the fundamental and simplified redox model for electrochemical activation utilizing SnCl₂ and PdCl₂ solutions. While the actual process does not produce metal Pd but rather a Sn-Pd complex [34], the activation is due to the presence of Pd. A more advanced model requires consideration of

³³ Photochemical activation includes any photon activation process, that utilizes energy from photons ($E = h\nu$) to generate catalytic sites for electroless deposition; this includes all processes that use photons to produce or deactivate the reducing agent as well as those processes where the catalytic metallic nuclei are formed by a subsequent electrochemical reaction. An example of photochemical activation is formation of catalytic palladium [Pd] from Pd acetate [Pd₂C₂H₃O₂]; PdAc → Pd +Ox, where Ox is the oxidation product of acetate ion [Ac] [28, 35].

³⁴ Silicon {Si} can be made catalytic for electroless deposition of Ni by replacing the surface Si atoms with Ni atoms; 2Ni²⁺ + Si → 2Ni + Si⁴⁺. A similar reaction also occurs with aluminum {Al} and palladium {Pd}; 3Pd²⁺ + 2Al → 3Pd + 2Al³⁺ [28].

³⁵ The surface of alumina {Al₂O₃}, may be activated by employing laser or ultraviolet irradiation to decompose Al₂O₃, generating catalytic aluminum particles for electroless Cu deposition [28].

the ligand behaviour of the chloride ion $\{Cl^-\}$, as well as the presence of mono-, di-, tri-, and tetra-chlorostannate(II) species; $\{SnCl^+\}$, $\{SnCl_2\}$, $\{SnCl_3^-\}$, and $\{SnCl_4^{2-}\}$, respectively [28]. Additional considerations are that the presence of Sn^{4+} cause by the oxidation of Sn^{2+} by atmospheric oxygen and subsequent colloid formation have been shown to improve deposition [36], and that deposition has been achieved on surfaces activated using a Sn^{2+} sensitizer after it has aged for 3 weeks and presumably exclusively contained Sn^{4+} [36] as well as Sn^{4+} sensitizer from tin(IV) chloride $\{SnCl_4\}$ [37].

The reduced Pd complexes on the surface of the substrate provide catalytic nucleation sites upon which deposition will occur. In the early thin film stages, deposition on a Pd activated surface is characterized by nucleation, growth and coalescence of three-dimensional crystallites [28], Figure 2.5c. Coalescence of the growing film and the formation of a continuous thin film occur within the thin film stage, which is characterized by the vertical and lateral growth of three-dimensional crystallites [28]. The thickness of the deposit required for the production of a continuous thin film is dependent on, among other factors, the density of nucleation sites; increased density results in a thinner film as coalescence occurs earlier. Once the film becomes continuous, the width of preferentially oriented grains becomes constant and bulk stage deposition, a deposition up to a thickness typically between 3 μm to 25 μm , takes place [28]. In most cases the bulk stage proceeds with: (1) preferential growth of favorably oriented grains, (2) restriction (inhibition) of vertical growth of unfavorably oriented grains³⁶, (3) lateral joining of preferentially growing grains, (4) cessation of growth of initial grains, and (5) nucleation of new layers of grains [28]. It should be noted that while the Sn/Pd electrochemical activation is effective for many surfaces, certain deposition baths require continuous metallic surfaces, or specific metallic surfaces for electroless plating to occur.

An additional benefit to the electrochemical activation of non-catalytic materials is that the process lends itself quite well to selective deposition by means of selective activation/deactivation of catalytic sites. This property of selective deposition by electrochemical activation for electroless deposition exists in addition to selective electroplating techniques, such as using photoresists, which are also viable so long as the

³⁶ While the nucleation about the Pd nuclei results in columnar deposit crystallization structure for electroless Ni-P, there is no adequate theory for lamellar growth aside from periodic fluctuations in the P content of in electroless Ni-P as a possible cause [28].

surface is catalytic. Selective activation/deactivation for the purpose of electroless deposition, like photolithography, is most easily carried out using an optical mask to enable selective photo-activation/deactivation of the surface. Additionally, photochemical activation and thermal decomposition of metal oxides, allow for selective activation and deposition by using the properties of the materials; while all techniques, including activation using displacement deposition, are easily controlled using photoresist technologies [38].

In the case of electrochemical activation using Sn/Pd pre-treatment, selective deposition can be achieved either by activating, or deactivating, the adsorbed elements at different points of the process with the application of ultraviolet (UV) light to the dried surface [39]. Specifically for Cu, Ni, or Co metalizing baths applied to activated glass substrates, it has been shown that no image is produced when the UV light is applied after the Sn sensitization; a positive image of the photomask is obtained when UV light is applied after either the post-sensitization rinse [40] or immediately after Pd activation [41]; and a negative image of the photomask is obtained when UV light is applied after the post-activation rinse [36]. The mechanism for post-sensitization deactivation of the adsorbed catalysts is attributed to the photo-oxidation of Sn^{2+} to Sn^{4+} [40], whereas the reaction producing positive and negative images post-activation are not explained by the simplified redox reaction for activation and require the consideration of the Sn-Pd complex. It should be noted that the Sn-Pd complex contains a non-reproducible amount of Cl within its structure after the activation bath, which is reduced to approximately one Cl atom per Sn atom and is likely related to the production of negative images [34]. Additional considerations for the selective deposition by means of selective activation of electrochemically activated surfaces are: the composition of the sensitization, activation, and metalizing baths; the duration of the post-treatment rinse baths; as well as the time between sensitization and activation, and between activation and metallization steps [36]. For instance, it has been shown that using a Sn^{4+} sensitizer, derived from dissolved SnCl_4 and aged for between 24 hours and 48 hours at 21 °C, allows deposition of Ni-P, and disallows deposition of Cu, independent of UV exposure when applied immediately after the sensitizer or post-sensitizer rinse [36]. When UV is applied to the surface after the activation or the post-activation rinse, no deposit occurs for Ni-P at sites exposed to the

UV light, while deposition of Cu occurs only where the surface has been exposed to UV light [36]. From an application perspective, the negative images have a much higher contrast [37], and are more useful for the electroless deposition such as for interconnects on computer chips [38].

While electrolessly deposited coatings are limited by the need for autocatalytic metals for successful deposition, coatings produced by electroless deposition tend to have benefits over similar coatings produced by methods such as electroplating and vacuum deposition. Further details and discussions of the superior mechanical, barrier, and magnetic properties of certain electroless coatings are contained throughout the following section of this chapter.

2.4 Single and Multi-layered Thin Film Deposit Properties

The variety of applications in which metallic thin films are utilized necessitates physical and mechanical properties that suit the operating condition of the coating. Some of the more commonly sought out and relevant properties include: the modulus of elasticity; the yield, tensile, and fatigue strengths; ductility; hardness; magnetic properties; as well as the corrosion, wear, and scratch resistance of coatings. Unlike the properties of a bulk alloy or metal, the properties of metal thin films have the additional parameter of layer thickness plays a significant role in controlling the behaviour of thin films. The behaviour of thicker alloy or single metal deposits are relatively straightforward in that their properties and behaviour approach that of the bulk metal or alloy; conversely, multi-layered metallic thin films have a number of unique properties including variable hardness and magnetic properties depending on layer thickness. The properties of all deposits, including multi-layers, depend on the ongoing coherency and stability of the properties of the coating with time. While coating properties vary based on the application and need, adequate adhesion of coatings is a largely universal requirement for all applied coatings, aside from electroforming applications. The maintenance of good adhesion is essential and adhesion failure at the interface may occur due to diffusion between the deposited film and the substrate, or result from stresses and fractures stemming from a brittle deposit.

2.4.1 Diffusion & Deposit Brittleness

Diffusion is a thermodynamically irreversible self-driven process that drives different atoms or molecules to a state of equilibrium. In the case of thin films, diffusion is a temperature dependent process analogous to the diffusion of gasses. It is well known that for a system of two different gasses initially separated by a partition, the removal of the partition will result in diffusion which drives the system to equilibrium, maximum-entropy state of a system. Likewise, for thin films, an increase in temperature weakens the ‘partition’ between the metal reservoirs thin films encouraging the elimination of concentration gradients between the thin films. The flux, or flow, of particles between the layers, J , known as Fick’s First Law of Diffusion, depends on the diffusion constant/coefficient, D , which has an exponential dependence on temperature, and the gradient of the concentration of the diffusing layer, C , Equation 2.37 [42]. The change in concentration as a function of time, Fick’s Second Law of Diffusion, predicts how diffusion causes the concentration to change as a function of time, Equation 2.38 [42].

$$J = -DVC = -D\left(\frac{\partial C}{\partial x_i}\right), \quad i = 1, 2, 3 \quad (2.37)$$

$$\frac{\partial C}{\partial t} = \frac{\partial}{\partial x}\left(D\frac{\partial C}{\partial x}\right) \quad (2.38)$$

A practical example of diffusion³⁷ in thin films is the gold plating of electronic contacts to prevent corrosion. The copper upon which the gold is typically deposited can diffuse through the gold during thermal processing, ultimately oxidizing on the surface and resulting in oxidation of the copper. The rate of diffusion of copper through the gold is of the order of one month for a 3 μm thick gold deposit at 300 °C and four to five days for a 30 μm thick gold deposit at 500 °C [5]. Despite the negative aspects of diffusion, for certain deposits and applications diffusion of metal thin films is very desirable. Diffusion is beneficial in the formation of thin film alloys by depositing alternate layers, or simple bi-layer, of different metals and heating the deposit to promote mutual diffusion [5]. The deposition may take place within a single deposition bath, as in the case of most

³⁷ In addition to the diffusion of metals, both of Fick’s Diffusion Laws provide a means of determining the impact of the deposition current on pH decreases during electroplating at the electrode–solution interface. Control of pH is essential to ensure limited non-magnetic and insoluble hydroxide inclusions permalloy, CoNiFe, and CoFe alloys for magnetic recording and microelectronic technologies [1].

multi-layers, or using two different baths in the case of a bi-layer deposit. Deposition of brass, a Zn-Cu alloy, using this method obviates direct brass deposition via a cyanide process [5]. This technique can also be used in the creation of an 80 % Ni – 20 % Cr alloy. Alternating layers of 19 µm-thick Ni and 6 µm-thick Cr followed by subsequent heating to 1000 °C for 4–5 hours produces completely diffused alloys of high quality in terms of corrosion properties [5].

The reason for diffusion occurring preferentially at elevated temperatures is that for diffusion to take place the atom or ion must overcome a potential energy barrier from neighbouring atoms. The probability of diffusion occurring may be calculated as based from a Boltzmann-type exponential, $\exp(-E/kT)$, taking into account the height of the energy barrier, E , the absolute temperature, T , and the characteristic atomic vibrational frequency, f , which provides the unit time of the diffusion of an atom and is of the order of 10^{14} Hz, Equation 2.39.

$$p \approx f \exp(-E/kT) \quad (2.39)$$

where:

- p = Probability the atom will pass the potential energy barrier
- f = Characteristic atomic vibrational frequency
- E = Energy of the potential barrier
- k = Boltzmann's constant $1.38 \times 10^{-23} \text{ m}^2 \cdot \text{kg} \cdot \text{s}^{-2} \cdot \text{K}^{-1}$
- T = Temperature, in Kelvin

To maintain the separation of differing layers, a diffusion barrier layer is often applied. A diffusion barrier is any layer, which due to crystallographic properties such as grain size or preferred orientation, prevents diffusion from taking place. One example of a diffusion barrier is a nickel {Ni} alloy, such as electroless nickel phosphorus {Ni-P}, layer on copper to block the diffusion of Cu into, and ultimately through, Au [5]. Layer thicknesses for Ni-P less than 1 µm provide an effective diffusion barrier; with the effectiveness increasing with layer thickness. A comparison between Ni and Co diffusion barriers produced by electroless, electro-, and evaporation deposition shows that only electrolessly deposited metals and alloys, at a thickness of 1000 µm, have barrier properties for Cu diffusion [28]. Electrolessly deposited Ni has been used as a barrier layer between Au and Cu in a tri-layer configuration, Cu/Ni/Au, for electronic connectors and solder interconnections, while both Co and Ni, as well as Ni-Co alloys, have been used as a barrier metals for diffusion barriers between a Cu conductor and an insulator [28]. Though electroless Ni-P provides superior barrier to Au than vacuum deposited Ni,

thereby preventing contamination of a substrate by an Au contact, greater diffusion of Ni into Au can occur from Ni-P than vacuum deposited Ni [43].

Diffusion barriers are also useful to prevent the formation of brittle layers, a result of alloying, or voids from preferred diffusion of one layer into another, known as Kirkendall void formation. Brittle layers result when the materials in contact have similar diffusion coefficients and the diffusion occurs by exchange mechanism. The formation of Kirkendall voids occurs when the diffusion coefficients of layers differ and one material preferentially diffuses into the other resulting in vacancies in the material with higher diffusion coefficient. Some examples of metal thin film pairs that lead to Kirkendall void formation include aluminum-gold {Al-Au}, platinum-copper {Pt-Cu}, and Cu-Au [5]. The formation of voids, such as in the case of Pt deposited on Cu, can be averted by making the appropriate selection of metal coating. The application of electrodeposited Ni rather than Pt is free of Kirkendall voids even if the surface is heated to as high as 600 °C for more than 10 hours [5]. Ultimately both scenarios of diffusion can lead to failure, loss of adhesion, of the coating.

A similar concern to diffusion, also resulting in the formation of a brittle deposit, is the presence of a hydrogen impurity, as solute, within metallic thin films. Hydrogen is co-deposited with most metals and is readily adsorbed during deposition due to its low atomic weight [5]. The source of the hydrogen incorporated into coatings varies and can be traced back to cleaning procedures, such as electro-cleaning where the cathode is cleaned by hydrogen evolution within an alkaline bath, or to chemical reactions during the plating process, including the reduction of hydrogen ions [5]. Regardless of its origin, the presence of hydrogen may result in embrittlement of the thin films leading to various fracture phenomena and substantial reduction in film ductility³⁸. No consensus exists on the mechanism of hydrogen embrittlement as it represents a number of fracture phenomena associated with the presence of hydrogen, though for steel it is posited, at least in part, that absorbed hydrogen interferes with the normal flow or slip of the lattice planes under stress [5]. The formation of voids between differing metal layers, film-film or film-substrate, can aggravate the phenomena of hydrogen embrittlement as molecular hydrogen {H₂} may accumulate within those regions and ultimately lead to adhesive

³⁸ Ductility - the ability of the coating to deform under tensile stress.

and/or mechanical failure of the coating. The inclusion of gases within deposits is not a phenomenon restricted to electroplating alone, hydrogen embrittlement is a concern in electroless deposition as both ionic and molecular hydrogen are present due to the deposition mechanism. Additionally, the inclusion of gasses within physical vapour-deposited and sputter-deposited films can increase film stress and raise annealing³⁹ temperatures; electron-beam-evaporated films are also subject to similar effects [5]. Both diffusion and embrittlement effects are of concern within any deposit; however, the aggregation of the effects is of special concern deposits composed of multiple layers.

2.4.2 Multi-Layers

As introduced in section 2.2.3, modern electroplated multi-layers are deposited from a single electrolyte by periodically alternating the deposition potential to selectively deposit two metals differing in nobility. The nobility of a metal, or degree to which the metal resists oxidation, giving up an electron, is measured by the standard electrode potential, E° , of the half-reactions of a metal in a solution of its ion. Metals of similar nobility, and hence similar E° , require similar potentials for reduction and are not suitable for the deposition of compositionally discrete multi-layers.

For the successful deposition of multi-layers, as outlined by Yahalom and Zadok [44] for the deposition of Cu-Ni multi-layers, two metals are chosen with different nobility with metal A, Cu, being nobler than metal B, Ni, or Co. Additionally, the pair of metals deposited must resist diffusion in order for the layers to remain distinct. The deposition of electroplated multi-layered structures from a single solution is limited by the E° of the metal pair, which must be distinct in order to avoid co-deposition and alloying. To enable the distinct layers traces of metal A ions are introduced into a concentrated solution of metal B. At sufficiently low, negative, polarization potential, the rate of reduction of metal B is high and the rate of reduction of metal A is slow and controlled by diffusion [5]. At a considerably less negative polarization potential only metal A is reduced. Deposition of the sequential layers occurs by periodically switching the potential between the two prescribed values for the potential. The resulting deposit is a modulated structure composed of pure A layers and layers of B with traces of metal A

³⁹Annealing - heat treatment for the purpose of increasing ductility.

[5]. As in the case of electroplating with an inert anode, the metal salts must be replenished, especially that of the more noble metal A which appears with significantly lesser concentration. The deposition of multi-layers can be carried out either under galvanostatic or potentiostatic conditions. For convenience, deposition of multi-layered films as presented here will be under potentiostatic conditions. Under potentiostatic conditions the thickness of each layer is controlled by the duration of the periodic potential applied, which in turn corresponds to a given current density applied over the same duration. A common technique to assure proper layer formation during multi-layer deposition is a brief, or pulsed, reverse, or zero, potential to help transition between the depositions of each layer by resetting the polarization of ions within the solution. The application of a reverse potential may also be used to strip a small amount of deposited material from the surface of the electrode.

Alternatives to electrodeposition from a single electrolyte for multi-layered coatings include vacuum deposition techniques as well as electro-, or electroless, plating from a dual bath system. Both vacuum and dual bath methods provide a means of depositing modulated layers of similar metals, though complications of oxidation can arise from a dual bath system. Vacuum deposition techniques typically provide the most cost effective means of producing pure, compositionally modulated, metal layers of similar metals; however, vacuum deposition is a more costly process than electroplating alternatives which are limited by trace elements and restrictions of metal nobility. Dual bath systems are frequently used for the deposition of multi-layers, including Cu-Ni multi-layers [45-47], but do not typically have the same control, less than 10 nm, over layer thickness as single electrolyte systems [48]. Multi-layer deposition is widely used in the electronics and semiconductor industries and has been used in the construction of read/write heads within computer hard disks among other components. Metallic multi-layer arrangements are of ongoing interest to both industry and academia due to the unique properties including enhanced hardness and magnetic properties arising from the presence of compositionally modulated layers. The periodic layered structure of two different materials, as is the case for multi-layers, is known as a super-lattice due to the repetitive lattice-like structure above, albeit at times just above, the atomic level. The

special properties of multi-layered deposits arise from the crystal structure, magnetic nature, as well as the thickness of each layer forming the super-lattice.

2.4.3 Hardness

The hardness of electroplated deposits be they single metal, alloyed, or multi-layered is a value which can provide insight into the wear resistance of a given coating. The hardness of a coating is the measure of the resistance of an aerial to permanent plastic deformation [49] and is of significance when it can be related to other quantities such as tensile strength, scratch resistance, or ductility. Establishing a relationship between hardness and other qualities must be assessed based on the type and composition of the coating as the relationship can differ from coating to coating. For example, while it is expected that hardness increases with tensile strength and decreases with ductility; the reverse is common among electrodeposits [5].

The measurement of hardness is generally accomplished using indentations tests which consist of applying a load on a diamond-tip indenter, the shape of which differs depending on the test, and measuring the features of the indent for a given load. For accurate results it is accepted that the coating thickness must be at least 14 times greater than the depth of the indent, otherwise the substrate will influence the hardness by what is commonly called the anvil effect [5]. Orienting the sample to measure cross-section hardness, using smaller loads are common ways of overcoming the anvil affect. Two common micro-hardness tests for thin-films are the Vickers and Knoop hardness tests. The Vickers test indenter produces an indent of equal length and width and was introduced in 1922 by R. L. Smith and G. E. Sandland of Vickers Ltd. as an alternative to Brinell hardness test; the first widely used hardness test developed by J. A. Brinell in 1900 which used a steel or tungsten carbide ball shaped indenter [50]. The Knoop test, named for Frederick Knoop who developed the test with colleagues at the US National Bureau of Standards (NBS)⁴⁰ in 1939, uses a symmetric, pyramidal indenter point that produces an indent of length ~7 times its width and 30 times its depth [5]. The Knoop test, which is more sensitive to surface variations than the Vickers test, provides a means of examining the hardness of the uppermost surface layers [51]. For greatest accuracy,

⁴⁰ The NBS was renamed the National Institute of Standards and Technology (NIST) in 1988.

the Knoop hardness test is used on cross-sections with the length of the indenter parallel to the substrate-deposit interface. Both the Knoop, Equation 2.40, and Vickers, Equation 2.41, hardness results provide both macro and micro-hardness values [52]. Nano-hardness measurements require specific nano-hardness testers which produce a small indent that can be used on the surface without causing the anvil effect [5].

$$H_K = \left(\frac{P}{c_p d_K^2} \right) = 14.229 \left(\frac{P}{d_K^2} \right) \quad (2.40)$$

$$H_V = 1.854 \left(\frac{P}{d_V^2} \right) \quad (2.41)$$

where: H_K = Knoop Hardness, in MPa
 H_V = Vickers Hardness, MPa
 P = Force, in N
 c_p = correction factor related to indenter shape, ideally 0.070279
 d_K = Length of the long diagonal of the indentation, mm.
 d_V = Average length of the diagonal left of the indent, in mm

Another method of determining coating hardness is known as scratch hardness testing. Scratch hardness tests consist of dragging a harder material, typically a diamond point, across the surface of an object made of a softer material. The test provides a measure of the hardness by determining the force necessary to cut through the film to the substrate. While the test does provide the resistance of a sample to fracture or permanent plastic deformation, interpretation of scratch experiments rely heavily on assumptions about the size of the contact area, as well as the coefficient of friction, between the material and the stylus [53]. Though sometimes used for thin films, scratch hardness tests are most often used in mineralogy where the comparison of the hardness based on the Mohs scale of mineral hardness.

The hardness of single metal or alloyed films results from the grain size, lattice dislocations, crystal structure, and impurities within the film. The composition of the film, including impurities, is fundamental to the crystal structure of the thin film and provides the basis for the related parameters of grain size and lattice dislocations. While impurities, such as hydrogen, often hinder deposit properties, the intentional inclusion of impurities can be beneficial enabling smaller grain sizes or limiting the propagation of dislocations, ultimately increasing hardness. Comparing the mechanical properties of

electrolessly deposited Ni-P thin films with those produced by electroplating, electrolessly deposited Ni-P is harder and has better corrosion resistance than that of electrodeposited Ni-P [28].

Crystalline deposits having many dislocations possess lower hardness than those with few dislocations as the dislocations can more easily propagate within the crystallite resulting in irreversible plastic, rather than reversible elastic, deformation. Once plastic deformation has occurred the hardness of the material can increase due to the aggregation and generation of dislocations which is known as strain, or work, hardening. The presence of grain boundaries and atomic mismatch between neighbouring grains creates a repulsive stress field to impede the propagation of dislocations to other grains [49]. When the concentration of stress from aggregate dislocations at the grain boundary reaches a critical value, the dislocations will propagate to an adjacent grain and yielding takes place. The propagation of the dislocations is driven by both the aggregation of dislocations at the boundary as well as local stress fields [54, 55], Equation 2.42, between dislocations that repel each other. Minimizing the grain size within deposits provides greater resistance to dislocation propagation as fewer dislocations are able to accrue at the boundary, increasing the amount of applied stress necessary for a dislocation to propagate across a grain boundary; a process known as grain boundary strengthening [49]. The relationship between the yield stress and grain size is described by the Hall-Petch equation which establishes the relationship between grain size and yield strength [56, 57], Equation 2.43. It should be noted that the Hall-Petch correlation tends to break for extremely small grain sizes, 5-20 nm, as strain hardening and reduction of tensile strength occur within that range for electrodeposited nano-crystal Ni and Co [5, 58].

$$\sigma \propto Gb/r \quad (2.42)$$

where: σ = Stress field
 G = Material's shear modulus
 b = Burgers vector (magnitude and direction of the lattice distortion of dislocation in a crystal lattice)
 r = Distance between dislocations

$$\sigma_y = \sigma_0 + k_y d^{-1/2} \quad (2.43)$$

where: σ_y = Yield stress
 σ_0 = Starting stress for dislocation movement
 k_y = Strengthening coefficient (unique to material)
 d = Average grain diameter

While the hardness of single metal or alloyed film is determined by the grain size, crystal structure, lattice dislocations, and impurities within the film; multi-layered thin films have the added parameter of layer thickness. Experimentally it has been shown that decreasing the layer thickness of a Cu-Ni super-lattice, deposited from using the dual bath technique, from 1 μm to 30 nm increased the hardness by more than two fold, consistent with the Hall-Petch relation [46]. The hardening effect of the layers is attributed to the large number of interfaces, brought about by optimal layer thicknesses and interface distances, which are able to act as barriers to plastic deformation by preventing dislocations from traveling across the super-lattice. Tench and White reported a sharp increase in the hardness of electrodeposited Ni/Cu multi-layers⁴¹ as Cu layer thickness decreased below 0.4 μm [59]. Further refining the thickness of the compositionally modulated nano-layers, to the near-angstrom range of the nanometer scale, has shown experimentally to further increase the hardness of the super-lattice provided the layer thickness of the super-lattice system is reduced to some optimal value [60]. For example, the Knoop hardness of softer Cu and harder Ni multi-layers increases up to 5.6 times the value of the harder electrodeposited nickel layer around an optimum layer thickness of 20 \AA is achieved [48], Figure 2.11.

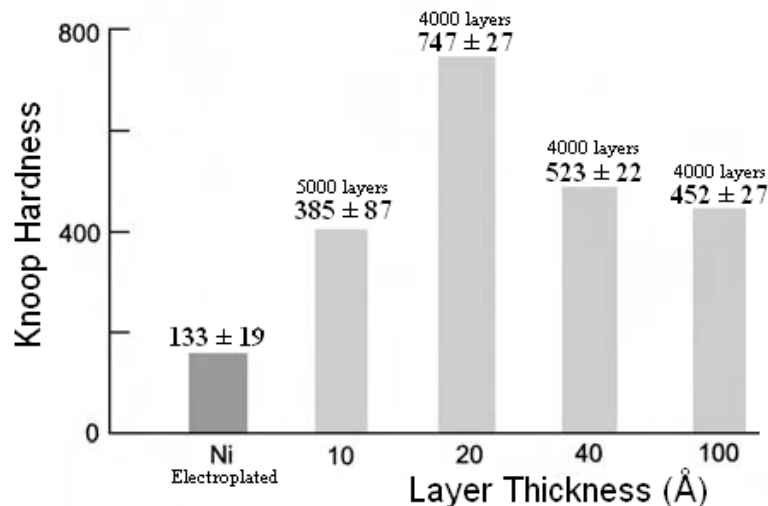


Figure 2.11: Hardness data for electrochemically grown Cu/Ni super-lattice multi-layers as a function of individual layer thickness compared to electroplated Ni from a sulfamate bath [48]. [Figure produced from table presented by Simunovich et al. (1994) by permission of The Electrochemical Society.]

⁴¹ In their work Tench and White had a 2% Cu impurity within the Ni layer.

As the thickness of the individual layers and distance between interfaces approaches the angstrom scale, atoms, the majority of which are then close to an interface, experience stress forces about lattice dislocations which result in hardening of the structure in a similar fashion to grain boundary strengthening. An interpretation of the emergence of increased hardness within epitaxial⁴² structures is the mismatch of both Young's modulus and lattice constants between adjacent layers [60]. The modulus mismatch introduces a force between a dislocation and its image in the interface, while the lattice parameter mismatch generates stresses and mismatch dislocations which interact with mobile dislocations [60]. Due to the large number of interfaces, hardening occurs as dislocations are subject to the mismatches at the interface/boundary of the layers that prevents the transit of dislocations through the structure. A peak in yield stress, stress at which irreversible plastic deformation occurs, occurs as feature size, both layers and grains for multi-layers, approaches an optimum value and single dislocations must overcome both mismatch barriers [60]. The unique properties of the super-lattice system that differ from the individual, bulk, components diminish with increasing layer thickness as a bulk region, and diminished density of interfaces, allow for the aggregation of dislocations resulting in a drop in yield stress. Other investigations of hardness above tens of angstroms have shown that the hardness of Cu-Ni super-lattice systems remain higher than Ni-Cu alloys even at layer thicknesses around 100 nm where bulk material properties begin to influence the multi-layer system [61]. Additionally, gradient multi-layer systems, where the composition of the layer changes gradually between pure metals due to a stepwise switching between potentials, have been shown to have greater Vickers hardness compared to traditional multi-layers [61]. For example, a Cu-Ni gradient multi-layer structure of 160 nm between 'pure' peaks has been shown to have Vickers hardness 1.8 times greater than that of traditional 100 nm thick multi-layers [61]. The findings of the gradient deposition, which is essentially a system of sequential layers of different alloy composition, may be related in part to the increased hardness of the nano-layers of Figure 2.11.

⁴² Epitaxial – Deposits of the crystals of one element, or alloy, on the crystal face of another such that the crystalline substrates of both materials have the same crystal symmetry.

Along with the mismatch of layers, the specific orientation of layers has also been put forward as part of the explanation for the special properties of epitaxial super-lattice systems, such as FCC for Cu-Ni multi-layers [60]. In the case of Cu-Ni multi-layers, structure is epitaxial in the sense that the lattice constant is intermediate between that of both materials and it is the modulated strain⁴³ resulting from intermediate epitaxial structure and applied stress field that is likely responsible for the increased hardness [60]. The epitaxial structure of super-lattice systems is not limited to metals of similar crystal structure and may be created from metals having dissimilar natural crystal structure provided the layers of the multi-layered thin-film system remain below a critical thickness. In the case of Cu-Co multi-layers with Cu layer thickness of 20 nm and Co layer thickness ranging from 20 nm to 500 nm, it has been shown that Co layers have an FCC structure below 100 nm, above which it forms its natural HCP phase consisting of a fine 3nm thick lamellar structure [62]. Though the Vickers hardness of the Cu-Co super-lattice has been shown to remain independent of Co layer thickness above 20 nm [62], the hardness has been shown to be layer dependent for layer thicknesses below of tens of nanometer [63]. Additionally, increased hardness has been measured for non-epitaxial super-lattice deposits [48], where the deposit occurred on amorphous nickel-phosphorus substrates; hence, the interplay of the aforementioned factors with the layer thickness continues to be investigated [60].

2.4.4 Magnetic Properties & Giant Magneto-Resistance (GMR)

Fundamentally the magnetic properties of pure metals arise from the aggregate orientation of atomic magnetic dipole moments of atoms/ions⁴⁴ that comprise the lattice. In the case of alloys and other composite materials, the magnetic properties become linked to the elemental composition and crystal structure of the material. Different types of magnetism arise from orientation and net effect of the magnetic moments of atoms with the lattice of a material. Materials in which the magnetic moments are ordered are

⁴³ Provided layers of equal thickness, the strain within the super-lattice may be modulated in a layered fashion with all Ni layers having near identical strain which differs from the strain within Cu layers of near identical strain. [60]

⁴⁴ A lattice of atoms can be equivalently viewed as a lattice of ions within a gas of conduction electrons.

ferromagnetic, ferrimagnetic, and anti-ferromagnetic, while disordered magnetic moments are present in paramagnetic and diamagnetic materials.

Ferromagnetic materials; such as Fe, Ni, and Co; consist of those materials in which atoms positively contribute to the net magnetization, while materials in which some of the atoms contribute negatively towards net magnetization of the material, as is possible with certain alloys, are termed ferrimagnetic; though historically some been confused as ferromagnetic. Anti-ferromagnetic materials; such as Cr and some other alloys; have oriented atomic dipole moments that cancel producing no net magnetization outside of a magnetic field; within a magnetic field a minor magnetization may arise. The ordering of the magnetic moments is temperature dependent and vanishes above critical temperatures⁴⁵. Above the critical temperatures, ordered magnetic materials become paramagnetic with individual atoms retaining a permanent magnetic dipole moment without any net magnetization outside of an applied external magnetic field. Within an external magnetic field, the magnetic moments of paramagnetic materials, such as Mg and Al, align with, and are attracted to, the external field, while the magnetic moments of atoms of diamagnetic materials, such as Cu and Zn, align to resist and repel an external magnetic field.

2.4.4.1 Magnetization & Coercivity of Thin Films

The magnetic properties of metallic thin films typically require an external magnetic field as no inherently ordered magnetization is typically present in as-deposited films. Application of an external magnetic field aligns the magnetic domains, regions of uniform magnetization within individual grains of the material, within a material with the magnetic field⁴⁶. The degree of alignment is a function of the applied magnetic field and the point at which further increase in the field strength produces no further increase in the magnetization of the material is known as the saturation point. In the case of ferromagnetic and ferrimagnetic materials, removal of the magnetic field following magnetic saturation results in residual magnetization within the material, which does not

⁴⁵ Critical temperature for ferromagnetic and ferrimagnetic materials is the Curie temperature, while the critical temperature for anti-ferromagnetic materials is known as the Néel temperature.

⁴⁶ Diamagnetic materials in an external magnetic field will exactly oppose the field unlike the other magnetic materials which align with the applied magnetic field.

occur for paramagnetic, diamagnetic, or anti-ferromagnetic materials. In addition to residual magnetization, the shape and volume of the materials may change under magnetization in what is known as magnetostriction. Magnetostriction, which equally refers strain resulting from the magnetization or magnetization due to strains, [5] occurs for all magnetized materials, though effects persist more for materials with residual magnetization.

The external magnetic field required to return a saturated ferromagnetic material to zero magnetization is known as the coercivity of the material. The coercivity provides the resistance of a material to return to zero magnetization is measured in oersted (Oe) in CGS⁴⁷ units and amperes per meter (A/m) in SI⁴⁸ units. Materials of coercivity below 200 Oe are termed ‘soft’ and are used as magnetic cores and within the write heads of magnetic recording devices due to the ease of magnetization. Materials with high coercivity above 200 Oe are termed ‘hard’ and are used for permanent magnets and magnetic storage media as the large coercivity prevents demagnetization [5]. The high coercivity of very small grains is attributed to the single magnetic domain of grains of diameter below 10^{-7} m or 10^{-8} m, or <100 nm [64]; larger grains split into multiple domains. The small grain size allows for magnetization to saturation, the reversal of which requires larger fields based on the shape of the particle. At sufficiently small grain size, materials can become super-paramagnetic depends on whether the grains are free to rotate, resulting in super-paramagnetism, or fixed, resulting in ferromagnetism [64].

The properties of coercivity and residual magnetization are summarized within a hysteresis loop which illustrates the response of the magnetic material to an external magnetic field. Hysteresis, the dependence of the system on a previous configuration, exists only for ferromagnetic and ferrimagnetic materials, Figure 2.12, as paramagnetic and anti-ferromagnetic materials relax to zero magnetization once the field is removed, Figure 2.13.

⁴⁷ CGS Units – Centimeter-Gram-Second based Units

⁴⁸ SI Units – System Internationale Units

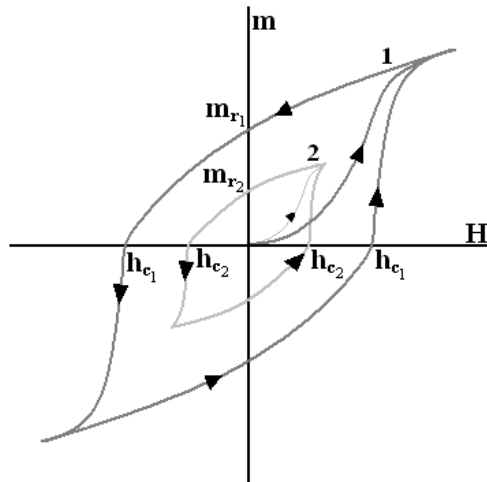


Figure 2.12: Schematic of two hysteresis loops for harder (1) and softer (2) magnetic materials, showing the residual magnetization, m_r , and coercivity, h_c , of each loop.

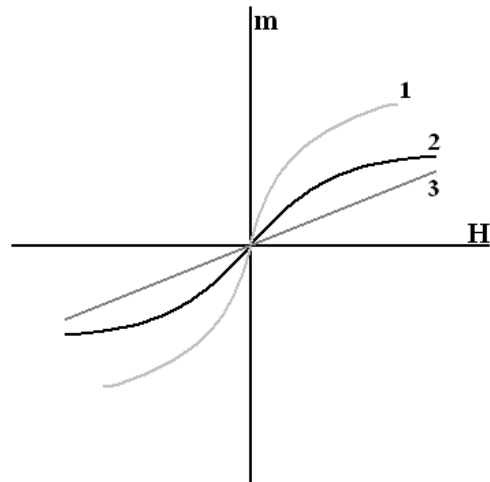


Figure 2.13: Schematic magnetization versus applied magnetic field for (1) Super-paramagnetic, (2) paramagnetic, and (3) anti-ferromagnetic materials.

Magnetic thin films of varying coercivity may be deposited using both electro- and electroless plating. An advantage of electroless deposition is the ability to control the coercivity of deposited magnetic materials, ranging from magnetically soft to hard, by changing a single component within the deposition solution. Hard magnetic films Co-P around $0.3 \mu\text{m}$ thick, with an in-plane coercivity of 514 Oe and no in-plane anisotropy, directional dependence, can be deposited from a 70°C solution containing: Co^{2+} ions from 0.02 M to 0.03 M cobalt sulfate $\{\text{CoSO}_4\}$, 0.07 M to 0.10 M citrate ions $\{\text{C}_6\text{H}_5\text{O}_7^{-3}\}$ as the complexing agent, 0.3 M to 0.4 M boric acid $\{\text{H}_3\text{BO}_3\}$ as the buffer, 0.05 M to 0.07 M sodium hypophosphite $\{\text{NaH}_2\text{PO}_2\}$ as the reducing agent; with pH adjusted to 8 by means of sodium hydroxide $\{\text{NaOH}\}$ [28]. The addition of 0.05 M of sulfamic acid $\{\text{H}_3\text{NO}_3\text{S}\}$ reduces the coercivity by half, while addition of 0.20 M of $\text{H}_3\text{NO}_3\text{S}$ results in a 100 fold reduction in the coercivity of the thin film [28]. Additionally, it has been shown to be possible to electrolessly deposit Co-P films with a coercivity of up to 1000 Oe [28].

2.4.4.2 Fundamentals of Magneto-Resistance

In addition to the magnetization of metal thin films, metals within a magnetic field experience a change in electrical resistance in a process known as magneto-resistance. As in all cases, the resistance of a material is the result of scattering processes which impede the flow of electrons within the material. Scattering can result from a

number of factors including impurities and natural periodic vibrations of atoms, phonons, within a crystal lattice. Scattering processes not only vary by external factors but also on the electronic configuration of the element. The 1936 work of Sir Nevil Mott suggested that the electrical conductivity of d transition metals was mainly determined by the easily mobile 4s electrons [65, 66]. Scattering of the s state electrons into the many d states which are available at the Fermi level, the topmost filled level in the ground state⁴⁹ of an N electron system, gives rise to a considerable resistance [65]. For Cu, a diamagnetic element that immediately follows Ni in the Periodic Table, all the 3d states are situated below the Fermi level and therefore not available for scattering which in turn results in the high conductivity of the metal [65, 66].

Magneto-resistance is the property of a material to change the value of its electrical resistance, R, in the presence, and as a function, of an external magnetic field, H; $\Delta R/R_0 = f(H)$. Magneto-resistance effects originate from the spin-orbit coupling of electrons within an atom and alter, increase or decrease, the electrical resistance of a material within an effective magnetic field⁵⁰. In broad terms, the change in resistance can be seen as a result of the interaction between the magnetic dipole moment of electrons, the magnetic domains within materials, as well as externally applied magnetic fields. For the commonly deposited transition metals, the properties of magneto-resistance arise due to the electronic configuration of the 3d and 4s shells of the atoms. In the free atoms, the 3d and 4s atomic energy levels of the 3d transition elements host the valence electrons and broaden into energy bands when confined within a lattice. Strong hybridization of the 3d and 4s orbitals of the transition metals render the shells largely indistinguishable as both shells hold conduction electrons. Additionally, the electrons in the 4s band are more mobile in part due to the large wide energy range of the band and significant overlap between the 4s orbitals of neighbouring atoms [66]. The occupation of the energy bands in accordance with the Pauli Exclusion Principle, electrons of identical spin cannot have

⁴⁹ To be in the ground state the atom is at absolute zero, 0 K. At higher temperatures, some electrons have sufficient thermal energy to occupy higher energy levels than the Fermi level, where electrons have energy E_F . The probability of occupation that any particular energy level, E, is occupied by an electron is provided by the Fermi-Dirac Distribution Function:

$$f(E) = \frac{1}{e^{(E-E_F)/kT} + 1}$$

⁵⁰ An effective magnetic field can include an externally applied magnetic field as well as magnetization.

identical orbital angular momentum, and Hund's rule, greater total spin results in greater atomic stability, results in the pairing of electrons in the lower energy bands and unpaired electrons having the same spin. For atoms in the ground state⁵¹, all the lowest energy levels are filled by electrons and the highest occupied energy level, Fermi Level, is called the Fermi energy, E_F . For conductors, the Fermi level is typically within the overlap of the valence and conduction bands. In the case of both insulators and semiconductors, the Fermi level at absolute zero lies within the gap between the valence and conduction bands. While in the case of insulators the gap is too large for electrons to traverse, the distance between each band, valence and conduction, to the Fermi level in semiconductors gives rise to different semiconductor properties. Within paramagnetic materials, both the 3d and 4s bands contain an equal number of spin up and spin down electrons resulting in no net spin polarization, Equation 2.44, which produces no net magnetization [66]. Within ferromagnetic materials the number of spin up electrons is larger than the number of spin down electrons, which results in a net spin polarization, Figure 2.14.

$$P = \frac{(N\uparrow - N\downarrow)}{(N\uparrow + N\downarrow)} \quad (2.44)$$

where: P = Spin Polarization
 $N\uparrow$ = Number of spin up electrons in the 3d and 4s shells
 $N\downarrow$ = Number of spin down electrons in the 3d and 4s shells

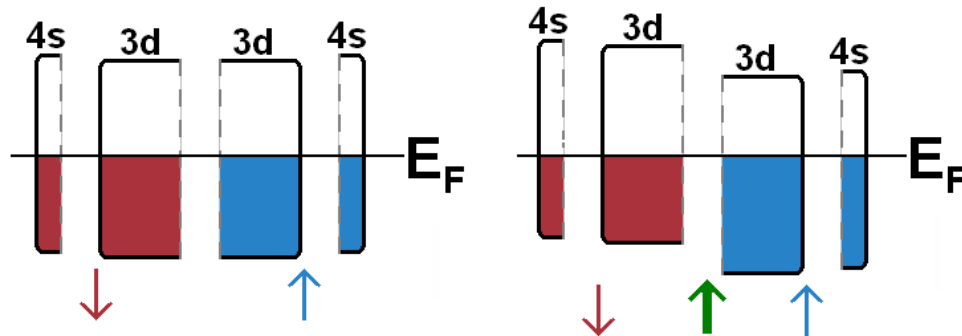


Figure 2.14: Spin polarization in (Left) paramagnetic and (Right) ferromagnetic materials. The blue and red arrows indicate spin up and spin down, respectively, and the green arrow indicates the net spin polarization. The density of states is shown separately for the spin up and down electrons with a separation shown between the 4s and 3d energy bands; E_F is the Fermi Energy.

The net spin polarization of the ferromagnetic material can be compared to paramagnetic materials, such as ferromagnetic materials above the Curie temperature, by

⁵¹ The ground state of an atom refers to the lowest energy state possible at absolute zero.

the transfer of spin down electrons from the spin down band into the spin up band which leads to more exchange energy in the system and lowers the total energy. The exchange energy results from the exchange and associated symmetry of identical of unpaired in the overlapping outer valence bands of neighbouring atoms. Parallel alignment of the unpaired electrons spins within the valence band lowers the electrostatic energy of electrons within the system with the increase in exchange energy lowering the energy of the system. Along with the exchange energy, realignment of the spin up and spin down states occurs to maintain the Fermi energy level; this displacement between the spin up and spin down allows very different densities of states for the two spin bands at the Fermi energy [66]. Given that the only electrons at or very close to the Fermi level participate in the electrical conduction process and that the density of states at the Fermi surface is quite different for the two spin states, there is a significant difference between the resistance of the spin up electrons and the spin down electrons within ferromagnetic materials due to spin-dependent scattering [66]. Within paramagnetic materials, there is no difference between the number of spin up and spin down electrons, or the density of the spin up and spin down states, and the electrons act as a single type of charge carriers contributing equally to the resistance [66]. Simply, the more spin-polarized the density of states at the Fermi energy, the greater the difference in number the spin up and spin down electrons, and the more pronounced the resulting efficiency of the magneto-electronic effects [66].

For ferromagnetic materials, materials of anisotropic magnetization, the magnitude of the magneto-resistance effect is dependent on the orientation of the external magnetic field and/or the magnetization of the material which contributes to the effective external magnetic field. The dependence on the orientation of the magnetization is known as the anisotropic magneto-resistance (AMR) effect and was initially discovered by Lord Kelvin in 1856 with the observation that resistivity is maximized when the current is in the same direction of magnetization, and is minimized when the current is at 90° to the magnetization [66, 67]. The change in the resistance is the result of spin-dependant scattering and a larger probability of s-d electron scattering in the direction of magnetization as a result of the interaction between the magnetic domains of the material and the magnetic dipole moments of the electrons, Figure 2.15.

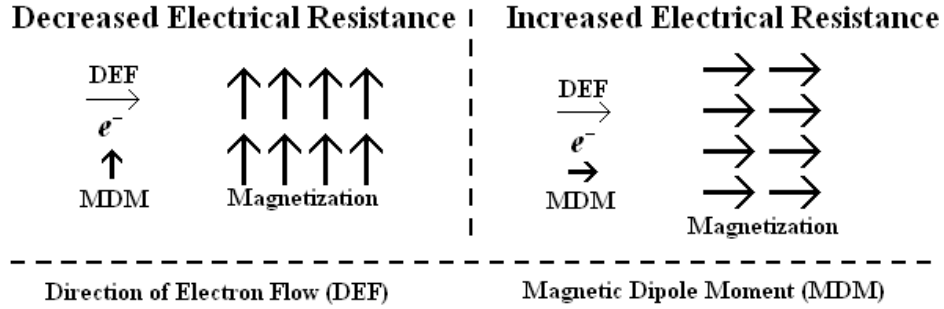


Figure 2.15: Schematic of the AMR effect indicating the change in resistance based on the motion of the electron current and the preferred orientation of the magnetic dipole moment of an electron within the effective magnetic field of the magnetized lattice. The decrease in resistance in the perpendicular case occurs due to the alignment of the spin induced magnetic moment with the magnetization of the material and lesser interaction/scattering compared to the parallel case where a magnetic resistance helps scatter the electrons.

The AMR ratio, or increase in the relative resistance of the film, depends on thickness, grain size, and film surface conditions, with measurements reliable only at room temperature [68]. The mathematical description of the AMR effect, put forward in 1975 by T. R. McGuire and R. I. Potter at IBM, describes the AMR effect as an anisotropic conductivity matrix term, σ_{ij} , in the microscopic Ohm's law, Equation 2.45, with the resistance resulting from the anisotropic scattering of electrons in an external electromagnetic field [67, 68].

$$\mathbf{J}_i = \sigma_{ij} \mathbf{E}_j \quad (2.45)$$

where: \mathbf{J}_i = Current Density
 σ_{ij} = Conductivity matrix (note: resistivity $\rho = 1/\sigma = RA/\ell$)
 \mathbf{E}_j = Electric field

Magneto-resistance effects cause by external magnetic fields apply to all metals independent of magnetic properties, though vanishingly isotropic materials, the effect is, in part, a direct result of the Lorentz force [60], Equation 2.46, which relates the force on a charge, in this case an electron, to the applied electric and magnetic fields.

$$\mathbf{F} = -e(\mathbf{E} + \mathbf{v} \times \mathbf{B}) \quad (2.46)$$

where: \mathbf{F} = Force experience by the charge
 e = Electron Charge
 \mathbf{E} = Electric field
 \mathbf{v} = Velocity of the charge
 \mathbf{B} = Magnetic field

Within paramagnetic and demagnetized ferromagnetic materials outside of an applied magnetic field, the effective magnetic fields produced by the disordered magnetic domains results in deflect electrons within the current resulting in scattering and base

resistance of the material. When the applied magnetic field or magnetization of the material is longitudinal, aligned with the electron flow, there is no contribution to the Lorentz force by the magnetic field and the electrons pass unabated and a decrease in resistance may be observed. Transversal alignment of the magnetization or magnetic field with respect to the electron flow produces deflections of the electrons increasing the likelihood of scattering, ultimately increasing the resistance [60]. For a magnetic field at 90° to the flow of a current, the deflection of charges by the Lorentz force results in aggregation of charge on one side of the medium. The aggregation of charge, or Hall Effect, discovered by Edwin Hall in 1879, produces a potential difference perpendicular to both the flow of current and magnetic field. The force of the electric field produced by the aggregation of charge ultimately counteracts the force exerted on the electrons by the magnetic field producing an eventual steady state for the current, Figure 2.16. Both prior to and during the steady-state system, the Hall Effect produces a small increase, $\ll 1\%$, in the resistivity of most materials [60].

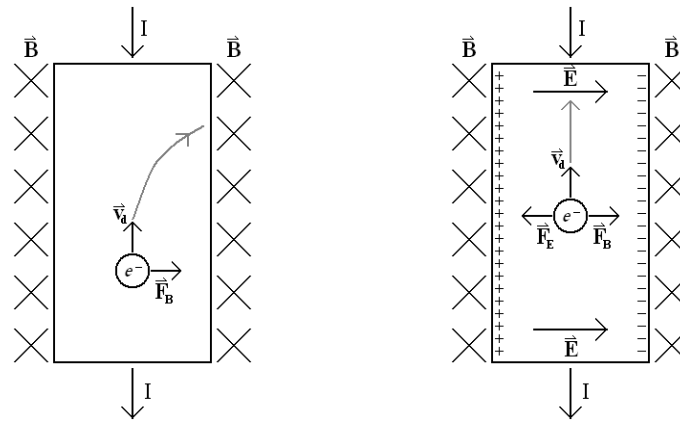


Figure 2.16: Diagram of the Hall Effect and resulting forces on an electron within a conducting metal before (left) and after (right) equilibrium.

In most, non-magnetic, conductors the Hall resistance exceeds the effect of magneto-resistance; however, in anisotropic magnetic materials, such as ferromagnetic materials, the AMR effect dominates dependent on the intensity of the effective magnetic field. Though not dominant within magnetic conductors, an effect known as the anomalous Hall Effect occurs simultaneously with AMR effects within transversally magnetized ferromagnetic materials in the absence of an externally applied magnetic field. The anomalous Hall Effect produces a Hall Voltage similar to the original effect, though the spin-dependent scattering of the electrons results in accumulation of electrons

of a single spin on each side of the material [69, 70]. The coefficient of the anomalous Hall Effect is about 100 times larger than that of the ‘ordinary’ Hall Effect near the Curie temperature for pure Ni, and about the same at very low temperatures [71]. Introduction of an external magnetic field to the AMR effect results in a modification of the magneto-resistance curve due to additional interactions. An external magnetic field can be oriented to enhance or diminish the magneto-resistance effect, by being aligned transversely or longitudinally, respectively, with the motion of the charge carriers [60]. Both the Hall and AMR effects contribute to scattering processes and magneto-resistance effects of bulk materials and thin films.

2.4.4.3 Larger Magneto-Resistance Effects

While magneto-resistance effects are larger than the ‘ordinary’ Hall Effect, the percentage change in magneto-resistance is, in general, smaller in films than bulk materials [68] and the maximum magneto-resistive change achieved in a magnetic metal, specifically permalloy, a 20 % Fe – 80 % Ni alloy, is only about 4 % [60]. Larger magneto-resistance effects, by one order of magnitude or more, are termed giant magneto-resistance (GMR) and are produced, mainly, by layered thin film structures. While GMR is indicative of the scale of magneto-resistance, and large magneto-resistance effects had been found around 1967 for some alloyed materials, the oscillatory hallmark of multi-layer GMR films was not present in alloyed deposits [72]. Discovery of GMR in layered materials occurred independently by the groups of Albert Fert and Peter Grünberg, both of whom shared the 2007 Nobel Prize in Physics [66]. Both groups discovered the GMR effect occurs within multi-layered systems consisting of ferromagnetic layers interspersed with non-magnetic metallic layers. The first successful experiments showing a significant GMR effect were produced using Fe and Cr layers; the group of Peter Grünberg [73] used a tri-layer system of Fe/Cr/Fe, while the group of Albert Fert [74] used multi-layers of the form $(\text{Fe/Cr})_n$ where n could be as high as 60 [66]. The experiments by Fert’s group utilized multi-layer systems constructed from 30 Å thick layers of iron interspersed with chromium layers between 9 Å and 18 Å [74]. For a Cr layer thickness of 9 Å at a temperature of 4.2 K, the resistivity was lowered by almost a factor of 2 in a magnetic field of 2 Tesla [74]. In order to exhibit the GMR

effect, the mean free path length for the conduction electrons has to greatly exceed the interlayer separations so as to allow the electrons to interact with multiple magnetic layers [66]. It is for this reason that thicker multi-layers of layer thickness above a few angstroms, such as those produced by D. Tench and J. White [59], possess only increased hardness and not GMR.

The fundamental process by which the GMR effect occurs in multi-layer systems is anti-parallel coupling/ordering of the magnetic layers through the non-magnetic ‘spacer’ layer in the absence of an external magnetic field. As a multi-layer sample is deposited, the minimum energy requirement of the system ensures that successive magnetic layers, such as Ni and Fe, will contain domains of anti-ferromagnetic orientation with respect to previous magnetic layers [63]. The orientation of the layers is not perfectly anti-ferromagnetic in nature as the orientation of the domains is dictated by the minimization of the free energy [63]. With no external magnetic field applied, the anti-parallel magnetizations of neighbouring magnetic layers result in spin-dependent electron scattering above the normal scattering of charge carriers, electrons. The increased scattering of electrons due to the anti-ferromagnetic coupling between the magnetic layers effectively increases the resistance of the material. Application of an external magnetic field, strong enough for saturation, aligns magnetizations of the magnetic layers in an essentially parallel structure, Figure 2.17, reducing spin-dependent scattering for those electrons of spin anti-parallel to the magnetization, spin-up electrons, decreasing the overall resistivity of the structure [72, 75].

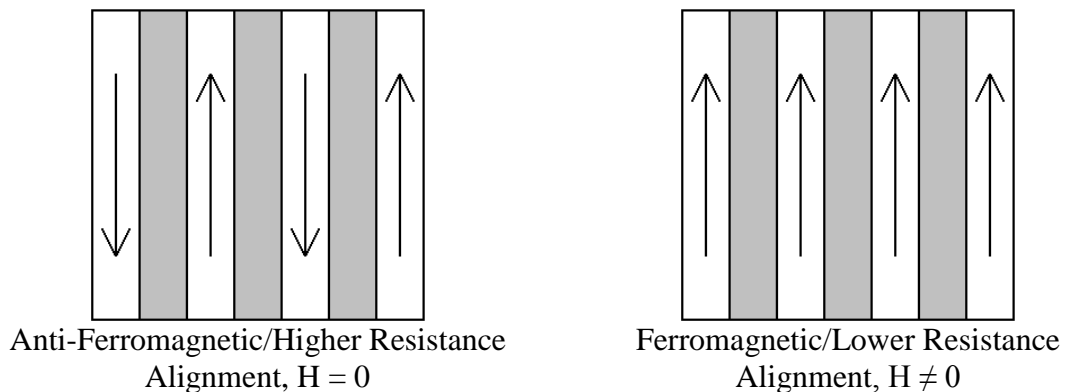


Figure 2.17: Schematic of the idealized magnetization of the super-lattice in multi-layers producing the GMR effect.

The dependence of the resistance on the relative magnetic alignment of sequential magnetic layers seen within the multi-layer system, and resulting binary configurations is commonly known as a spin valve. Spin valves using non-magnetic metal spacers allow for current to pass through the multi-layer system even under anti-ferromagnetic alignment of the adjacent magnetic layers, and the binary system exists between high and low resistance. Replacement of the non-magnetic metal with a half-metal; a material in which the spin down band is metallic, bisected by the Fermi Level, while the spin up band is an insulator, below the Fermi Level; such as CrO_2 ; results in 100 % spin polarization at the Fermi level. The complete polarization of the spin results in the creation of a perfect spin valve that does not allow the passage of current in the anti-ferromagnetic alignment of adjacent magnetic layers [66].

The effect of GMR occurs for current flow both along, current in plane (CIP), and perpendicular, current perpendicular to plane (CPP), to the planar orientation of the layers. As in normal magneto-resistance, the CPP arrangement generally provides larger changes in the resistance than the CIP arrangement, Figure 2.18, and has the added benefits of being less sensitive to inhomogeneity within the sample while having a simpler theory for the magneto-resistance effect [76]. While both the CPP and CIP orientations operate as spin valves, the CPP alignment is favoured for device creation due to increased sensitivity to magnetic fields [76].

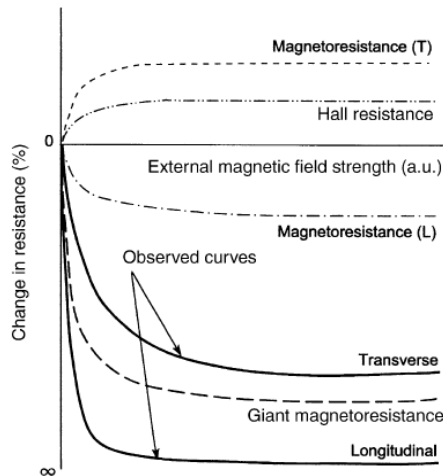


Figure 2.18: Superposition of all contributions toward observed GMR.

[Figure reproduced from Figure 17.8 in “Fundamentals of Electrochemical Deposition, 2nd Edition”, with permission from John Wiley & Sons Inc. (2006).]

Ideally, GMR values depend on the materials used, the super-lattice structure of the multi-layers, and the electromagnetic conditions imposed, and not the method of multi-layer preparation; though preparation methodology does impact the lattice and super-lattice characteristics of the sample [63]. Of the deposition methods, electroless deposition suffers from impractical need of mechanical switching between solutions. Vapour deposition and sputtering are rather cost intensive with vapour deposition creating quasi-amorphous interfaces and time consuming for alternating the deposited material, and sputtering unable to be extended to industrial usage [63]. While electro-deposition is practical, relatively inexpensive, the fundamentals of multi-layer deposition are restrictive in the choice of lattice materials. Critical to the GMR effect is the thickness of the non-magnetic interlayer and resulting spacing of the magnetic layers. The saturation value of the GMR in ferromagnetic/non-ferromagnetic multi-layers oscillates with the thickness of the spacer layer with the changes in the magneto-resistance more pronounced for thinner layers, Figure 2.19. The oscillation is due to the exchange coupling of the layers to one another with a sign that oscillates with the thickness of the spacer layer, alternating between ferromagnetic and anti-ferromagnetic coupling [77].

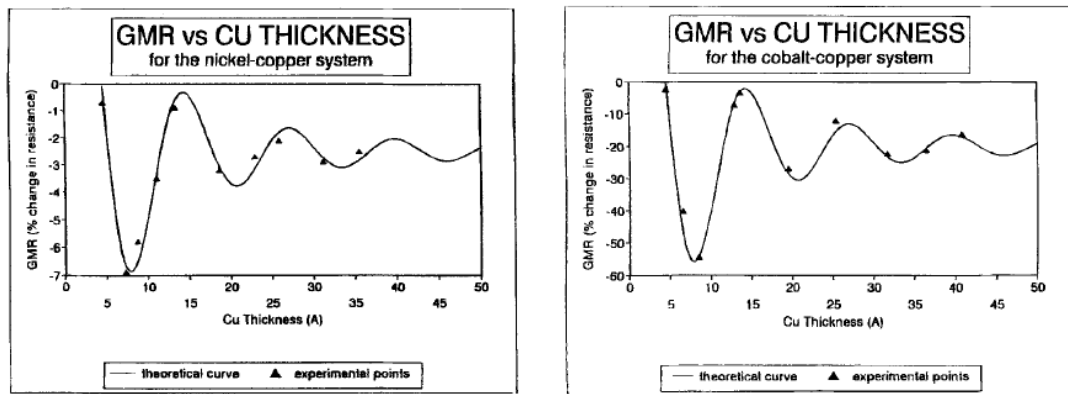


Figure 2.19: Examples of the dependence of spacer layer thickness, Cu, on GMR at magnetic saturation for Ni-Cu and Co-Cu multi-layers. The fitted theoretical curves are Ruderman-Kittel-Kasuya-Yosida (RKKY) curves⁵². [77] [Figures reproduced from Bird et al. (1995) by permission of The Electrochemical Society.]

Other magneto-resistance effects include tunnelling magneto-resistance (TMR) and colossal magneto-resistance (CMR). For TMR, the interlayer is a thin non-

⁵² RKKY interaction refers to the coupling mechanism of nuclear magnetic moments in a metal by means of conduction electron interaction. The ferromagnetic/antiferromagnetic oscillation due coupling between thin layers of magnetic materials separated by a non-magnetic spacer, as observed in GMR, is one prediction of the RKKY theory. [60]

conducting, non-magnetic insulator where any electron flow between the layers is due to quantum mechanical tunnelling and ferromagnetic ordering of the ferromagnetic layers of the super-lattice increases the likelihood of tunnelling. The change in the magneto-resistance of TMR films is of the order of 50 % at room temperature with barriers of Fe/MgO/Fe shown to give rise to magneto-resistance changes that sometimes exceeded 200 % [66]. Unlike TMR, which produces magneto-resistance effects larger than GMR using a multilayer configuration, CMR provides magneto-resistance of several orders of magnitude beyond that of GMR without any multi-layer structure; magneto-resistance properties in CMR alloys remain an ongoing field of research [78-80]. The ongoing development to produce larger magneto-resistance effects is to further increase the sensitivity of magnetic sensors, such as read heads, and hence further increasing the density of magnetic storage; however, it is unlikely that CMR will become of technological interest as the required magnetic fields are very high [66].

While substantial technological interest exists in TMR technologies, as they have become dominant over the GMR sensors [66], several avenues of GMR research continue to be of significant interest. Among the topics of interest is the question of “how far can spin-polarized electrons travel in a material while maintaining their spin polarization” [66]. Additionally, very intense work is now being directed towards magnetic switching induced by spin-currents [66]. As magnetic recording devices approach the size limit imposed by quantum mechanics, magnetic switching by spin-currents allow the motion of magnetic domain walls along a nano-wire [81]. The construction of such memory has the potential to provide a means of creating memory devices of the reliability and speed of current solid state drives at the capacity of traditional hard disk drives [81].

Both the coercivity and magneto-resistance properties of metal thin films are of significant importance to a number of modern applications, including within sensors and magnetic storage devices, or more commonly computer hard disks. While modern magnetic storage devices utilize more sophisticated technology, especially for reading encoded data, the fundamental processes associated with writing and reading of data to and from a magnetic media remains largely unchanged.

2.5 Magnesium & Corrosion

Magnesium {Mg} is the eighth most abundant element in the earth's continental crust and present at a concentration of about 1.33 gram per kilogram ($\text{g}\cdot\text{kg}^{-1}$) of seawater [82]. At 2.1 %, Mg is the third most abundant industrial metal behind aluminum {Al}, 8.1 %, and iron {Fe}, 5.0 % in the earth's continental crust [83]. The abundance of Mg along with the many excellent properties associated with Mg alloys, most notably excellent relative properties (property/density) and light weight, Table 2.6, make it an increasingly desirable material within a number of sectors and industries including automotive, aerospace, electronics, and medical.

Common Name	Thermal conductivity ($\text{W}\cdot\text{m}^{-1}\cdot\text{K}^{-1}$)	Density ($\text{g}\cdot\text{cm}^{-3}$)	Coefficient of linear expansion ($10^{-6}\cdot\text{C}^{-1}$)	Electrical Resistivity ($\mu\Omega\cdot\text{cm}$)	Elastic Modulus (GPa)	Tensile Strength (MPa)	Melting Point ($^{\circ}\text{C}$)
Plain Carbon Steel AISI-SAE ⁵³ 1020	0.52	7.86	11.7	18	205	450	1515
Stainless Steel type 304	0.15	7.90	17.3	72	195	550	1425
Al alloy 3003 (rolled ⁵⁴)	1.9	2.73	23.2	3.7	70	110	650
Al alloy 2014 (annealed ⁵⁵)	1.9	2.80	23.0	3.4	70	185	650
AZ31B Mg alloy	1.0	1.77	26	9	45	260	620
Copper (electrolytic ⁵⁶)	3.9	8.94	16.5	1.7	120	300	1080
Nickel	0.9	8.89	13.3	10	200	460	1440

Table 2.6: Comparison of properties of selected alloys of Fe, Al, and Mg as well as common pure Cu and Ni [84]

Specific advantages of Mg alloys include higher relative tensile strength⁵⁷ than Al or steel alloys, and relative elastic modulus⁵⁸ superior to many steels and similar to Al alloys. Further advantages of Mg alloys include superior damping capacity⁵⁹, high thermal conductivity, high dimensional stability, good electromagnetic shielding characteristics, good machinability, and easy recyclability [85]. Despite many

⁵³ AISI-SAE – American Iron and Steel Institute-Society of Automotive Engineers

⁵⁴ Rolled – metal forming where metal stock is passed through a pair of rollers and made flat

⁵⁵ Annealed – heat treatment that increases ductility increasing ease of work with the material

⁵⁶ Electrolytic – derived by electrolysis

⁵⁷ Tensile strength – maximum amount of tensional force over an area, tensile stress, a material can take before breaking

⁵⁸ Elastic modulus – also known as Young's modulus, the ratio of the stress along an axis over strain along the axis up to which a material deforms reversibly/elastically obeying Hooke's Law

⁵⁹ Damping capacity – relative ability of a material to absorb vibration

advantageous properties, industrial use of Mg alloys, although increasing, remains limited due to its poor wear resistance and reactive properties, including poor corrosion resistance and high chemical reactivity, arising, in part, from the very anodic standard electrode potential of pure Mg, $E^\circ = -2.37$ V vs. SHE. Pure Mg corrodes rapidly in humid atmospheric and/or aqueous environments and anions such as Cl^- , Br^- , I^- , and SO_x^- further promote local electrolytic corrosion [86]. Even the limited protections afforded by oxidative films are ineffective in saline environments as chloride solutions, even in small amounts, usually break down the thin protective Mg oxide film [86]. Further limiting the use of Mg alloys is the perception that Mg is flammable, a result of the violent oxidation reaction observed when Mg is heated [87].

While industrial use is at the forefront of Mg alloy applications, potential applications of Mg alloys in medicine are important to bear in mind when investigating properties of Mg alloys. On the medical side, Mg has been investigated for the purpose of biodegradable implants including sutures, stents, and orthopaedic implants [88]. The concept of biodegradable implants dates back to the very early work of physician Edward C. Huse in 1878 with the use of Mg wires as ligatures for bleeding vessels [89]. Though today's ligatures are most often organic polymers which degrade and are absorbed within the body's biological processes, the use of Mg alloys as biodegradable implants has found new life in the resurgence of Mg alloy research. As one of only two biodegradable metals, the other being Fe which oxidizes into ferrous $\{\text{Fe}^{2+}\}$ and ferric $\{\text{Fe}^{3+}\}$ ions subsequently dissolving into the biological media, Mg corrodes into soluble Mg hydroxide $\{\text{Mg}(\text{OH})_2\}$, Mg chloride $\{\text{MgCl}_2\}$, as well as produces hydrogen gas $\{\text{H}_2\}$ which in low quantities can be managed by the body [90]. While comparative studies of Fe and Mg as biodegradable stent materials have shown that Mg is of limited use in vascular applications, with Fe being a superior stent material⁶⁰, Mg alloys have excellent characteristics for use as orthopaedic biomaterials. Beneficial characteristics of Mg as an orthopaedic biomaterial include an elastic modulus, compressive yield strength, and density close to, 16 % more than, bone, an ability to promote osteogenesis, fracture

⁶⁰ As a stent material the low elastic modulus, resulting in poor radial strength of the stents and requiring a larger volume of Mg for thicker struts and larger area of metal–artery interaction in order to provide proper vessel wall support; lack of high ductility, needed to withstand deformation during expansion; and radiolucence, transparency to X-rays, of Mg alloys make Fe a better choice as a stent material [90].

toughness greater than osteogenic ceramic materials such as synthetic hydroxyapatite, and most importantly good biocompatibility with Mg alloys not typically reducing the viability of cells, including nerve and muscle cells [88, 91-95].

2.5.1 Corrosion

Corrosion is the thermodynamically favourable, gradual chemical destruction of materials where the chemical reaction produces one, or more, compound(s) that are more stable than the initial material. Corrosion is a costly process which, in 1995, was estimated to cost the United States \$296 billion per year with as much as 35 %, or \$104 billion, deemed preventable [96]. At the same time, the cost of corrosion related to motor vehicles was estimated at \$94 billion per year with nearly 70 %, \$65 billion, deemed avoidable [96]. More recent estimates of the cost of corrosion have placed the overall cost at in the United States at \$276 billion per year, or approximately 3.1 % of the nation’s gross domestic product (GDP) [97]. Though percentage of avoidable cost corrosion to overall corrosion has been dropping since 1975, due to anti-corrosion technologies, corrosion remains as an economic drag as all metals are prone to corrosion which can significantly hinder material properties, Table 2.7, and shorten the life cycle of machines and infrastructure.

Material	Corrosion rate (µm/year)		Loss of tensile strength after 2.5 years (%)	
	Marine Atmosphere	Industrial Atmosphere	Marine Atmosphere	Industrial Atmosphere
Al Alloy 2024	2.0	2.0	2.5	1.5
Mg Alloy AZ31	18.0	27.7	7.4	11.2
Low Carbon Steel (0.27 %C)	150.0	25.4	75.4	11.9

Table 2.7: Select results of 2.5 year corrosion exposure tests on sheet alloys. [98]

In metals, corrosion is caused by oxidation, the donation of electrons by a material, which increases the metals susceptibility to react with other chemicals in the environment. Corrosion is a natural process that returns refined, pure metals to a lower energy state as they would be found naturally, as ores, in the environment. Notable exceptions to corrosion are gold and platinum as both are found in metallic form in nature due to their more positive standard electrode potentials and hence lower reactivity. Common corrosion products in aqueous systems are oxides and hydroxides; however,

other metal salts may be formed depending on the availability and reactions with chemicals species in the environment.

Thermodynamics and thermodynamic data may be used to determine the spontaneity, or non-spontaneity, of corrosion reactions for specific metals within specified environments by calculating the change in Gibbs free energy, ΔG° , of the system [99]. These calculations center upon a determination of the change in free energy of the system, where a positive change, $\Delta G^\circ > 0$, is indicative of a non-spontaneous reaction and a negative change, $\Delta G^\circ < 0$, is indicative of a spontaneous reaction. The calculation of the free energy may be carried out from actual experimental measurements which give the equilibrium constant, Equation 2.47; from knowledge of the absolute entropies of all substances involved in the reaction and the heats of formation of the compounds involved, Equation 2.48; or, as in the case of electroless deposition, from reversible oxidation potentials, or single electrode potentials, for electrode reactions which can be combined to give the overall corrosion reaction, Equation 2.30 [99].

$$\Delta G^\circ = -RT \ln K \quad (2.47)$$

$$\Delta G^\circ = \Delta H - T\Delta S^\circ \quad (2.48)$$

$$\Delta G^\circ = -nFE^\circ \quad (2.30)$$

where: ΔG° = Change in standard free energy
 R = Gas constant
 T = Absolute temperature
 K = Equilibrium constant.
 ΔH = Change in the heat of reaction, or enthalpy (total energy)
 ΔS° = Standard entropy change in the reaction.
 n = number of equivalents reacting, moles of electrons
 F = Faraday constant, $96\,485 \text{ C}\cdot\text{mol}^{-1}$, or $23.061 \text{ kcal}\cdot\text{V}^{-1}\cdot\text{g}_{\text{eq}}^{-1}$
 E° = Standard electrode potential of the reaction

As in the case of electroless deposition, Equation 2.30 is equivalent to the determination of spontaneity using the standard electrode potentials alone, Equation 2.2, $\Delta G^\circ < 0$ and $E^\circ > 0$ once again indicate a spontaneous reaction, while $\Delta G^\circ > 0$ and $E^\circ < 0$ indicate a non-spontaneous reaction. Calculations of spontaneity rely on the understanding that a spontaneous reaction is the time-evolution of a system in which free energy is released, usually as heat, resulting in the system moving to a lower, and more thermodynamically stable energy state. The process of determining the corrosion products is carried out by determining the possible corrosion products that could form

within the environment and calculating the change in free energy of the system for each possible process. In addition to the spontaneity of corrosion product formation, which can be measured by E° alone, the thermodynamic interpretation provides information on the stability of corrosion products. The interpretation of the stability results from the number of moles taken into account in the determination of ΔG° , where the more negative ΔG° represents greater stability of the corrosion product. For the corrosion of manganese {Mn} in water containing no dissolved oxygen, or hydrogen type corrosion, the stability of corrosion products matches E° with the most positive reaction being the most stable [99], Table 2.8. For the corrosion of Mn in water saturated with dissolved oxygen, or oxygen type corrosion, manganese(III) hydroxide {Mn(OH)₃} is a more stable corrosion product than manganese(II) hydroxide {Mn(OH)₂} despite having a lower E° for the reaction [99], Table 2.8.

Metal	Corrosion Product	E° (V)	ΔG° per g·mol metal (calories)	Spontaneity/Stability
Mn	Mn(OH) ₂	+0.60	-27 600	Spontaneous/Most Stable
Mn	Mn(OH) ₃	+0.256	-17 700	Spontaneous
Mn	MnO ₂	-0.14	+12 700	Non-Spontaneous
Medium: Water unsaturated by oxygen; partial pressure 1 atmosphere (air)				
Mn	Mn(OH) ₂	+1.81	-83 200	Spontaneous
Mn	Mn(OH) ₃	+1.50	-103 000	Spontaneous/Most Stable
Mn	MnO ₂	+1.11	-101 000	Spontaneous
Medium: Water saturated with oxygen; partial pressure of 0.21 atmosphere (air)				

Table 2.8: Comparison of spontaneity and stability for the corrosion of Mn in water with, and without, dissolved oxygen. [99]

Alloying, the introduction of small quantities of other elements into a metal forming a quasi-homogeneous mixture, is a common way to improve and/or modify the natural qualities, including corrosion properties, of the base metal. Alloying improves the qualities of materials via a number of processes. Within both cast and deposited alloys, inhomogeneity of the solid mixture results in secondary particles of crystal structures that differ from the bulk or from other constituents. The differing crystal structures with alloys, known as intermetallics, are defined as solid phases containing two or more metallic elements, or at least one metal and non-metallic element. Paired with heat treatment regiments, alloyed materials can have a vast change in their behaviour compared to the base material or untreated alloy resulting in significant enhancement mechanical properties, such as tensile strength, Table 2.9. The naming of alloys typically

follows the American Society for Testing and Materials (ASTM) standard⁶¹, which uses a two letter-two number system where each number represents the percentage of the element, rounded to the nearest one, associated with the corresponding letter; i.e.: Mg alloy AZ31 contains 3 % Al and 1 % Zn with bulk Mg.

Alloy (ASTM designation)	Alloy Type	Condition	Composition (weight %) [balance Mg]					Tensile Strength (GPa)
			Al	Zn	Mn	Zr	Cu	
AZ31	Wrought	annealed sheet	3	1	0.2	–	–	240
AZ91	Casting	as sand cast	9.5	0.5	0.3	–	–	135
		T4 heat treatment						230
AM50	Casting	as die cast	5	–	0.3	–	–	200
ZK61	Casting	T5 heat treatment	–	6	–	0.7	–	275
ZMC711	Wrought	T6 heat treatment	–	6.5	0.75	–	1.25	325

Table 2.9: Type, condition, composition, and tensile strength of select Mg alloys

The tensile strength of Mg alloys typically ranges from around 120 MPa to 300 MPa depending on the alloy and heat treatment performed, though extraordinary high-strength Mg alloys, ultimate tensile strength of 542 MPa, have been produced using gadolinium, yttrium, zinc, and zirconium, {Mg – 1.8 Gd – 1.8 Y – 0.7 Zn – 0.2 Zr} [100]. While enhancement of mechanical properties is often the desired goal of alloying, the identity and quantity of alloying elements can have a significant impact the corrosion behaviour of the base metal. Creating strong and corrosion resistant materials often requires compromise; some of the strongest Al alloys are alloyed with Cu hindering the corrosion resistance [101]. Additionally, intermetallics formed by alloying may be noble to the base metal matrix, thereby facilitating galvanic corrosion, see Section 2.5.2, or enrich the corrosion product thereby possibly inhibiting the corrosion rate [98]. Like pure metals, intermetallics within a metal possess a distinctive corrosion potentials defined by half-cell measurements similar to the standard electrode potential of metals, Table 2.10.

⁶¹ ASTM Designations: A – aluminum {Al}; B – bismuth {Bi}; C – copper {Cu}; D – cadmium {Cd}; E – rare earths; F – iron {Fe}; H – thorium {Th}; K – zirconium (Zr); L – Lithium {Li}; M – manganese {Mn}; N – nickel {Ni}; P – Lead (Pb); Q – silver {Ag}; R – chromium {Cr}; S – silicon {Si}; T – Tin {Sn}; W – yttrium {Y}; Y – antimony {Sb}; Z – zinc {Zn}

Inter-metallic Compound	Corrosion Potential vs. SHE (V)
Al ₃ Fe	-0.50
Al ₃ Fe*	-0.71
Mg ₁₇ Al ₁₂ Mn	-0.93
Mg ₁₇ Al ₁₂ (β -phase)	-0.96
Mg ₂ Si	-1.41
Mg (99.99 %)	-1.42

* indicates Mn presence.

Table 2.10: Select corrosion potentials of synthetically prepared intermetallic phases after 2 h in de-aerated 5 % NaCl solution saturated with Mg(OH)₂ at pH 10.5 [98].

The half-cell measurements provide the open-circuit, or corrosion, potential of the system, which is defined as the potential of the working electrode relative to the reference electrode in a standard solution when no potential or current is being applied to the cell. The corrosion potential not only provides a measure of the susceptibility of a material to corrosion, it can also provide a comparative measure between uncoated/alloyed samples with those that have been modified to resist corrosion.

While each group of alloys has characteristic corrosion behaviour resulting from properties of the alloy and the presence of certain intermetallics [102], certain elements are preferentially alloyed with certain metals to elicit certain desirable qualities. Aluminum is commonly included in Mg alloys in the amounts of 2 % wt. to 9 % wt. to increase strength, fluidity, ease of casting, along with creep⁶² and corrosion resistance, and can be included up to a maximum solid solubility of 12.7 % at 473 °C [103]. The presence of Al above 2 % wt. results in the formation of Mg₁₇Al₁₂ intermetallics which exist as a β -phase to the bulk Mg α -phase [98]. Low, 2 % wt. to 4 % wt., Al content results in α -phase, Mg, dendrites⁶³ surrounded by the two-phase, $\alpha + \beta$ eutectic⁶⁴ mixture at grain boundaries [98]. Higher concentrations of Al, 6-9 % wt., tend to precipitate distinct β particles along grain boundaries, depending on alloy solidification rates and local concentrations of up to 10 % wt. Al can surround the β phase as a result of micro-segregation during solidification [98]. The Al-rich β -phase results in a low corrosion rate over a wide pH range for Al containing Mg alloys. In alkaline media, the Al component dissolves and a passive Mg-enriched film forms. In neutral and slightly acidic

⁶² Creep – tendency of a solid material to permanently deform under long-term exposure to stress; the tendency increases at higher temperatures closer to the melting point of the material.

⁶³ Dendrite – a crystal that develops with a typical multi-branching, tree-like form.

⁶⁴ Eutectic – a mixture of compounds or elements in which the mixture solidifies at temperature lower than that needed for the solidification of either of the separate constituents

environments the Mg component of the Mg alloy dissolves allowing the formation of a passive Al-enriched film [98]. A variety of microstructures may be produced within Mg alloys by manipulating the Al content and using heat treatment to control the precipitation of intermetallics through the eutectic reaction. Controlling precipitation of the β particles through the eutectic reaction at 28 % wt. Al can produce a variety of microstructures including a lamellar β -phase in heat treated AZ91 Mg alloy [98]. Other elements commonly alloyed with Mg are Zn, which increases the electrochemical nobility of the alloy thereby minimizing the corrosion rate, and Si, which strengthens Mg by the formation of Mg_2Si precipitates in the alloy and is electrochemically just as reactive as pure Mg [98], Table 2.10. Most significant to the corrosion behaviour of Mg alloys is the presence of tramp, or trace, elements that are typically the result of the manufacturing process. The influence of trace elements on the corrosion behaviour of Mg alloys can be significant. Elements to which Mg alloys are most sensitive and which significantly increase the corrosion rate of Mg alloys when present in as little as a few hundred ppm are Fe, Cu, and Ni, Figure 2.20 [98].

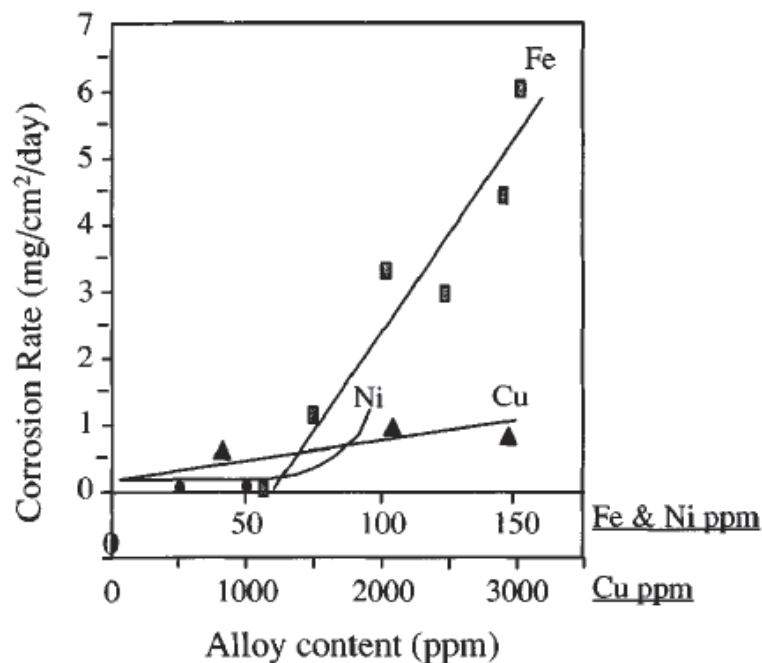


Figure 2.20: Die cast AZ91D salt spray performance versus Fe, Ni, and Cu tramp element content. [98]
 [Figure reproduced from SAE paper No. 850417 [104] © 1989 with the permission of the Society of Automotive Engineers, Inc.]

Mitigation of tramp inclusions within alloys is typically achieved by means of further alloying. The inclusion of Mn, typically below 1 %, helps control the high

cathode corrosion potential of trace Fe, which has a very low solubility of 9.9 ppm in Mg. In the absence of Mn, Fe precipitates as Al_3Fe and behaves like a cathode to the more anodic Mg alloy [98]. In excess, Mn may result in higher corrosion with the formation of binary Al-Mn phases. The beneficial effect of Mn is attributed to the combination of Mn with the Fe causing Fe complexes to precipitate to the bottom of the crucible during alloying and /or reacting with the Fe left in suspension during solidification [98].

2.5.2 Galvanic Corrosion

In addition to the general corrosion experienced from the environment, galvanic corrosion is of serious concern particularly for Mg alloys. Galvanic corrosion occurs wherever two metals of differing nobility are brought together in contact by an electrolyte forming a galvanic cell. Electrochemically, the galvanic coupling of metals results in oxidation of the less noble metal species, while reduction occurs on the other, more noble metal. The open-circuit potential produced across two dissimilar metals immersed within the same electrolyte provides a measure of the galvanic corrosion of the less noble metal relative to the more noble metal. The process of galvanic corrosion is defined by an initial difference in potential, the corrosion, or open-circuit, potential, E_{corr} , between the dissimilar metals generating a corrosion current, I_{corr} , which is responsible for mass transport within the system. Measure of E_{corr} and I_{corr} are dependent not only on the materials comprising the galvanic couple but also the electrolytic environment. For practical purposes, the galvanic series for various metals is given by the anodic index, Table 2.11, where the difference in potential between metals in a galvanic couple should not exceed 0.15 V in harsh, high humidity and salt, environments; 0.25 V in normal environments, such as a warehouse without temperature and humidity controls; and 0.50 V in controlled temperature and humidity environments [105].

Metal Index	(V)
Gold (solid and plated), gold-platinum alloys, wrought platinum, graphite carbon	-0.00
Rhodium plated on silver-plated copper	-0.05
Rhodium plating	-0.10
Silver (solid or plated), high silver alloys	-0.15
Nickel (solid or plated), nickel Copper alloys, titanium and its alloys, Monel metal	-0.30
Copper (solid or plated), low brasses or bronzes, silver solder, nickel silver (CuNiZn), NiCr alloys, CuBe alloys, CuNiSn alloys, CuTi alloys, austenitic stainless steels	-0.35
Yellow brass and bronzes	-0.40
High brasses and bronzes, naval brass, Muntz metal	-0.45
18 %Cr type corrosion-resistant steels, 300 series stainless steels	-0.50
Tin plating, chromium plating, 12 %Cr-type corrosion-resistant metal, 400 series stainless steels	-0.60
Tin-plating (Terne plate), tin-lead solder	-0.65
Lead (solid or plated), high-lead alloys	-0.70
Aluminum; 2000 series wrought aluminum alloys	-0.75
Iron (wrought, gray or malleable), plain carbon and low alloy steels, cold-rolled steel	-0.85
Aluminum alloys other than 2000 series, cast Al-Si alloys	-0.90
Cast aluminum alloys other than Al-Si, cadmium plating	-0.95
Hot-dip galvanized or electro-galvanized steel	-1.20
Wrought zinc, zinc die casting alloys, zinc plating	-1.25
Magnesium & its alloys (cast or wrought)	-1.75
Beryllium	-1.85

Table 2.11: Anodic Index [105]

Galvanic corrosion can result either from internal alloy composition, where a difference in corrosion potential between intermetallic species and/or the bulk of an alloy can promote galvanic corrosion, or external contact between two dissimilar metals within an assembly. Galvanic corrosion arising from alloy composition can, depending on the composition, be limited to the grain boundary, or inter-granular, with no appreciable attack of the grain body or matrix. Most alloys possessing intermetallics are susceptible to inter-granular corrosion; Al alloys containing > 3 % Mg become susceptible due to preferential anodic attack of the Mg_2Al_3 intermetallic [101]. Matching of the corrosion potential within an alloy, such as Mg alloys containing Si, specifically the Mg_2Si intermetallic, is an effective means to limit inter-granular corrosion as no phase is a natural cathode or anode to other phases. In addition to inter-granular corrosion, galvanic corrosion arising from intermetallic species can result in pitting corrosion, defined by the

formation of small pits on the surface of a metal/alloy. Pitting corrosion, often resulting from galvanic corrosion of a surface defect, progresses similar to crevice corrosion, where stagnant liquid in a crevice begins oxidizing the metal and/or its passive layer. Pitting corrosion can propagate quickly below the surface masked by surface corrosion and can remain undetected until mechanical failure occurs. Due to the anodic nature of Mg alloys, pitting of Mg alloys can progress rapidly; alloying Mg with rare earths is an often used method to minimize pitting corrosion of Mg alloys. The high corrosion resistance of Mg alloyed with rare earths appear related to the presence of passive Al-rich zones along the grain boundaries, which act as barriers against pit propagation [98].

Magnesium, the most anodic of all engineering metals, Table 2.1, is prone to severe galvanic attack when coupled to most other metals. One notable exception is the coupling of Mg and very pure Al, Fe content below 200 ppm; the Al forms a passive oxide layer and is similarly anodic producing a negligible galvanic effect [98]. While the interplay between localized sites of differing corrosion potential within an alloy may be remedied by alloying and/or heat treatments [98], neither practise is particularly effective in mitigating external galvanic coupling. An often used remedy to galvanic corrosion is the application of inert spacers/coatings which can also be used for mitigation of general electrolytic corrosion. Within the automotive industry complete sequestration of Mg alloy parts, such as in the dashboard or steering wheel, in plastic is a common to avert corrosion of interior parts.

Another means of corrosion mitigation, often used to prevent the general form of corrosion, is the exploitation of galvanic coupling using a sacrificial anode, a material that is more anodic than the material requiring protection. The placement of a sacrificial anode on a material can protect it from corrosion by changing the potential of the system and allowing for corrosion of the sacrificial anode in place of the material to be protected. Similarly, connecting a direct current (D/C) power supply to the anode and cathode materials in a system of mismatched metals of differing standard electrode potential can be used to oppose the potential difference between the metals and hence eliminate the corrosion current that would be established.

Of the many treatments available for corrosion mitigation, by far the most used is the deposition of metallic coatings. While corrosion resistant claddings are the norm, in

some instances a sacrificial coating may be deposited, rather than a corrosion resistant coating, in order to preserve the integrity of sensitive parts. Metallic coatings, which are typically more mechanically robust than inert organic coatings, can be selected to match almost any metal eliminating galvanic coupling. The complete sequestration of the metal within a cladding prevents electrolytic coupling between the metals and, provided there is negligible diffusion, retains the properties of the coated alloy. For instance, coatings, such as Zn, Cd, or Sn, on steel can substantially reduce the galvanic attack of Mg compared to uncoated steel [98]. Metallic coatings, such as those deposited by electro- or electroless deposition, are often best suited to afford Mg alloys the necessary corrosion resistance to allow for wider industrial use. Controlling for diffusion, ensuring no electrolyte becomes trapped between the alloy substrate and cladding, ensuring any potential intermetallics within the cladding do not create a system where the coating may act as a solid electrolyte, and ensuring the coating has necessary mechanical properties are some of the factors taken into account for corrosion resistant metallic coatings.

2.6 Summary

The purpose of this dissertation is to present the processes and applied solutions for practical problems regarding the galvanic corrosion of magnesium and the deposition of multi-layered coatings. Specifically new work on the electroless coating of magnesium alloys for galvanic corrosion prevention, Chapter 3, selective electroless deposition on silicon, Chapter 4, and new hybrid deposition using wet chemistry techniques, Chapter 5, are presented herein. The background presented within Chapter 2 represents an overview of deposition techniques and coating properties integral to this work. Specifically, hardness and GMR properties, while relevant to the produced coatings, were not measured within this current work. Additionally, detailed and specific mechanisms for the electro- and electroless deposition, such as the identity of metal ion complexes, were not pursued as part of the work or considered beyond what is presently available in literature.

2.7 References

- [1] S. R. Brankovic, N. Vasiljevic, and N. Dimitrov; Chapter 27: Applications to Magnetic Recording and Microelectronic Technologies, in “Modern Electroplating, Fifth Edition”, p.573-615, eds: M. Schlesinger and M. Paunovic, (2010) John Wiley & Sons, Inc., Hoboken, NJ, USA, DOI: 10.1002/9780470602638.ch27
- [2] M. Paunovic, M. Schlesinger; Chapter 5: Equilibrium Electrode Potential, in “Fundamentals of Electrochemical Deposition, Second Edition”, p.55-76, (2006), John Wiley & Sons, Inc., Hoboken, NJ, USA
- [3] D.A. Skoog, F.J. Holler, S. R. Crouch, Chapter 23: Potentiometry, in “Principles of Instrumental Analysis, 6th edition”, p.659-696, (2007), Thomson Brooks/Cole, Belmont, CA, USA
- [4] P. Vanýsek, Section 8: Analytical Chemistry, Electrochemical Series, in “CRC Handbook of Chemistry and Physics, Internet Version 2005”, p.8-23–8-33, ed: David R. Lide, <<http://www.hbcpnetbase.com>>, CRC Press, Boca Raton, FL, 2005.
- [5] M. Paunovic, M. Schlesinger, and D.D. Snyder; Chapter 1: Fundamental Considerations, in “Modern Electroplating, Fifth Edition”, p.1-32, eds: M. Schlesinger and M. Paunovic, (2010) John Wiley & Sons, Inc., Hoboken, NJ, USA, DOI: 10.1002/9780470602638.ch1
- [6] M. Paunovic, M. Schlesinger; Chapter 6: Kinetics and Mechanism of Electrodeposition, in “Fundamentals of Electrochemical Deposition, Second Edition”, p.77-112, (2006), John Wiley & Sons, Inc., Hoboken, NJ, USA
- [7] M. Paunovic, M. Schlesinger; Chapter 16: Structure and Properties of Deposits, in “Fundamentals of Electrochemical Deposition, Second Edition”, p.273-288, (2006), John Wiley & Sons, Inc., Hoboken, NJ, USA
- [8] P. A. Kohl; Chapter 4: Electrodeposition of Gold, in “Modern Electroplating, Fifth Edition”, p.115-130, eds: M. Schlesinger and M. Paunovic, (2010) John Wiley & Sons, Inc., Hoboken, NJ, USA, DOI: 10.1002/9780470602638.ch4
- [9] P. L. Redmond, A. J. Hallock, and L. E. Brus, Electrochemical Ostwald Ripening of Colloidal Ag Particles on Conductive Substrates, *Nano Letters*, 5(1), (2005), p.131-135
- [10] B. Conway, “Electrochemical Kinetics of Hydrogen Evolution at Cu-Ni Alloys: Relation to Electronic Properties of the Electrodes” *Electrochimica Acta*, 1, (1962), p.39
- [11] M. Paunovic, "Chronopotentiometry", *Journal of Electroanalytical Chemistry*, 14(4), (1967), p.447-474, DOI: 10.1016/0022-0728(67)80026-3
- [12] M. Paunovic, “Ligand Effects in Electroless Copper Deposition”, *Journal of the Electrochemical Society*, 124(3), (1977), p.349-354, DOI: 10.1149/1.2133304
- [13] M. Paunovic, “Computer Study of pH Effect in Electroless Copper Deposition”, 125(1), (1978), p.173-174, DOI: 10.1149/1.2131388
- [14] R. P. Seisyan, “Nanolithography in Microelectronics: A Review”, *Technical Physics*, 56(8), (2011), p.1061-1073
- [15] R. A. Robison, “Moore's Law: Predictor and Driver of the Silicon Era”, *World Neurosurgery*, 78(5), (2012) p.399-403

- [16] S. Armini, Z. El-Mekki, J. Swerts, M. Nagar, and S. Demuynck, "Direct Copper Electrochemical Deposition on Ru-Based Substrates for Advanced Interconnects Target 30 nm and 12 Pitch Lines: From Coupon to Full-Wafer Experiments", *Journal of The Electrochemical Society*, 160(3), (2013), p.D89-D94
- [17] J. Belledent, M. Smayling, J. Pradelles, P. Pimenta-Barros, S. Barnola, L. Mage, B. Icard, C. Lapeyre, S. Soulan, L. Pain, "Sub-20nm Hybrid Lithography using Optical plus Pitch-Division and e-Beam, Alternative Lithographic Technologies IV", *Book Series: Proceedings of SPIE*, Editors: W.M. Tong; D.J. Resnick, Vol.8323, Article #:83230F, (2012) DOI: 10.1117/12.916486
- [18] International Technology Roadmap for Semiconductors, 2011 Edition, Lithography, (<http://www.itrs.net>)
- [19] M. Paunovic, M. Schlesinger; Chapter 1: Overview, in "Fundamentals of Electrochemical Deposition, Second Edition", p.1-6, (2006), John Wiley & Sons, Inc., Hoboken, NJ, USA
- [20] G. O. Mallory, Chapter 1: The Fundamental Aspects of Electroless Nickel Plating, in "Electroless Plating: Fundamentals and Applications", Eds: G. O. Mallory, J. B. Hajdu; (1990), American Electroplaters and Surface Finishers, Orlando, Florida
- [21] M. Schlesinger; Chapter 18: Electroless Deposition of Nickel, in "Modern Electroplating, Fifth Edition", p.447-458, eds: M. Schlesinger and M. Paunovic, (2010) John Wiley & Sons, Inc., Hoboken, NJ, USA, DOI: 10.1002/9780470602638.ch18
- [22] R. Petro, M. Schlesinger, and G.-L. Song; Chapter 30: Ionic Liquid Treatments for Enhanced Corrosion Resistance of Magnesium-Based Substrates, in "Modern Electroplating, Fifth Edition", p.665-686, eds: M. Schlesinger and M. Paunovic, (2010) John Wiley & Sons, Inc., Hoboken, NJ, USA. doi: 10.1002/9780470602638.ch30
- [23] M. Schlesinger, X. Meng, D. D. Snyder; "Electroless Ni-Zn-P Films", *Journal of the Electrochemical Society*, 137(6), (1990), p.1858-1859
- [24] W. T. Evans, M. Schlesinger, "The Effect of Solution pH and Heat-Treatment on the Properties of Electroless Nickel Boron Films", *Journal of the Electrochemical Society*, 141(1), (1994), p.78-82
- [25] R.H. Petrucci, W.S. Harwood, and F.G. Herring, Chapter 25: Complex Ions and Coordinate Compounds, in "General Chemistry: Principles and Modern Applications, Eighth Edition", p.985-1023, (2002), Prentice Hall Inc., Upper Saddle River New Jersey
- [26] A. K. Covington and W. Davison, Section 8: Analytical Chemistry, Dissociation Constants of Inorganic Acids and Bases, in "CRC Handbook of Chemistry and Physics, Internet Version 2005", p.8.44-8.45, David R. Lide, ed., <<http://www.hbcpnetbase.com>>, CRC Press, Boca Raton, FL, 2005.
- [27] A. K. Covington and W. Davison, Section 8: Analytical Chemistry, Dissociation Constants of Organic Acids and Bases, in "CRC Handbook of Chemistry and Physics, Internet Version 2005", p.8-46-8-57, David R. Lide, ed., <<http://www.hbcpnetbase.com>>, CRC Press, Boca Raton, FL, 2005.
- [28] M. Paunovic, M. Schlesinger, Chapter 8: Electroless Deposition, in "Fundamentals of Electrochemical Deposition, Second Edition", p.139-168, (2006), John Wiley & Sons, Inc., Hoboken, NJ, USA

- [29] M. Paunovic, "Electrochemical aspects of electroless deposition of metals", *Plating*, 55(11), (1968), p.1161
- [30] M. Paunovic, "Electrochemical Aspects of Electroless Nickel Deposition", *Plating and Surface Finishing*, 70(2), (1983), p.62-66
- [31] Izumi Ohno; Chapter 22: Electroless Deposition of Alloys, in "Modern Electroplating, Fifth Edition", p.499-506, eds: M. Schlesinger and M. Paunovic, (2010) John Wiley & Sons, Inc., Hoboken, NJ, USA. doi: 10.1002/9780470602638.ch22
- [32] N. Feldstein, Chapter 11: Composite Electroless Plating, in "Electroless Plating: Fundamentals and Applications", p.269-287, Eds: G. O. Mallory, J. B. Hajdu; (1990), American Electroplaters and Surface Finishers, Orlando, Florida
- [33] J. P. Marton and M. Schlesinger, "The Nucleation, Growth, and Structure of Thin Ni-P Films", *Journal of the Electrochemical Society: Electrochemical Science*, 115(1), (1968), p.16-21
- [34] C. H. de Minjer and P. F. J. v.d. Boom, "The Nucleation with SnCl₂-PdCl₂ Solutions of Glass Before Electroless Plating", *Journal of the Electrochemical Society: Electrochemical Science and Technology*, 120(12), (1973), p.1644-1650
- [35] M. Paunovic; Chapter 17: Electroless Deposition of Copper, in "Modern Electroplating, Fifth Edition", p.433-446, eds: M. Schlesinger and M. Paunovic, (2010) John Wiley & Sons, Inc., Hoboken, NJ, USA, DOI: 10.1002/9780470602638.ch17
- [36] B.K.W. Baylis, A. Busuttill, N. E. Hedgecock, M. Schlesinger, "Tin(4) Chloride Solution as a Sensitizer in Photo-Selective Metal Deposition", *Journal of the Electrochemical Society*, 123(3), (1976), p.348-351, DOI: 10.1149/1.2132823
- [37] B.K.W. Baylis, A. Busuttill, N. E. Hedgecock, M. Schlesinger, "Long-Lived Sn(IV) Sensitizer Baths for Photo-Selective Metal-Deposition", *Journal of the Electrochemical Society*, 123(9), (1976), p.1376-1377, DOI: 10.1149/1.2133078
- [38] M. Paunovic, M. Schlesinger, Chapter 19: Applications in Semiconductor Technology, in "Fundamentals of Electrochemical Deposition, Second Edition", p.321-331, (2006), John Wiley & Sons, Inc., Hoboken, NJ, USA
- [39] M. Schlesinger, "Ultraviolet Inhibition of Electroless Plating on Glass", *Journal of the Electrochemical Society: Electrochemical Science and Technology*, 121(5), (1974), p.667-668
- [40] J. F. D'Amico, M. A. De Angelo, J. F. Henrickson, J. T. Kenney, and D. J. Sharp, "Selective Electroless Metal Deposition Using Patterned Photo-Oxidation of Sn(II) Sensitized Substrates", *Journal of the Electrochemical Society: Electrochemical Technology*, 118(10), (1971), p.1695-1699
- [41] S. L. Chow, N. E. Hedgecock, M. Schlesinger, and J. Rezek, "The Role of U.V. Light in the Inhibition of Electroless Deposition", *Journal of the Electrochemical Society: Electrochemical Science and Technology*, 119(8), (1972), p.1013-1016
- [42] W. D. Callister Jr., D. G. Rethwisch, Chapter 6: Diffusion, in "Fundamentals of Materials Science and Engineering: An Integrated Approach, 4th Edition"; p.170-199, (2012), John Wiley & Sons, Inc. Hoboken, New Jersey, USA.
- [43] A. van Wijngaarden, M. Schlesinger, N. E. Hedgecock, and B. K. W. Baylis, "Interdiffusion Studies of Au/Ni and Au/Ni-P", *Journal of the Electrochemical Society: Solid-State Science and Technology*, 127(5), (1980), p.1124-1128

- [44] J. Yahalom and O. Zadok, "Formation of Composition-Modulated Alloys by Electrodeposition", *Journal of Material Science*, 22(2), (1987), p.499-503
- [45] M. Matlosz, D. Landolt, R. Aogaki, Y. Sato, J. B. Talbot, "Fundamental aspects of electrochemical deposition and dissolution", *Electrochemical Society Proc.*, New Jersey, 2000, p. 263.
- [46] J. Lamovec, V. Jović, M. Vorkapić, B. Popović, V. Radojević, and R. Aleksić, "Microhardness Analysis of Thin Metallic Multilayer Composite Films on Copper Substrates", *Journal of Mining and Metallurgy Section B – Metallurgy*, 47(1)B, (2011), p. 53 – 61
- [47] F.Z. Ren, S.Y. Zhao, W.H. Li, B.H. Tian, L.T. Yin, A. A. Volinsky, "Theoretical Explanation of Ag/Cu and Cu/Ni Nanoscale Multilayers Softening", *Materials Letters*, 65 (2011) p.119–121
- [48] D. Simunovich, M. Schlesinger, and D.D. Snyder, "Electrochemically Layered Copper - Nickel Nanocomposites with Enhanced Hardness", *Journal of the Electrochemical Society*, 141(1), (1994), L10-L11
- [49] W. F. Smith, with the collaboration of J. Hashemi; Chapter 5: Mechanical Properties of Metals I, in "Foundations of Materials Science and Engineering, 3rd edition", p.181-237, (2004), McGraw-Hill Professional, ISBN: 0072402334
- [50] D. Tabor, Chapter 2: Hardness Measurements by Spherical Indenter, in "The Hardness of Metals", p.6-18, (2000), Oxford University Press
- [51] D. Tabor, Chapter 7: Hardness Measurements with Conical and Pyramidal Indenters, in "The Hardness of Metals", p.95-114, (2000), Oxford University Press
- [52] Standard Test Method for Knoop and Vickers Hardness of Materials, ASTM E384 - 11e1, American Society for Testing and Materials (ASTM) International, West Conshohocken, Pennsylvania, United States
- [53] F. Wredenber, P.-L. Larsson, "Scratch testing of metals and polymers: Experiments and numerics", *Wear*, 266(1–2), (2009), p.76-83
- [54] A. D. Brailsford, "Stress Field of a Dislocation", *Physical Review*, 142(2), (1966), p.383-387
- [55] C. Kittel, Chapter 21: Dislocations, in "Introduction to Solid State Physics, Eighth Edition", p.597-618, (2005), John Wiley & Sons, Inc.
- [56] W. D. Callister Jr., D. G. Rethwisch, Chapter 8: Deformation and Strengthening Mechanisms, in "Fundamentals of Materials Science and Engineering: An Integrated Approach, 4th Edition", p.260-307, (2012), John Wiley & Sons, Inc. Hoboken, New Jersey, USA.
- [57] Y. T. Chou, "Dislocation Pileups and the Hall-Petch Relation", *Canadian Journal of Physics*, 45 (1967), p.559-566
- [58] N. Hansen, "Hall-Petch Relation and Boundary Strengthening", *Scripta Materialia*, 51, (2004) p.801-806
- [59] D. Tench and J. White, "Enhanced Tensile Strength for Electrodeposited Nickel-Copper Multilayer Composites", *Metallurgical Transactions A*, 15(11), (1984), p.2039-2040
- [60] M. Paunovic, M. Schlesinger, Chapter 17: Electrodeposited Multilayers, in "Fundamentals of Electrochemical Deposition, Second Edition", p.289-306, (2006), John Wiley & Sons, Inc., Hoboken, NJ, USA

- [61] K. Uemori and Y. Kaneko, "Fabrication and Vickers Hardness of Electrodeposited Ni-Cu Alloy with Composition Gradient", *Journal of the Japan Institute of Metals and Materials*, 76(5) (2012), p.309-313
- [62] N. Sato, Y. Kaneko, and S. Hashimoto, "Layer Thickness Dependence of Hardness and Microstructure in Electrodeposited Co/Cu Multilayers", *Journal of the Japan Institute of Metals and Materials*, 73(3) (2009), p. 234-237
- [63] M. Schlesinger, Chapter 14: Superlattice Multilayers Formed via Electrochemical Deposition Methods, in "Electrochemical Technology: Innovation and New Developments", p.265-277, Eds: N. Masuko, T. Osaka, and Y. Ito, (1996), Kodansha, Tokyo, Japan; Gordon and Breach Amsterdam, The Netherlands
- [64] C. Kittel, Chapter 12: Ferromagnetism and Antiferromagnetism, in "Introduction to Solid State Physics, Eighth Edition", p.321-360, (2005), John Wiley & Sons, Inc.
- [65] N. F. Mott, "The Electrical Conductivity of Transition Metals", *Proceedings of the Royal Society A*, 153, (1936), p.699-717
- [66] The Royal Swedish Academy of Sciences, AAPPS Bulletin December 2007, Vol. 17, No. 6, Compiled by the Class for Physics of the Royal Swedish Academy of Sciences
- [67] D. Wei, Chapter 1: Exordium, in "Micromagnetics and Recording Materials", p.1-20, (2012), Springer Heidelberg New York Dordrecht London, DOI 10.1007/978-3-642-28577-6
- [68] T. R. McGuire, R. I. Potter, "Anisotropic Magnetoresistance in Ferromagnetic *3d* Alloys", *IEEE Transactions on Magnetics*, 11(4), (1975), p.1018-1038
- [69] S. Zhang, "Spin Hall Effect in the Presence of Spin Diffusion", *Physical Review Letters*, 85(2), (2000), p.393-396
- [70] J. Inoue and H. Ohno, "Taking the Hall Effect for a Spin", *Science*, 309, (2005), p.2004-2005
- [71] R. Karplus and J. M. Luttinger, "Hall Effect in Ferromagnetics", *Physical Review*, 95(5), (1954), p.1154-1160
- [72] T. Miyazaki, Chapter 14: Giant Magnetoresistance Effect in Superlattice Multilayers, in "Electrochemical Technology: Innovation and New Developments", p.279-300, Eds: N. Masuko, T. Osaka and Y. Ito, (1996), Kodansha, Tokyo, Japan; Gordon and Breach Publishers Amsterdam, The Netherlands
- [73] G. Binasch, P. Grünberg, F. Saurenbach, and W. Zinn, "Enhanced Magnetoresistance in Layered Magnetic Structures with Antiferromagnetic Interlayer Exchange", *Physical Review B*, 39, (1989), p.4828-4830
- [74] M. N. Baibich, J. M. Broto, A. Fert, F. Nguyen Van Dau, F. Petroff, P. Eitenne, G. Creuzet, A. Friedrich, and J. Chazelas, "Giant Magnetoresistance of (001)Fe/(001)Cr Magnetic Superlattices", *Physics Review Letters*, 61(21), (1988), p.2472-2475
- [75] C. Chappert, A. Fert and F. Nguyen Van Dau, "The Emergence of Spin Electronics in Data Storage", *Nature Materials*, 6(11), (2007) p.813-823
- [76] J. Bass, W.P. Pratt Jr., "Current-Perpendicular (CPP) Magnetoresistance in Magnetic Metallic Multilayers", *Journal of Magnetism and Magnetic Materials*, 200, (1999) p.274-289
- [77] K. D. Bird and M. Schlesinger, "Giant Magnetoresistance in Electrodeposited Ni/Cu and Co/Cu Multilayers", *J. Electrochem. Soc.*, 142(4), (1995), p.L65-L66

- [78] Advances on Condensed Matter Science: Volume Two; Colossal Magnetoresistive Oxides, ed: Yoshinori Tokura, (2000), Gordon and Breach Science Publishers, The Netherlands
- [79] H Sakurai, "Colossal Magnetoresistance and Magnetism of NaCr_2O_4 ", JPS Conference Proceedings, Proceedings of the 12th Asia Pacific Physics Conference (APPC12), Article: 012006 (2014), p.1-4
- [80] L. Hellwig, C. Beckner, M. Eblen-Zayas, "The Colossal Magnetoresistance Response of EuO_{1-x} Thin Films" American Physical Society, APS March Meeting 2013, March 18-22, (2013), abstract #V1.132
- [81] S. S. P. Parkin, M. Hayashi, L. Thomas, "Magnetic Domain-Wall Racetrack Memory", Science, 320, (2008), p.190-194
- [82] A.G. Dickson & C. Goyet, Chapter 5: Physical and Thermodynamic Data, in "Handbook of methods for the analysis of the various parameters of the carbon dioxide system in sea water, Version 2", Eds: A.G. Dickson & C. Goyet, Prepared for US Department of Energy, Special Research Grant Program 87-7A: Global survey of carbon dioxide in the oceans, (1994), <http://cdiac.esd.ornl.gov/ftp/cdiac74/>
- [83] F. K. Lutgens, E. J. Tarbuck, illustrated by D. Tasa, Chapter 2: Matter and Materials, in "Essentials of Geology, 11th Edition", p.36-61, (2012), Prentice Hall
- [84] L. I. Berger, Section 12: Properties of Solids, Commercial Metals and Alloys, in "CRC Handbook of Chemistry and Physics, Internet Version 2005", p.12-204, David R. Lide, ed., <<http://www.hbcpnetbase.com>>, CRC Press, Boca Raton, FL, 2005.
- [85] Y. Kojima, "Platform science and technology for advanced magnesium alloys", Material Science Forum, 350-351, (2000), p.3-18
- [86] G. L. Song and A. Atrens, "Corrosion Mechanisms of Magnesium Alloys", Advanced Engineering Materials, 1(1), (1999), p.11-33
- [87] United States Automotive Materials Partnership (USAMP) Automotive Metals Division (AMD) at the office of the United States Council for Automotive Research (USCAR), "Magnesium Vision 2020: A North American Automotive Strategic Vision for Magnesium", (2006), <http://www.uscar.org/guest/teams/28/U-S-Automotive-Materials-Partnership>
- [88] R. Petro and M. Schlesinger, Chapter 1: Applications of Electrochemistry in Medicine, in "Modern Aspects of Electrochemistry Vol:56 - Applications of Electrochemistry in Medicine", p.1-32, ed. M. Schlesinger, (2013), Springer Science+Business Media New York, ISBN 978-1-4614-6148-7
- [89] F. Witte, "The history of biodegradable magnesium implants: a review", Acta Biomaterialia., 6, (2010) p.1680-1692
- [90] G. Mani, M. D. Feldman, D. Patel, C. M. Agrawal, "Coronary stents: a materials perspective", Biomaterials 28, (2007), p.1689-1710
- [91] D. Xue, Y. Yun, Z. Tan, Z. Dong, M. J. Schulz, "In vivo and in vitro degradation behavior of magnesium alloys as biomaterials", Journal of Material Science and Technology, 28(3), (2012), p.261-267
- [92] M. P. Staiger, A. M. Pietak, J. Huadmai, G. Dias, "Magnesium and its alloys as orthopedic biomaterials: a review. Biomaterials", 27, (2006), p.1728-1734
- [93] G. L. Song, S. Song, "A possible biodegradable magnesium implant material", Advanced Engineering Materials, 9(4), (2007), p.298-302

- [94] G. L. Song, “Control of biodegradation of biocompatible magnesium alloys”, *Corrosion Science*, 49, (2007), p.1696-1701
- [95] D. F. Williams, Titanium and titanium alloys, in “Biocompatibility of clinical implant materials, vol. II”, Ed. D. F. Williams, Boca Raton, FL, CRC Press, (1981) p. 9-44
- [96] J. Kruger, Chapter 1: Cost of Metallic Corrosion, in “Uhlig's Corrosion Handbook, Second Edition”, Ed: R. W. Revie, (2000), John Wiley & Sons Inc
- [97] G. H. Koch, M. P. H. Brongers, N. G. Thompson, P. Virmani, J.H. Payer, “Corrosion Costs and Preventative Strategies in the United States”, PUBLICATION NO. FHWA-RD-01-156, National Association of Corrosion Engineers (NACE) International & U.S. Federal Highway Administration (FHWA), <http://www.nace.org/uploadedFiles/Publications/ccsupp.pdf>
- [98] E. Ghali, Chapter 44: Magnesium and Magnesium Alloys, in “Uhlig's Corrosion Handbook, Second Edition”, p.793-830, Ed: R. W. Revie, 2000, John Wiley & Sons Inc.
- [99] J. C. Warner, “Thermodynamic Considerations in the Corrosion of Metals”, *Journal of the Electrochemical Society*, 83(1), (1943), p.319-333, DOI: 10.1149/1.3071547
- [100] T. Homma, N. Kunito, S. Kamado, “Fabrication of extraordinary high-strength magnesium alloy by hot extrusion” *Scripta Materialia*, 61(6), (2009), p.644-647
- [101] E. Ghali, Chapter 40: Aluminum and Aluminum Alloys, in “Uhlig's Corrosion Handbook, Second Edition”, p.677-716, Ed: R. W. Revie, (2000), John Wiley & Sons Inc.
- [102] N. Hort, Y. Huang, K. U. Kainer, “Intermetallics in Magnesium Alloys”, *Advanced Engineering Materials*, 8(4), 2006, p. 235–240, DOI: 10.1002/adem.200500202
- [103] E. Ghali, Chapter 9: Properties, Use, and Performance of Magnesium and its Alloys, in “Corrosion Resistance of Aluminum and Magnesium Alloys: Understanding, Performance, and Testing”, p.321-347, (2010), John Wiley & Sons Inc
- [104] K. N. Reichel, K. J. Clark, and J. E. Hillis, “Controlling the Salt Water Corrosion Performance of Magnesium AZ91 Alloy”, SAE Technical Paper, No. 850417, 1985.
- [105] X. C. Tong, Chapter 2: Characterization methodology of EMI shielding materials, in “Advanced Materials and Design for Electromagnetic Interference Shielding”, p.37-66, (2009), CRC Press, Taylor & Francis Group LLC

Chapter 3: Electroless Cladding of Magnesium {Mg}	106
3.1 Introduction to Applications of Magnesium {Mg}	107
3.2 Current Anti-Corrosion Practises	107
3.3 Materials and Methodology	112
3.3.1 Sample Analysis	113
3.4 Results	114
3.4.1 Early Work	115
3.4.2 Electroless Copper {Cu} and Nickel Boron {Ni-B}	129
3.4.2.1 Surface Treatments	137
3.4.2.2 Immersion Coatings and Electrolyte Modifications	141
3.4.2.3 Metallic, Electroless Cu Coating of AZ91D Mg Alloys	160
3.4.3 Electroless Nickel Phosphorous {Ni-P} and Other Binary Alloys	162
3.4.4 Electroless Nickel-Zinc-Phosphorus {Ni-Zn-P} and Other Ternary Alloys	177
3.5 Summary	195
3.6 References	197

3.1 Introduction to Applications of Magnesium {Mg} Alloys

Magnesium {Mg} alloys possess many advantageous properties due largely to low density compared to other metals, such as aluminum {Al}, titanium {Ti}, and steel, iron {Fe}, alloys. Despite the advantageous properties Mg alloys have long been hindered by the high reactivity of Mg which results in corrosion and ultimately the loss of the attractive properties. Options to allow greater industrial use of Mg parts, particularly in the automotive industry, have centered on sequestration measures, often using plastic [1], as fastening Mg alloys to other metals while protecting against galvanic corrosion pose several technical challenges. These challenges essentially require the sequestration of Mg such that it does not chemically react with electrolytes present within the environment that might electrically couple the Mg to another metal, or intermetallics of the alloy, creating a galvanic cell. The establishment of a galvanic cell, either from the electrolyte connecting the metal contact with the alloy or intermetallics within the alloy itself, results in galvanic corrosion, which can cause pitting corrosion, and exists in addition to the more general surface corrosion. As outlined in Chapter 2.5, these corrosion issues take away from the beneficial properties of Mg alloys limiting wider use. As fuel efficiency, by way of lighter vehicles, becomes increasingly essential, the establishment of corrosion resistant, specifically galvanic corrosion resistant, coatings on Mg alloys have become an increasing focus of research especially in the automotive sector. The ideal anti-corrosion coating is defined by a coating which 1) protects the alloy from both general and galvanic corrosions, 2) preserves the bulk conductivity of the substrate, 3) can act as a base coating able to accept further deposits to match other metals, and 4) uses simple techniques allowing for relatively low cost industrial implementation.

3.2 Current Anti-Corrosion Practises

The industrial need of lightweight alloys has resulted in significant research regarding the development of anti-corrosion coatings for Mg alloys. Anti-corrosion studies can be put into one of two broad categories, 1) the deposition of a weakly or non-conducting corrosion resistant layer, often referred to as an interlayer when a subsequent metallic coating is deposited, or 2) the deposition of metallic coatings ‘directly’ on the

Mg alloys, often paired with multi-stepped, sometimes complicated and/or toxic, pre-treatments. In the case of the deposition of an interlayer, the non-conducting nature of the coating is at times sufficient to sequester Mg alloys and prevent corrosion. Examples of weakly/non-conductive coatings include surface conversion treatments where the surface of the Mg alloy is made passive to secondary deposition [2] as well as the coating of the alloy with an organic/resin coating [3, 4], which includes the coatings of organosilicon heat-resisting varnishes to provide an interlayer for subsequent metallic deposition [5].

Conversion treatments can be carried out by exposing surfaces to a number of aqueous electrolytes [2, 6], as well as certain ionic liquids [6]. The more common aqueous-based surface conversion of an Mg alloys typically center upon the creation of less active Mg compounds such as magnesium fluoride $\{\text{MgF}_2\}$, which can be used separately and more often within the metallization electrolyte [7, 8], and magnesium stannate hydrate $\{\text{MgSnO}_3 \cdot \text{H}_2\text{O}\}$ which is used separately from the metalizing electrolyte [2] among many others¹. The $\text{MgSnO}_3 \cdot \text{H}_2\text{O}$ coating was reported to reach a thickness of 3-5 μm after 60 min immersion in an electrolyte containing 10 g/L sodium hydroxide $\{\text{NaOH}\}$, 50 g/L sodium stannate trihydrate $\{\text{Na}_2\text{SnO}_3 \cdot 3\text{H}_2\text{O}\}$, and 10 g/L sodium acetate trihydrate $\{\text{NaCH}_3\text{COO} \cdot 3\text{H}_2\text{O}\}$ at 90 °C [2]; though just as other conversions, the stannate conversion coating requires further metal deposition to establish more robust corrosion resistance. The conversion coatings produced by ionic liquids, such as the ionic liquid formed by the mixture of the tri(hexyl)tetradecyl phosphonium cation and bis(trifluoromethanesulfonyl)amide anion ($\text{P}_{6,6,6,14}^+ \text{TFSA}^-$), result from the unique film-forming environment, an environment free of water, provided by the organic salts [6]. It has been shown that the corrosion current densities conversion films produced on AZ31 Mg alloys by the $\text{P}_{6,6,6,14}^+ \text{TFSA}^-$ electrolyte shift the open-circuit potential of samples to more noble potentials by more than 500 mV, reduce corrosion current densities of in a 0.1 M NaCl aqueous environment by up to 50 times compared to untreated samples, and reduce pitting and corrosion within the Cl^- containing environment [9].

¹ Other aqueous conversion baths include (di)chromate, permanganate, fluoride, phosphate [6].

Much like secondary deposition on passive/converted surfaces, the application of an organosilicon heat-resisting varnish² often requires subsequent pre-treatment and activation for deposition of metallic layers [5]. The deposition of metallic coatings on any weakly/non-conductive interlayer carries with it risks of brittleness, lower mechanical strength, questionable adhesion from bonding either between the interlayer and substrate or the metal and interlayer. Furthermore, depending on the choice of interlayer, the bulk conductivity of the part may be minimization or even altogether eliminated placing the burden of conductivity entirely on the thin film. The coating methods for organic/inorganic organosilicon coatings varies and includes coatings that dry quickly upon removal from a dip [3]; varnishes that require baking at 180 °C post dip [5]; and the plasma enhanced chemical vapor deposition (PECVD) of silicon containing organic compounds for the purpose of creating inorganic SiO_x coatings [4]. The use of organic and resin coatings is a widely researched anti-corrosion method in part due to the simplicity of the procedure which, in most cases, requires only a short dip in the resin bath allowing for inline inclusion within the assembly process. Direct application of a resin coating is exemplified by the 10 s immersion of Mg alloys in a ‘Du Pont, Electroshield 21 Gray Bath’, containing 71-82 wt. % water, 16-26 wt. % epoxy resin, and 1.3 wt. % titanium dioxide [3]. The coatings produced by the immersion in the resin dry quickly and produce coatings that are sufficient to reduce corrosion rates [3]. Given the limitations of non-metallic and organosilicon-based coatings, the direct coating of Mg alloy substrates is also well studied for industrial applications.

The application of non-metallic coatings is also of significant interest for medical applications where pure Mg and Mg alloys have garnered interest as biodegradable implants [10-12]. In the case of a biodegradable implant, the coating on the Mg-based material is in place to regulate and slow the corrosion of Mg rather than eliminate it entirely [10, 13]. The effectiveness/value of Mg as an orthopaedic material is centered upon the solubility of Mg compounds produced as well as close matching of the properties of the metal, such as density, to bone itself, Chapter 2.5. Coatings for orthopaedic purposes often include calcium hydroxyapatite {Ca₅(PO₄)₃(OH)}, also

² Specific varnish used in that study was the “8604 organosilicon heat-resisting varnish” from Changjiang Paint Co. Ltd. which requires baking prior to any activation procedure.

known simply as either hydroxyapatite or as hydroxylapatite. Hydroxyapatite is a naturally occurring component of bone and is used as a synthetic analogue to the naturally occurring inorganic mineral phase of bone itself, carbonated hydroxyapatite [13]. The inclusion of $\text{Ca}_5(\text{PO}_4)_3(\text{OH})$ either as a second layer [11] on, or as nanoparticles within, biodegradable organic films, such as poly(lactic acid) and poly(ϵ -caprolactone), which are in some ways similar to organic coatings for industrial purposes. The organic coatings incorporation hydroxyapatite allow for the production of biologically active and safe implants with acceptable corrosion rates which allow sufficient time for healing and promote cell attachment, cell growth, and cell proliferation [12]. Understanding of the effectiveness of these coatings within the human body is at present only in the early stages of development due to in part to disagreements on proper analogues to extracellular fluid, a lack of an electrochemical understanding of *in vivo* corrosion, and few animal trials [13].

The insufficiencies of poorly/non-conductive and organosilicon-based coatings, including potential brittleness and lower mechanical strength, have necessitated the continued study of the direct metallic coating of Mg alloy substrates for industrial applications. The deposition of metallic coatings directly on the Mg alloys is often somewhat of a misnomer as conversion treatments routinely occur within the metalizing electrolyte if such treatments are not part of the multi-stepped, sometimes complicated and/or toxic, pre-treatment process. A large number of past and ongoing studies use various pre-treatments as a means to overcome the reactivity of Mg alloys within electrolytes. Common pre-treatments include pickling, activation, and zinc immersion treatments all of which play important roles in the deposition of metallic coatings on Mg alloys as they strongly influence the adhesion, corrosion resistance, and structure of the plated coatings [7]. Pickling, the first step in most pre-treatment processes, is defined as the removal of loose films, including oxides, hydroxides, embedded sand, passivation film, dust, and lubricants for the surface of Mg alloys [7]. Activation, required to catalytically or electrically activate the surface for electroless and electroplating, respectively, is a passivation process carried out in order to allow deposition and avoid fierce replacement and corrosion reactions between the bare Mg alloy matrix and the plating solution [7]. Zinc immersion is the term used for the coating of a substrate with a

transition zinc layer and is carried out on Mg substrates in order to reduce the potential difference, galvanic corrosion, between Mg alloy substrates and the subsequent coatings, such as Cu or Ni [7]. Zinc immersion is also widely used to increase the conductance of Mg substrates for electrodeposition and increase the adhesion between substrates and coatings [7]. The purpose of pre-treatments can generally be separated into 3 categories: 1) surface cleaning/degreasing, or pickling; 2) surface activation/catalytic, or activation, which in some instances includes zinc immersion; and 3) pre-treatments to render the substrate passive, commonly known as passivation pre-treatments, of which activation and zinc immersion both play part.

One of the more common activation pre-treatments for Mg alloys is the use of hydrofluoric acid {HF} to form MgF_2 on the surface of the alloy. The primary utility of the MgF_2 films is the prevention of excessive dissolution of Mg alloys due to strong adhesive attraction to the substrate and insolubility [7], as well as prevention of oxidation of the surface in the electrolyte [14]. Though the production of MgF_2 activation films are not suitable for electroplating without a prior zinc immersion, MgF_2 pre-treatment films are suitable for direct electroless Ni-P plating. The direct electroless plating of the converted/activated surface is carried out by the replacement of the film with Ni-P and subsequent deposition by the growth and coalescence of Ni-P nuclei [7, 14]. The appeal of HF pre-treatments for Mg alloys lies not only with the ease of use but also with the decrease in toxicity compared to standard activation pre-treatments, such as those using chromic acid { H_2CrO_4 }. The purpose of the chromic acid treatment is the formation of chromium(III) oxyhydroxide { $CrOOH$ } on the surface of Mg alloys which serve to etch the surface as well as protect/insulate the Mg substrate from corrosion [7]. It should be understood that while less toxic than H_2CrO_4 activation treatments, which use hexavalent chromium { Cr^{6+} }, the use of HF, or similar F^- containing chemicals, for MgF_2 activation of Mg alloys do pose significant health hazards³ [15].

In addition to the application of activation pre-treatments, certain compounds used for the chemical activation of Mg alloy surfaces can also be incorporated into electrolytes for the deposition of Ni-P. The most common activation additives for the production of MgF_2 are HF or ammonium hydrogen difluoride { NH_4HF_2 } [7, 8], which

³ In addition to being corrosive, fluoride can cause fluorosis which damages bones and joints. [15]

produce MgF₂ films on Mg alloys. While MgF₂ itself is well adhered to the surface of the alloy, as reported by others [14] some uncertainties exist as to the adhesion of the coatings. When incorporated directly into the metalizing electrolyte, HF, despite its highly corrosive nature, is expected to form MgF₂ and slow corrosion on the surface of the Mg alloy similar to the film produced from by the pre-treatment process. Furthermore, as with the HF pre-treatment itself, inclusion of HF within the electrolyte often results in micro-porous coatings as a consequence of low coating density [16, 17], for which further deposition, such as a layer of Ni-B, is required [8].

3.3 Materials and Methodology

The Mg alloy substrates used within the body of this work were the AZ91D and AM50 Mg alloys, Table 3.1, which are commonly used in the automotive sector and were supplied by researchers at General Motors.

Alloy	Al	Zn	Mn	Ni	Cu	Si	Fe	Mg
AZ91D	8.3-9.7	0.35-1.0	0.5-0.15	<0.002	<0.03	<0.10	<0.005	Balance
AM50	4.9	0.5-0.2	0.45	<0.01	<0.008	<0.05	<0.004	Balance

Table 3.1: Nominal compositions of the AZ91D and AM50 Mg alloys by wt. %

The Mg alloy substrates were cut into coupons of varying size no smaller than 1.85 cm × 2.3 cm × 0.3 cm. The cut samples were normally wet polished using a LECO SS200 grinder/polisher, most often using 240-grit SiC emery paper, to ensure a uniform surface and remove any potential surface contaminants. Polishing was most often conducted in the vertical sense so as to minimize the trapping of hydrogen gas liberated as part of the anodic reaction. In some instances the grinder/polisher was used to round the edges of the samples. After polishing, the samples were wiped clean with laboratory clean wipes and were left out to oxidize. In most cases a hole was drilled at the top of the large face of the sample to hang the sample within the electrolyte. In early experiments, Section 3.4.1, thin strips of folded over masking tape, or tape string, were used as a non-conducting wire to hold the samples. The tape strings later replaced by an inert, non-conducting polymer wire, Mako (10 lbs.) fishing line. The deposition procedure used beyond sample preparation varied based on the process and electrolyte investigated and further details as to both are provided in the various results sections of Section 3.4. It should be noted that a number of different preparation methods were explored in early

work conducted on Mg metallization; those procedures along with subsequent metallization are presented within Section 3.4.1.

3.3.1 Sample Analysis

Macroscopic images of the samples were taken using a Hewlett-Packard Scanjet G4010 scanner at a resolution of 600 dpi (dots per inch) or, in those instances where samples could not be adequately scanned, a 7.2 Megapixel Sony Cyber-shot digital camera using the macro setting. Scanning electron microscope (SEM) images were taken using an FEI Quanta 200 Environmental SEM with a Field Emission Gun (FEG) the beam strength kept between 10 kV and 20 kV. Compositional analysis of the claddings was obtained using energy-dispersive X-ray spectroscopy (EDS) as part of the SEM system. Acquisition of the EDS data occurred using an EDAX SiLi Detector with Super Ultra Thin Window (SUTW) and EDAX Genesis software. Analysis of all samples, including those discussed in Chapters 4 and 5, was carried out using the same equipment and general procedures.

The use of EDS provided the average composition of the outer few microns of the deposit weighted toward the outer layers of coating. The beam strength/potential used for EDS measurements also varied between 10 kV and 20 kV as in acquisition of SEM images. The selection of beam strength for EDS measurements was a compromise between higher beam strengths, which provided for better and more rapid EDS data acquisition but deeper x-ray penetration into the coating, and lower beam strengths, which resulted in slower data acquisition but provided for less penetration into the coating thereby producing a better compositional analysis of the surface. The choice of beam strength was also dependent on coating thickness as well as composition given that x-ray penetration is shallower in coatings comprised of heavier elements. A common feature of backscatter SEM images is darker regions surrounding larger grains which are due to shadowing from elevation differences. Other dark regions between grains are most often the cause of minor divots in the coating due to H₂ bubbles from the anodic reaction as well as a lack of agitation of the solution. Additionally, striations seen on the surface of samples, in both macroscopic and SEM images are the result of surface polishing.

3.4 Results

Fundamentally, there are two issues to overcome in order to deposit a metal onto Mg alloys; 1) corrosion of Mg in the electrolyte and 2) galvanic corrosion between nucleated metal, and/or grains, and the Mg alloy substrate. As presented in Section 3.2 of this chapter, many different methods have been proposed to mitigate and eliminate various forms of corrosion experienced by Mg alloys. The techniques proposed often are multi-stepped, complex, toxic, or produce coatings that are not functional over a wide range of applications. Notably, rendering the surface passive for electroless deposition; while helping to mitigate in situ corrosion as well as poor adhesion from stress within a rapidly deposited coating; can itself result in poor adhesion of the coating, or hinder the properties of the metal by creating an insulating barrier between a metallic coating and the metal substrate.

The electroless deposition of corrosion resistant, specifically galvanic corrosion resistant, claddings on Mg alloys was here established by considering many different processes and electrolytes. Early work centered on achieving an initial understanding of the interaction between Mg and various electrolytes and included the replication and modification electroless plating techniques put forward by other researchers for the cladding of Mg alloys. Once a good understanding of the limitation of other methods was established, work was conducted on achieving a minimalist process for the cladding of Mg alloys that 1) provided galvanic corrosion resistance, 2) provided a simple method of substrate preparation, 3) provided a simple deposition procedure, 4) used electrolytes similar to those currently used in industry, and 5) limited toxicity of the electrolyte.

Given the large number of important results obtained regarding the galvanic corrosion resistant cladding of Mg alloys, this section, 'Results', is divided into four sections which follow the chronological order in which the work was completed. Section 3.4.1, 'Early Work', represents initial work on understanding the relationship between common electrolytes and Mg alloys as well as the replication and modification electroless plating techniques put forward by outside studies. Sections 3.4.2, 3.4.3, and 3.4.4 contain work previously co-published by the author of this dissertation in the Journal of the Electrochemical Society in the form of three separate papers. Specifically, Section 3.4.2, 'Electroless Cu', contains the work presented within "Direct Electroless Deposition of

Nickel Boron Alloys and Copper on Aluminum Containing Magnesium Alloys” [18]; Section 3.4.3, ‘Electroless Ni-P’, contains the work presented within “Direct Electroless Deposition of Low Phosphorous Ni-P Films on AZ91D Mg Alloy” [19]; Section 3.4.4, ‘Electroless Ni-Zn-P’, contains the work presented within “Direct Electroless Deposition of Ni-P-Zn Films on AZ91D Mg Alloy” [20]. It should be noted that the term “direct” as it applies to this body of work refers to Mg alloys having undergone minimal surface treatment that is limited to mechanical polishing/preparation of the surface. Testing was not conducted to determine whether a non-conductive interlayer formed as part of the natural electroless metallization process. Additional details concerning the metalizing electrolytes used throughout sections 3.4.2, 3.4.3, and 3.4.4 are found in Appendix A.

3.4.1 Early Work

Initial experiments on the electroless cladding of Mg alloys focused on the behaviour of Mg alloys in known electrolytes and on replicating the work of others in connection with corrosion resistant claddings on Mg alloys. The early work concerning Mg alloys was conducted principally using AZ91D coupons machined to dimensions in the range of 10 mm – 25 mm × 20 mm – 40 mm × 3 mm – 10 mm. Several experiments were conducted as part of the initial testing for the provision of corrosion resistant claddings in order to determine the criteria for adequate corrosion resistant thin film deposits on Mg alloys. The electrolytes chosen for those experiments were of the Ni-P and Ni-B varieties as both Ni alloys are known to be corrosion resistant; in particular Ni-B alloys are known to be mechanically hard alloys, reaching up to 1500 kg/mm² Vickers hardness after annealing [21]. It should be noted that due to the large body of work, the experiments discussed within this section include only the most significant. Results of note include deposition of Ni-P from typical acidic deposition baths; the deposition of Ni-B from an alkaline deposition bath; the passivation of the Mg alloy for subsequent Ni deposition, Huo et.al. [2]; and the deposition of Ni-P from an acidic deposition bath containing hydrofluoric acid {HF}, Zhang et al. [8]. As a first step, both oxidized and polished samples were exposed to Sn/Pd activation, Table 3.2a, followed by metallization an acidic electroless Ni electrolyte, Table 3.2b.

Deposition Steps	Chemical Name	Chemical Formula	Bath Composition	Step Details
Sensitization	Tin Chloride	SnCl_2	10 g/L	pH 1.42, 20 s, 25 °C
	Hydrochloric Acid (36.5 % - 38 %)	HCl	5 mL/L	
H ₂ O Rinse	Water	H ₂ O	Distilled H ₂ O	pH 7, 20 s, 25 °C
Activation	Palladium Chloride	PdCl_2	0.4 g/L	pH 2.34, 20 s, 25 °C
	Hydrochloric Acid (36.5 % - 38 %)	HCl	0.5 mL/L	
H ₂ O Rinse	Water	H ₂ O	Distilled H ₂ O	pH 7, 20 s, 25 °C

Table 3.2a: Pre-treatment process by J. Marton and M. Schlesinger (1968) [22]

Deposition Steps	Chemical Name	Chemical Formula	Bath Composition	Step Details
Ni-P Metallization	Nickel Sulphate Hexahydrate	$\text{NiSO}_4 \cdot 6\text{H}_2\text{O}$	29.5 g/L	pH 4.7-5.3 2-20 min 65 °C
	Sodium Hypophosphite Hydrate	$\text{NaPH}_2\text{O}_2 \cdot \text{H}_2\text{O}$	17.5 g/L	
	Sodium Succinate	$(\text{NaOOCCH}_2)_2$	15.0 g/L	
	Succinic Acid	$\text{C}_4\text{H}_6\text{O}_4$	1.5 g/L	

Table 3.2b: Electroless Ni-P electrolyte formulation by J. Marton and M. Schlesinger (1968) [22]

The process described in Table 3.2 has several major issues due to the acidity of all electrolytes at each step of the process. Both the sensitising Sn bath and the activation Pd bath provide a corrosive environment for the Mg alloy from which even oxidized surfaces offer little protection. The corrosion from the acidic environments not only contaminated the pre-treatment baths with Mg, but galvanic corrosion between the Mg substrate and Pd nucleation sites continued the corrosion in the post-Pd rinse bath as well as the metalizing electrolyte. Metallization within the acidic electrolyte liberated large amounts of hydrogen {H₂} gas as a corrosion reaction occurred in parallel with the anodic reaction. Deposits formed from this process were very thin as the metallization bath decomposed due to the free catalytic particulate within the bath providing nucleation sites. Given the aggressive reaction of the pre-treatment and metalizing electrolytes, passivation of the surface was explored as a method of providing corrosion resistant claddings. Keeping the same metalizing electrolyte and pre-treatment process,

Table 3.2, the stannate conversion treatment, Table 3.3, was explored means to diminish the corrosion reactions in the acidic sensitizing and activation electrolytes, Table 3.2a.

The goal of the conversion as laid out by Huo et al. [2] is the formation of magnesium stannate hydrate $\{MgSnO_3 \cdot H_2O\}$ on the surface of the alloy upon which sensitization and activation are carried out. After the chemical surface conversion of the AZ91D alloys was complete, activation and metallization steps, as summarized in Table 3.2, were carried out. The deposits produced on the converted surface from the acidic electrolyte initially appeared dark with the colour changing to a light grey, likely due to oxidation, as the coating dried. In addition to the stone-like appearance, Figure 3.1, the deposits produced were very brittle, crumbling easily. The brittleness of the deposit was attributed to the oxidizing environment provided by the intense H_2 evolution liberated by the deposition and corrosion reactions.

Step	Chemical Name	Chemical Formula	Bath Composition	Step Details
Pre-cleaning	Hydrochloric Acid (36.5 % - 38 %)	HCl	3 % HCl solution	pH 1.4, 2 min, 25 °C
H ₂ O Rinse	Water	H ₂ O	Distilled H ₂ O	pH 7, 20 s, 25 °C
Degreasing	Acetone	(CH ₃) ₂ CO	Pure Acetone	pH 1.8, 60 s, 25 °C
Stannate Chemical Conversion (Passivation)	Sodium Hydroxide	NaOH	10 g/L	pH 12.5, 60 - 120 min, 90 °C, Light agitation
	Sodium Stannate	Na ₂ SnO ₃	50 g/L	
	Sodium Acetate	NaCH ₃ COO	6 g/L	
H ₂ O Rinse	Water	H ₂ O	Distilled H ₂ O	pH 7, 30 s, 25 °C
Drying	Open atmosphere for at least 24hours prior to further treatments.			

Table 3.3: Stannate surface conversion treatment for Mg alloys as modified from Huo et al. [2]

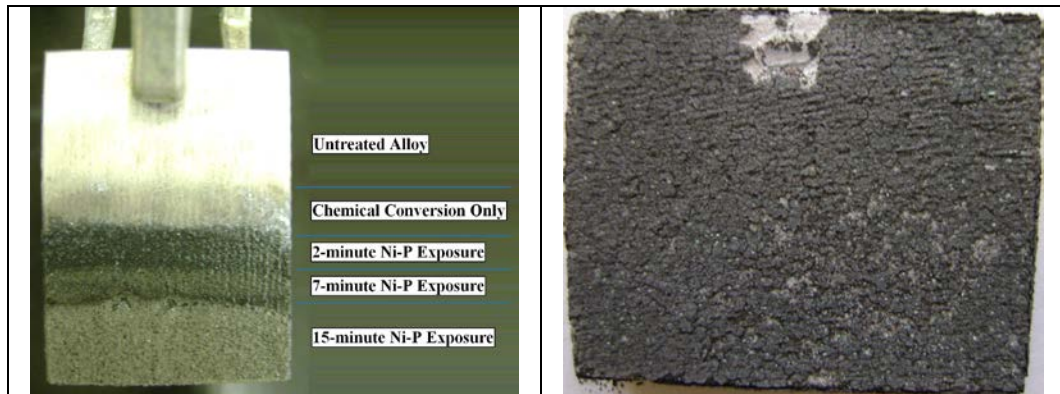


Figure 3.1: (Left) Incremental and (Right) 30 minute deposits of acidic Ni-P deposit on stannate surface converted AZ91D Mg alloy. Deposition process: cleaning/etching in a 3 % HCl solution [2 min, 25 °C], acetone rinse [2 min, 25 °C], stannate conversion treatment [60 min, 85 °C], sensitization, activation, and Ni-P metallization in accordance with Table 3.2.

Along with the acidic electrolytes, an alkaline Ni-P electrolyte was tested for the metallization of the stannate conversion surface, Table 3.4. Deposition from the alkaline electrolyte occurred with light agitation from a magnetic stir bar.

Deposition Steps	Chemical Name	Chemical Formula	Bath Composition	Step Details
Alkaline Ni-P Metallization	Nickel Sulphate Hexahydrate	$\text{NiSO}_4 \cdot 6\text{H}_2\text{O}$	30.0 g/L	pH 8.0 7 min 60 °C, Light agitation
	Sodium Hypophosphite Hydrate	$\text{NaPH}_2\text{O}_2 \cdot \text{H}_2\text{O}$	10.75 g/L	
	Sodium Citrate Tribasic Dihydrate	$\text{Na}_3\text{C}_6\text{H}_5\text{O}_7 \cdot 2\text{H}_2\text{O}$	10.0 g/L	
	Ammonium Chloride	NH_4Cl	53.75 g/L	

Table 3.4: Common alkaline Ni-P metallization electrolyte [23]

During deposition, a black magnetic Ni precipitate was observed in the electrolyte. The magnetic precipitates were assumed to be caused by a combination of dislodged poorly adhered nucleation sites due to agitation as well as some corrosion of the sample due to dissolution of the conversion layer during pre-treatment and/or metallization steps. Darkening of the sample occurred after 2 minutes and the sample possessed a dark, grainy surface once it was removed from the electrolyte after 7 minutes. As mentioned in Section 2.5.1, acidic environments, especially those containing Cl^- anions produce intense corrosion responses. At this stage of the research, the grainy condition of the deposit was not linked to Cl^- ions and electrolytes of this type were

revisited once a good understanding of issues surrounding the electroless cladding of Mg were better understood, Section 3.4.3. To this end the presence of Cl^- ions were not recognized as potentially harmful to thin film deposition on Mg alloys for the deposition of Ni-P and Ni-B thin films.

As a final test of the conversion coatings, Ni-B was electroless deposited on a converted AZ91D Mg alloy surface as well as an acid etched surface; both processes followed alkaline cleaning of previously polished surfaces, Table 3.5. The deposition of Ni-B, which can only be achieved from alkaline media, Table 3.6, resulted in substantial deposition over the surface of the Mg alloys, though corrosion was also visibly present with the formation of Mg oxide/hydroxide $\{\text{Mg}(\text{O})_x/(\text{OH})_y\}$ complexes.

Deposition Steps	Chemical Name	Chemical Formula	Bath Composition	Step Details
Alkaline Cleaning	Sodium Hydroxide	NaOH	45 g/L	pH 14, 10 - 20 min, 65 °C
	Sodium phosphate Tribasic Dodecahydrate	$\text{Na}_3\text{PO}_4 \cdot 12\text{H}_2\text{O}$	10 g/L	
H ₂ O Rinse	Water	H ₂ O	Distilled H ₂ O	pH 7, 20 s, 25 °C
Pre-Treatment Option 1				
Acidic Etch	Phosphoric Acid (85 %)	H ₃ PO ₄	150 mL/L	2 min, 25 °C
	Acetic Acid	CH ₃ COOH	200 mL/L	
	Ethanol	CH ₃ CH ₂ OH	500 mL/L	
	Nitric Acid (80 %)	HNO ₃	50 mL/L	
Ni-B Metallization				
Pre-Treatment Option 2				
Stannate Chemical Conversion (Passivation)	Sodium Hydroxide	NaOH	10 g/L	pH 12.5, 60 - 120 min, 90 °C Light agitation
	Sodium Stannate	Na ₂ SnO ₃	50 g/L	
	Sodium Acetate	NaCH ₃ COO	6 g/L	
Air Dry of the Conversion Coating				
Ni-B Metallization				

Table 3.5: Electrolytes for the pre-treatment of AZ91D Mg alloy samples prior to metallization from a Ni-B electrolyte. Acidic etch electrolyte is based on that provided within Zhang et al. [8], Note: No Sn/Pd activation occurred on the surface of the stannate conversion surface.

Bath	Chemical Name	Chemical Formula	Bath Composition
Bath A	Nickel Chloride Hexahydrate	$\text{NiCl}_2 \cdot 6\text{H}_2\text{O}$	60.0 g/L
Bath B	Sodium Hydroxide	NaOH	80.0 g/L
	Ethelenediamine (>99.5 %)	$\text{H}_2\text{NCH}_2\text{CH}_2\text{NH}_2$	120 mL/L
	Sodium Borohydride	NaBH_4	9.6 g/L
Operating Temperature: 80 to 90 °C			

Table 3.6: Electroless Ni-B electrolyte formulation modified from Gorbunova et al. (1973) [21]

The $\text{Mg(O)}_x/(\text{OH})_y$ complexes, include the formation of Mg(OH)_2 , MgO and other more complex oxide hydroxide products. The growth of $\text{Mg(O)}_x/(\text{OH})_y$ crystallites on the surface of the acid pre-treated surface post-metallization were, at least in one case, sufficient to shed the coating from the surface, Figure 3.2. The shed coating, which was colloquially name the “Hulk”⁴ coating, appeared to have been lifted from the surface by the growing crystallites. The lack of metallization of the crystallites, which is expected of non-conductive and non-catalytic oxides, indicates that such formations must be mitigated as sequestration under a deposit is, at best, impractical.



Figure 3.2: Electroless Ni-B “Hulk” coating of an AZ91D Mg alloy substrate. Deposition Process: fly cut sample, 15 min alkaline cleaning at 50 °C, 2 min acidic pre-treatment at 25 °C, 3 h metallization at 90 °C.

Despite the damage and removal of the coating from the surface, the Ni-B deposit retained the smoothness expected of Ni-B thin films indicating that significant autocatalytic metallization took place. Reducing the duration of the metallization determined that the formation of the $\text{Mg(OH)}_x/\text{O}_x$ crystallites occurred simultaneously with the coating formation, Figure 3.3, for both stannate and acid pre-treated samples.

⁴ The term “Hulk” deposit came about due to the fact the coating, while shed by out of control oxidation, remained intact much like the pants of the Marvel comics character “The Incredible Hulk”.



Figure 3.3: Electroless Ni-B coatings on fly-cut AZ91D Mg alloys; (Left) Deposition Process: 15 min alkaline cleaning at 50 °C, 2 min acidic pre-treatment at 25 °C, 45min metallization of the lower half of the sample at 90 °C; (Right) Deposition Process: 20min alkaline cleaning at 57 °C, 60 min stannate conversion at 90 °C, 45 min metallization of the entire sample at 85 °C

The presence of crystallites on the stannate converted surface, though smaller even with the 300 % longer metallization compared to the acidic treatment, indicated that conversion of the surface was not an effective means of providing corrosion protection within the metalizing electrolyte. Moreover, the apparent rainbow-like shine of the dried stannate conversion illustrated the difficulty in establishing a uniform surface. Further issues arising from the stannate surface conversion treatment, in addition to the difficulty in the formation of a uniform surface conversion, included poor/inconsistent adhesion and an the insulating nature of the stannate layer. The questionable protection from the electrolyte afforded by the stannate layer along with the lack of reliable adhesion and the insulating nature of the layer between the substrate and metallic thin film led to the exploration of other, pre-treatments regiments outside of passivation.

Aside from passivation techniques, prominent pre-treatment regiments for the metallization of Mg alloys involve acidic environments meant to etch and electrochemically activate the surface. Many forms of acidic pre-treatment exist and several variations were produced and attempted based on the work of Zhang et al. [8], Table 3.7. In addition to a more robust acidic pre-treatment and the addition of manganese {Mn} to the acidic etch; the metalizing electrolytes make use of fluoride {F} ions in order to minimize the corrosion of the Mg substrate within the metalizing electrolyte.

Deposition Steps	Chemical Name	Chemical Formula	Bath Composition	Step Details
Alkaline Cleaning	Sodium Hydroxide	NaOH	45 g/L	pH 14, 10 - 20 min, 65 °C
	Sodium phosphate Tribasic Dodecahydrate	Na ₃ PO ₄ · 12H ₂ O	10 g/L	
H ₂ O Rinse	Water	H ₂ O	Distilled H ₂ O	pH 7, 20 s, 25 °C
Acidic Mn-cocktail Pre-treatment	Manganese Dihydrogen Phosphate	Mn(H ₂ PO ₄) ₂	5 g/L	2 min, 25 °C
	Phosphoric Acid (85 %)	H ₃ PO ₄	150 mL/L	
	Acetic Acid	CH ₃ COOH	200 mL/L	
	Ethanol	CH ₃ CH ₂ OH	500 mL/L	
	Nitric Acid (80 %)	HNO ₃	50 mL/L	
H ₂ O Rinse	Water	H ₂ O	Distilled H ₂ O	pH 7, 20 s, 25 °C
Ni-P Metallization	Nickel Sulphate Hexahydrate	NiSO ₄ · 6H ₂ O	15.0 g/L	pH 5.0, 40 min, 90 °C
	Sodium Hypophosphite Hydrate	NaPH ₂ O ₂ · H ₂ O	26.0 g/L	
	Sodium Acetate	NaCH ₃ COO	13.0 g/L	
	Hydrofluoric Acid (40 %)	HF	12.0 mL/L	
	Ammonium Hydrogen Difluoride	NH ₄ HF ₂	8.0 g/L	
	Thiourea	SC(NH ₂) ₂	0.076 g/L	
H ₂ O Rinse	Water	H ₂ O	Distilled H ₂ O	pH 7, 20 s, 25 °C
Ni-B Metallization	Nickel Chloride Hexahydrate	NiCl ₂ · 6H ₂ O	30.0 g/L	pH > 13, 4 h, 85 °C
	Ethelenediamine (>99.5 %)	H ₂ NCH ₂ CH ₂ NH ₂	100 mL/L	
	Sodium Borohydride	NaBH ₄	0.794 g/L	
	Sodium Hydroxide	NaOH	90.0 g/L	
	Thiourea	SC(NH ₂) ₂	0.001 g/L	

Table 3.7: Composition and operating conditions for the pre-treatment and subsequent Ni-P and Ni-B metallization of Mg alloys. Formulation modeled after Zhang et al. [8]

The acidic nature of the Ni-P metallization bath provides an environment whereby corrosion occurs simultaneously with the metallization reaction. In addition to the stabilizing role of F^- ions, the concentration of thiourea $\{SC(NH_2)_2\}$ within the electrolyte was determined to be a major influence of the structure and quality of the deposit. The difficulty in establishing the correct ratio of $SC(NH_2)_2$ within the Ni-P electrolyte along with depletion of the bath over several cycles resulted in variability of the deposit quality. Tandem Ni-P metallization trials on AM50 and AZ91D demonstrated no discernable difference between the two alloys in the context of Ni-P metallization in accordance with the procedure of Table 3.7, Figure 3.4.



Figure 3.4: Ni-P metallization, Table 3.7, of fly-cut (Left) AM50 and (Right) AZ91D Mg alloys samples. Deposition Process: alkaline cleaning [20 min, 64 °C], acidic Mn-cocktail pre-treatment [2 min, 25 °C], Ni-P metallization [15 min, 90 °C].

Testing for the role of HF and $SC(NH_2)_2$ within 90 °C Ni-P metalizing electrolyte, it was observed that those electrolytes containing neither HF or $SC(NH_2)_2$ blackened and succumb to breakdown within 3 minutes. Electrolytes containing $SC(NH_2)_2$ without HF remained stable for over 20 minutes with samples possessing an iridescent metallic, albeit rough, coating, Figure 3.5. Deposits from electrolytes containing HF without $SC(NH_2)_2$ were more stable than those which contained neither; however, the significant formation of black precipitates was observed within the electrolyte after 7 minutes. The black precipitates were magnetic indicating that this was likely precipitated Ni-products as no other metal within the electrolyte was magnetic. The quality of the deposit from the $SC(NH_2)_2$ -free electrolyte was poor and appeared very grainy and discontinuous, Figure 3.5. The ensemble of images in Figures 3.4 and 3.5 demonstrate the large change resulting from small changes in the composition, especially the $SC(NH_2)_2$. The inclusion of 0.25 g/L $SC(NH_2)_2$ within a typically HF-free, $SC(NH_2)_2$ -free acidic Ni-P electrolyte,

Table 3.2, slowed deposition to the point that the Ni-P thin film, while still flaking similar to Figure 3.1(Left), possessed a green color.

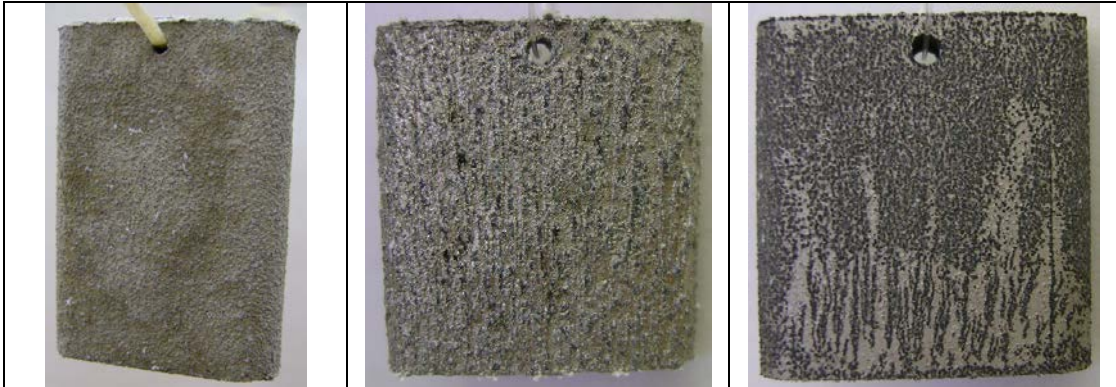


Figure 3.5: Comparison of Ni-P deposits from (Left) Standard, slightly more $SC(NH_2)_2$ [105min, 90 °C] (Center) HF-free [7 min, 90 °C], and (Right) $SC(NH_2)_2$ -free [20 min, 90 °C] Ni-P electrolytes. Ni-P electrolytes were modified from Table 3.7 and included increased $NiSO_4 \cdot 6H_2O$, 20 g/L from 15 g/L. Pre-treatment for the deposits consisted of those listed in Table 3.7.

Further pre-treatment testing using Ni-P electrolytes focused on the role of HF pre-treatments in acidic Ni-P baths both with, Table 3.7, and without, Table 3.2, HF, along with a Zn conversion pre-treatment for metallization from an HF containing Ni-P electrolyte, Table 3.8.

Deposition Steps	Chemical Name	Chemical Formula	Bath Composition	Step Details
HF Treatment	Hydrofluoric Acid (40 %)	HF	20.0 mL/L	2 min, 25 °C
Zn Treatment	Zinc Sulfate Heptahydrate	$ZnSO_4 \cdot 7H_2O$	11.5 g/L	pH 10, 25 - 35 min, 25 °C
	Ethylenediamine-tetraacetic Acid	$C_{10}H_{16}N_2O_8$ Linear Formula: $(HO_2CCH_2)_2NCH_2CH_2N(CH_2CO_2H)_2$	95.0 g/L	
	Citric Acid Monohydrate	$C_6H_8O_7 \cdot H_2O$ Linear Formula: $HOC(COOH)(CH_2COOH)_2 \cdot H_2O$	42.0 g/L	
	Ammonium Hydroxide	NH_4OH	250 mL/L	

Table 3.8: Acidic HF and alkaline Zn surface treatments for AZ91D and AM50 Mg alloys
The Zn pre-treatment is modified from a formulation by Bai et al. [24].

Directly comparing the HF treatment, Table 3.8, with the acidic Mn-cocktail treatment, Table 3.7, the HF treatment provides minimal surface modification and retains the morphology of the surface, whereas the acidic Mn-cocktail treatment creates a rough surface, Figure 3.6.

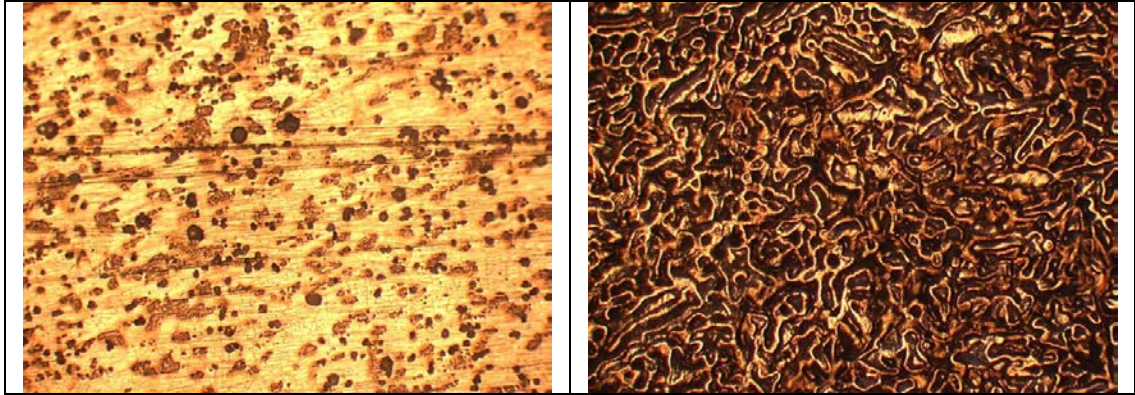


Figure 3.6: Magnification (10×) of (Left) and (Right) acidic Mn-cocktail pre-treated AZ91D Mg alloy surfaces using an optical microscope. Scale bars not available, magnification indicates the objective used.
Note: The yellow colour comes from the light source of the microscope.

The better adhesion of the deposit on the acidic Mn-cocktail treated surface, Figure 3.7, is attributed to the rough surface providing better anchoring of the deposit compared to the smoother HF treatment.





Control (Mn-treated)	HF-Treated	Control (Mn-treated)	HF-Treated
			
Ni-P metallization: 20 min, 85 °C		Ni-P metallization: 10 min, 84 °C	

Figure 3.7: Comparison of Ni-P metallization of fly-cut AZ91D Mg alloy samples with acidic Mn-cocktail and HF pre-treatments. Deposition process: alkaline cleaning, Table 3.7, [20 min, 65 °C]; acidic pre-treatment [2 min, 25 °C] (Control) acidic Mn-cocktail, Table 3.7, (HF) HF, Table 3.8; Ni-P metallization.

Comparing both pre-treatments, it is apparent that both are susceptible to poor quality resulting from prolonged metallization. The cracks developing in the very metallic deposit on HF are attributed to stress and hydrogen embrittlement of the metal. Conversely, deposits on acidic Mn-cocktail treated surfaces were less brittle and less metallic compared to the HF treated surfaces. The fracturing of the surface and poor adhesion of the deposit to the acidic Mn treated surface were attributed to remnant bubbles/cavities. The formation of the cavities was attributed to H₂ evolution trapped between the coating and the rough surface during deposition. A second, shorter, period of metallization, Figure 3.6, demonstrates that the HF treatment produces something of a better coating than the Mn-cocktail treatment as it more matches the smoothness of the

initial surface. Additionally, due to the smooth surface, the HF treated sample is free of lines formed by H₂ evolution, which are apparent on the acidic Mn-cocktail treated surface.

Using HF as the acidic pre-treatment, in place of the Mn containing acidic cocktail presented in Table 3.7, was found to improve the quality of the deposit from non-HF containing acidic Ni-P electrolytes, Figure 3.8. The improvement, which is attributed to the formation of more passive MgF₂ on the alloy surface, was insufficient to prevent contamination and decomposition of the electrolyte within the first 3 minutes.



Figure 3.8: Electroless Ni-P coating on fly-cut AZ91D Mg alloys after alkaline cleaning [20 min, 68 °C], Table 3.7, and HF pre-treatment [2 min, 20 °C], Table 3.8, from (Left) HF-containing, Table 3.7, [Deposit: 7 min, 86 °C, pH 3.4], (Right) HF-free, Table 3.2, Ni-P electrolytes [Deposit: 3 min, 74 °C, pH 5.4].

The original formulation of the Zn immersion treatment called for 23 g/L ZnSO₄ · 7H₂O, 190 g/L C₁₀H₁₆N₂O₈, 84 g/L C₆H₈O₇ · H₂O, with an unknown volume of NH₄OH and immersion for only 1 minute [24]. The modifications were carried out as the treatment in the cited study was applied to the 5051 Al alloy and initial testing did not improve the quality of the deposit compared to untreated Mg alloys. The modified Zn pre-treatment allowed for metallic coatings of the AZ91D and AM50 Mg alloys though poor adhesion, attributed to H₂ trapping under the film, was observed. Furthermore, the Zn pre-treatment clearly demonstrated the temperature sensitivity of the metalizing electrolyte which requires temperatures of 90 °C to be most-effective, Figure 3.9.

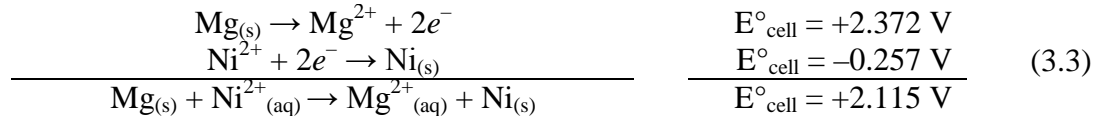
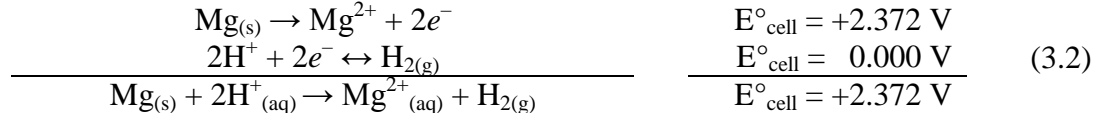
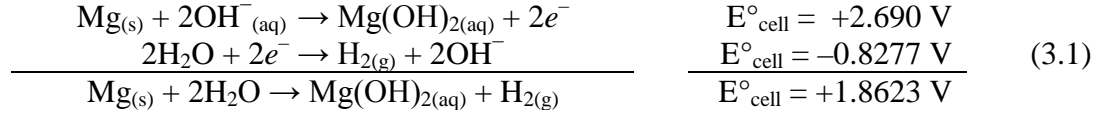


Note: Sample images were taken immediately after metallization when the samples were still damp.

Figure 3.9: Comparison of electroless Ni-P deposits from an electrolyte containing HF, Table 3.7, on Zn treated Mg alloys. Samples underwent alkaline cleaning [20min 65 °C] prior to Zn treatment and Ni-P metallization (Left) Zn [25 min, 90 °C], Ni-P [4 min, 82 °C] on AZ91D; (Center) Zn [35 min, 90 °C], Ni-P [4 min, 92 °C] on AZ91D; (Right) Zn [30 min, 90 °C], Ni-P [4 min, 93 °C] on AM50. The striations on the samples are principally due to the evolution of hydrogen as part of the anodic reaction and associated corrosion, though the vertical direction of polishing may have also played a minor role.

While both HF and Zn treatments performed well, Figures 3.6 and 3.7, neither provided superior coatings compared to the unaltered pre-treatment, Figure 3.5. Furthermore, while somewhat effective, none of the pre-treatment regimens tested were able to overcome the inherent multi-cycle inconsistency and sensitivity of the deposit structure and morphology to minute changes in the acidic Ni-P electrolyte.

The testing of common electrolytes provided insight regarding the activity of Mg and the hazard posed by contamination of the deposition bath. The exposure of oxidized, or polished, Mg alloy substrates to most electrolytes of metal ions more noble than the substrate will, as in the case of other similar metal pairs, result in a displacement reaction. Given that Mg is the least noble industrial metal, having a standard electrode potential of -2.37 V vs. SHE, commonly used electrolytes will produce an immersion reaction along with the autocatalytic reaction. Furthermore, the presence of an immersion reaction requires modification of the metalizing electrolytes in order to prevent corrosion, specifically galvanic corrosion, of the substrate. In particular, exposure of Mg alloys to acidic electrolytes results in intense spontaneous corrosion/displacement reactions due to the aqueous, Equation 3.1, acidic, Equation 3.2, environment and the metal ions in solution, Equation 3.3.



The exposure of the Mg alloy to the acidic deposition bath not only results in corrosion of the substrate but also in the contamination and plate-out/precipitation of metal from the metalizing electrolyte. Notable exceptions to the decomposition of the electrolytes presented in this section are those containing HF and $\text{SC}(\text{NH}_2)_2$. The presence of HF provides free F^{-} ions in solution which likely bonded with the Mg forming stable MgF_2 . Similarly, $\text{SC}(\text{NH}_2)_2$ is used as a stabilizer and likely plays a role as a complexing agent within the electrolyte.

The ubiquitous pursuit of acidic metalizing environments for Mg alloys appears to originate from the fact that the Mg component of the Mg alloy dissolves in neutral and slightly acidic environments allowing the formation of a passive Al-enriched film [25]. This pursuit, while attempting to produce a more passive substrate, essentially sets up a race between the corrosion and metallization reactions with stabilizers and pre-treatments providing something of a head start to the metallization. Rather than pursue this approach further experiments centered upon the behaviour of Mg alloys in alkaline environments. The lesser corrosion experience by the substrate in highly alkaline environments, such as the electrolyte for electroless Ni-B deposition, suggest that other alkaline electrolytes allow for deposits on Mg. The formation of $\text{Mg}(\text{OH})_x/\text{O}_x$ crystallites during Ni-B deposition was not explored, though EDS was performed to verify that the crystallites contained Mg and large amounts of oxygen {O}. The minimal pre-treatment of the surface prior to Ni-B deposition differed from outside studies which utilize several pre-treatment steps in order to establish Ni-B coatings on Mg alloys. Aside from Ni-B, few studies take place concerning the metallization of Mg from alkaline electrolytes. Therefore, the shift to alkaline media appears to diverge somewhat from the approach of

acidic electrolytes in which the deposition reaction attempts to outpace any corrosion reaction; typically by making use of some form of surface passivation. Furthermore, even with the formation of $Mg(O)_x/(OH)_y$ crystallites during Ni-B deposition, the surface of the coating remained smooth indicating that the coating was likely lifted rather than shed from the Mg substrate.

3.4.2 Electroless Copper {Cu} and Nickel Boron {Ni-B}

From the Ni-B results, it is apparent that, despite the potential formation of $Mg(O)_x/(OH)_y$ complexes, the muted corrosion rate of Mg alloys within alkaline environments allows for superior film formation. Additionally, the natural propensity for displacement reactions to occur on naturally anodic metals, such as Mg, is impossible within acidic environments due to corrosion. Therefore, immersion of active anodic metals within less corrosive, alkaline, media allows a higher likelihood of a displacement/immersion reaction than more acidic environments. Electrolytes suitable for studying the role of pH in the metallization of Mg are effectively limited to select Ni-B and Cu electrolytes which possess a pH above 12.5. Given the high alkalinity possible for electroless Cu electrolytes, Table 3.9, and the lack of an anodic component within the deposit; Cu electrolytes provide an ideal environment study the role of pH on corrosion during metallization within alkaline electrolytes.

Bath	Chemical Name	Chemical Formula	Bath Composition
Bath A	Copper Sulphate Pentahydrate	$CuSO_4 \cdot 5H_2O$	40.0 g/L
	Potassium Sodium Tartrate Tetrahydrate (Rochelle's Salt)	$KNaC_4H_4O_6 \cdot 4H_2O$	100.0 g/L
	Sodium Hydroxide	NaOH	25.0 g/L
Bath B	Paraformaldehyde	$HO(CH_2O)_nH$ ($n = 8-100$)	65.0 g/L
	Sodium Hydroxide	NaOH	40.0 g/L
Operating Temperature: 20 to 25 °C			

Table 3.9: Electroless Cu thin film electrolytes

*Formulation by Schlesinger et al. (1976) [26]

Immersing oxidized AM50 and AZ91D Mg alloys within alkaline Cu electrolytes, Table 3.9 – Bath 1, provided no reaction even after 30 minutes exposure. By contrast, exposing the same Mg alloys to a pH 7 electrolyte containing 30 g/L $CuSO_4 \cdot 5H_2O$

resulted in an intense corrosion reaction along with the formation of precipitates. Repeating the experiment for Bath 1, Table 3.9, without the presence of NaOH resulted in the same corrosion of the Mg indicating that the acidity of the metalizing electrolyte, or rather lack thereof, greatly influences degree of corrosion experienced by the substrate.

A qualitative test of AZ91D submerged in an aqueous solution containing sodium chloride {NaCl} and NaOH revealed that corrosion due to NaCl, seen as H₂ evolution from the sample, was suppressed by NaOH up to a point. The suppression of the corrosion reaction is attributed to the dissolution of the Al component of the Al containing Mg alloys and the formation of a passive Mg-enriched film within the alkaline media [25]. Specifically, within an alkaline environment Mg is likely to form Mg hydroxide {Mg(OH)₂}, Equation 3.4, in addition to any oxidation that has occurred prior to immersion.



The likely formation of Mg(OH)₂ on the surface of bare Mg alloys necessitated the comparison of oxidized and polished Mg to compare the role of surface oxides on deposit formation. In order to ensure a uniform surface, samples were wet polished using 240-grit SiC emery paper, dabbed dry and allowed to oxidize over a period of 3 weeks. After oxidation of both samples occurred, a hole was drilled at the top of each sample to allow the samples to be hung in the electrolytes by a nylon wire. One sample was left oxidized while the other was dry polished in open atmosphere using 240-grit SiC emery paper to remove the oxide/hydroxide layer. The polishing was carried out slowly to ensure minimal heating, and thus minimal oxidation, of the sample before immediate immersion within the alkaline Cu electrolyte. Both oxidized and polished samples were immersed within identical electrolytes for 20 minutes. Post-deposition, samples were rinsed in distilled water and dabbed dry using the laboratory clean wipes thereafter. Macroscopic as well as EDS inspection of the surface, Figure 3.10, clearly demonstrated that no deposition occurred on the unpolished, oxidized, surface, while a significant deposit formed on the polished, oxide-free, surface.

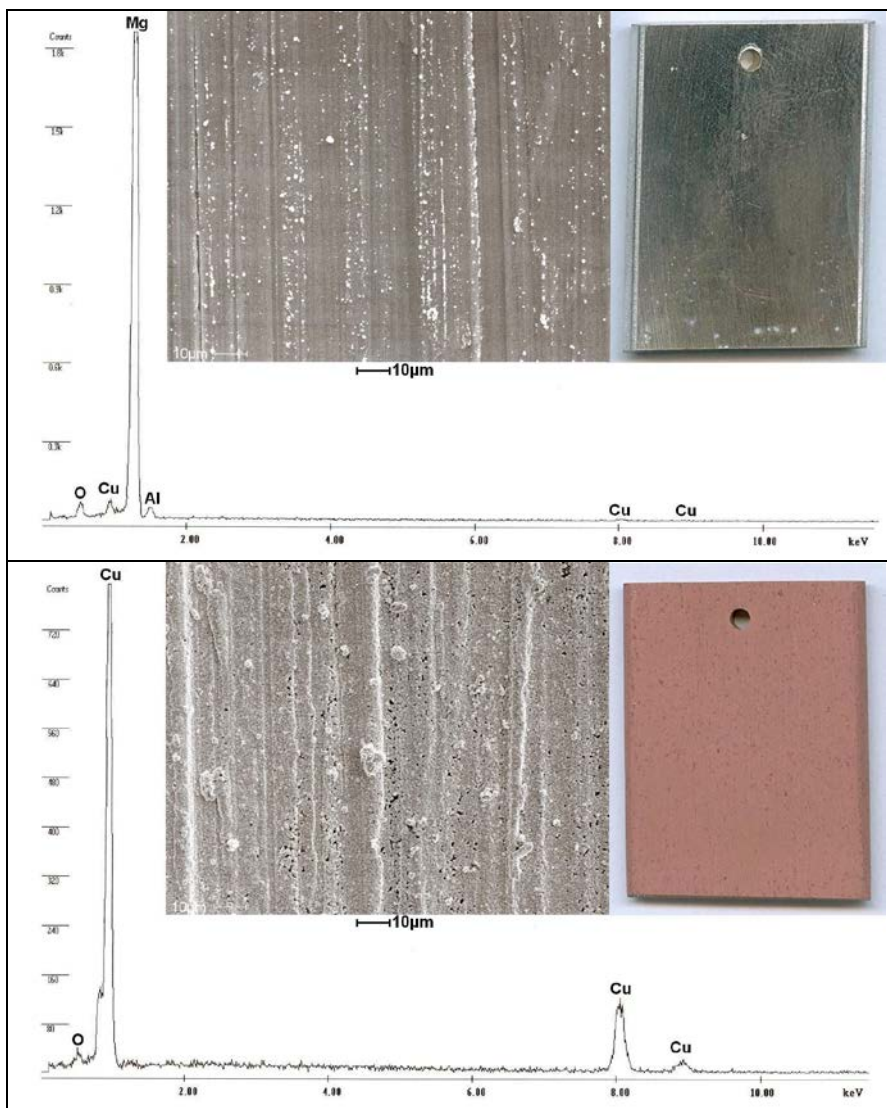


Figure 3.10: Macroscopic, backscatter SEM, and EDS analysis comparison of electroless deposits formed by a room temperature, alkaline Cu electrolyte over 20 minutes on (Top) oxidized and (Bottom) polished AZ91D Mg alloy substrates [18]. The oxidized sample, Top, possesses no Cu deposit whereas the polished sample, Bottom, is entirely coated with a layer of Cu which masks the EDS signal of the substrate.

As can be seen on the oxidized surface, top image in Figure 3.10, some corrosion similar to that formed in the Ni-B electrolyte appears to be present near the base of the sample. The slight formation of $MgO_x/(OH)_y$ crystallites near the base of the sample was attributed to a significantly suppressed reaction within the electrolyte compared to previous Ni-B deposits, Figure 3.3. Additionally, the samples were briefly hung to dry with the base of the sample in contact with a paper towel for about 15 minutes prior to being dabbed dry. The delay in the drying, which occurred equally for both samples, may have contributed to the appearance of the crystallites on the unpolished sample. The

quality of the electroless Cu thin film was generally good; however, immersion in post-deposit rinse baths was associated with the formation and evolution of some small bubbles. These bubbles, which were slow to form, were attributed to the anodic part of the corrosion reaction from the galvanic coupling of Cu and Mg through pinholes/micropores in the coating and assumed to be H₂ gas. As can be seen in the SEM image of the Cu coating, Figure 3.10, the pores in the coating measured, on average, less than 1 μm. Despite the small dimension of the pores, those pores which penetrate to the substrate provide channels between the coating and substrate which, when filled by an electrolyte, effectively form micro-galvanic cells. Thicker coatings, while minimizing pores some, do not eliminate their presence within the thin film as some channels between the coating surface and substrate persist. Moreover, the presence of a single pore or defect can, in the 'right' environment, effectively destroy any protection afforded by the deposited thin film.

Given that the pH of both the Cu and Ni-B electrolytes are about pH 14, that the Cu coating was stable on Mg and, once removed from the rinse and dried, did not show signs of corrosion, it was concluded that the pre-treatments of the initial Ni-B deposits oxidized the surface and encouraged the formation of the MgO_x/(OH)_y crystallites. Dry polishing the Mg substrates rather than subjecting them to acidic etching allowed for successful Ni-B metallization, Figure 3.11, using the same electrolyte that produced the 'Hulk' sample, Table 3.6.

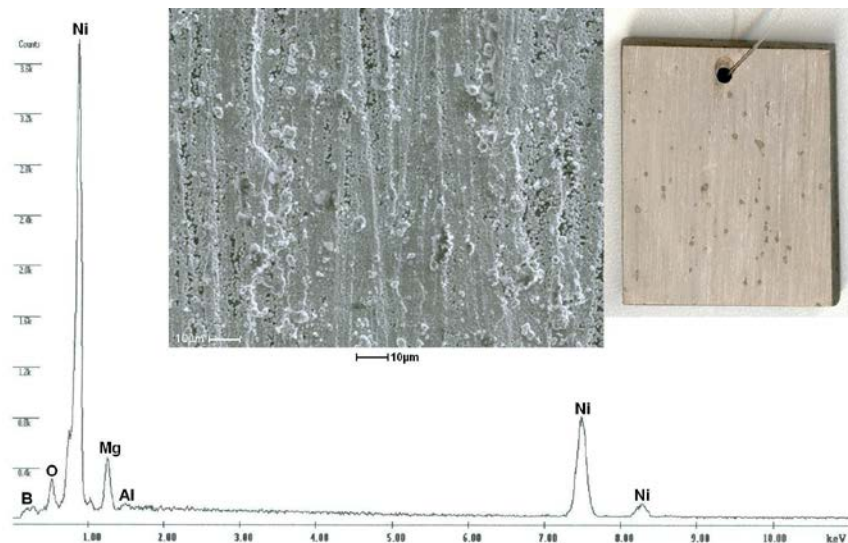


Figure 3.11: Macroscopic scan, backscatter SEM image (1000× magnification), and EDS analysis of a Ni-B coated AZ91D substrate. Coating took place over 5 min at 85 to 90 °C.

The Ni-B deposit, while somewhat more discontinuous than the Cu deposits, did not possess the significant $Mg(O)_x/(OH)_y$ crystallites present after Ni-B deposition on either the stannate conversion or acidic pre-treatments, Figure 3.3. Longer metallization attempts resulted in the growth of some $Mg(O)_x/(OH)_y$ in those darker regions of the macroscopic image, though the crystallites remained small. Additionally, though choices are limited within highly alkaline environments, other metals, such as cobalt {Co}, Table 3.10, can be co-deposited with Ni, Figure 3.12, allowing for possibility of different coating properties.

Bath	Chemical Name	Chemical Formula	Bath Composition
Bath A	Nickel Chloride Hexahydrate	$NiCl_2 \cdot 6H_2O$	49.0 g/L
	Cobalt Chloride Hexahydrate	$CoCl_2 \cdot 6H_2O$	1.0 g/L
Bath B	Sodium Hydroxide	NaOH	80.0 g/L
	Ethelenediamine (>99.5 %)	$H_2NCH_2CH_2NH_2$	120 mL/L
	Sodium Borohydride	$NaBH_4$	9.6 g/L
Operating Temperature: 80 to 90 °C		pH \approx 14	

Table 3.10: Formulation for co-deposition of Co with Ni-B modified from Table 3.5. Original formulation by Gorbunova et al. (1973).

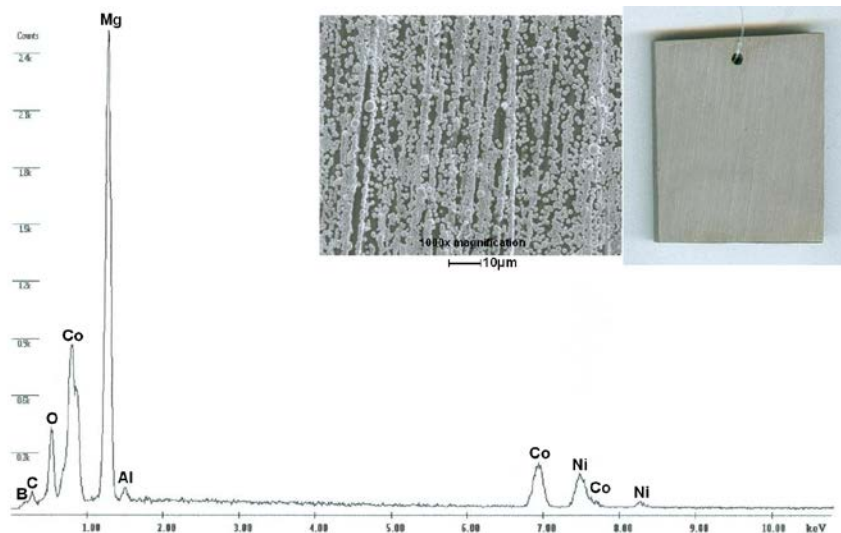


Figure 3.12: Macroscopic scan, backscatter SEM image (1000x magnification), and EDS analysis of an AZ91D substrate coated with a Co doped Ni-B layer [10 min, 80 °C].

The reduced formation of visible $MgO_x/(OH)_y$ crystallites in Figures 3.11 and 3.12 suggests that the formation of crystallites is due to, among other possible factors, the presence of surface oxides coupled with an electrolytic environment. It was also determined from other samples that increasing the temperature of the electrolyte appeared

to form more crystallites than lower temperature deposits. The formation of crystallites at higher electrolyte temperatures suggests that the reaction forming the crystallites surpasses the deposition reaction with increasing temperature.

Most importantly, the Ni-B coating allowed for subsequent Cu metallization on both the AZ91D and AM50 Mg alloys, Figure 3.13. The secondary metallization of the substrate, which was not possible with any of the processes outlined in the early work, Section 3.4.1, is essential for industrial applications where properties of scratch and wear resistance are a necessity. Additionally, it is not only the Ni-B cladding that allowed for subsequent metallization but also the Cu electrolyte, as an acidic electrolyte would have resulted in corrosion and the formation of aggressive galvanic cells.

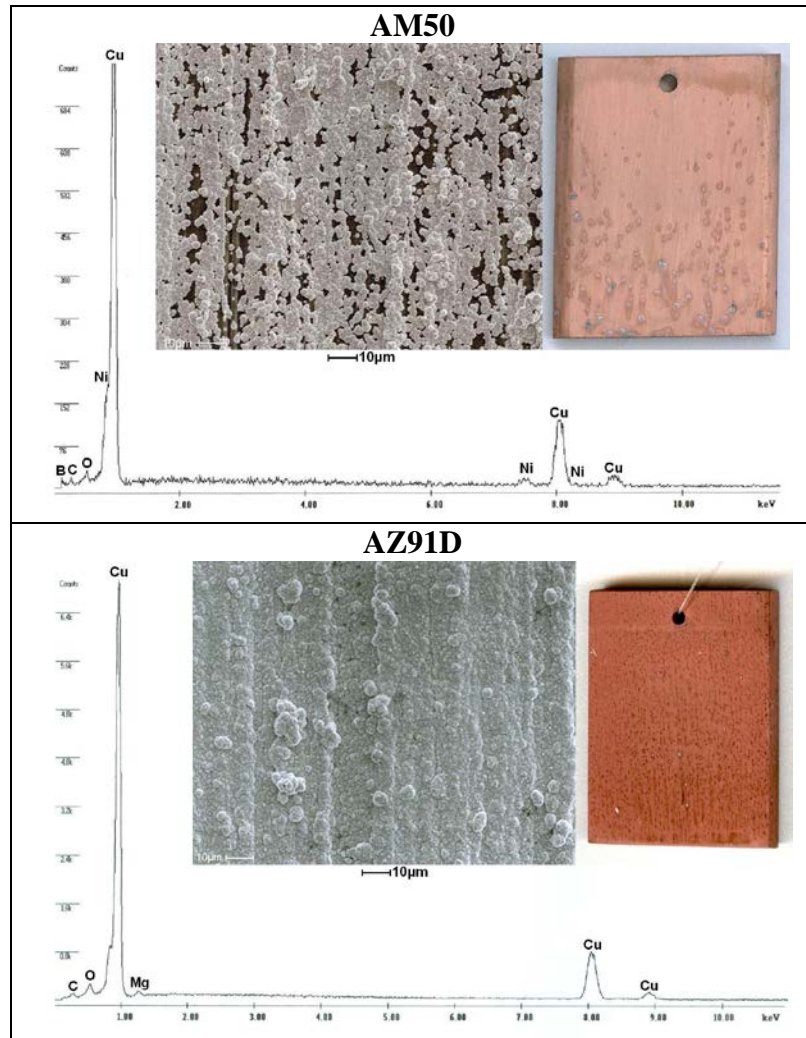


Figure 3.13: Macroscopic scan, backscatter SEM image (1000x magnification), and EDS analysis for (Top) Cu particles in the upper, corrosion free, region of an AM50 substrate coated with a Ni-B layer [15 min, 85 °C] and subsequent Cu layer [5 min, 21 °C] and (Bottom) the upper region of an AZ91D substrate coated with a Ni-B layer [15 min, 80 °C] and subsequent Cu layer [22 min, 21 °C]. [18]

The clear formation of $\text{Mg(O)}_x/(\text{OH})_y$ crystallites on the surface of the AM50 Mg alloy, Figure 3.13, resulted in a shorter Cu metallization period, 5 minutes, compared to the AZ91D Mg alloy, 22 minutes. From the EDS provided in Figure 3.13, it can be inferred that a more continuous Ni-B layer was formed on the AM50 sample compared to the AZ91D sample. The thicker more continuous Ni-B deposit on AM50, a likely consequence of better polishing and a higher metallization temperature, produced a Ni signal from EDS of the coating. Conversely, the lower metallization temperature of the AZ91D sample was observed to produce a much thinner coating which was not picked up in the region of the AZ91D sample analyzed by EDS. Combining the lack of Ni signal and presence of Mg in the EDS analysis of the AZ91D sample, it may be concluded that Ni-B was not present on the surface of AZ91D in any significant quantity at the time of Cu deposition and that the masking of the Ni by a thick Cu was unlikely. Moreover, the spotted macroscopic surface of the Cu deposit is indicative of the limited Ni-B presence producing small corrosion cells. Comparing the secondary, Figure 3.13, and direct, Figure 3.10, Cu claddings, it is clear that the secondary Cu coatings, independent of thickness, produce some $\text{Mg(O)}_x/(\text{OH})_y$ crystallites, likely due to the formation of galvanic cells. Along with other secondary deposits on both AM50 and AZ91D, the results within Figure 3.13 demonstrate that the continuity and quality of the initial Ni-B layer are the principal factors in the formation of $\text{Mg(O)}_x/(\text{OH})_y$ crystallites during secondary deposition. Simply, it appears that a critical amount of surface coverage is needed for successful secondary deposition of Cu on the Ni-B layer. In order to determine the improvement to coating continuity offered to the initial Ni-B coating by a secondary Cu deposit, a sample was only partially immersed in the Cu electrolyte after initial Ni-B metallization, Figure 3.14.

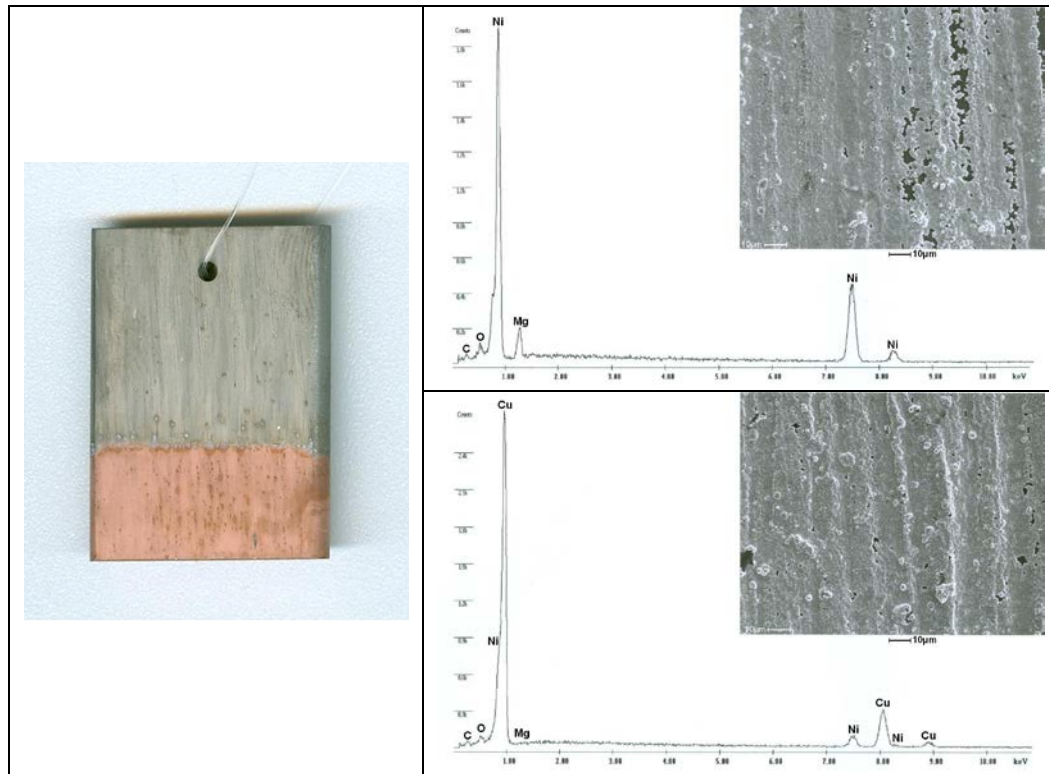


Figure 3.14: Macroscopic scanned image accompanied by EDS analysis and SEM images of an AZ91D sample having both initial Ni-B [5 min, 89 °C] (top) and secondary Cu [5 min, 25 °C] (bottom) deposits. A 25 minute drying period was used between initial and secondary metallization.

As with thicker deposits, the secondary metallization, while successful in reducing the porosity of the initial layer, did not entirely eliminate pinholes/micro-pores present within the coating. While some pores were not aligned, the alignment of pores from the Ni-B and Cu layers produce channels from the surface down to the substrate. The channels, when filled with any electrolyte, produce galvanic cells and cause the evolution of small bubbles assumed to be $H_{2(g)}$. Comparing the Cu deposit of Figure 3.14 with those presented in Figure 3.13, it is clear that too little Ni-B coverage is a significant issue for the secondary deposition of Cu. Furthermore, the results indicate that there exists a minimum porosity for the initial layer to produce a good quality Cu deposit and that shorter electroless Cu deposits, such as those on the AM50, Figure 3.13, and AZ91D, Figure 3.14, alloys produced more metallic quality deposit. The complexities and inconsistencies associated with the Ni-B electrolyte, including the need to maintain a high temperature, Appendix A, led to the selection of the easier to use and more successful alkaline Cu electrolyte for investigation of methods to reduce the porosity of the coating.

Investigation of the film forming environment for better understanding of the metallization process and mitigation of the porosity centered on various metallization techniques, including agitation of the metalizing electrolyte and the application of pre-treatments, as well as modification of the electrolyte. Utilizing a magnetic stir bar for agitation, it was determined that weak agitation of the electrolyte, ~60 rpm, did not alleviate the formation of pores within the coating. More mild agitation, >200 rpm, only served to change the angle of the pores from normal to the surface to having some angle along coating in the direction of the motion of the rotating electrolyte. The presence of non-perpendicular, angled, pores, while difficult to clearly identify on SEM, was strongly suggested by the same formation and evolution of small bubbles from the surface within a post-deposit rinse bath. The bubbles evolving from the surface in the post deposit rinse bath were consistent with those produced from coatings having pores normal to the surface. Bubbling argon {Ar} gas as a means of agitation, and in the process removing dissolved oxygen {O₂} from the electrolyte to minimize oxidation of the Mg within the electrolyte, proved ineffective in the minimization of pores/pinholes. Not only was the quality of the deposit essentially identical to those formed without agitation, no difference was observed when using air in place of Ar. A final agitation method of providing a vertical mechanical shock to the sample appeared to provide the best improvement of the Cu coating of the sample, though pinholes/pores remained in the coating. Further investigation of mechanical shaking of the sample was not pursued due to the lack of practicality, though it stands to reason that the agitation method proved most effective as it removed from the surface bubbles formed by the anodic or corrosion reactions.

3.4.2.1 Surface Treatments

The application of pre-treatments focused on the stannate pre-treatment, Table 3.3, and acidic etching in dilute nitric {HNO₃} and sulphuric {H₂SO₄} acids. Application of the stannate conversion provided slightly better results than the Ni electrolytes as the high pH minimized any possible corrosion of the surface. The superior quality of the coating was predicated on the MgSnO₃ · H₂O surface remaining intact after the required acidic activation, Figure 3.15.

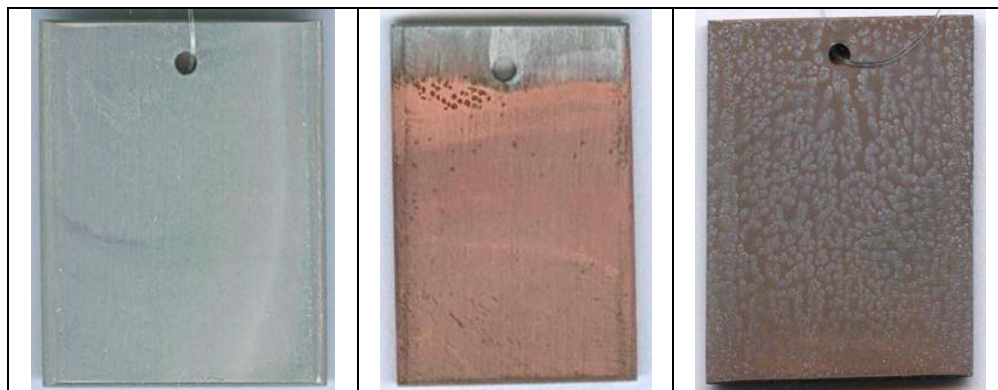


Figure 3.15: Macroscopic scanned images of a stannate treated [2 h, 90 °C] AZ91D samples; (Left) without a Cu deposit, (Center) after a 25 min Cu deposit and adhesion test, specifically cellulose tape test, and (Right) after a 25 min Cu deposit.

Difficulties regarding the stannate conversion rested largely with the uneven coating which produced patterns on the Cu deposit, Figure 3.14. Furthermore, the required acidic activation, using either Sn/Pd or Pd alone, for deposition on stannate conversion surface had to be carried out with extreme care so as to not damage the sensitive $\text{MgSnO}_3 \cdot \text{H}_2\text{O}$ surface. While the adhesion of the Cu on the stannate surface was excellent, the unreliable quality of the conversion and the variability required for proper activation, along with the conversion forming an insulator surface, meant that the conversion technique was not viable.

Exploring acidic etching, another common practise within industry, variations in the composition of the acidic etch including the selection of the acid itself were explored. Comparing HNO_3 and H_2SO_4 etch baths, it was found that immersion within an H_2SO_4 etch prior to metallization allowed for superior Cu deposits compared to immersion within an HNO_3 etch bath, Figure 3.16.

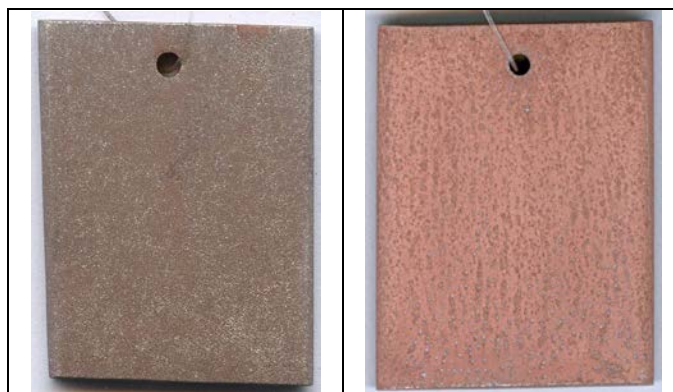


Figure 3.16: Macroscopic images of 20 min electroless Cu deposits on 30 s acid pre-treated Mg alloy samples. (Left) concentrated HNO_3 [50 mL/L] and (Right) dilute [20 mL/L] H_2SO_4 .

The superiority of the H_2SO_4 immersion was attributed in part to the presence of sulphate $\{\text{SO}_4^{2-}\}$ ions in both the acidic etch as well as the electrolyte. The difference in hue/colour between the two deposits is attributed to a combination of adsorption of the acidic anion to the Mg surface along with a more discontinuous deposit on the HNO_3 treated alloy. Investigation as to the reason of the poorer quality of coatings after acidic treatments was not conducted as several experiments demonstrated similar results as provided in Figure 3.16. Differences between acidic etches are expected as anions are easily adsorbed onto the Mg substrate. Concerns about anion adsorption was the principle reason that HCl was not included in the acidic etch testing, as Cl^- ions are known to enhance corrosion of Mg alloys. Another point of note is the formation of $\text{MgO}_x/(\text{OH})_y$ crystallites visible on the surface of the H_2SO_4 treated sample. The formation of the crystallites is consistent with their appearance on other samples and is attributed, here as before, to oxidation of the Mg surface. Further testing of the acidic etch baths included the addition of CuSO_4 to the bath in an effort to produce a limited, discontinuous, catalytic, immersion coating for better the nucleation of growth on Mg. While some very limited success was achieved in the formation of a sparse Cu immersion coating, no deposit of quality was formed during subsequent Cu deposition.

Comparing the various pre-treatment methods, the stannate conversion provided the best adhesion as measure by means of a simple tape test. The test, which consisted of placing a strip of packing tape over the deposit and removing it as quickly as possible, was unable to remove any amount of coating from the stannate conversion sample. Of the adhesion tests carried out, Figure 3.17, the stannate performed best followed by the H_2SO_4 treatment, a short deposit on a polished surface and finally a longer deposit on the polished surface.

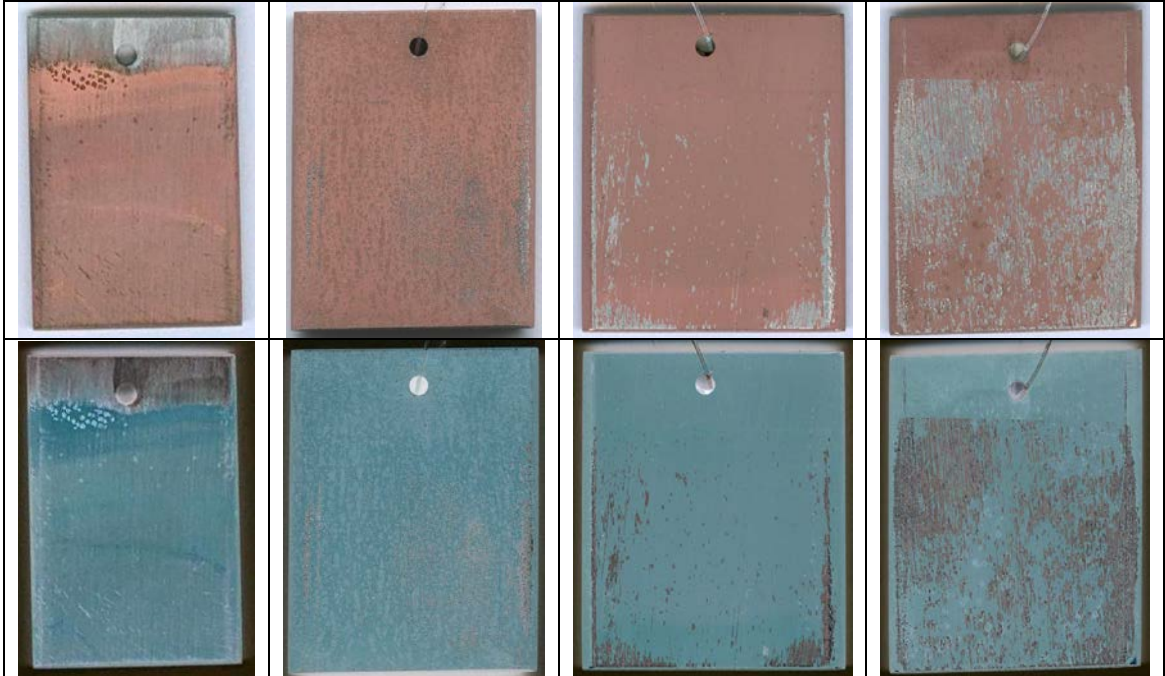


Figure 3.17: Macroscopic images, and their negatives, comparing the post-tape test surfaces of Cu deposits on (Left) stannate conversion [20 min Cu deposit, dabbed dry], (Center-Left) H_2SO_4 etched [20 min Cu deposit, dabbed dry], (Center-Right) polished [15 min Cu deposit, dabbed dry] and (Right) polished [20 min Cu deposit, 5 min air dry, then dabbed dry], AZ91D Mg alloy samples.

The superior adhesion of Cu coatings on stannate and H_2SO_4 treated alloys is attributed to increased roughness of the surface by the acidic Pd activation of the stannate and acidic pre-treatments, respectively. The increased surface roughness produces a larger surface area for which the cladding is in contact with the substrate and allows anchoring of the deposit into the substrate. The smoother, polished, surfaces provided a lower adhesion though shorter deposits allowed the surface texture from the polishing to contribute to the adhesion. Longer deposits on polished surfaces produced thicker coatings which kept together and were stronger than thin coatings decreasing the adhesion. Dabbing dry the sample appeared to result slightly better adhesion for thin deposits than air drying prior to dabbing away excess water. The slight difference in dabbing versus air dry was attributed to the removal of latent water inundating the pores forming galvanic cells.

3.4.2.2 Immersion Coatings and Electrolyte Modifications

Considering that none of the pre-treatment techniques were capable of successfully resolving issues of consistency and the formation of pinholes/pores, modifications of the electrolyte were considered. Electrolyte modifications included decreasing the NaOH content from 32.5 g/L in the original formulation, as well as removing any ‘superfluous’ anions, such as SO_4^{2-} , from the electrolyte, Table 3.11. The presence of SO_4^{2-} ions provide a means of corrosion of the Mg surface, albeit to a lesser degree than Cl^- ions. While both types of modification produced similar, good quality, deposits independent of the presence of ‘superfluous’ anions, the pinholes in the deposit remained present. The only substantial change provided by the modified electrolytes was the coloring of the deposits, which became more metallic compared to the previous matted coloring when the concentration of NaOH was reduced.

Bath	Chemical Name	Chemical Formula	Bath Composition (g/L)		
			Bath 1	Bath 2	Bath 3
Bath A	Copper Sulphate Pentahydrate	$\text{CuSO}_4 \cdot 5\text{H}_2\text{O}$	35.0	25.0	—
	Copper Hydroxide	$\text{Cu}(\text{OH})_2$	—	—	13.9
	Potassium Sodium Tartrate Tetrahydrate (Rochelle’s Salt)	$\text{KNaC}_4\text{H}_4\text{O}_6 \cdot 4\text{H}_2\text{O}$	65.0	65.0	65.0
	Sodium Hydroxide	NaOH	15.0	10.0	10.0
Bath B	Paraformaldehyde	$\text{HO}(\text{CH}_2\text{O})_n\text{H}$ ($n = 8-100$)	65.0	65.0	65.0
	Sodium Hydroxide	NaOH	15.0	10.0	10.0
Operating Temperature: 20 to 25 °C					

Table 3.11: Modified electroless Cu thin film electrolytes

The apparent lack of corrosion within the alkaline Cu electrolyte, despite the large difference between the standard electrode potentials of Mg (-2.372 V vs. SHE) and Cu (+0.340 V vs. SHE), indicates that highly alkaline electrolytes are, to some extent, able to inhibit both general corrosion and galvanic corrosion between Cu and Mg. Given the vigorous reaction between Cu and Mg in neutral, pH 7, electrolytes, investigation into corrosion as the source of the pinholes was carried out by immersing Mg alloy samples in ‘Bath A’ of the alkaline Cu electrolyte. Polishing one side of an oxidized AZ91D Mg alloy samples and exposing it to ‘Bath A’ of the original Cu electrolyte, Table 3.9, for 48 hours resulted in a Cu immersion coating only the polished face, Figure 3.18.

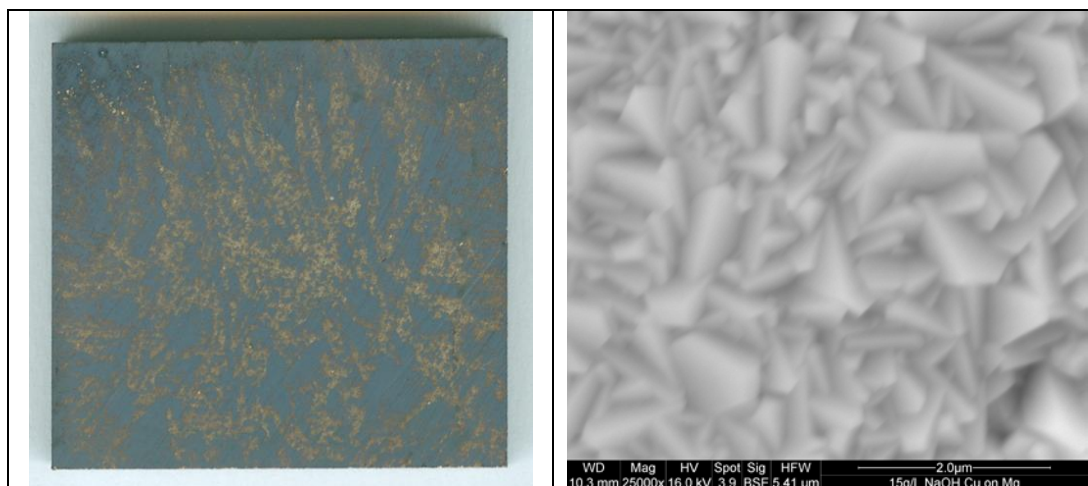
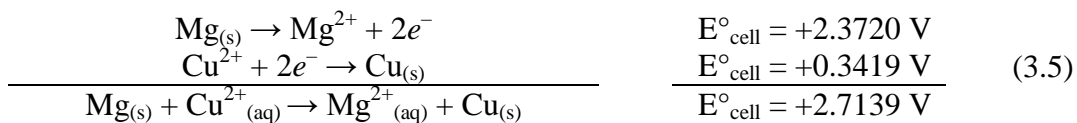


Figure 3.18: Macroscopic and backscatter SEM image of a Cu immersion deposit formed at pH 11.5 in an electrolyte containing 35 g/L $\text{CuSO}_4 \cdot 5\text{H}_2\text{O}$, 75 g/L $\text{KNaC}_4\text{H}_4\text{O}_6 \cdot 4\text{H}_2\text{O}$, and 15 g/L NaOH on an AZ91D Mg alloy.

Displacement/immersion reactions are formed by the displacement, oxidation, of a less noble metal by more noble metal ions, which are reduced from the environment. The formation of an immersion deposit, which, due to corrosion, does not occur in neutral and acidic environments, is consistent with a simple displacement reaction where Cu displaces Mg on the surface of the alloy, Equation 3.5.



The Cu deposition on Mg alloys from ‘Bath A’, Bath 1 – Table 3.11, which does not contain the $\text{HO}(\text{CH}_2\text{O})_n\text{H}$ ($n = 8-100$) reducing agent, suggests that electroless Cu deposition on Mg alloys is initiated by a simple displacement, or immersion, reaction upon which autocatalytic deposition occurs. Better understanding of immersion formation and autocatalytic Cu deposition on the Mg alloys, was achieved by immersing polished alloys in alkaline Cu electrolytes of varying NaOH concentration and without reducing agent, Table 3.12. The slightly higher pH of the electrolyte containing 15.0 g/L NaOH compared to the electrolyte containing 20.0 g/L NaOH, which is effectively within the uncertainty of the pHmeter, is attributed to small differences in the concentration of other constituent chemicals as well as interaction of the electrolyte with the environment.

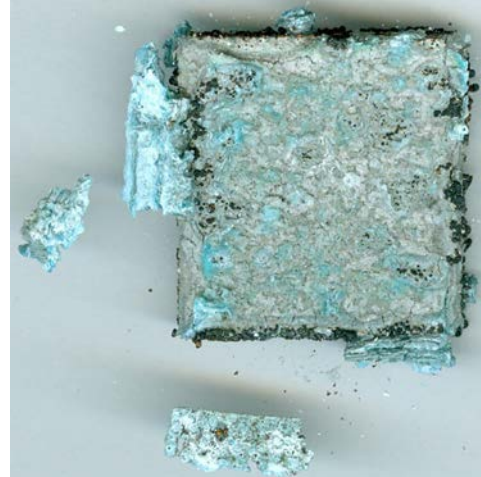
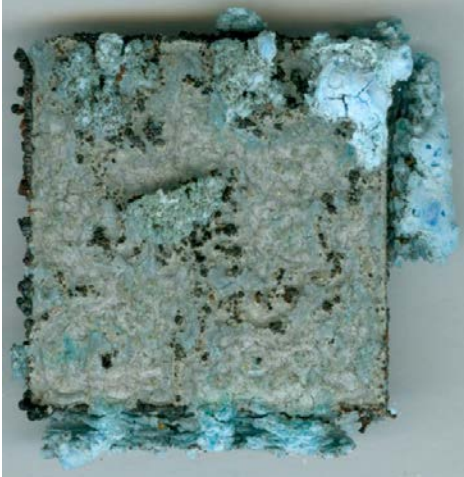
Chemical Name	Chemical Formula	Bath Composition (g/L)				
		Bath 1	Bath 2	Bath 3	Bath 4	Bath 5
Copper Sulphate Pentahydrate	$\text{CuSO}_4 \cdot 5\text{H}_2\text{O}$	35.0	35.0	35.0	35.0	35.0
Potassium Sodium Tartrate Tetrahydrate (Rochelle's Salt)	$\text{KNaC}_4\text{H}_4\text{O}_6 \cdot 4\text{H}_2\text{O}$	75.0	75.0	75.0	75.0	75.0
Sodium Hydroxide	NaOH	10.0	12.5	13.0	15.0	20.0
	pH	10.35	11.50	12.70	13.90	13.80

Table 3.12: Alkaline Cu electrolytes for immersion deposits on Mg alloys

To adequately compare the behaviour of the Mg alloys in the various electrolytes, the AZ91D Mg alloys were wet polished on all sides creating uniform oxidized surfaces. A final dry polish was applied to one of the larger faces immediately before immersion in the alkaline Cu electrolyte just as in the initial test. Initial formation of the immersion coating began immediately upon immersion of the alloy within the electrolyte. The immersion coatings were formed on only the dry polished faces, Figures 3.19 & 3.20, though coatings from electrolytes containing NaOH at less than 15 g/L were not affixed to the Mg substrate, Figures 3.19.

It should be understood that the reflective, textured, surfaces produce two slightly different images depending on whether the scan is carried out across, bright, or along, dark, the polishing lines of the sample. The difference in the image is due to the reflection of the scanning light source which passed from top to bottom along the sample and was minimal in the case of images of Figure 3.19.

10.0 g/L, pH 10.35



Outside Surfaces

Inside Surfaces

12.5 g/L, pH 11.50

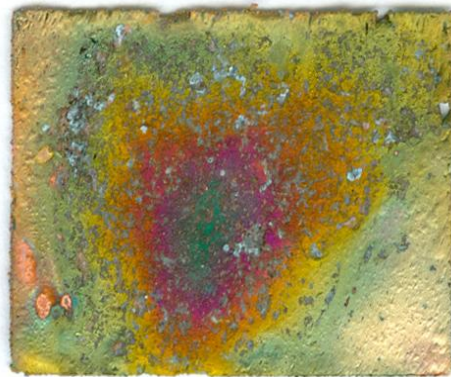


Figure 3.19: Continues on Next Page with Caption

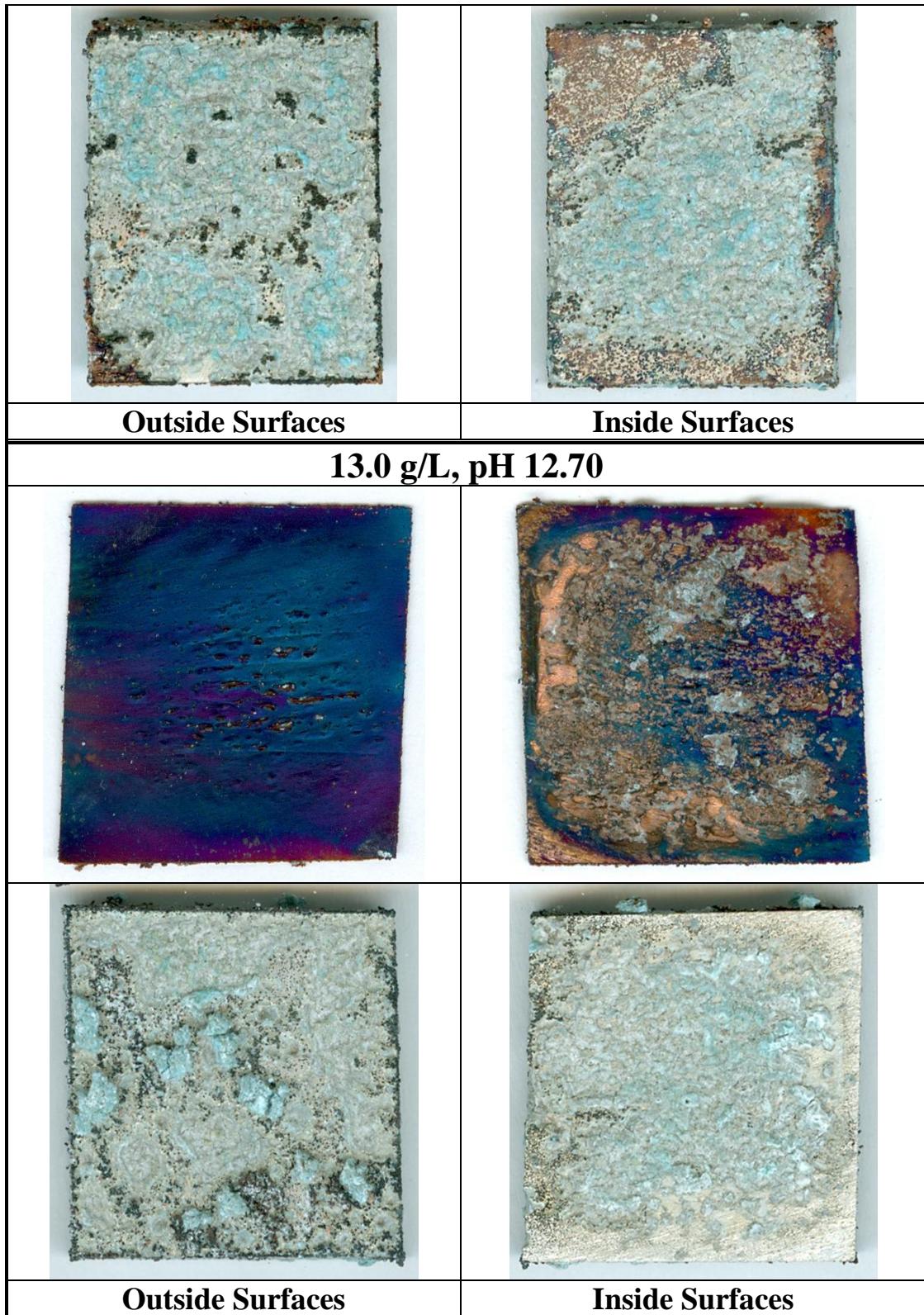
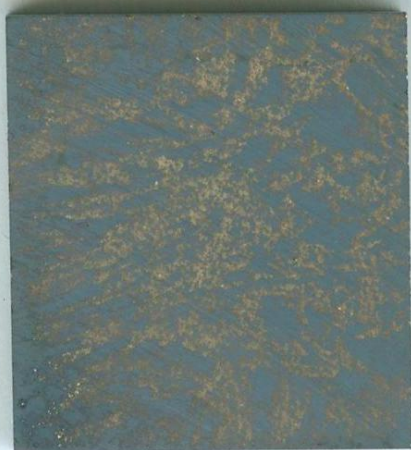


Figure 3.19: Macroscopic image of 48 hour Cu immersion deposits formed on 15 mm – 20 mm × 20 mm AZ91D Mg alloys within room temperature electrolytes of varying NaOH concentrations, < 15 g/L. Macroscopic images of samples from 10 g/L, 12.5 g/L, and 13 g/L NaOH electrolytes show (Left) the front and back of the sample as well as the (Right) inside face of the deposit and the face upon which it formed.

15.0 g/L pH 13.90



Horizontal orientation

Vertical Orientation

20.0 g/L, pH 13.80



Figure 3.20: Continues on Next Page with Caption

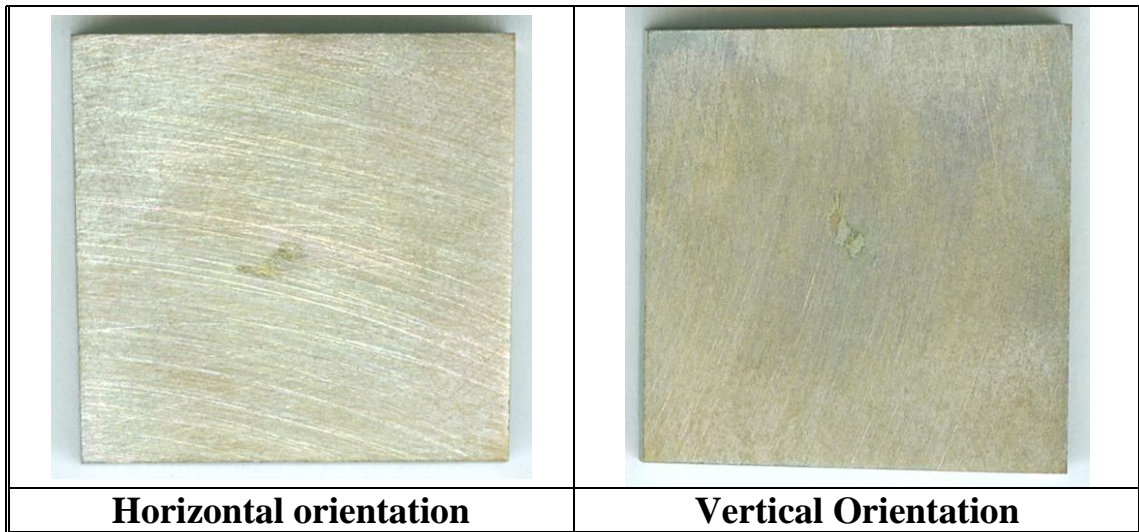


Figure 3.20: Macroscopic image of 48 hour Cu immersion deposits formed on 15 mm – 20 mm × 20 mm AZ91D Mg alloys within room temperature electrolytes of varying NaOH concentrations, ≥ 15 g/L. Macroscopic images of samples from 15 g/L and 20 g/L NaOH electrolytes show two scans of the front and back surfaces of the deposit showing different features due to the reflective surface.

As is clearly visible from the macroscopic images, Figures 3.19 & 3.20; the degree of substrate corrosion decreases with increasing alkalinity of the electrolyte. Specifically, no clear signs of corrosion products are observed on samples exposed to electrolytes containing NaOH at, or above, a concentration of 15 g/L, Figure 3.20. Those samples immersed in electrolytes containing NaOH at concentrations above 10 g/L but below 15 g/L, Figure 3.19, produced well complete Cu layers of better quality than electrolytes containing NaOH at, or above, a concentration of 15 g/L, Figure 3.20. The Cu thin films produced on Mg alloys within alkaline electrolytes, while not always affixed to the substrate, are not produced within neutral environments due to aggressive corrosion of the Mg substrate. For this reason the Cu cladding produced from the electrolyte containing 10 g/L NaOH was very brittle compared to the more metallic coatings produced from electrolytes having 12.5 g/L and 13.0 g/L NaOH concentrations. The high quality of the metallic coatings can also be seen on SEM no porosity, aside from those inflicted by the growing $\text{MgO}_x/(\text{OH})_y$ crystallites, is observed, Figure 3.21.

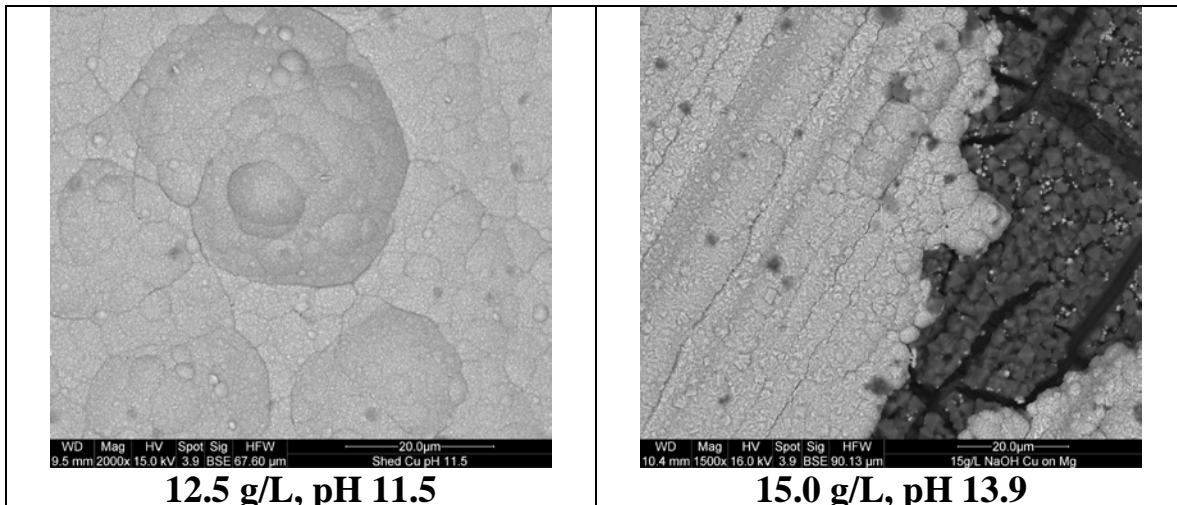


Figure 3.21: Backscatter SEM images of immersion Cu coatings formed on AZ91D Mg alloys at (Left) pH 11.5, metallic and shed from the surface, and (Right) pH 13.9, adhered and discontinuous. The corrosion product from the immersion at pH 11.5 is not shown. Lighter coloring on backscatter images indicate heavier elements.

Given the large difference between the pH of electrolytes containing NaOH at 12.5 g/L and 13.0 g/L, pH of 11.5 and 12.7, respectively, titration measurements were carried out to determine the pH response of the electrolyte for increasing NaOH, Figure 3.22.

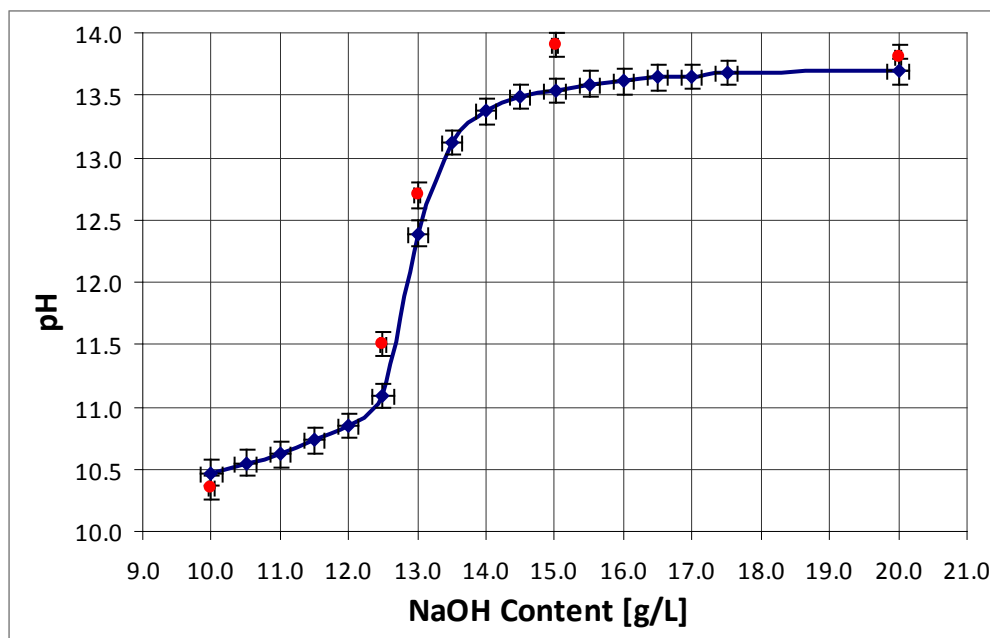


Figure 3.22: Titration curve for the alkaline Cu electrolyte containing 35 g/L $\text{CuSO}_4 \cdot 5\text{H}_2\text{O}$ and 75 g/L $\text{KNaC}_4\text{H}_4\text{O}_6 \cdot 4\text{H}_2\text{O}$. The volume of the electrolyte used was 60 mL. Error bars for NaOH determined by the average of value produced from the propagation of uncertainty. Error bars for pH determined by the difference in readings after recalibration of the meter at the end of the titration. Red data points show the pH of the immersion Cu electrolytes, Figure 3.19.

Note: Data points connected rather than fitted to a curve.

The clear presence of a titration curve suggests that the ligand structure around the Cu^{2+} ions changes significantly between NaOH concentrations of 12.5 g/L and 13.5 g/L. Overlaying the pH of the immersion electrolytes presented in Figure 3.19 on the titration curve for electrolytes containing 35 g/L $\text{CuSO}_4 \cdot 5\text{H}_2\text{O}$ and 75 g/L $\text{KNaC}_4\text{H}_4\text{O}_6 \cdot 4\text{H}_2\text{O}$, provides a rough pH dependence providing the conditions for a brittle shed coating, shed metallic coatings, and adhered matted coatings, Figure 3.22.

According to the titration curve, brittle Cu immersion coatings are expected to be formed below around pH 11. Metallic coatings appear to be produced between pH 11 and pH 13 in the steep portion of the titration curve, with adhesion improving with pH. Well adhered, discontinuous immersion deposits form above pH 13 suggesting that it is likely that a precise concentration of NaOH providing a precise pH would offer reasonably well adhered, continuous, metallic coatings. The provision of such a good quality immersion coating, when paired with an electrolyte, provide an excellent quality electroless Cu deposit. Lowering the concentration of CuSO_4 within the electrolyte produces shifted titration curve, Figure 3.23

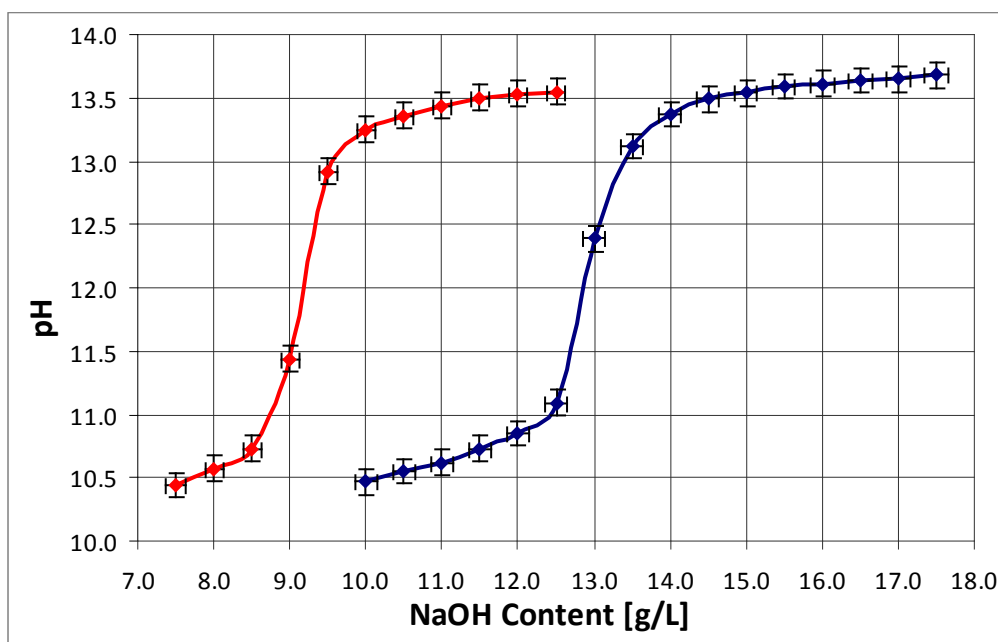


Figure 3.23: Titration curves for the alkaline Cu electrolytes containing 75 g/L $\text{KNaC}_4\text{H}_4\text{O}_6 \cdot 4\text{H}_2\text{O}$, along with (Blue) 35 g/L $\text{CuSO}_4 \cdot 5\text{H}_2\text{O}$, and (Red) 25 g/L $\text{CuSO}_4 \cdot 5\text{H}_2\text{O}$.

Note: Data points connected rather than fitted to a curve.

A critical point worth mention within this work is that the pH of the electrolytes does fall over time. After 96 hours, the final pH measured in the titration curve presented

in Figure 3.22 fell to around 11.30. The decline is a result of reactions of the electrolyte with the atmosphere. The decline in pH did not influence the immersion results as the electrolytes were always used fresh and the formation of coatings were observed within the first few minutes. The decline in pH is greater than what would have been expected had no titration curve been observed with the addition of NaOH, Figure 3.24. The decrease in the pH beyond the extrapolated linear increase with NaOH is indicative of some reaction did taking place.

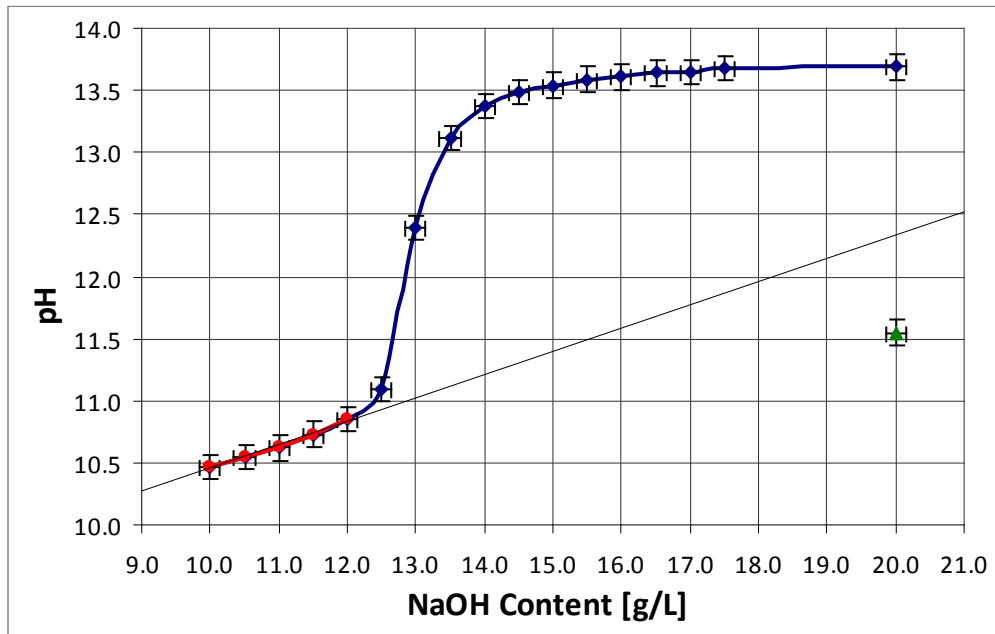


Figure 3.24: Titration curve for the alkaline Cu immersion electrolyte containing 35 g/L $\text{CuSO}_4 \cdot 5\text{H}_2\text{O}$ and 75 g/L $\text{KNaC}_4\text{H}_4\text{O}_6 \cdot 4\text{H}_2\text{O}$ along with (Black) a curve representing the trend of the initial climb in pH pre-equilibrium point and (Green) pH of the electrolyte after 96 hours.
Note: Data points connected rather than fitted to a curve.

Further evidence of a reaction taking place within the electrolyte can be shown by comparing a deposit from the electrolyte that experienced a pH drop, Figure 3.25, with those deposits from freshly made electrolytes, shown in Figure 3.19 and 3.20. A clear difference in the quality of the deposit is compared to both the pH 11.5 electrolyte containing 12.5 g/L of NaOH, shown in Figure 3.19, as well as the pH 13.8 electrolyte containing 20.0 g/L of NaOH, shown in Figure 3.20. The deposit from the pH 11.6, 20.0 g/L NaOH electrolyte, Figure 3.25, has the same matted colour as the deposit shown in Figure 3.19, but is less metallic and continuous. Similarly, deposit shown in Figure

3.25 is discontinuous, similar to the deposit shown in Figure 3.20, but appears to have corroded the surface due to a lower alkalinity.

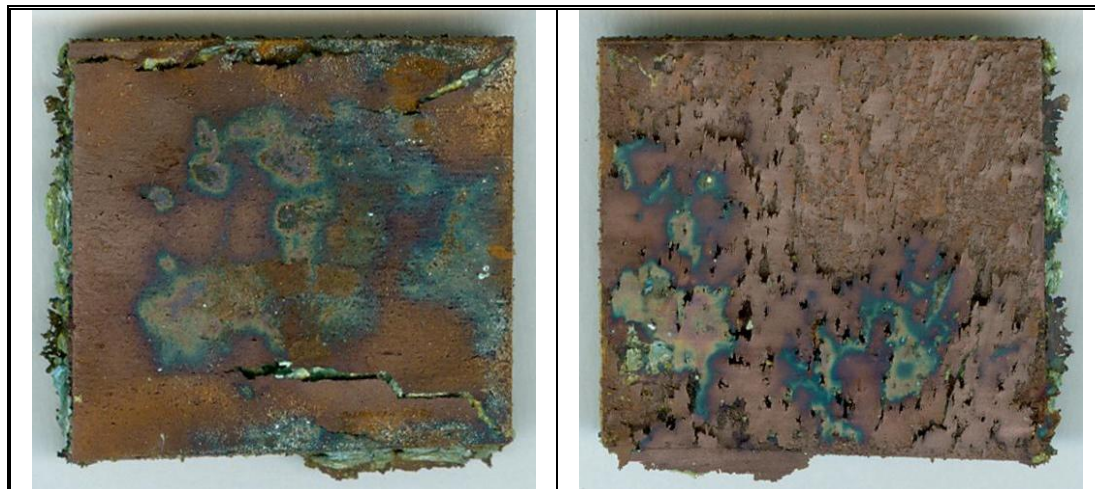


Figure 3.25: Macroscopic scanned image of both large faces of a polished AZ91D Mg alloy sample after 40 h immersion in a pH 11.6 Cu electrolyte containing 20 g/L NaOH, 35 g/L $\text{CuSO}_4 \cdot 5\text{H}_2\text{O}$, and 75 g/L $\text{KNaC}_4\text{H}_4\text{O}_6 \cdot 4\text{H}_2\text{O}$.

The difference in the immersion results compared to other, newer electrolytes indicates that the concentration of the constituent chemicals, here OH^- , is a factor in the formation of the immersion coating. Hence, the difference in the quality of the deposit is attributed not only to the change, decrease, in pH, which enhances corrosion; but also likely side reactions between the atmosphere and the electrolyte that presumably change the composition of the electrolyte. Identifying the ions, and the surrounding ligand structure, within the electrolyte after the equilibrium point would presumably allow the immersion coating of Mg by Cu at lower pH values. The formation of the coatings at lower pH values is notably predicated on the formation of similar ionic complexes within the electrolyte.

Analyzing the corrosion product present on the reverse side of the Cu immersion coating from the 10 g/L NaOH electrolyte, Figure 3.26, Mg and O feature most prominently within the EDS results; though small quantities of Cu, Na, and K are also present. While the formation of hydroxide $\{\text{OH}^-\}$ complexes is supported by the colouring of the debris as well as the environment in which it was formed, EDS cannot quantify hydrogen $\{\text{H}\}$ and hence cannot explicitly identify the presence of OH^- . Given the ratio of Mg to O, it appears that most of the corrosion product is MgO_2 , though due to the appearance $\text{Mg}(\text{OH})_2$ is more likely. The minimal sulphur content within the debris

suggests that the light blue color is due to $\text{Cu}(\text{OH})_2$ rather than CuSO_4 , and the slight reddish coloring in some regions suggest that Cu_2O is also present, though in smaller quantities. Given that the presence of carbon {C} is detected even on metallic samples due to environmental contamination from previous samples in the SEM and handling it left out from EDS quantification. The ubiquitous presence of carbon clouds the possible presence of carbonates $\{\text{CO}_3^{2-}\}$ within the oxide/hydroxide debris. The presence of other materials, namely Na and K, are produced by the dissociation of the $\text{KNaC}_4\text{H}_4\text{O}_6$ and are likely trapped in the debris as O containing complexes.

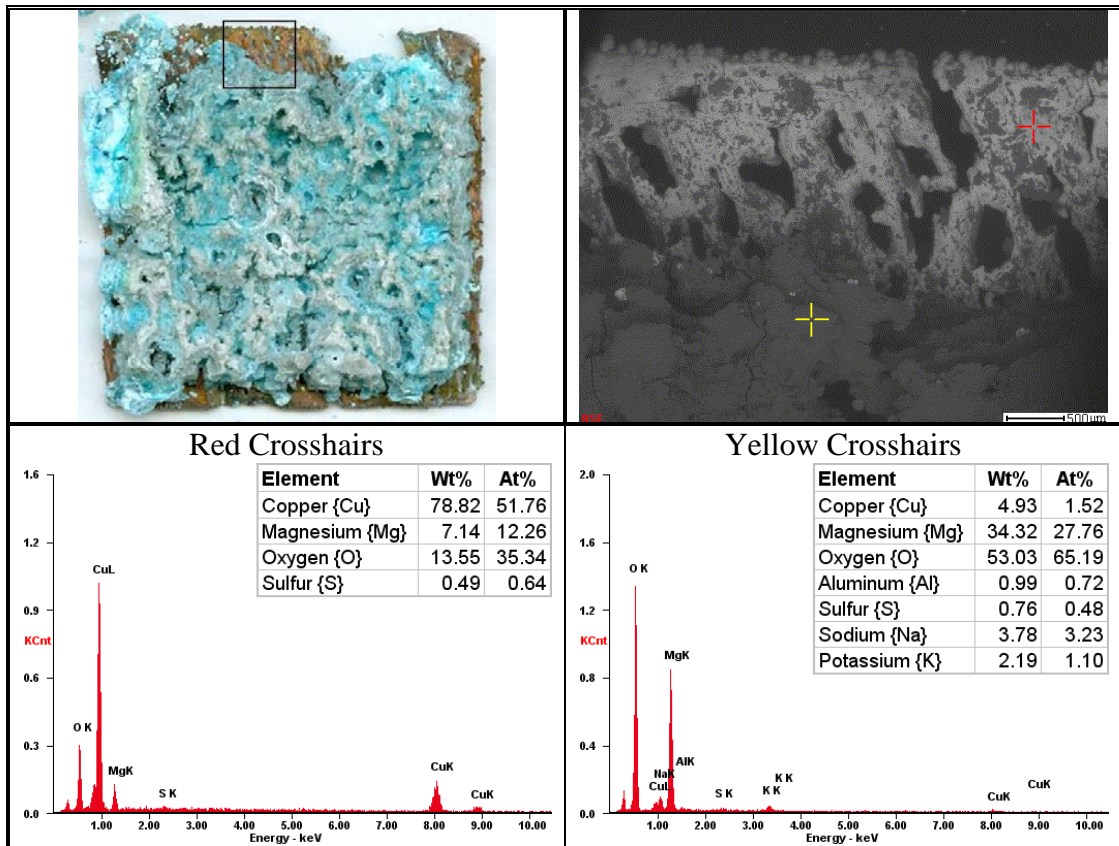


Figure 3.26: Compositional EDS analysis of the oxide/hydroxide crystallites on the reverse of the Cu film formed on AZ91D Mg from a pH 10.5 electrolyte containing 10 g/L NaOH, 35 g/L $\text{CuSO}_4 \cdot 5\text{H}_2\text{O}$, and 75 g/L $\text{KNaC}_4\text{H}_4\text{O}_6 \cdot 4\text{H}_2\text{O}$.

The oxygen {O} quantified as part of the yellowish Cu thin film produced from the 12.5 g/L NaOH electrolyte, Figure 3.27, is near 2:1 which suggests the presence of Cu_2O . The presence of other oxides, such as CuO , is discounted by both the blackish colour of CuO as well as EDS which suggests the presence of Cu_2O , though some minor $\text{Cu}(\text{OH})_2$ may be mixed in with CuO .

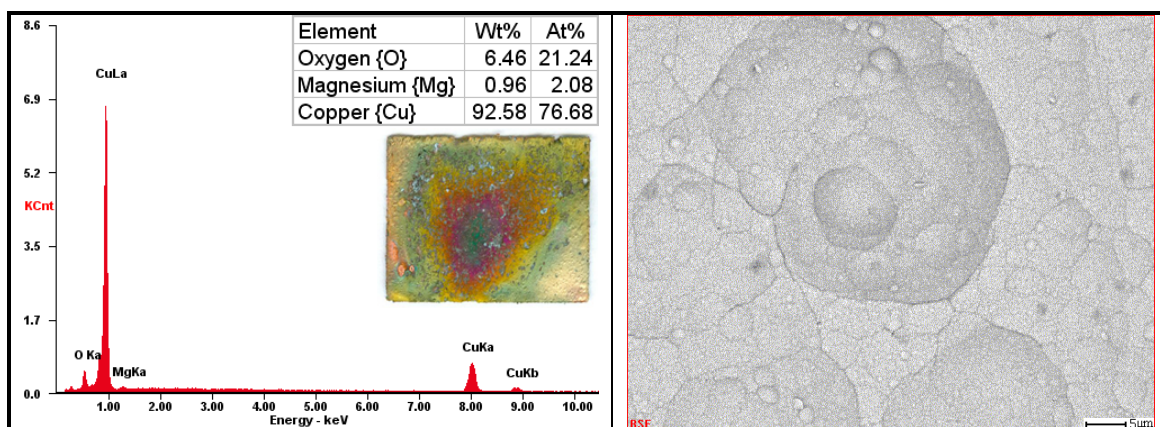


Figure 3.27: Compositional EDS analysis of the shed Cu thin film produced on AZ91D Mg from an electrolyte containing 12.5 g/L NaOH, 35 g/L CuSO₄ · 5H₂O, and 75 g/L KNaC₄H₄O₆ · 4H₂O at pH 11.5.

Specifically concerning the Cu deposit and the presence of Cu₂O, the large Cu amount of Cu quantified by EDS suggests oxidation of the deposit as Cu is present at more than twice the O content. Additionally, deposition of Cu₂O is very unlikely as oxides are not easily deposited. The composition of the Mg materials, as before, Section 3.4.1, appears to be some combination of MgO and Mg(OH)₂ structures. As the samples are exposed to dissolved oxygen {O₂} within the electrolyte, as well as from the environment upon removal, it is impossible to determine the exact composition of the debris beyond the general statement of MgO_x/(OH)_y complexes. Regarding processes within the formation of the immersion film, the likely reactions taking place are oxidation and reduction of Cu by means of galvanic displacement, Table 3.13.

Half-Reaction	E° (V)
$\text{Mg}_{(s)} + 2\text{OH}^{-}_{(aq)} \rightarrow \text{Mg}(\text{OH})_{2(aq)} + 2e^{-}$	+2.690
$\text{Mg}_{(s)} \rightarrow \text{Mg}^{2+} + 2e^{-}$	+2.372
$\text{Cu}_{(s)} + 2\text{OH}^{-}_{(aq)} \rightarrow \text{Cu}_2\text{O}_{(s)} + \text{H}_2\text{O} + 2e^{-}$	+0.360
$\text{Cu}_{(s)} + 2\text{OH}^{-}_{(aq)} \rightarrow \text{Cu}(\text{OH})_{2(s)} + 2e^{-}$	+0.222
$\text{Cu}^{+} + e^{-} \rightarrow \text{Cu}_{(s)}$	+0.521
$\text{Cu}^{2+} + 2e^{-} \rightarrow \text{Cu}_{(s)}$	+0.3419

Table 3.13: List of likely half-reactions along with associated standard electrode potentials for the formation of Cu immersion coatings on Mg alloys.

While these equations, which do not take into account any ligand structure, are not entirely representative of deposition processes, they do provide some idea as to the processes at work. Most notably, the equations for the oxidation of Mg, E°_{cell} = +2.372 V, and reduction of Cu, E°_{cell} = +0.3419 V, suggest that the coating on Mg

should not be stable as corrosion due to galvanic coupling between the substrate and coating appears to be a thermodynamically favoured process. Aside from diffusion, which was not measured and may be occurring, the stability of the Cu claddings is remarkable provided no electrolytic contact is made between the Cu cladding and substrate. Further investigation to the immersion deposit was conducted with the addition of NH_4OH . The inclusion of NH_4OH within the immersion electrolytes, Table 3.14, was attempted as it is a common additive within electroless Ni-P electrolytes.

Chemical Name	Chemical Formula	Bath Composition (g/L)		
		Bath 2A	Bath 3A	Bath 4A
Copper Sulphate Pentahydrate	$\text{CuSO}_4 \cdot 5\text{H}_2\text{O}$	35.0	35.0	35.0
Potassium Sodium Tartrate Tetrahydrate (Rochelle's Salt)	$\text{KNaC}_4\text{H}_4\text{O}_6 \cdot 4\text{H}_2\text{O}$	75.0	75.0	75.0
Sodium Hydroxide	NaOH	20.0	20.0	15.0
Ammonium Hydroxide	NH_4OH	10.0	20.0	83.3

Table 3.14: Alkaline Cu electrolytes for immersion deposits on Mg alloys

The inclusion of NH_4OH served only to thin the immersion coating when included up to a concentration of 20 mL/L, Figure 3.28. Further addition of NH_4OH appeared only to oxidize and further limit the immersion coating rather than generate any improvement.

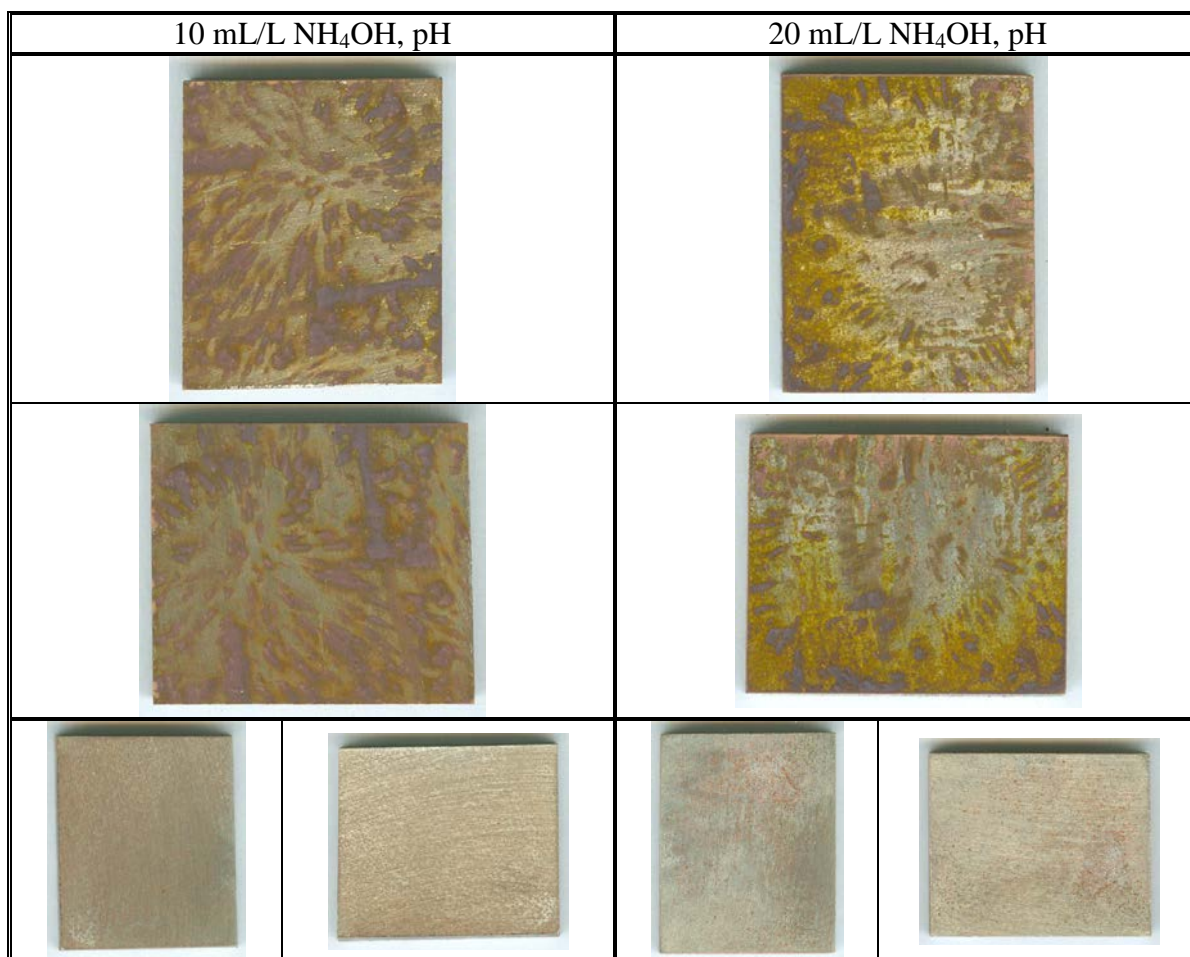


Figure 3.28: Macroscopic image of 14 hour, room temperature, Cu immersion deposits, Table 3.14, formed on the (Top) dry polished and (Bottom) oxidized, sides of wet polished AZ91D Mg alloys.

Given that ammonia {NH₃} dissolves Cu and that NH₄OH contains dissolved NH₃, apparent thinning of the coating is expected along with reduction of Cu coverage. The presence of minor Cu deposits on the reverse, oxidized, sides presented in Figure 3.28 are attributed to incomplete oxidation of the surface prior to immersion within the Cu electrolyte. Microscopic, SEM, images of the Cu immersion surface on the Mg alloys from electrolytes containing NH₄OH demonstrate diminishing coverage of the substrate with increasing NH₄OH, Figure 3.29.

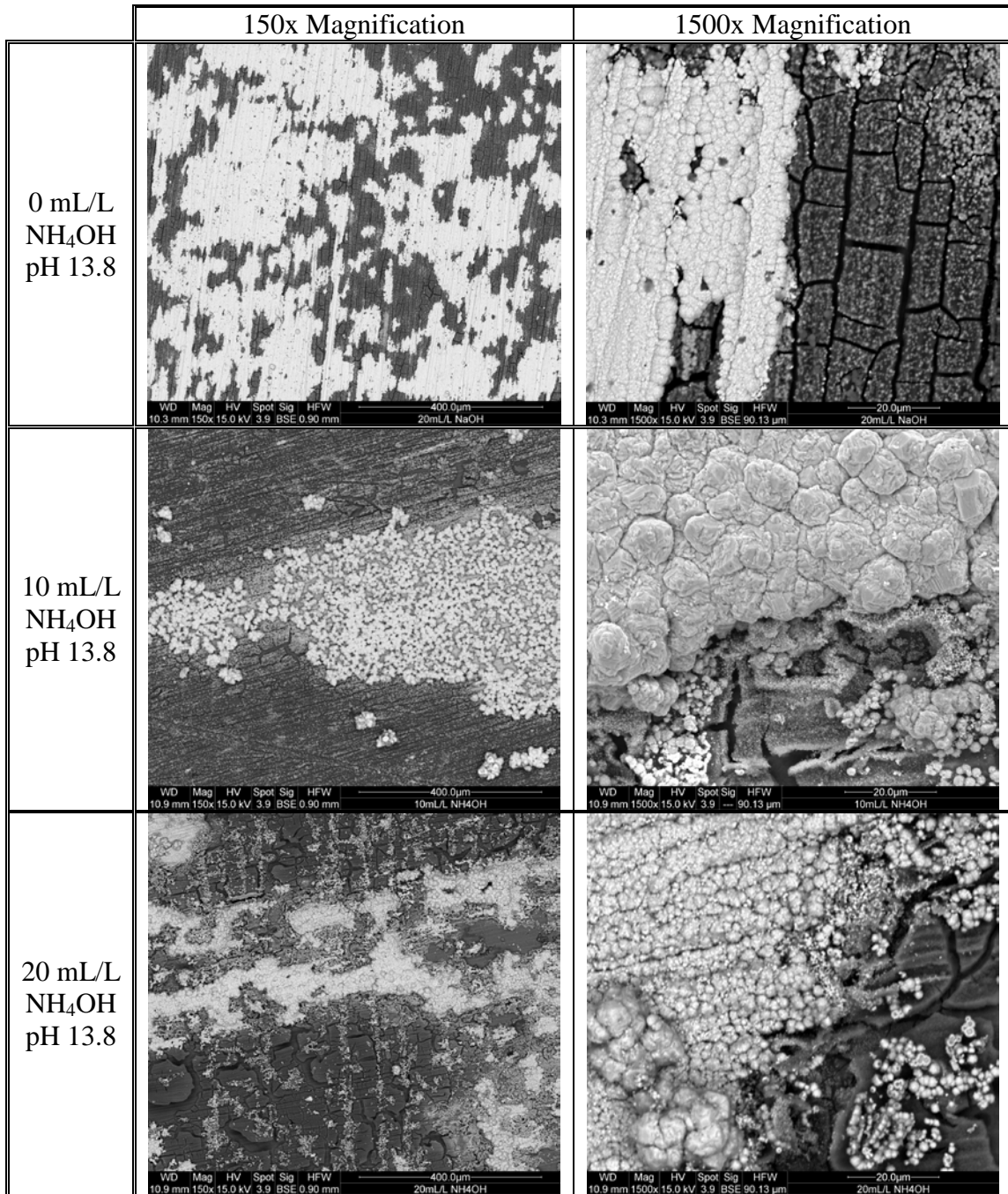


Figure 3.29: Backscatter SEM images comparing of Cu immersion deposits formed over 14h 20min on AZ91D Mg alloys within room temperature electrolytes containing 20 g/L NaOH, 35 g/L CuSO₄ · 5H₂O, 75 g/L KNaC₄H₄O₆ · 4H₂O, and varying concentrations NH₄OH.

Higher NH₄OH concentrations, of the order of 83.3 mL/L, limit Cu deposition only to localized regions, Figure 3.30. The large size of the Cu clusters in those electrolytes with a high NH₄OH concentration suggests that some form of reduction beyond a simple displacement reaction takes place.

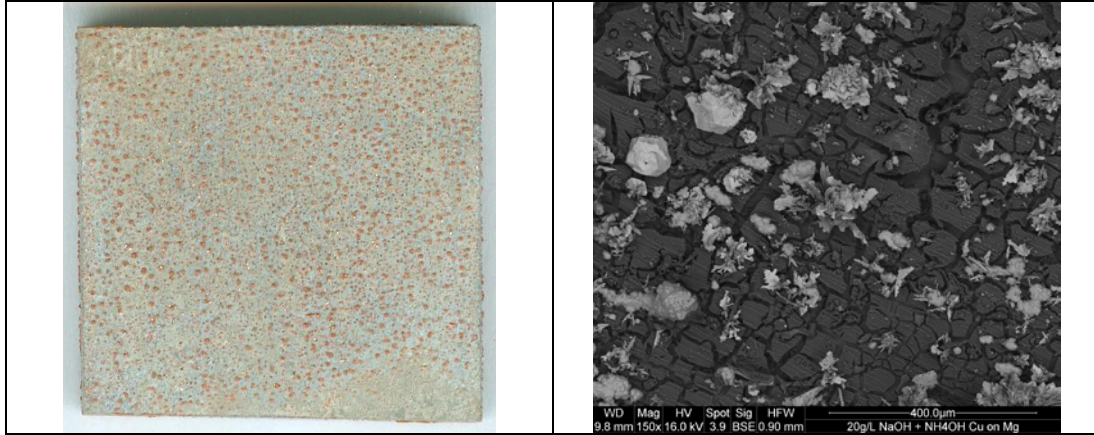


Figure 3.30: Macroscopic image along with backscatter SEM image of a Cu immersion coating formed on an AZ91D Mg alloy [48 h, pH 13.9, 25 °C] from an electrolyte containing 35 g/L $\text{CuSO}_4 \cdot 5\text{H}_2\text{O}$, 75 g/L $\text{KNaC}_4\text{H}_4\text{O}_6 \cdot 4\text{H}_2\text{O}$, 20 g/L NaOH, and 83.3 mL/L NH_4OH .

The presence of Mg and common use of MgSO_4 as a reducing agent for electroless silver {Ag}, Appendix A, suggests it may be possible that Mg^{2+} ions within the Cu electrolytes encourage some form of reduction beyond the immersion coating. Verification of this possibility was carried out with the addition of MgSO_4 to the ‘Bath A’ electrolyte. Immersion of Sn/Pd treated glass within the electrolyte produced a yellowish deposit that appears similar to those produced at the early stages of Cu deposition, Figure 3.31.



Figure 3.31: Macroscopic scans of (Top) 23 h and (Bottom) 68 h electroless immersion deposits on Sn/Pd treated glass slides, treated region 45 mm × 25 mm, from an electrolyte containing 25 g/L $\text{MgSO}_4 \cdot 7\text{H}_2\text{O}$, 20 g/L NaOH, 35 g/L $\text{CuSO}_4 \cdot 5\text{H}_2\text{O}$, and 75 g/L $\text{KNaC}_4\text{H}_4\text{O}_6 \cdot 4\text{H}_2\text{O}$.

The formation of the thin Cu deposit, which does not occur in electrolytes not containing MgSO_4 , required a relatively high concentration, 25 g/L, of $\text{MgSO}_4 \cdot 7\text{H}_2\text{O}$

within the electrolyte. The inclusion of the MgSO_4 at such a high concentration resulted in a separation of the electrolyte and may have simply displaced Cu from the ligand structure resulting in the formation of the deposit. Microscopic investigation of the coating on the 68 hour immersion sample, Figure 3.32, demonstrates that the deposit is composed mostly of an organic type structures with Cu deposited only at the lowest extremity, rightmost part in Figure 3.31, of the sample.

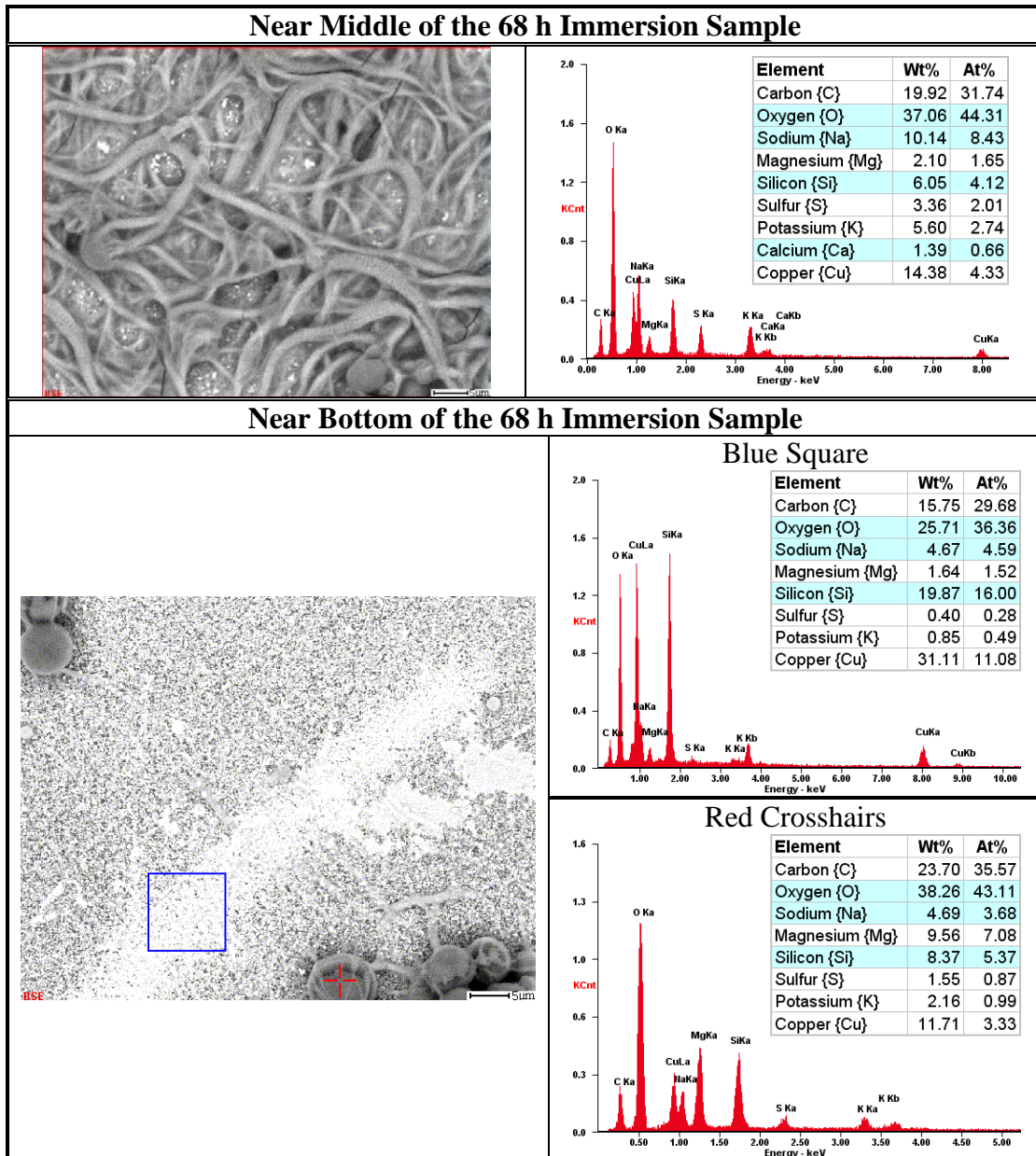


Figure 3.32: Backscatter SEM images and EDS of a 68 hour deposit on Sn/Pd treated glass from an electrolyte containing 25 g/L $\text{MgSO}_4 \cdot 7\text{H}_2\text{O}$, 20 g/L NaOH, 35 g/L $\text{CuSO}_4 \cdot 5\text{H}_2\text{O}$, and 75 g/L $\text{KNaC}_4\text{H}_4\text{O}_6 \cdot 4\text{H}_2\text{O}$. (Top) SEM and EDS of the deposit near the top of the sample, (Middle) SEM of deposit formed near the bottom of the sample, (Bottom) EDS of (Left) Cu and (Right) organic structures near the bottom of the sample. Highlighted in light blue in the EDS composition are the components attributed to the glass substrate.

The slow formation of an ostensibly monolayer deposit at the lowest end of the substrate suggests that any contribution to film formation is limited for the short immersion of Mg in the electroless Cu electrolyte. Furthermore, while Cu and Ag have similar nobility, increasing the likelihood of reduction enhancement of some sort by Mg ions alongside immersion deposits, it is not likely a major factor in the thickness of Cu immersion coatings. Hence, explanations as to the apparent thickness of the immersion coatings formed in electrolytes containing NaOH, CuSO₄, and KNaC₄H₄O₆ are reasoned as an ongoing reaction with the uncovered substrate rather than the presence of Mg ions acting as a reducing agent.

An additional, but unrelated, exercise in developing a pre-treatment for electroless Cu produced what is best described as a corrosion/displacement reaction. The observation of a displacement/corrosion reactions occurred during a investigation of ionic liquids as electrolytes for the metallization of Mg alloys. As ionic liquids do not contain water it was felt that they would provide superior, corrosion free deposition environments. Difficulties in keeping water out of the hygroscopic mixtures led to the abandonment of this approach as the application of a metallic thin film must be as simple as possible in order to be embraced by industry. One result of note was the observation of what appeared to be a selective displacement reaction on the surface of Mg alloys. The addition of water to a < 2 mm thick layer of Zn containing ionic liquid, specifically zinc chloride-1-ethyl-3-methylimidazolium chloride (ZnCl₂-EMIC), on the surface of Mg produced a corrosion reaction which resulted in the uneven reduction of Zn. The reaction, which appeared to be catalyzed by adding water to the ionic liquids, was best described as a corrosion/simple displacement reaction as the mixture was acidic and contained Cl⁻ ions. The uneven coating, which was composed mainly of Zn oxide {ZnO}, was tested as a Cu pre-treatment but produced poor quality deposits. The poor quality was attributed to the lack of a catalytic surface for electroless Cu deposition and the discontinuities of the treatment resulting in discontinuous deposits. These results, while interesting, are not relevant to the successful metallization of Mg alloys for the purpose of corrosion resistance but serve to demonstrate the intricacies and difficulties in the successful cladding of Mg alloys.

3.4.2.3 Metallic, Electroless Cu Coating of AZ91D Mg Alloys

Combining the many novel observations, methods, and techniques obtained from the work with electroless Cu; good, metallic quality deposits have been successfully deposited on Mg alloys, Figure 3.33. These deposits, which are produced in electrolytes of around pH 13, Table 3.15, are just above where corrosion would occur as can be seen by the same immersion pattern present from immersion electrolytes around pH 13.8.



Figure 3.33: Macroscopic scanned images of an electroless Cu deposit [20 min, 25 °C] on a dry polished 25 mm × 25 mm × 5mm AZ91D Mg alloy.

Bath	Chemical Name	Chemical Formula	Bath Composition (g/L)
Bath A	Copper Sulphate Pentahydrate	$\text{CuSO}_4 \cdot 5\text{H}_2\text{O}$	35.0
	Potassium Sodium Tartrate Tetrahydrate (Rochelle's Salt)	$\text{KNaC}_4\text{H}_4\text{O}_6 \cdot 4\text{H}_2\text{O}$	75.0
	Sodium Hydroxide	NaOH	12.5
Bath B	Paraformaldehyde	$\text{HO}(\text{CH}_2\text{O})_n\text{H}$ ($n = 8-100$)	65.0
	Sodium Hydroxide	NaOH	12.5
Operating Temperature: 20 to 25 °C		pH: 12.95	

Table 3.15: Modified electroless Cu thin film electrolyte

The metallic coating of Cu on the Mg alloy is not without defects as some corrosion is present on faces where the oxide layer was not entirely removed. Furthermore, the well formed deposit on the edges of one of the larger faces match the place at which the sample was held with a latex glove during polishing. The presence of the latex glove appears to have limiting oxidation improving the deposit in that region. Efforts to improve electroless Cu on Mg alloys rests with the improvement of oxide removal regiments and some minor tuning of the alkaline electroless Cu electrolyte. Tuning of the electroless Cu electrolyte presented is restricted to the alkaline regime as a mixture of CuSO_4 and $\text{KNaC}_4\text{H}_4\text{O}_6$ produces precipitates within the aqueous solution. The addition of NaOH to the CuSO_4 and $\text{KNaC}_4\text{H}_4\text{O}_6$ mixture initially does not change the pH, which remains around 5.6, until sufficient NaOH is added so that the precipitates are dissolved into the electrolyte.

The application of alkaline electrolytes, though creating $\text{Mg}(\text{O})_x/\text{OH}_y$ complexes in the case of Ni-B deposition, provide the best way in which to allow deposition directly on Mg alloys using minimal surface preparation. Given the ubiquity of Ni-P coatings within both industry and scientific research, the methods and techniques established for electroless Cu were applied to the formation of Ni-P coatings.

3.4.3 Electroless Nickel Phosphorous {Ni-P} and Other Binary Alloys

In the early work, Section 3.4.1, exposure of Mg alloys to alkaline Ni-P electrolytes resulted in decomposition of the electrolyte similar to that observed within acidic electrolytes. As dry polishing immediately prior to immersion was not attempted, the acidic Ni-P electrolyte, Table 3.16, was revisited as a means of coating formation.

Chemical Name	Chemical Formula	Bath Composition (g/L)
Nickel Sulfate Hexahydrate	$\text{NiSO}_4 \cdot 6\text{H}_2\text{O}$	29.0
Succinic Acid Disodium Salt	$\text{Na}_2\text{C}_4\text{O}_4\text{H}_4$	15.0
Succinic Acid	$\text{C}_4\text{O}_4\text{H}_6$	1.3
Sodium Hypophosphite Hydrate	$\text{NaPH}_2\text{O}_2 \cdot \text{H}_2\text{O}$	17.0
Deposition Temperature: 65 to 80°C		pH before bath use (20 °C): 5.40

Table 3.16: Acidic Ni-P electrolyte, essentially identical to the electrolyte presented in Table 3.2b [22]. Minor alterations have no impact on the electrolyte and serves to accurately reflect the used electrolyte.

The application of the oxide removal technique, established for alkaline electroless Cu deposits, allowed the successful formation of a deposit albeit at an inferior quality compared to electroless Cu, Figure 3.34. The formulation of the acidic electrolyte was chosen as it did not contain Cl^- ions, which are known to be most aggressive in promoting corrosion of Mg surfaces; though nitrates $\{\text{NO}_3^-\}$ and sulphates $\{\text{SO}_4^{2-}\}$ also attack Mg albeit to a somewhat lesser extent [27]. As the most aggressive corrosion promoting ion was not present within the electrolyte, the poor quality of the coating was attributed mostly to the active, acidic environment. The presence of SO_4^{2-} ions within the electrolyte, though likely to have contributed to corrosion within the acidic environment, were not the major factor in corrosion as SO_4^{2-} ions were present as part of the electrolytes which successfully deposited Cu on Mg.

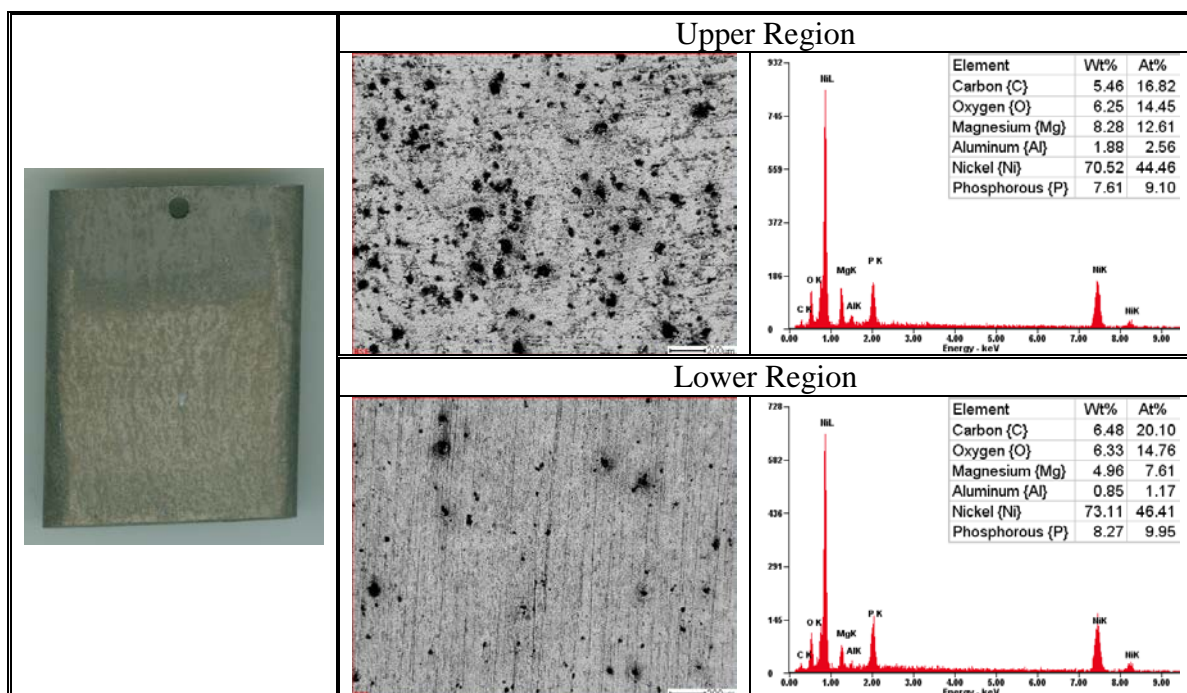


Figure 3.34: Macroscopic image, backscatter SEM images, with 200 μm scale bars, and EDS analysis of the upper and lower portions of the acidic Ni-P coating [9 min, 65 $^{\circ}\text{C}$] on a AZ91D Mg alloy. [19]
Note: The dark regions on the SEM image are both rich in Mg and represent protrusions from the surface according to secondary emission images.

In order to provide a less active environment the alkaline electroless Ni-P electrolyte was also revisited. Taking cues from the attempted minimization of ions within the alkaline Cu electrolyte, Section 3.4.2, NH_4Cl and NaOH were both replaced by NH_4OH . Additionally, NiSO_4 was replaced by Ni-acetate $\{\text{Ni}(\text{C}_2\text{H}_3\text{O}_2)_2\}$, as SO_4^{2-} ions can contribute to corrosion, Table 3.17. While the NH_4Cl was entirely replaced, NaOH remained in the electrolyte to provide pH stability. The resulting Ni-P electrolyte was capable of metalizing Sn/Pd treated glass, indicating the changes in formulation were appropriate.

Chemical Name	Chemical Formula	Bath Composition (g/L)
Nickel Acetate Tetrahydrate	$\text{Ni}(\text{C}_2\text{H}_3\text{O}_2)_2 \cdot 4\text{H}_2\text{O}$	9.94
Sodium Citrate Tribasic Dihydrate	$\text{Na}_3\text{C}_6\text{H}_5\text{O}_7 \cdot 2\text{H}_2\text{O}$	23.50
Sodium Hypophosphite Hydrate	$\text{NaH}_2\text{PO}_2 \cdot \text{H}_2\text{O}$	17.50
Sodium Hydroxide	NaOH	1.25
Ammonium Hydroxide* (28.0 % - 30.0 %)	NH_4OH	12.50
Deposition Temperature: 68 to 72 $^{\circ}\text{C}$	Average pH before use (20 $^{\circ}\text{C}$): 11.81	

* NH_4OH was measured in mL/L.

Table 3.17: Electroless Ni-P thin film electrolyte for successful deposition on Mg alloys. [19]

Immersion of dry polished Mg alloys in the electrolyte produced a vigorous initial reaction attributed to the active Mg surface. The initial reaction, which liberated a large amount of bubbles assumed to be H₂ gas, lasted for approximately 5 minutes before eventually subsiding into a steady state metalizing reaction. The coating produced by the Ni-P metallization, Figure 3.35, did not flake from the surface and had a mimetic morphology effectively copying the polishing pattern left on the substrate.

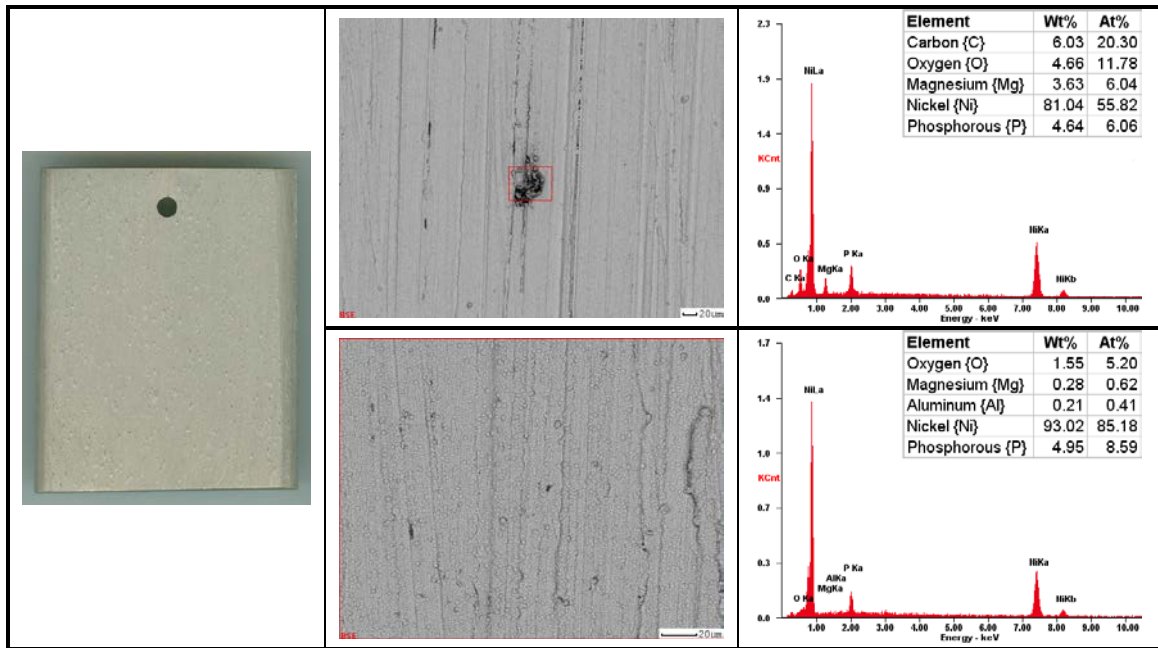


Figure 3.35: Macroscopic image, backscatter SEM images, with 20 μm scale bars, and EDS analysis of an alkaline electroless Ni-P coating [9 min, 68 °C] on a AZ91D Mg alloy. [19]

The rough quality of the surface and minor Mg protrusions were initially attributed to the polishing of the surface, though breakdown of the electrolyte after several uses required investigation. In keeping with the C₆H₅O₇³⁻ stabilizer and H₂PO₂⁻ reducing agent, only the identity of the metal salt and source of alkalinity remained variable across the formulations. In attempting to isolate the role of the metal salt and source of alkalinity within the electrolyte, a number of electrolyte variants, Tables 3.18 & 3.19, were tested on polished Mg alloys.

Chemical Name	Chemical Formula	Bath Composition (g/L)					
		S1	S2	S3	S4	S5	S6
Nickel Acetate Tetrahydrate	$\text{Ni}(\text{C}_2\text{H}_3\text{O}_2)_2 \cdot 4\text{H}_2\text{O}$	9.94	—	—	9.94	—	—
Nickel Sulphate Hexahydrate	$\text{NiSO}_4 \cdot 6\text{H}_2\text{O}$	—	10.5	—	—	10.5	—
Nickel Sulfamate Tetrahydrate	$\text{Ni}(\text{H}_2\text{NSO}_3)_2 \cdot 4\text{H}_2\text{O}$	—	—	12.9	—	—	12.9
Sodium citrate Tribasic Dihydrate	$\text{Na}_3\text{C}_6\text{H}_5\text{O}_7 \cdot 2\text{H}_2\text{O}$	23.5	23.5	23.5	23.5	23.5	23.5
Sodium Hypophosphite Hydrate	$\text{NaH}_2\text{PO}_2 \cdot \text{H}_2\text{O}$	17.5	17.5	17.5	17.5	17.5	17.5
Sodium Hydroxide	NaOH	1.25	1.25	1.25	—	—	—
Ammonium Hydroxide* (28.0 % - 30.0 %)	NH_4OH	12.5	12.5	12.5	37.5	37.5	37.5
Average pH before use (20 °C)		11.81	11.98	11.85	11.86	11.92	11.93
Deposition temperature:		68 to 72 °C.					

* NH_4OH was measured in mL/L.

Table 3.18: Formulations of successful electroless Ni-P thin film electrolytes for deposition on Mg alloys. [19]

The electrolytes presented in Table 3.18 are numbered as S# as they represent successful electrolytes. Similarly, the less successful, or failed electrolytes of Table 3.19 are numbered as F#. Additionally, to allow for adequate comparison of all alkaline electrolytes tested, both the molar concentration of the Ni^{2+} ions, as well as the pH of the electrolyte, remained fixed, or as fixed as possible in the case of pH. The molar concentration of the Ni^{2+} ions in the electrolytes was of the order of $3.995 \cdot 10^{-2}$ M. Changes in concentration of the metal salt were not explored. Increasing the concentration of the metal salt is expected to require changes in both the stabilizer and source of alkalinity. Specifically, the $\text{C}_6\text{H}_5\text{O}_7^{3-}$ stabilizer is present at twice the concentration of Ni^{2+} ions in solution, $7.990 \cdot 10^{-2}$ M, and is responsible, in part, for the stability of the electrolyte during deposition as some Mg^{2+} is likely present from corrosion.

Chemical Name	Chemical Formula	Bath Composition (g/L)					
		F1	F2	F3	F4	F5	F6
Nickel Sulfate Hexahydrate	NiSO ₄ · 6H ₂ O	29.0	—	—	—	10.5	10.5
Nickel Chloride Hexahydrate	NiCl ₂ · 6H ₂ O	—	9.495	9.495	—	—	—
Nickel Acetate Tetrahydrate	Ni(C ₂ H ₃ O ₂) ₂ · 4H ₂ O	—	—	—	9.94	—	—
Succinic Acid Disodium Salt	Na ₂ C ₄ O ₄ H ₄	15.0	—	—	—	—	—
Succinic Acid	C ₄ O ₄ H ₆	1.3	—	—	—	—	—
Sodium Citrate Tribasic Dihydrate	Na ₃ C ₆ H ₅ O ₇ · 2H ₂ O	—	23.5	23.5	23.5	23.5	23.5
Sodium Hypophosphite Hydrate	NaPH ₂ O ₂ · H ₂ O	17.0	17.5	17.5	17.5	17.5	17.5
Sodium Hydroxide	NaOH	—	1.25	—	1.938	1.875	11.91
Ammonium Hydroxide* (28.0 % - 30.0 %)	NH ₄ OH	—	12.5	37.5	—	—	—
Ammonium Sulfate	(NH ₄) ₂ SO ₄	—	—	—	—	—	19.25
Average pH before use (20 °C)		5.40	11.86	11.77	12.32	11.97	11.30
Deposition temperature:		68 to 72 °C.					

*NH₄OH was measured in mL/L.

Table 3.19: Formulations of unsuccessful electroless Ni-P thin film electrolytes for deposition on Mg alloys. [19] Note: Bath F1 is a reproduction of that found in Table 3.16 as it was part of the wider set of electrolytes presented in the original published table.

A notable feature regarding all electrolytes is a drop in alkalinity, as measured by the pH meter, due to heating, immediately prior to use. The measured, temperature adjusted, pH of all alkaline electrolytes was of the order of 9.5 at temperature immediately prior to deposition and returned to around 10.5 after use of the electrolyte. The pH drop between the initial room temperature electrolyte and the post-deposit room temperature electrolyte is a reflection of the acidity provided by the liberation of hydrogen ions {H⁺} from the reducing agent and corrosion reactions. As P content in the deposit is a function of the acidity/alkalinity of the electrolyte [28] and control of the alkalinity was not practical, a consistent amount of P may not be present throughout the coatings.

Results from the electrolytes tested demonstrated that electrolytes containing Cl^- ions, which were initially discounted as a concern in the early work, play a critical role regarding both stability of the electrolyte and quality of the deposit. Those electrolytes containing Cl^- ions were more prone to decomposition and formed deposits with a significant presence of $\text{MgO}_x/(\text{OH})_y$ crystallites, Figure 3.36, than those electrolytes free of the Cl^- ions, Figures 3.38 & 3.39.

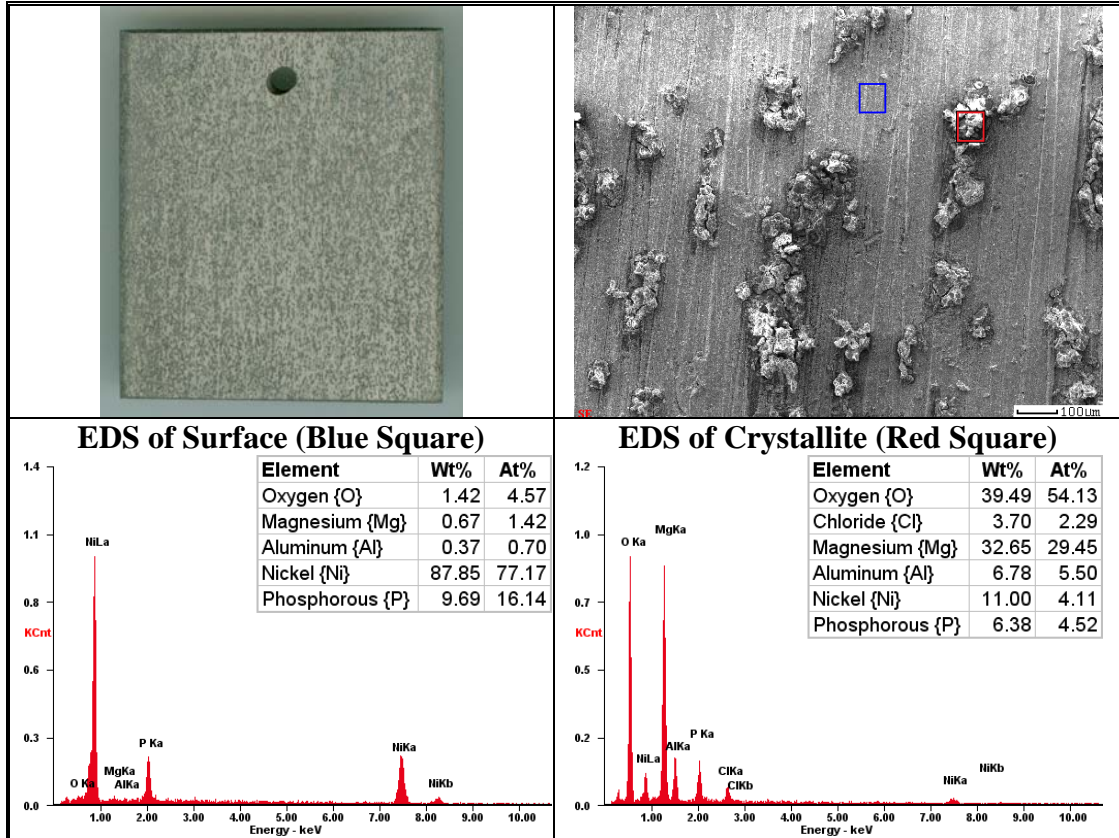


Figure 3.36: Macroscopic scan, backscatter SEM image, scale bar: 100 μm , and EDS analyses of an alkaline electroless Ni-P deposit [2 min, 70 $^{\circ}\text{C}$] from Bath F3, containing Cl^- ions, on a dry polished AZ91D Mg alloy. [19]

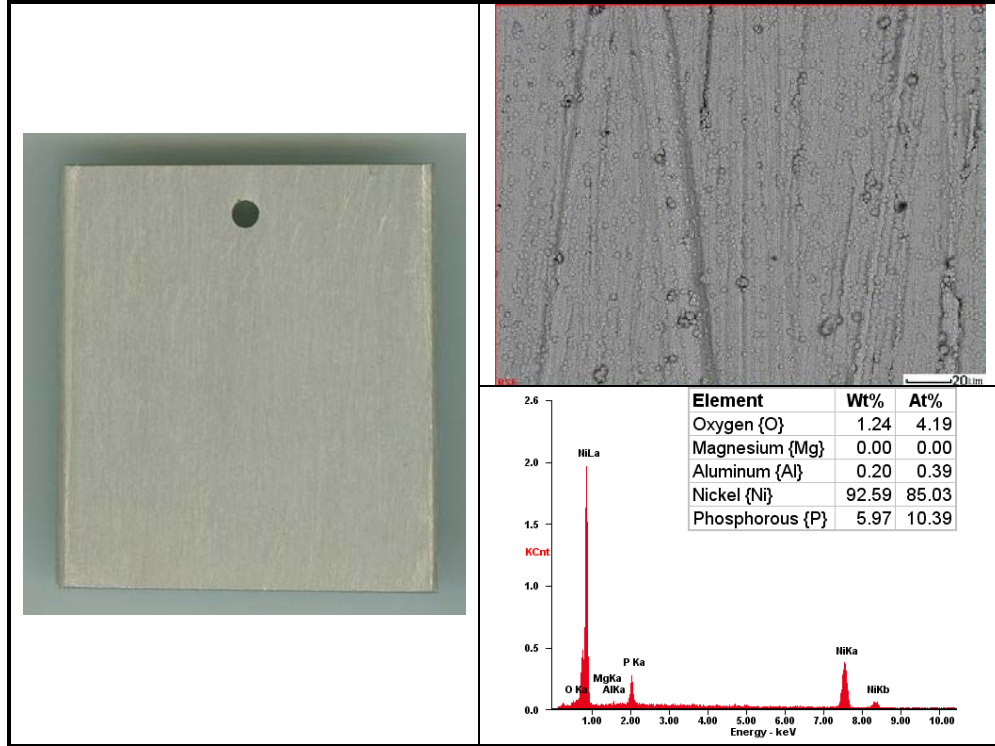


Figure 3.37: Macroscopic scan, backscatter SEM image, scale bar: 20 μm, and EDS analysis of an alkaline electroless Ni-P deposit [5 min, 68 °C], from Bath S2, on a dry polished AZ91D Mg alloy. [19]

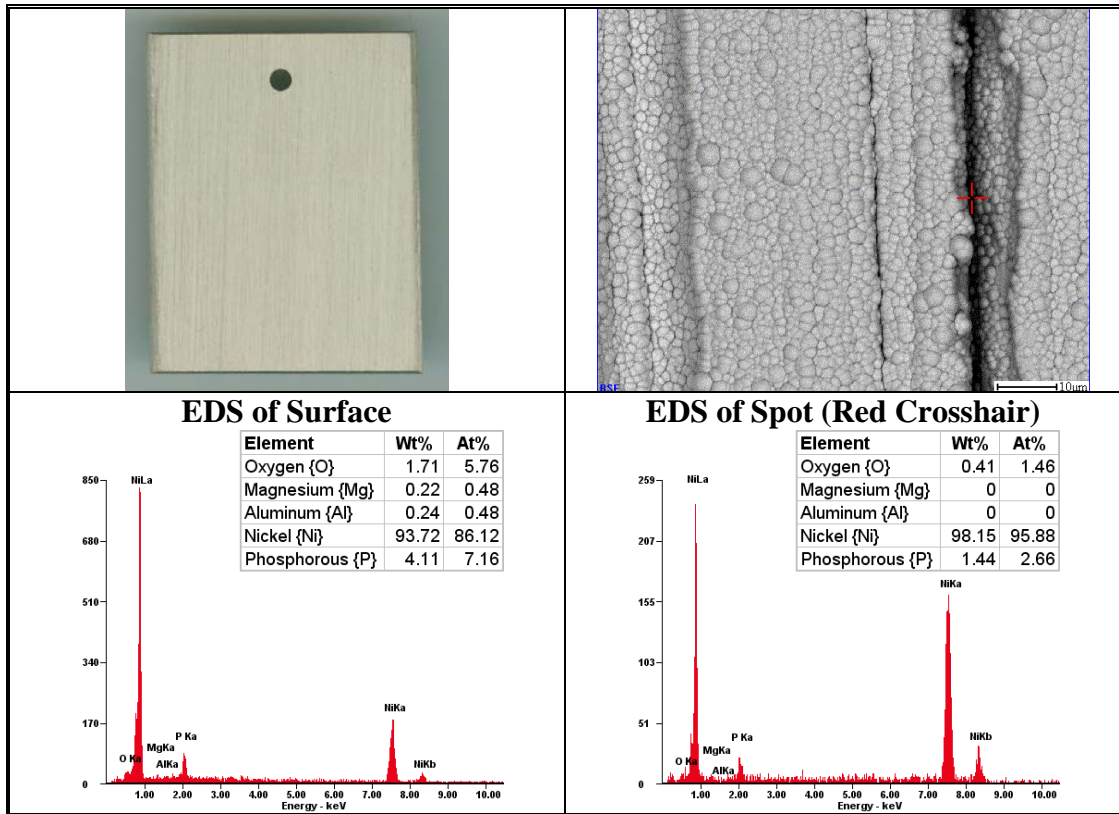


Figure 3.38: Macroscopic scan, backscatter SEM image, scale bar: 10 μm, and EDS analyses of an alkaline electroless Ni-P deposit, from Bath S4 [10 min, 68 °C], on a dry polished AZ91D Mg alloy. [19]

While electrolytes containing a mixture of NaOH and NH₄OH, Baths S1, S2, & S3, were reasonably stable and provided good quality deposits, electrolytes containing NaOH as the only source of alkalinity, Baths F4 and F5, were prone to decomposition and produced significantly poorer quality deposits, Figure 3.39. The stability of electrolytes F4 and F5 was of the order of less than 30 minutes while electrolytes S1, S2 and S3 were stable for well over an hour.

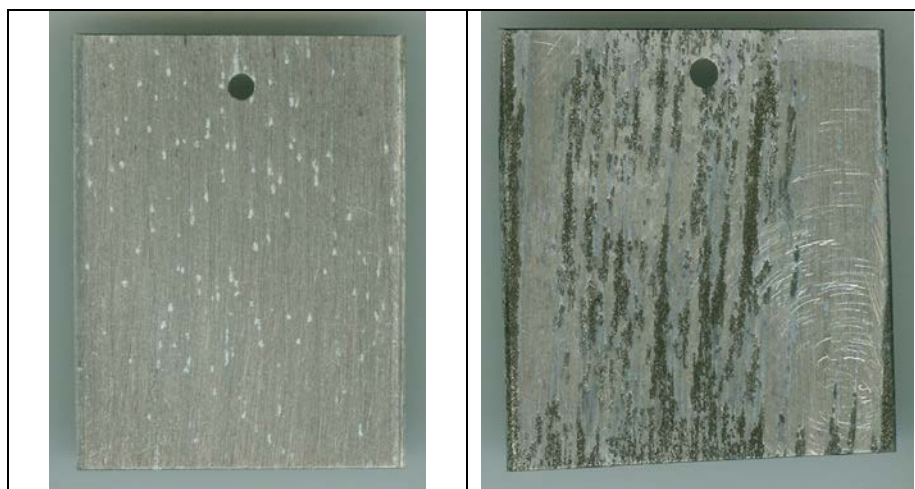


Figure 3.39: Macroscopic scans of failed deposits from (Left) Bath F4 [5 min, 69 °C] and (Right) Bath F5 [5 min 74 °C] on AZ91D Mg alloys. [19]

As the electrolyte already contains a stabilizer, C₆H₅O₇³⁻, the addition of NH₃ acts as a further buffer for the electrolyte and provides additional stability needed for deposition on Mg substrates. The change in the colour of the electrolyte upon the addition of NH₄OH suggests a mixed ligand structure; without the C₆H₅O₇³⁻, complexing agent the dissolved NH₃ would form [Ni(NH₃)₆]²⁺ complexes. Further benefits of NH₄OH within the electrolyte include buffering against increasing acidity, NH₃ is a buffer of pKa 9.25, as well as the lack of superfluous, corrosive, ions such as Cl⁻ and SO₄²⁻, which are liberated by the use of NH₄Cl and (NH₄)₂SO₄. The liberation of corrosive anions, especially Cl⁻, is another factor in the stability of the electrolyte as corrosion of the substrate can catalyze decomposition. While it is possible that maintaining both the pH and NH₃ in solution would increase the usable lifetime of electrolytes containing Cl⁻ ions, electrolytes free of Cl⁻ ions, such as the ‘S’ class baths, Table 3.18, require no maintenance, at least within the first few hours of use, in order to prevent decomposition.

Electrolytes containing $(\text{NH}_4)_2\text{SO}_4$ and NaOH, Bath F6, while able to produce reasonable quality deposits, were also found to have limited stability and could decompose in as little as under 30 minutes. Conversely, electrolytes free of Cl^- ions and containing NH_4OH as the sole source of alkalinity produce good quality and are exceptionally stable with decomposition having yet to be observed despite several hours of use and cycles of use and inactivity. Evaporation of NH_3 from the 90 °C electrolyte along with increased acidity from many deposits are factors which are expected to hinder the stability of the electrolyte in the longer term; though these factors have yet to be fully examined.

The presence of two complexing agents, NH_3 and $\text{C}_6\text{H}_5\text{O}_7^{3-}$, appears to be a central factor in the successful formation of electroless Ni deposits on Mg surfaces. It is thought that, in addition to preventing harmful galvanic reactions between the Ni^{2+} ions and Mg substrates, and buffering against increased acidity from corrosion of the Mg substrate; the complexing agents also help sequester any Mg^{2+} ions liberated into the solution from the corrosion of the Mg substrates.

Perhaps the most interesting and useful result provided by the S-class electrolytes, Table 3.18, is the capacity of the electrolytes to provide Ni-P deposits on oxidized Mg surfaces, Figure 3.40. Oxidized surfaces are typically insufficiently catalytic to allow electroless deposition unless some component of the electrolyte renders the surface catalytic in a parallel process.

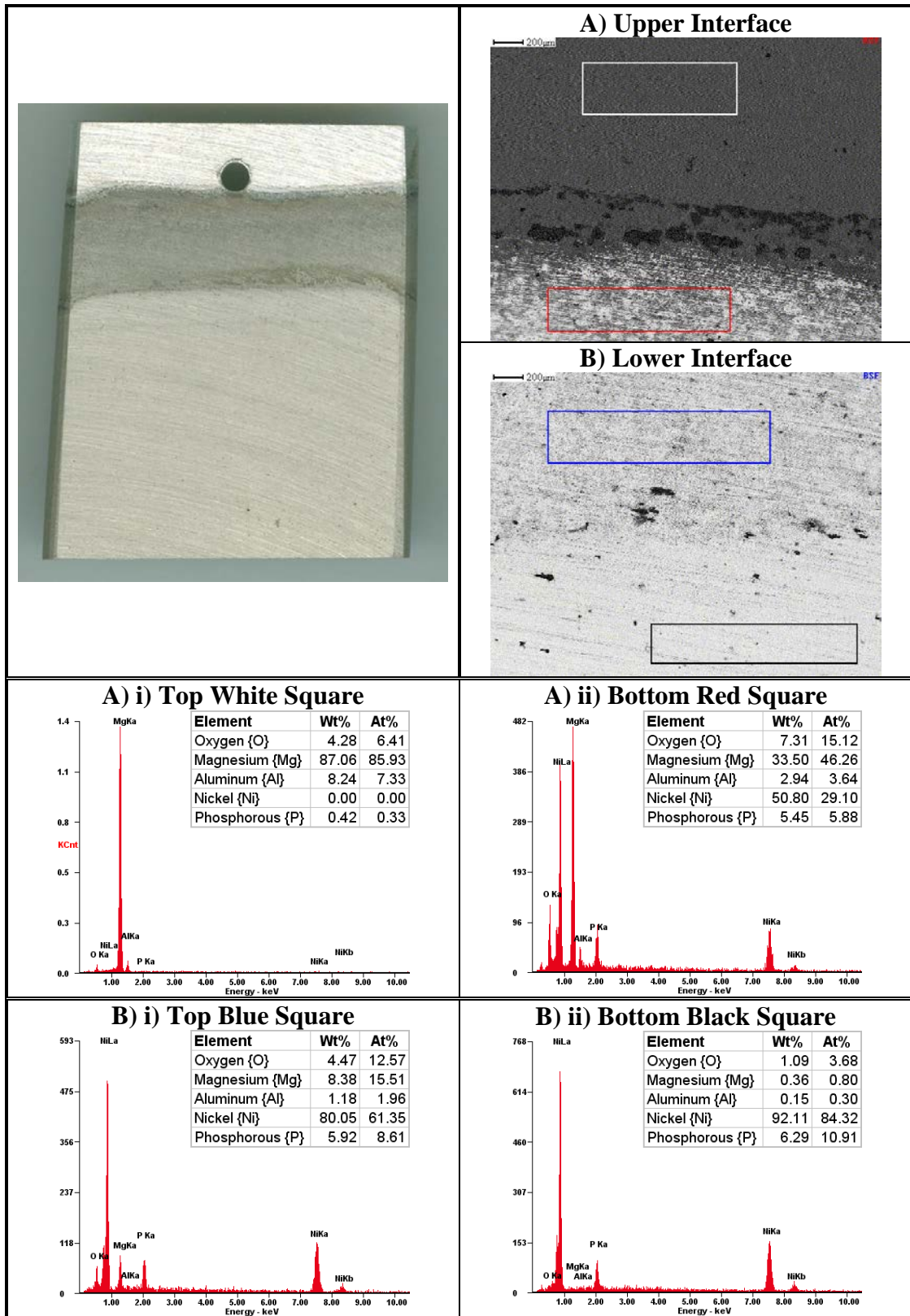


Figure 3.40: Macroscopic image of an oxidized AZ91D Mg alloy with No, 2 min, and 5 min deposits from electrolyte S6 at 75 °C along with backscatter SEM images, with 200 μm scale bars, and EDS provided for the regions highlighted on each side of the interface. [19]

Unlike the polished samples, which immediately produced a vigorous response upon immersion, a short dwell time was associated with the immersion of oxidized Mg alloys in the electrolyte. The presence of a dwell time is attributed to initial corrosion resistance of the oxide layer which is dissolved by a consequent corrosion reaction during the initial stages of deposition. As with the case of polished samples, the intense initial evolution of bubbles subsided into a steady state deposition reaction. The well formed deposits were of equal quality as those produced on polished surfaces indicating that oxide removal was more likely than deposition over the oxidized layer. The minimal oxide content indicated by EDS of the substrate is due to the thinness of the oxide layer rather than the apparent polishing. Wet polishing of the surface was carried out 24 hours prior to deposition and about one week prior to EDS measurements. Even formed under ideal conditions, such as 60 hours at 20 kPa in pure oxygen {O₂} on pure Mg, oxide layers on Mg measures only of a few, 4.3, nanometers in thickness [29].

Immersion of the Ni-P deposited Mg alloy sample within post-deposit, distilled water, rinse baths did not, in most cases, produce any reaction, indicating a good quality deposit. In certain cases immersion within the distilled water rinse produced some bubbles originating from the surface of the deposit. The observation of the bubbles was associated with the presence of micro-pores/pinholes as observed by SEM. The evolution of bubbles in the post-deposit rinse was hence attributed to galvanic corrosion between the substrate and coating for which immersion in distilled water was an adequate test. The presence of pinholes was associated with higher temperature deposits where H₂ evolution from the surface was greater and a higher deposition rate produced greater stresses within the cladding. Managing the deposition rate is hence a critical component of the successful formation of Ni-P claddings on Mg alloys.

The production of an immersion coating in the case of alkaline Cu suggests that a similar process is likely in the formation of Ni-P deposits. The capacity of deposits to form on oxidized surfaces, which differs from electroless Cu deposits, suggests the presence of an immersion reaction and/or mild corrosion of the oxide layer. Testing for the presence of a Ni immersion coating within a reducing agent free electrolyte was conducted using electrolyte S5, Table 3.18. In order to observe any difference between oxidized and polished surfaces, AZ91D Mg alloy samples were prepared in the same way

as Cu immersion testing, with the entire sample wet polished and a dry polish applied to one surface immediately prior to immersion. Upon immersion of the Mg alloy within the electrolyte, the evolution of small bubbles was observed primarily from the freshly polished face. The production of bubbles from the oxidized face was minimal by comparison and was associated with incomplete formation of the oxide layer after wet polishing, which had occurred only 15 minutes prior to immersion. The formation of some form of deposit was observed both macroscopically as well as with SEM and EDS analysis, Figure 3.41. The maintenance of the electrolyte at 80 °C resulted in bubbling off of the NH_3 which in turn allowed for a greater reaction. After 5 minutes immersion excess NH_4OH , to the order of 50 mL/L was added to the electrolyte. The addition of the excess NH_4OH arrested most of the bubbles evolving from the polished surface indicating the increased alkalinity stabilized, and likely also created, an oxide layer on the surface of the alloy.

As can be seen by the SEM images, an incomplete Ni immersion deposit was formed on polished surface. The deposit, blue crosshairs, did not contain P as no reducing agent, the source of P, was present. The presence of Al rich regions, red square, is somewhat at odds with the typical response of Al containing Mg alloys in alkaline environments as the Al component dissolves and a passive Mg-enriched film forms within alkaline media [25]. The presence of MgO regions, yellow square, are indicative of corrosion which is expected as the Mg electrolyte was not saturated with NH_4OH for the initial immersion.

The subsequent introduction of an identically prepared Mg alloy sample within the electrolyte containing an excess of NH_4OH produced only a rapid initial reaction. The reaction, which appeared to be mainly one of oxidation, produced almost no Ni clusters on the surface of the deposit. Based on the results obtained for immersion coatings, it appears that both immersion and corrosion reactions are present; though unlike Cu immersion a definitive transition is difficult to observe.

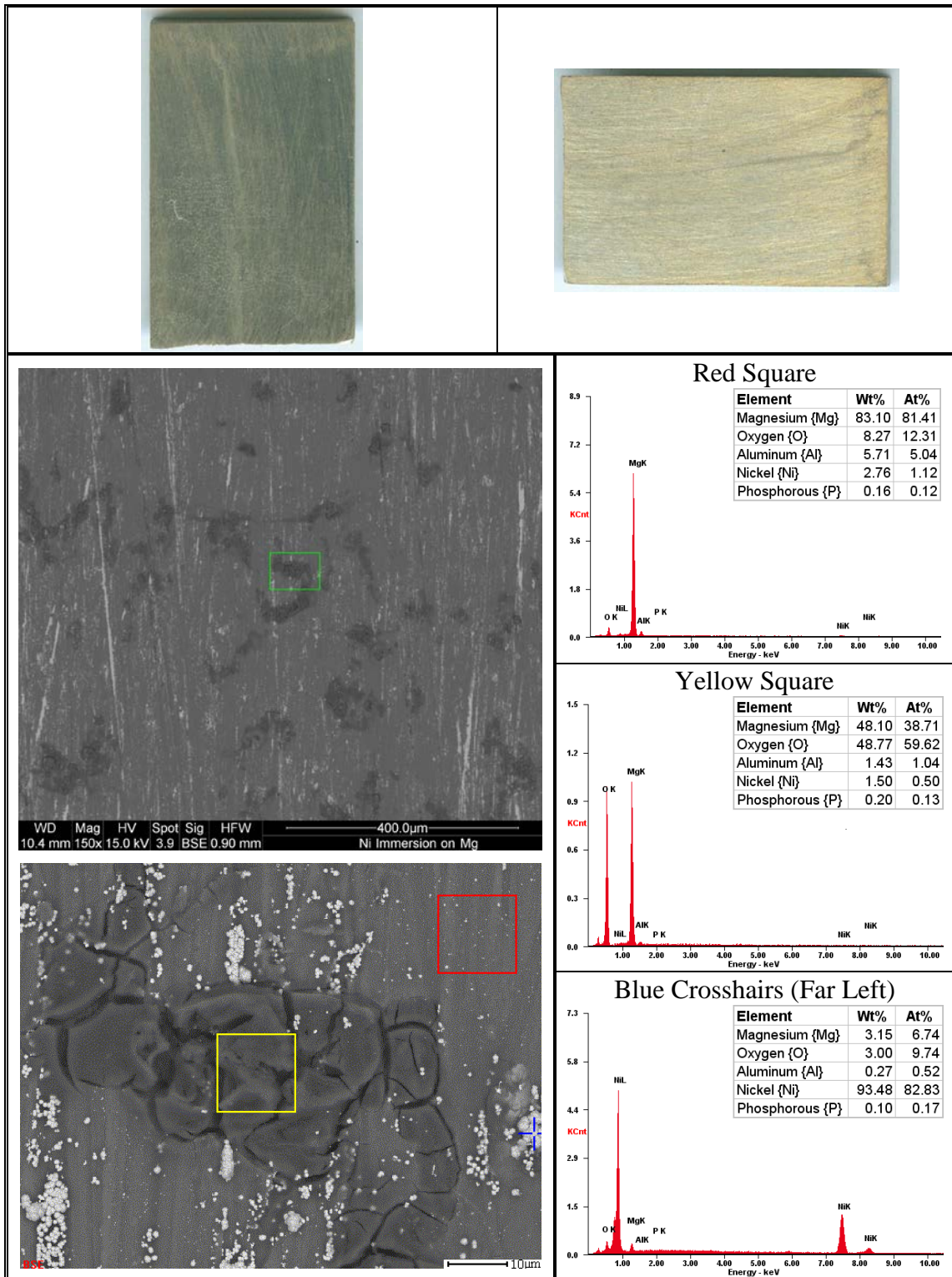


Figure 3.41: (Top) Macroscopic, vertical and horizontal, scans, (Bottom - Left) backscatter SEM images, and (Bottom - Right) EDS analysis, of a Ni immersion deposit [5 min 82 °C] formed on a freshly polished AZ91D Mg alloy from an electrolyte containing 10.5 g/L NiSO₄ · 6H₂O, 23.5 g/L Na₃C₆H₅O₇ · 2H₂O, and 50 mL/L NH₄OH. The green square in the 150x magnification image contains the regions of EDS analysis, shown in the backscatter image below, with the EDS results shown on the right.

The observation of deposition within electrolytes containing a reducing agent along with excess NH_4OH is attributed to the presence and adsorption of the reducing agent on the surface of the substrate. The stark difference of the electrolyte dependent on the presence of a reducing agent indicates that adsorption of the reducing agent is key to overcoming the oxidation of the substrate. A determination as to whether the oxide layer is preserved or corroded away requires the use of more sophisticated techniques such as laser ablation of the surface for spectroscopic analysis. Additionally, the role of the reducing agent in deposits on oxide surfaces within NH_4OH saturated electrolytes suggests the presence of a P-rich interlayer similar to the B-rich interlayer observed by others [30] in the formation of Ni-B deposits on Mg substrates.

As in the case of a polished surface, it is by way of speculation assumed that, a deposition reaction outpaces a simultaneous, though due to the alkalinity a somewhat suppressed, corrosion reaction. Specifically regarding deposition on an oxidized surface, observation of the increased H_2 evolution upon immersion of the Mg substrate within the electrolyte suggests removal of the oxide layer. Comparing to the results for alkaline electroless Cu, the alkaline environment under pH 13 suggests that corrosion, in addition to deposition and the possible formation of an immersion coating, is taking place. The destabilization of the oxide layer due to a corrosion reaction suggests strongly that oxide removal occurs during the initial stages of deposition. Though the surface becomes catalytic, the dwell time, which suggests that some of the oxide is removed/dissolved, allows for the possibility that discontinuities within the oxide surface allow the deposit to 'creep' overtop of some MgO and $\text{Mg}(\text{OH})_2$ areas. Additionally, dissolution of the oxide layer may be a result of discontinuities present, due to grain boundary effects [29], when MgO , in open air, reacts with water and forms hydroxide.

The effectiveness of the Ni-P electrolyte in forming quality electroless deposits on Mg alloys, suggests that other, similar, electrolytes are capable of the same. The similarities between cobalt {Co} and Ni electrolytes allows for deposition from electrolytes that are identical to those for Ni, Table 3.20.

Chemical Name	Chemical Formula	Composition (g/L)
Cobalt Sulphate Heptahydrate	$\text{CoSO}_4 \cdot 7\text{H}_2\text{O}$	11.23
Sodium Citrate Tribasic Dihydrate	$\text{Na}_3\text{C}_6\text{H}_5\text{O}_7 \cdot 2\text{H}_2\text{O}$	23.50
Sodium Hypophosphite Hydrate	$\text{NaH}_2\text{PO}_2 \cdot \text{H}_2\text{O}$	17.50
Ammonium Hydroxide* (28.0 % - 30.0 %)	NH_4OH	75.0
Deposition Temperature: 85 °C	Average pH before use (20 °C): 11.85	

* NH_4OH was measured in mL/L.

Table 3.20: Alkaline electroless Co electrolyte based on alkaline Ni electrolytes of Table 3.18.

Initial immersion of wet polished AZ91D Mg alloys within the electroless Co-P electrolyte produced few bubbles, either from corrosion or the anodic reaction, similar to the immersion of oxidized Mg alloys within alkaline electroless Ni-P electrolytes. After 60 seconds the reaction intensified and continued at a high rate until the sample was removed. The ongoing intense formation of bubbles, beyond the initial corrosion of the Mg after the breach of the passive oxide layer, was attributed to a heightened deposition rate which was a consequence of the alkaline environment and elevated temperature. Further uses of the alkaline Co-P electrolyte necessitated the addition of NH_4OH as the liberation of H^+ ions from electroless deposition increased the acidity of the electrolyte. Due to the buffering action of the electrolyte, introduction of excess NH_4OH served only to maintain the alkalinity of the solution, around pH 12, as well as the increase deposition rate. Deposits from the electrolyte were well formed and continuous with variation of the Co and P content within the deposit measured at $\pm 0.60\%$ from the average, Figure 3.42.

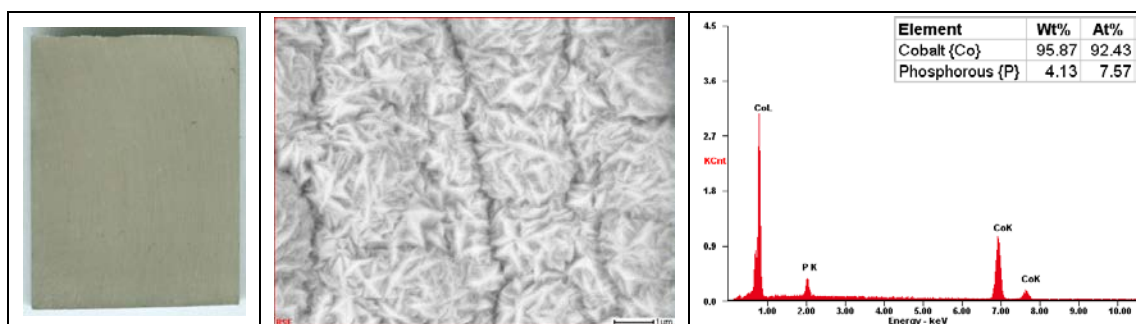


Figure 3.42: Macroscopic image, SEM image, scale bar 1 μm , and EDS analysis of an electroless Co-P thin film [20 min, 85 °C] on a polished AZ91D Mg alloy.

In addition to the electroless deposition of binary alloy thin films such as Ni-P and Co-P, formulations which contain NH_4OH as well as $\text{Na}_3\text{C}_6\text{H}_5\text{O}_7$ also allow for the co-deposition of additional metals forming ternary alloys. The deposition of ternary alloys is of significant interest as the properties of the coating, including both mechanical and electrochemical, can change drastically with the addition of another element.

3.4.4 Electroless Nickel-Zinc-Phosphorus {Ni-Zn-P} and Other Ternary Alloys

The deposition of ternary alloys can include both the co-deposition and incorporation of autocatalytic metals, such as Co and Cu, as well metals which cannot be deposited by autocatalytic means, such as tungsten {W} or zinc {Zn}. Of electrolytes for ternary alloy deposition, those which most closely resemble the alkaline Ni-P electrolytes of Table 3.18 are electroless Ni-Zn-P electrolytes. Electroless Ni-Zn-P electrolytes have the further advantage of having been previously researched and patented for use within the automotive industry [31-33]. Deposits of Ni-Zn-P alloys exhibit an electrochemical potential in sodium chloride solution very close to that of pure nickel, but are also at risk of acting as a sacrificial layer against the corrosion of more noble metals, such as steel [32]. Enhancement of the corrosion protection compared to electroplated Zn and Zn alloys rests with the incorporation of P within the deposit and refinement of the microstructure of the deposit [33]. Additionally, Zn is somewhat of a poison to electroless deposition, slowing the cathodic reaction. The slowing of the cathodic reaction allows for slower deposition rates and less stress within the thin film as well as allows for investigations as to the conditions for the minimum deposition rate needed to produce a coating. Hence, the Ni-Zn-P electrolytes provide the ideal environment for the understanding of ternary alloy deposits on Mg alloys.

Initial testing of Ni-Zn-P electrolytes focused on the inclusion of Zn in electrolytes used for successful alkaline Ni-P deposition, Table 3.18. The Ni-Zn-P electrolytes maintained the same molar concentration of metal ions within the solution as those electrolytes presented in Table 3.18, with 60 % of the ions from Ni and the other 40 % from Zn, Table 3.21.

Chemical Name	Chemical Formula	Composition (g/L)
Nickel Sulphate Hexahydrate	$\text{NiSO}_4 \cdot 6\text{H}_2\text{O}$	6.3
Zinc Sulphate Heptahydrate	$\text{ZnSO}_4 \cdot 7\text{H}_2\text{O}$	4.6
Sodium Citrate Tribasic Dihydrate	$\text{Na}_3\text{C}_6\text{H}_5\text{O}_7 \cdot 2\text{H}_2\text{O}$	23.5
Sodium Hypophosphite Hydrate	$\text{NaPH}_2\text{O}_2 \cdot \text{H}_2\text{O}$	17.5
Ammonium Hydroxide* (28.0 % - 30.0 %)	NH_4OH	40.0
Deposition temperature: 68 to 72 °C		Average pH before use (20 °C): 11.69

* NH_4OH was measured in mL/L.

Table 3.21: Alkaline electrolyte for the deposition of electroless Ni-Zn-P alloys on Mg alloys. [19]

Deposition from the Ni-Zn-P electrolyte progressed similarly to deposits formed within the Ni-P electrolytes of Table 3.18. Initial immersion of the Mg alloy sample within the electrolyte produced a vigorous reaction which persisted for around 5 minutes. After the initial reaction a steady state reaction was observed with the bubbles from the surface attributed to H₂ evolution as a result of the anodic reaction of electroless deposition. The deposits formed on AZ91D Mg alloys after short, 10 minute, immersions within the Ni-Zn-P electrolyte were dark with EDS indicating the deposits were thin and somewhat discontinuous as a significant signal was measured from the Mg substrate, Figure 3.43. The composition of the surface clusters identified on SEM images was determined by EDS to be rich in Zn; the cause of the clusters was initially unknown but has since been attributed, in part, to a low deposition temperature.

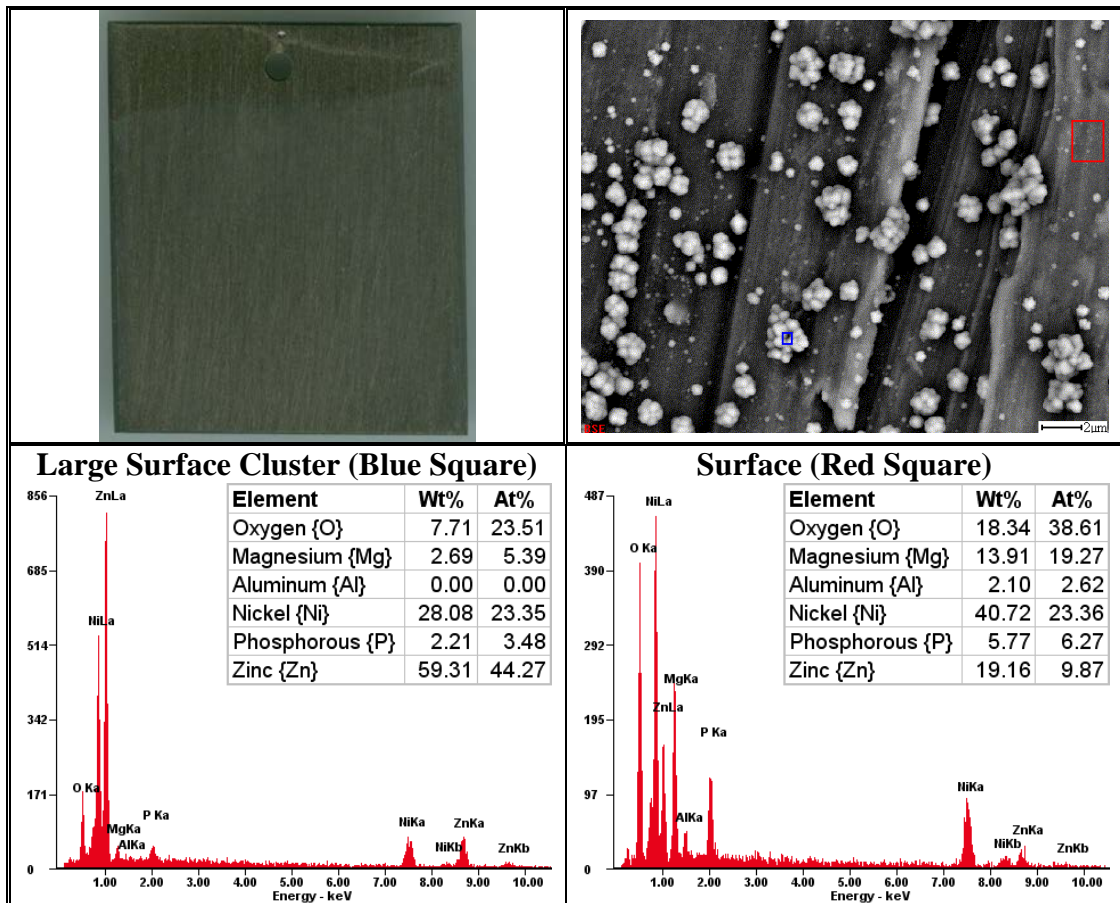


Figure 3.43: Macroscopic scan, backscatter SEM image, scale bar: 2 μm, and EDS analyses of a Ni-Zn-P deposit [10 min, 72 °C] on a polished AZ91D Mg alloy. [19]

As in the case of Ni-P deposition, introducing an oxidized Mg alloy part to the electrolyte resulted in the successful formation of a deposit, Figure 3.44. Longer

immersion time within the same electrolyte, of the order of 2 hours, produced deposits that remained somewhat thin as the EDS signal from the substrate persisted. The cause of the thin deposit was again attributed to a low deposition temperature resulting in a low deposition rate. The Zn-rich clusters present in the shorter deposits continued to be present, though now apparently covered in a Ni-Zn-P coating. The covering of the Zn clusters is attributed to a slight, but unmeasured, decline in the alkalinity of the electrolyte during the prolonged deposition.

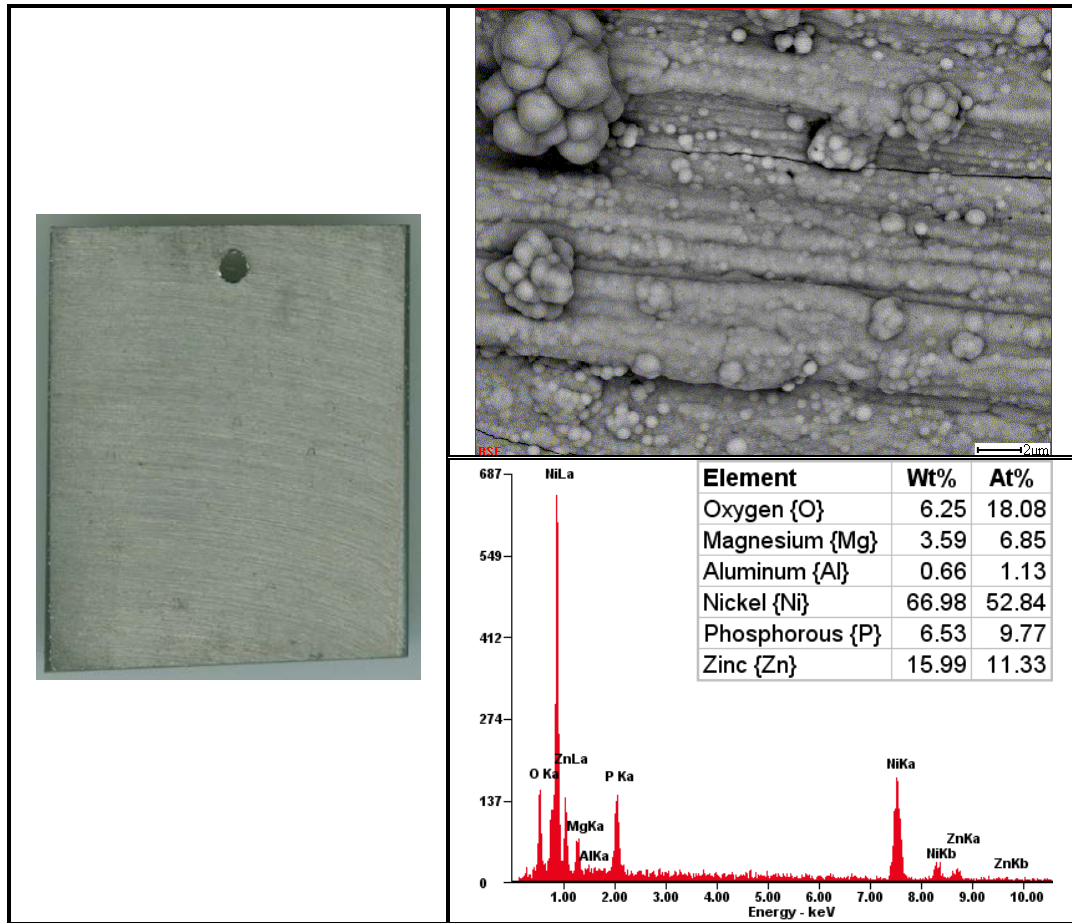


Figure 3.44: Macroscopic scan, backscatter SEM image, scale bar: 2 μm , and EDS analysis of a Ni-Zn-P deposit [2 h, 72 $^{\circ}\text{C}$] on an oxidized AZ91D Mg alloy. [19]

Given that Zn deposition inhibits the catalytic activity of Ni on hypophosphite oxidation, thus inhibiting the cathodic reduction of Ni and slowing the deposition rate [28], several of ratios of Ni to Zn were attempted to determine the best ratio for deposition on Mg alloys, Table 3.22.

Chemical Name	Chemical Formula	Bath Composition (g/L)			
		25%Zn	35%Zn	50%Zn1	50%Zn2
Nickel Sulphate Hexahydrate	NiSO ₄ · 6H ₂ O	7.87425	6.82435	5.2495	6.82435
Zinc Sulphate Heptahydrate	ZnSO ₄ · 7H ₂ O	2.87125	4.01975	5.7425	7.46525
Sodium Citrate Tribasic Dihydrate	Na ₃ C ₆ H ₅ O ₇ · 2H ₂ O	23.500	23.500	23.500	23.500
Sodium Hypophosphite Hydrate	NaPH ₂ O ₂ · H ₂ O	17.500	17.500	17.500	17.500
Ammonium Hydroxide*	NH ₄ OH	37.5	37.5	62.5	50.0
Average pH before use (20 °C):		11.61	11.63	11.96	11.63
Deposition temperature:		80 to 85 °C			

*NH₄OH was measured in mL/L.

Table 3.22: Formulations of alkaline electrolytes for the deposition of various electroless Ni-Zn-P alloys on Mg alloys. [20]

The formulations for the Ni-Zn-P electrolyte maintained the established molar concentration of metal ions, $3.995 \cdot 10^{-2}$ M, used in the deposition of Ni-P alloys, Table 3.18. An additional electrolyte for the 50 % molar ratio of the metal salts, Bath 50%Zn2, was produced to determine the effect of increase metal ion concentration. The total molar concentration of metal ions in solution for Bath 50%Zn2 was increased to $5.193 \cdot 10^{-2}$ M from $3.995 \cdot 10^{-2}$ M; an increase of just over 25 % compared to the other Zn electrolytes, including Bath 50%Zn1. Additionally, as reported by Bouanani et al. regarding the effective deposition of Ni-Zn-P thin films, the deposition rate of Ni-Zn-P begins to increase significantly above 80 °C [28]. Considering Zn has an inhibiting effect on the deposition rate, deposits from the electrolytes provided in Table 3.22 were conducted at $80 \text{ °C} \pm 2 \text{ °C}$. In addition to increasing temperature, the deposition rate also increases exponentially with increasing alkalinity of the electrolyte. The effect of increasing alkalinity on the deposition rate occurs beyond pH 10 [28] and additional NH₄OH was added to the electrolyte immediately prior to sample immersion to ensure sufficient alkalinity and NH₃ in solution. The volume of NH₄OH added to the electrolytes varied, but in all cases was sufficient to produce a temperature adjusted pH of 10 within the electrolyte. Depletion of NH₃ was qualitatively observed by the color of the electrolyte turning from a blue to a lighter sky blue color; addition of NH₄OH for the

pH restored the darker blue color of the electrolyte. Maintaining a sufficiently high deposition rate is essential as too slow a deposition results in corrosion and the inability of the bath to form a deposit. Conversely, too large a deposition rate introduces stresses into the coating and can potentially increase porosity of the deposit due to adsorbed bubbles from the anodic reaction. Additionally, the large deposition rates also risk creep of the deposit over non-catalytic, or oxidized, regions which harm adhesion.

The AZ91D Mg alloy samples used in connection with Ni-Zn-P deposits from electrolytes of Table 3.21 differed from other samples by the application of a non-catalytic silicone mask which exposed only one side of the sample to the electrolyte. The application of a silicone mask, produced using “587 Blue Loctite High Performance RTV Silicone Gasket Maker”, was carried out after wet-polishing of the surface. The purpose of masking the other side of the sample was to allow better comparison of the surfaces and allow the sample to rest on the bottom of the beaker during electroless deposition. The gasket maker, which had no apparent influence on the selected deposition baths, allowed the bubbles from the anodic reaction to rise from the surface and minimize any trapping of H₂ within the deposit. No polishing of the surface occurred after application of the mask, effectively allowing the formation of a thin oxide layer.

Exposure of the Mg alloys to each of the 80 °C Ni/Zn electrolytes produced successful electroless deposits in as little as 15 minutes, Figure 3.45. Rinsing the samples in distilled water did not produce any bubbles associated with galvanic cell formation. The better quality of the thin films compared to Co-P and Ni-P films was attributed to a somewhat reduced deposition rate and less stress within the deposit. As with other deposits, the Ni-Zn-P deposits matched polishing marks left on the surface and were sufficiently thick to block any EDS signal from the Mg substrate, Figure 3.45.

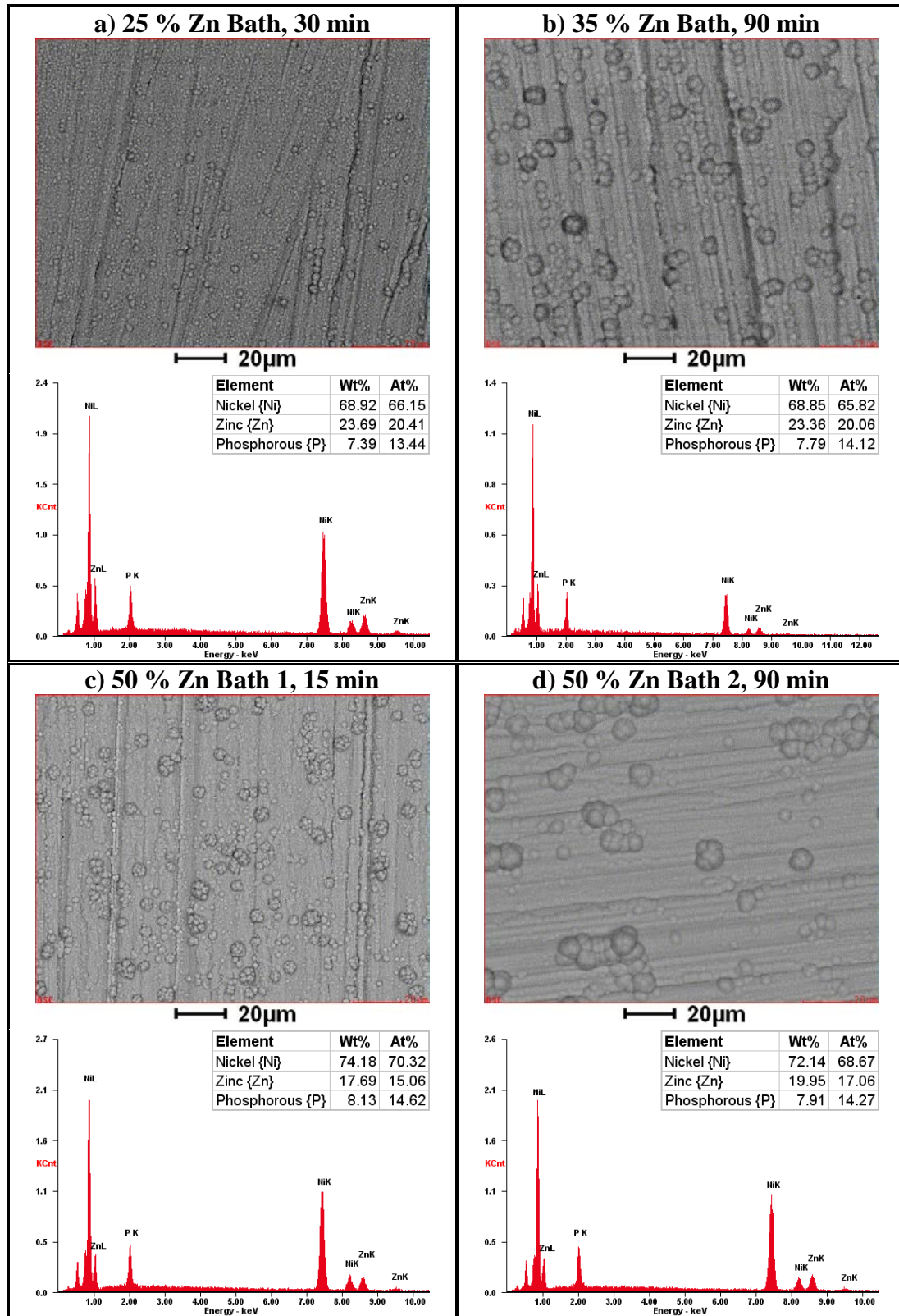


Figure 3.45: Backscatter SEM images and EDS analyses of Ni-Zn-P deposits, on oxidized AZ91D Mg alloys, from electrolytes containing various relative concentration of Ni^{2+}/Zn^{2+} . [20]

The concentration of Zn in the electrolyte compared to that is the resulting deposits appears to indicate that an excess of Zn in the solution limits the amount of Zn incorporated into the Ni-P-Zn thin films [20]. Deposits from both electrolytes containing 50 % mol Zn contained marginally less Zn, 17-20 wt. %, compared to those electrolytes containing the lesser 25 % mol and 35 % mol Zn, which similarly contained Zn at about 23 to 25 wt. % of the coating. The lesser concentration of Zn in deposits from 50 % mol Zn electrolytes appear to be independent of deposition time and total metal ion concentration in electrolyte. The main conditions for Zn inclusion in the deposit appear to be the ratio of metal ions in solution and the concentration of NH_4OH , indirectly pH, within the solution. Arguably, the slightly higher Zn content within the deposit from electrolytes having greater total metal ion concentration is attributed to falling alkalinity during the prolonged deposit. The role of the NH_4OH , and hence NH_3 , as a buffer suggests that the excess NH_4OH required to maintain the same alkalinity of the electrolytes of lower mol % Zn inhibits the inclusion of Zn within the deposit. The argument of excess NH_4OH , and hence alkalinity near pH 12, decreasing the Zn content within the films is supported by literature [28] as the Zn content within deposited films is pH dependent. Specifically, for a 90 °C electrolyte containing 0.01 M Zn^{2+} , 0.1 M Ni^{2+} , and 0.3 M H_2PO_2^- , the Zn content has been reported to increase with pH until reaching a maximum at around pH 10 and decreasing thereafter [28]. Similarly, the P content within the deposit is reported to fall to only a few percent with increasing alkalinity [28, 32, 33]. Further comparison with literature regarding the inclusion of Zn within the deposited film, the thin films produced on Mg alloys contained slightly more Zn, 17 to 23 wt. %, than the 13 to 20 wt. % put forward in those other studies [28, 32, 33].

Given that NH_3 , with a boiling point -33.33 °C, is a gas at room temperature, maintaining a constant concentration of NH_3 within the electrolyte is a significant challenge. Additionally, the role of $\text{NH}_4\text{OH}/\text{NH}_3$ as a buffer suggests that maintaining a constant pH is also a challenge given the presence of anodic and corrosion reactions. Investigation as to the effects of likely diminishing alkalinity of the electrolyte was conducted using the 25 % mol Zn electrolytes. A single 25 % mol Zn electrolyte was split into three identical electrolytes with samples immersed within the electrolytes for

30, 60, & 90 minutes. The NH_4OH was not replenished so as to compare the effects of diminishing NH_3 and alkalinity on the deposits, Figure 3.46.

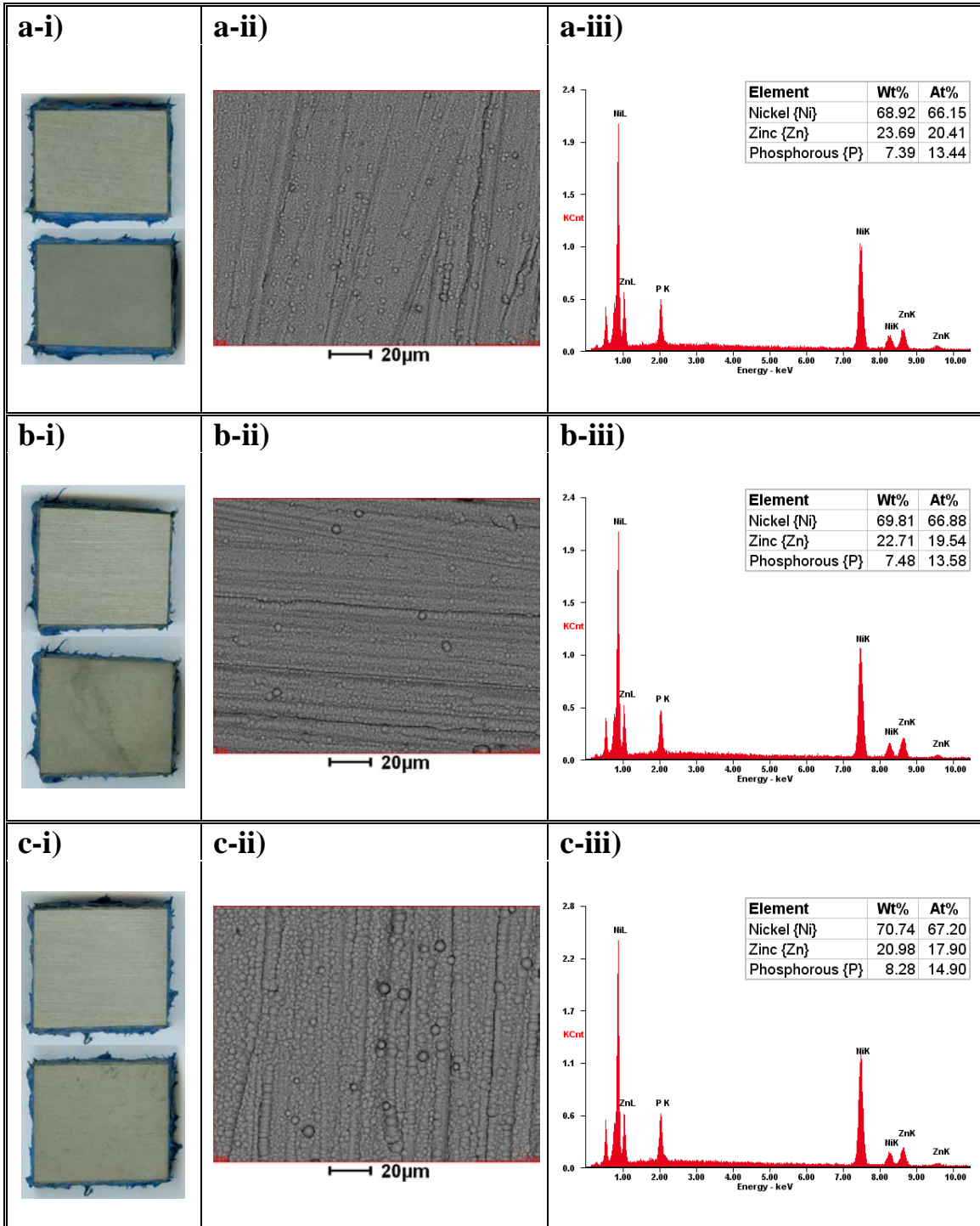


Figure 3.46: i) Macroscopic scan, ii) backscatter SEM image, and iii) EDS analyses of Ni-Zn-P deposits [a) 30 min / b) 60 min / c) 90 min, 80 °C] from electrolytes containing 25 % mol Zn on oxidized AZ91D Mg alloys [20]. Note: The blue material surrounding the sample is the silicone mask.

As expected, EDS analysis indicated an decrease in Zn concentration as well as increase in P concentration with increasing deposition time, which are both consistent within increased acidity. Most telling of the pH decrease is the increase in the P content, which is only pH dependent, as the concentration of Zn^{2+} relative to Ni^{2+} increased as time progressed due to a greater ratio of Ni within deposits. The method of analysis, namely EDS, penetrates into the coating and provides a measurement which is more correctly seen as the average of the layers. As the beam was set to 20 kV for all analysis, EDS provides a comparison of the average composition over essentially identical depths rather than of the outer most layers. The overall homogeneity of deposited coatings was relatively high with EDS analysis showing variation from the average Zn composition, taken over at least $100 \mu m^2$, limited to about ± 1 % between sites tested on a given sample [20]. Greatest differences in composition were observed about atypical surface clusters which had a tendency to possess slightly higher Zn content, usually < 1 % more than the average. The greatest variation, of about 2 % from the average was observed in the case of samples deposited over shorter durations. The cause of the variation is not entirely clear, but likely has to do with initial nucleation of the thin film [20].

As in the case of Ni-P, immersion of the Ni-Zn-P coated samples within distilled water rinse baths provided a means of determining the quality of the coating. The quality of most coatings was excellent with only some minor bubble evolution emanating from the edges of the coating near where the silicone mask prevented the formation of a deposit. The benefit of the distilled water environment, over conventional saline environments, is that distilled water does not corrode the surface but rather provides a means for galvanic coupling and exchange between metals. While the non-heat-treated Ni-P-Zn coating does not render the surface immune to conventional corrosion, it is expected to provide some degree of galvanic corrosion resistance/protection. Extending the qualitative measure of film continuity, a piece of 99 % pure Ni was rested over-top of a Ni-Zn-P coated Mg sample in order to determine the galvanic corrosion resistance of the coating, Figure 3.47.

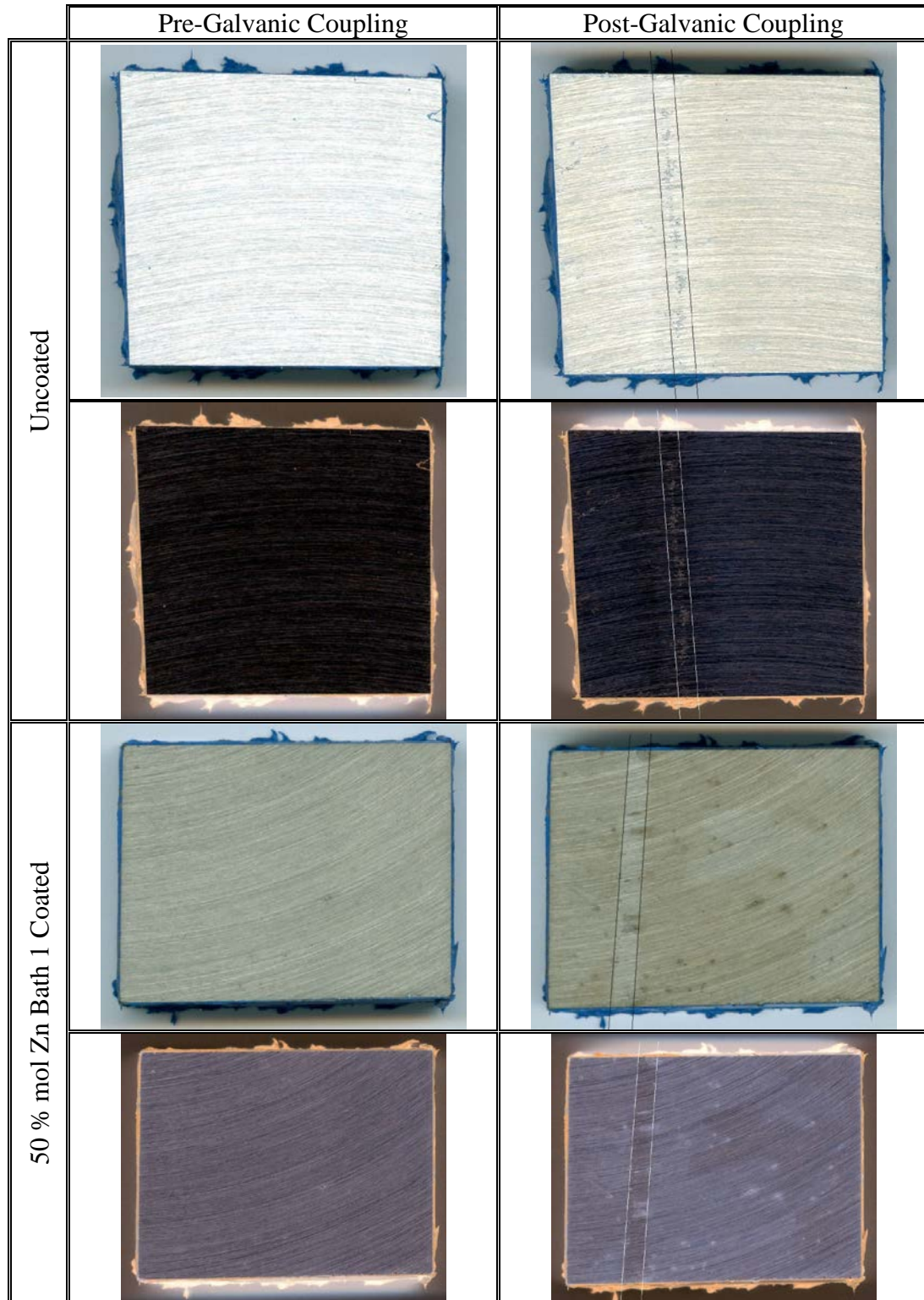


Figure 3.47: Macroscopic scans, and the negatives, of pre-, and post-, galvanic coupling of (Top) uncoated and (Bottom) Ni-Zn-P coated [50%molZn1: 45min, 82 °C] AZ91D Mg alloy samples to 99 % Ni plate for 2 hours in distilled water. Black lines illustrate where the Ni part rested. [20]

The size of the Mg alloy sample was approximately 25 mm × 30 mm; the edge of the Ni plate in contact with the coated and uncoated Mg samples measured 30 mm × 2mm.

Inspecting the macroscopic images makes it is apparent that some minor galvanic corrosion occurred over the entirety of the coated sample with small spots likely the corrosion of Zn rich zones. Looking at the region where the Ni plate rested, it is apparent that, after 2 hours in galvanic contact, the Ni-Zn-P coating afforded superior galvanic corrosion resistance than the uncoated AZ91D Mg alloy. Specifically, the Mg alloy possesses some oxide/hydroxide granules at the contact point between the surface and the Ni plate, whereas the Ni-P-Zn thin film has only a lighter color at the point of contact. The lighter coloured line across the Ni-Zn-P deposit, constrained by the added black lines, demonstrates the coating produced a weakened galvanic couple compared to the uncoated Mg alloy part. Immersion testing of this sort, which is not meant to measure the overall corrosion resistance of the coating, does provide a comparison of galvanic corrosion resistance of the cladding and bare Mg alloy when coupled with pure Ni.

The capacity of any cladding to provide protection from galvanic corrosion alone is insufficient for industrial applications which require robust resistance to all forms of corrosion. In connection with overall corrosion resistance, coatings containing higher amounts of P are known to provide superior corrosion resistance provided the Zn concentration remains significant [32]. Specifically, deposits containing Ni-Zn-P at atomic percentages of 73-12-15 provide better corrosion protection than those containing both more P (less Zn) and less P (more Zn) [32]. Establishing the correct ratio of Zn to P within the deposit for maximum corrosion resistance requires precise control of the alkalinity of the solution. Increasing the alkalinity of the electrolyte results in greater inclusion of Zn, up to pH 10 [28], and lesser inclusion of P within the deposit; similarly, decreasing pH lessens the Zn concentration within the deposit falls and increases the concentration of P. In addition to changes in the composition of the deposit, increasing alkalinity also increases the deposition rate. As both increasing alkalinity and increasing temperature increase the deposition rate, managing both the alkalinity and temperature of the electrolyte are necessary to produce robust deposits.

Slightly lowering the pH and increasing the temperature, to offset any impact on the deposition rate, of a 50 % mol ratio Zn^{2+}/Ni^{2+} containing electrolyte $3.995 \cdot 10^{-2}$ M of metal ions produced a coating containing atomic percentages of Ni-Zn-P at around 57 %, 12.5 %, and 30.5 %, respectively, Figure 3.48.

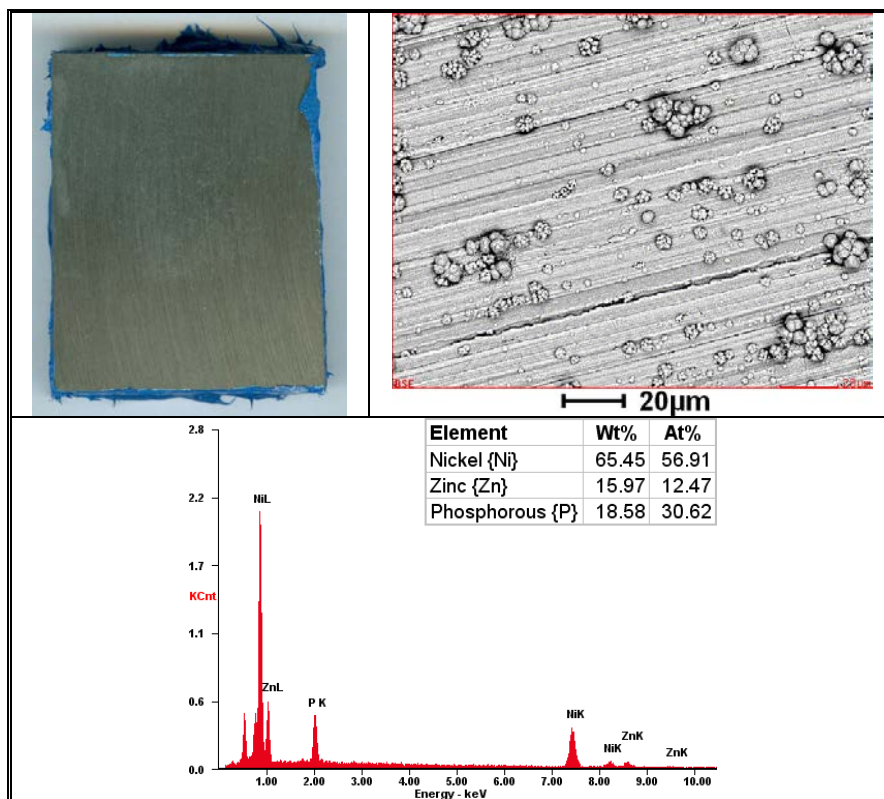


Figure 3.48: Macroscopic scan, SEM image, EDS analysis of a 45 minute Ni-Zn-P deposit from the 50 % mol Zn bath 1 at 85 °C on AZ91D Mg alloy containing higher concentration of P [20]. The post deposit room temperature for this bath was pH 10.8.

Though further investigation would be desirable, the inclusion of up to 30 % atomic P within the Ni-Zn-P film demonstrates the ability to tune the composition of the film on the Mg substrate. More generally, provided appropriate electrolyte composition and deposition conditions, Ni-Zn-P electrolytes allow for the control of P and Zn concentrations within deposits with the capacity of reaching up to 20 % atomic Zn and 30 % atomic P within claddings. The coatings are largely homogeneous with variation of the Zn content, from the average, on a given sample at less than ± 1 % between sites. Most importantly, similar to the alkaline Ni-P electrolytes, the alkaline Ni-Zn-P electrolytes remain stable and functional, at temperature, over more than 10 hours and multiple uses.

Investigating the role of an immersion layer, similar to investigations carried out for both electroless Cu and Ni-P deposits, AZ91D Mg alloy samples were wet polished and immersed within identical Ni-Zn-P electrolytes, Table 3.23. As previous immersion

tests, one side of the sample was dry polished immediately prior to immersion in order to compare the effect of oxidized and polished surfaces.

Chemical Name	Chemical Formula	Composition (g/L)
Nickel Sulphate Hexahydrate	$\text{NiSO}_4 \cdot 6\text{H}_2\text{O}$	7.886
Zinc Sulphate Heptahydrate	$\text{ZnSO}_4 \cdot 7\text{H}_2\text{O}$	2.875
Sodium Citrate Tribasic Dihydrate	$\text{Na}_3\text{C}_6\text{H}_5\text{O}_7 \cdot 2\text{H}_2\text{O}$	23.50
Ammonium Hydroxide* (28.0 % - 30.0 %)	NH_4OH	25.00
Operating Temperature: 80 °C	Average pH before use (20 °C): 11.3	

* NH_4OH was measured in mL/L.

Table 3.23: Electrolyte for Ni-Zn-P 25 % Zn immersion deposit

Unlike the Ni-P immersion deposit, Figure 3.41, and similar to Cu immersion deposits, Figures 3.19 and 3.20, a significant difference between the polished and unpolished surfaces was observed for Ni-Zn-P immersion deposits, Figure 3.49. As is clearly visible from SEM images, the reduction of metal species did take place predominantly on the polished surface. The reason for the sparse deposit on the oxidized surface is attributed to the oxide layer, while the overall deposit of metal on the polished surface is attributed to the presence Zn as a similar deposit was not seen for Ni-P immersion on polished AZ91D Mg alloy.

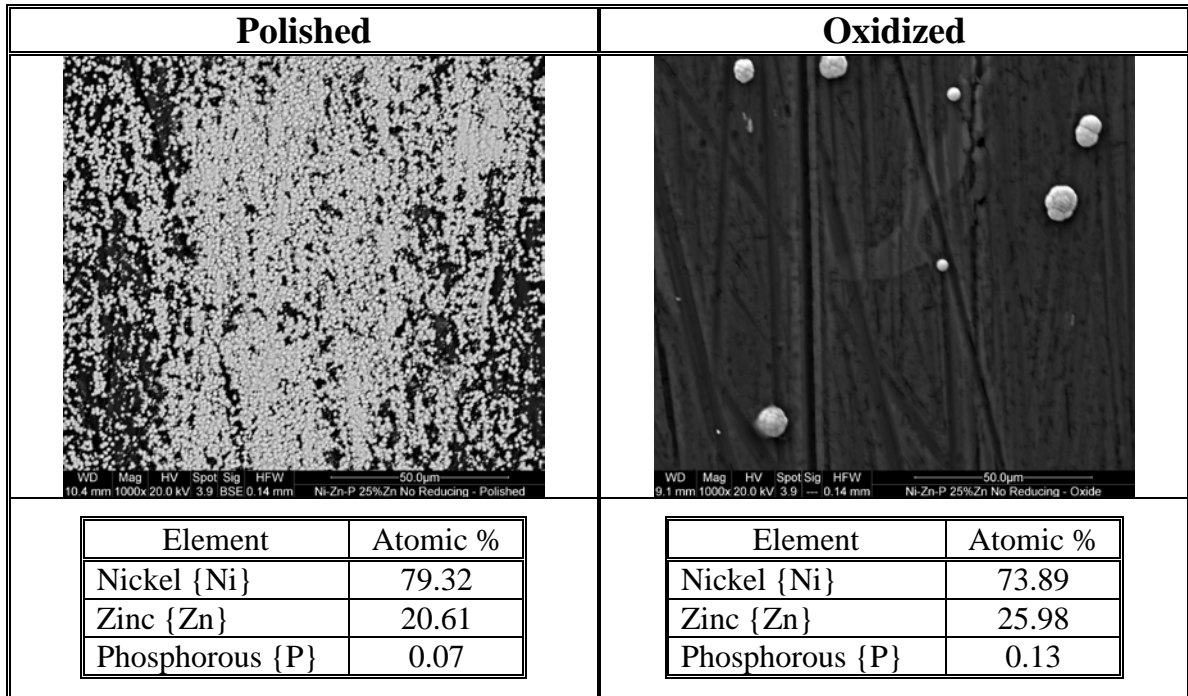


Figure 3.49: SEM image and EDS results for metal particulates deposited [20 min, 80 °C] (Left) polished and (Right) oxidized on AZ91D Mg alloys from a Ni-Zn-P immersion electrolyte.

Note: No phosphorous {P} was present within the electrolyte; the value expressed by EDS is only from the background and should be taken as zero.

At this stage, the difference in the Zn content between polished and oxidized surfaces cannot be conclusively attributed to the quality of the surface. Additionally the exact role of the Zn concentration within the electrolyte remains unexplored. Given the inability of the electrolyte to produce a Ni-Zn-P immersion on the oxidized surface and the similar deposit qualities for on both oxidized and polished surfaces when using a reducing agent, it is speculated that the adsorption of the reducing agent is key to overcoming the oxidation of the substrate. As with the immersion results from Ni-P, it again speculated that the adsorption of the reducing agent in some way allows at least the partial dissolution of the oxide layer by means of a corrosion type reaction.

Along with Ni-Zn-P, the deposition of other ternary alloys on Mg alloys was also investigated. Deposition of Ni-Co-P was attempted as good quality Ni-P and Co-P alloy deposits were each produced on Mg alloys. The composition of the Ni-Co-P electrolyte remained effectively identical to those used for Ni-P, Table 3.18, and Co-P, Table 3.20, with the total molar concentration of the metal ions maintained at $3.995 \cdot 10^{-2}$ M. The molar ratio of the metal ions was set to 60/40 Ni/Co in order to investigate the formation of films with near equal amounts of Ni and Co, Table 3.24.

Chemical Name	Chemical Formula	Composition (g/L)
Nickel Sulphate Hexahydrate	$\text{NiSO}_4 \cdot 6\text{H}_2\text{O}$	6.3 g/L
Cobalt Sulphate Heptahydrate	$\text{CoSO}_4 \cdot 7\text{H}_2\text{O}$	4.5 g/L
Sodium Citrate Tribasic Dihydrate	$\text{Na}_3\text{C}_6\text{H}_5\text{O}_7 \cdot 2\text{H}_2\text{O}$	23.50 g/L
Sodium Hypophosphite Hydrate	$\text{NaH}_2\text{PO}_2 \cdot \text{H}_2\text{O}$	17.50 g/L
Ammonium Hydroxide (28.0 % - 30.0 %)	NH_4OH	75.0 mL/L
Deposition Temperature: 80 to 85 °C	Average pH before use (20 °C): 11.85	

* NH_4OH was measured in mL/L.

Table 3.24: Alkaline electroless Ni-Co-P electrolyte based on electrolytes for Ni-P, Table 3.18, and Co-P, Table 3.20.

As in the case of alkaline electroless Co-P, a high deposition rate was produced due to the need of a large amount of NH_4OH to maintain the pH. Deposits from the electrolyte were fully formed within 3 minutes with longer deposits prone to shedding. Deposits from the Ni-Co-P electrolyte were of high quality, Figure 3.50, and appeared continuous as no bubbles were observed from the surface when immersed in a post deposit rinse. Immersion within the electrolyte beyond 5 minutes produced cracks in the coating which ultimately led to shedding of the coating from the surface. Initial stages of shedding can be seen in the top right corner of the 5 minute Ni-Co-P deposit, Figure 3.50.

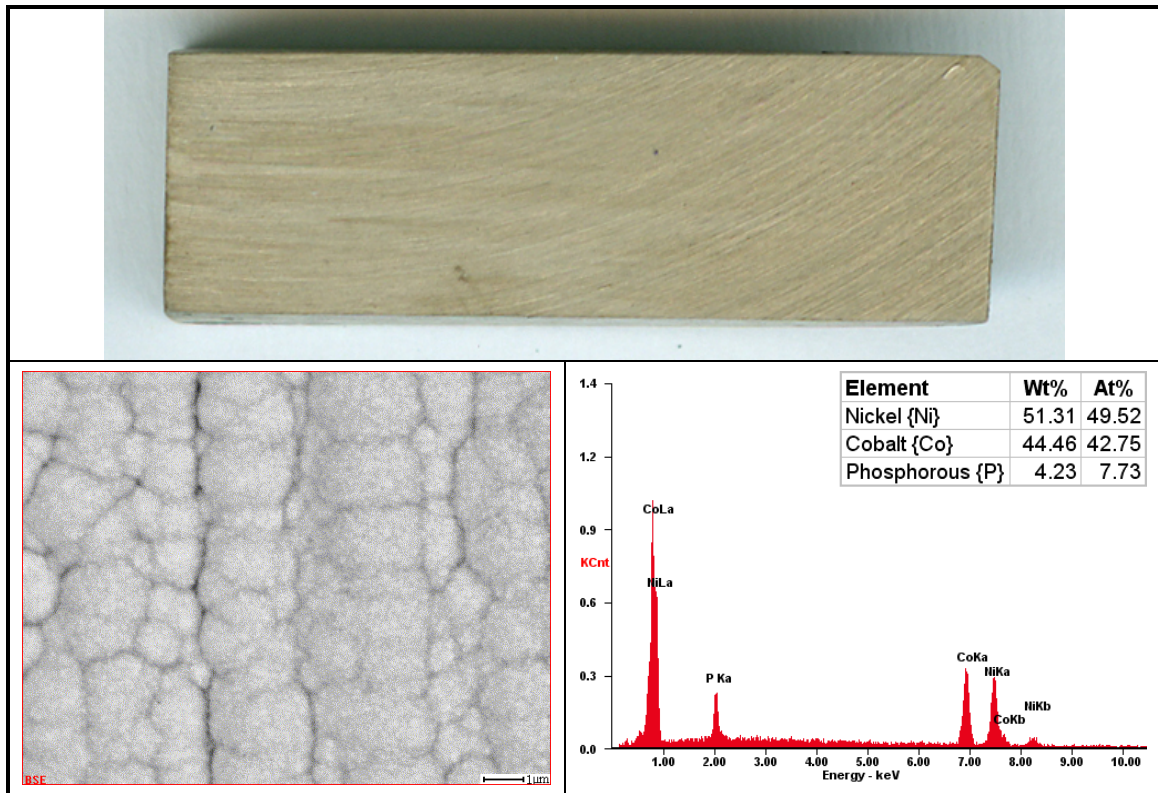


Figure 3.50: Macroscopic scan, SEM image, EDS analysis of a Ni-Co-P deposit [5 min, 82 °C] on a 25 mm × 7.5 mm × 5 mm AM50 Mg alloy.

In regions where shedding occurred, the formation of a new coating could be observed underneath, Figure 3.51, suggesting that the cause of shedding was a combination of stress within the coating and the smooth surface.



Figure 3.51: Macroscopic scanned image of a Ni-Co-P deposit [10 min, 82 °C] on a 65 mm long, 8mm wide at the base, AZ91D Mg alloy sample.

As no corrosion was visible in places where the coating had shed, shedding of the coating was attributed to internal stresses within the deposit resulting from the rapid deposition rate. In addition to shedding, the quick formation of the deposits led to poorer adhesion than that observed from slower Ni-P deposits. Control deposits on Sn/Pd treated glass, used to qualitatively verify the deposition rate, were fully formed within

40 s. As with the Mg substrates, deposits on glass also shed after similar immersion time indicating that the rapid deposition rate, and resulting internal stress within the thin film, was the reason for the shedding.

Another successfully deposited ternary alloy was Ni-Fe-P, which unlike all other Ni baths tested was not $C_6H_5O_7^{3-}$ based, Table 3.25. The change in the composition of the electrolyte, which included $KNaC_4H_4O_6$ similar to the electroless Cu electrolytes, indicates that other electrolytes aside from those using $Na_3C_6H_5O_7$ are able to successfully form deposits on Mg alloys.

Chemical Name	Chemical Formula	Composition (g/L)
Nickel Sulphate Hexahydrate	$NiSO_4 \cdot 6H_2O$	14.72
Ammonium Iron(II) Sulphate Hexahydrate	$Fe(NH_4)_2(SO_4)_2 \cdot 6H_2O$	37.20
Potassium Sodium Tartrate Tetrahydrate (Rochelle's Salt)	$KNaC_4H_4O_6 \cdot 4H_2O$	65.00
Sodium Hypophosphite Hydrate	$NaPH_2O_2 \cdot H_2O$	10.00
Ammonium Hydroxide (28.0 % - 30.0 %)	NH_4OH	37.50
Operating Temperature: 75 to 95 °C		Approximate pH: 9.2

* NH_4OH was measured in mL/L.

Table 3.25: Alkaline electroless Ni-Fe-P electrolyte [34, 35]

The Ni-Fe-P deposits produced, though well formed, contained cracks which indicate the coatings was brittle and stress within the deposit was high, Figure 3.52. These cracks may have been the result of the deposition rate or the pH of the electrolyte which was lower than the 11.2 called for in literature. Despite the fissures in the coating, no signal for the Mg substrate was produced suggesting the cracks did not penetrate to the substrate.

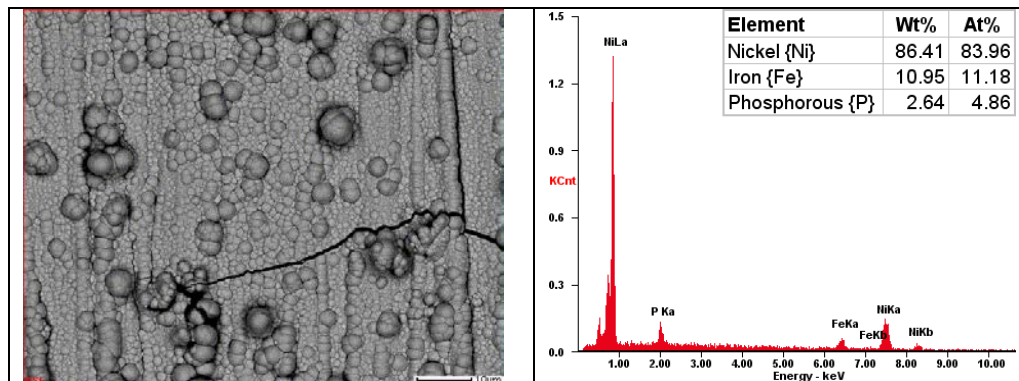


Figure 3.52: Backscatter SEM image, 10 µm scale bar, and associated EDS of a Ni-Fe-P deposit [5 min 75 °C] on an AZ91D Mg alloy.

Other electrolytes of similar composition to the alkaline Ni-P and Co-P electrolytes tested for deposit formation on Mg alloys include the Ni-W-P and Ni-Re-P electrolytes, Table 3.26.

Chemical Name	Chemical Formula	Bath Composition (g/L)	
		Ni-Re-P	Ni-W-P
Nickel Sulphate Hexahydrate	$\text{NiSO}_4 \cdot 6\text{H}_2\text{O}$	35.0	7.0
Potassium Perrhenate	KReO_4	0.2	—
Sodium Tungstate Dihydrate	$\text{Na}_2\text{WO}_4 \cdot 2\text{H}_2\text{O}$	—	3.5
Sodium Citrate Tribasic Dihydrate	$\text{Na}_3\text{C}_6\text{H}_5\text{O}_7 \cdot 2\text{H}_2\text{O}$	8.5	40.0
Sodium Hypophosphite Hydrate	$\text{NaPH}_2\text{O}_2 \cdot \text{H}_2\text{O}$	10.0	10.0
Ammonium Hydroxide (28.0 % - 30.0 %)	NH_4OH	50.0	50.0
Approximate pH		8.8 to 9.2	8.2
Operating Temperature (°C)		85 to 95	85 to 95

* NH_4OH is measured in mL/L and not g/L

Table 3.26: Alkaline electroless Ni-Re-P and Ni-W-P electrolytes [35, 36]

Note: $\text{NiSO}_4 \cdot 6\text{H}_2\text{O}$ content in Ni-Re-P was 10× that in the original formulation which nominally produces a coating containing 46 % Re.

While neither of the two electrolytes listed in Table 3.26 were pursued beyond the initial stages, some deposit attempts were conducted from both electrolytes. Experiments using the Ni-W-P electrolyte resulted in well formed Ni-P deposits though the presence of W remained questionable its presence was not definitively identified according to EDS. Experimental work conducted using the Ni-Re-P electrolyte produced well formed coatings though SEM images of the surface indicated significant unevenness within the deposit, Figure 3.53.

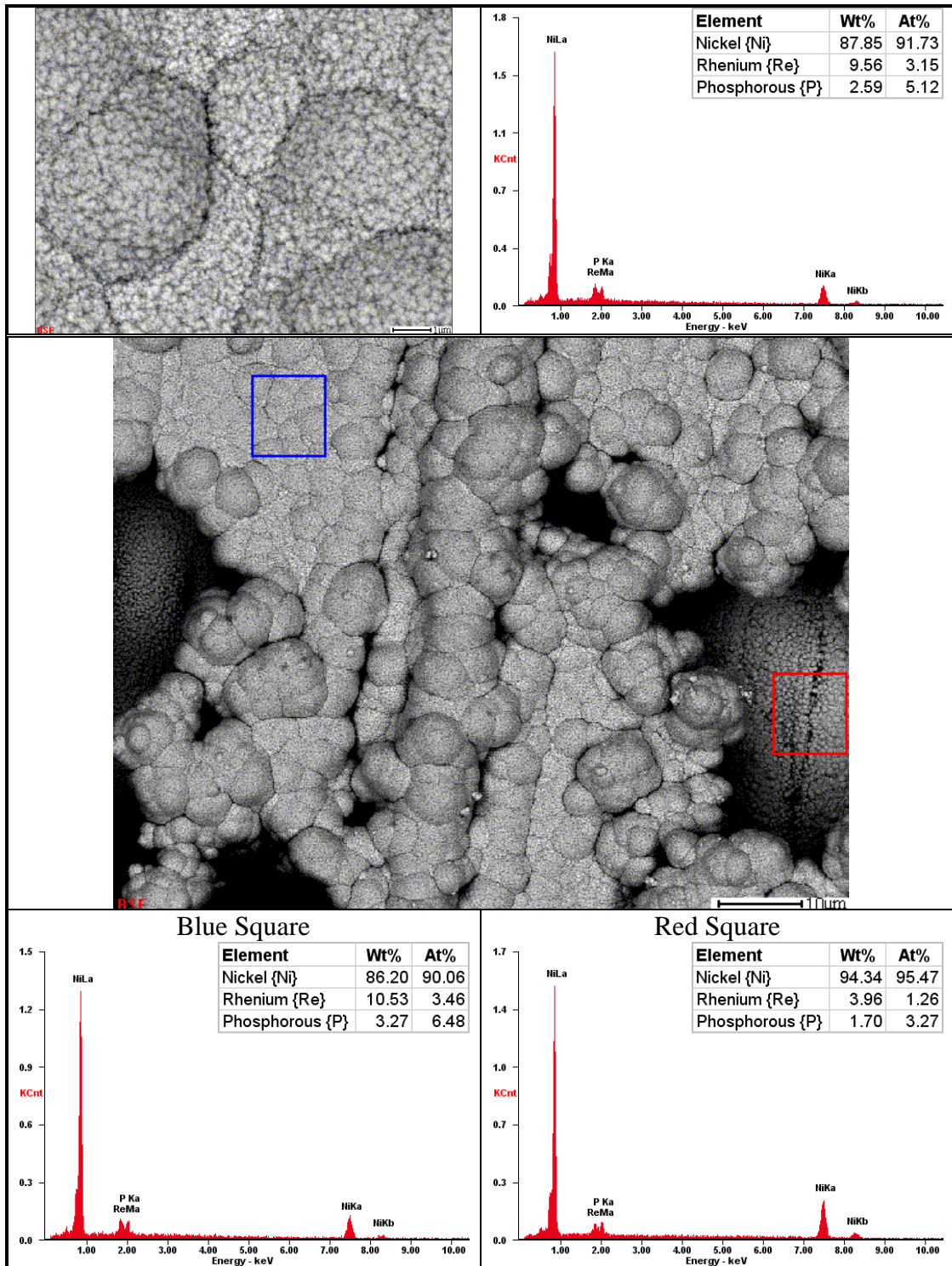


Figure 3.53: Backscatter SEM images and associated EDS of a Ni-Re-P deposit [10 min, 72 °C, pH 11.72] on an AZ91D Mg alloy. (Top) SEM image, scale bar: 1 μm, and EDS of the outer-layer coating, (Middle) SEM image, 10 μm scale bar, showing both the over- and under-layer deposits, along with EDS of the (Bottom-Left) over and (Bottom-Right) under layer deposits.

Specifically of note within the Ni-Re-P films are the deposits on what appear to be recessed pores, as well as the low P concentration within the recessed deposits. The uneven quality of the deposit is attributed to the lower than nominal temperature of the electrolyte during deposition. Though further improvement of the cladding is required, the overall good quality of the thin film is promising for the deposition of other ternary alloys using $C_6H_5O_7^{3-}/NH_3$ combination electrolytes.

The successful deposition of Zn, Co, Fe, and Re as ternary metals within Ni-P alloys indicates that the basic use of NH_4OH and an appropriate complexing agent/stabilizer provide excellent electrolytes for deposit formation on Mg alloys. Specifically regarding Ni-Me-P (Me = Fe, W, Re) electrolytes, significant work remains in order to conclusively comment on the effectiveness, though initial results are positive. The unique film forming environment, which allows for the deposition on/over oxide surfaces indicates that the deposition techniques are of use within industrial applications. Concerns regarding adhesion can be overcome by applying appropriate surface treatments prior to deposition, setting the suitable deposition conditions, and post-deposit heat treatment.

3.5 Summary

Magnesium {Mg} alloys, while possessing many industrially advantageous properties, have seen limited use due to the high reactivity of Mg which results in corrosion. The techniques established within this chapter demonstrate that direct cladding of Mg alloys can be achieved using simple techniques, such as mechanical oxide removal, and the use of appropriate electrolytes. As demonstrated in Section 3.4.2, the electroless cladding of Mg alloys with copper {Cu} is possible provided deposition occurs in a sufficiently alkaline environment and no electrolyte is trapped between the cladding and the substrate. The successful deposition of nickel phosphorous {Ni-P} alloys, Section 3.4.3, as well as several ternary alloys of Ni-Me-P, Section 3.4.4, from alkaline electrolytes demonstrates the advantage of alkaline electrolytes in the mitigation of corrosion. The utility of alkaline deposition environments is the suppression of corrosion which allows for slower deposition rates compared to acidic environments in which the rapid deposition rate attempts to outpace the corrosion rate. Additionally, the

deposition within alkaline environments ensures a low level of P within deposits, typically under 10 % atomically, that, while not ideal for corrosion protection, allows subsequent deposition.

Best results for the deposition of Ni-P alloys were obtained using those electrolytes containing a mixture of citrate $\{C_6H_5O_7^{3-}\}$ and ammonium $\{NH_4^+\}$ ions, though the replacement of $C_6H_5O_7^{3-}$ ions with tartrate $\{C_4H_4O_6^{2-}\}$ ions also proved effective. Most importantly, electrolytes for the successful deposition of coatings on Mg alloys must contain as few corrosion promoting ions, such as chloride $\{Cl^-\}$ ions, as possible. The capacity of the Ni-P and Ni-Me-P electrolytes to deposit on/over oxides, attributed to a maximum pH of 12 for the electrolytes, requires additional investigation in order to ensure adequate adhesion, though the process itself is ideal for industrial incorporation. In general, the conditions needed for better adhesion and the elimination of micro-pores lies in managing the deposition rate and minimizing stress within deposits. Slowing electroless depositions rate along with removal before excess thickening produces unmanageable stresses within the coating are two methods of alleviating internal stresses within the cladding. The conditions and electrolyte compositions for good quality Ni-P, Ni-Co-P, and Ni-Zn-P deposits on Mg alloys are delineated in Table 3.27.

Another significant result from the work on coatings for Mg alloys is the qualitative measurement of the continuity of the coating by immersing the samples distilled water baths. The evolution of bubbles from porous claddings, attributed to hydrogen $\{H_2\}$ gas released as the anodic part of the corrosion reaction, identified, and was associated with, the presence of micro-pores/pinholes subsequently observed by SEM. Using the standard of immersing samples in distilled water, most Ni-P and Ni-Me-P alloy samples were free of bubbles and hence failed to produce any reaction indicating a good quality deposits.

Chemical Name	Chemical Formula	Bath Composition (g/L)		
		Ni-P	Ni-Zn-P	Ni-Co-P
Nickel Sulphate Hexahydrate	NiSO ₄ · 6H ₂ O	10.5	7.87425	6.3
Zinc Sulphate Heptahydrate	ZnSO ₄ · 7H ₂ O	—	2.87125	—
Cobalt Sulphate Heptahydrate	CoSO ₄ · 7H ₂ O	—	—	4.5
Sodium Citrate Tribasic Dihydrate	Na ₃ C ₆ H ₅ O ₇ · 2H ₂ O	23.5	23.5	23.5
Sodium Hypophosphite Hydrate	NaPH ₂ O ₂ · H ₂ O	17.5	17.5	17.5
Ammonium Hydroxide (28.0 % - 30.0 %)	NH ₄ OH	37.5	37.5	75.0
Surface Quality	Clean, oxidized or polished			
Approximate pH (Pre-use 20 °C)	11.9	11.6	11.8	
Operating Temperature (°C)	80 to 90	80 to 95	80 to 90	
Approximate Deposit Composition in Atomic %	92.5 % Ni 7.5 % P	66.0 % Ni 20.5 % Zn 13.5 % P	49.50 % Ni 42.75 % Co 7.75 % P	

*NH₄OH is measured in mL/L and not g/L

Table 3.27: Summary of electrolyte compositions, and conditions, for electroless Ni-P, Ni-Zn-P, and Ni-Co-P deposits on Mg alloys. Note: The Ni-Co-P electrolyte can be made into a Co-P electrolyte by removing the replacing the Ni²⁺ ions with an equivalent amount of Co²⁺ ions. The composition of Co-P deposits mirrors that of Ni-P deposits.

3.6 References

- [1] United States Automotive Materials Partnership (USAMP) Automotive Metals Division (AMD) at the office of the United States Council for Automotive Research (USCAR), "Magnesium Vision 2020: A North American Automotive Strategic Vision for Magnesium", 2006, <http://www.uscar.org/guest/teams/28/U-S-Automotive-Materials-Partnership>
- [2] H. Huo, Y. Li, F. Wang, "Corrosion of AZ91D magnesium alloy with a chemical conversion coating and electroless nickel layer", Corrosion Science, 46, (2004), p.1467-1477
- [3] G.-L. Song and M. Liu, "The effect of Mg alloy substrate on "electroless" E-coating performance", Corrosion Science, **53**, (2011), p.3500–3508
- [4] F. Fracassi; R. d'Agostino; F. Palumbo; E. Angelini; S. Grassini; F. Rosalbino, "Application of plasma deposited organosilicon thin films for the corrosion protection of metals", Surface and Coatings Technology, 174-175, (2003), p.107-111

- [5] H. Zhao, Z. Huang, and J. Cui, "A novel method of electroless plating on AZ31 magnesium alloy sheet", *Journal of Materials Processing Technology*, 203, (2008), p.310–314
- [6] R. Petro, M. Schlesinger, G.L. Song, Chapter 30: Ionic Liquid Treatments for Enhanced Corrosion Resistance of Magnesium-based Substrates, in "Modern Electroplating, Fifth Edition", p.655-686, eds: M. Schlesinger and M. Paunovic, (2010) John Wiley & Sons, Inc., Hoboken, NJ, USA, DOI: 10.1002/9780470602638.ch30
- [7] Y. Zhu, G. Yu, B. Hu, X. Lei, H. Yi, J. Zhang, "Electrochemical behaviors of the magnesium alloy substrates in various pretreatment solutions", *Applied Surface Science*, 256(9), (2010), p.2988-2994
- [8] W.X. Zhang, Z.H. Jiang, G.Y. Li, Q. Jiang, J.S. Lian, "Electroless Ni-P/Ni-B duplex coatings for improving the hardness and the corrosion resistance of AZ91D magnesium alloy", *Applied Surface Science*, 254, (2008), p.4949-4955
- [9] M. Forsyth, P. C. Howlett, S. K. Tan, D. R. MacFarlane, and N. Birbilis, "An ionic liquid surface treatment for corrosion protection of magnesium alloy AZ31", *Electrochemical Solid-State Letters*, 9(11), (2006), p.B52-B55
- [10] F. Witte, "The history of biodegradable magnesium implants: a review", *Acta Biomater.*, 6, (2010) p.1680-1692
- [11] J.-H. Jo, Y. Li, S.-M. Kim, H.-E. Kim, and Y.-H. Koh, "Hydroxyapatite/poly(ϵ -caprolactone) double coating on magnesium for enhanced corrosion resistance and coating flexibility" *Journal of Biomaterials Applications*, 28(4), (2012), p.617-625
- [12] A. Abdal-hay, N.A.M. Barakat, J. K. Lim, "Hydroxyapatite-doped poly(lactic acid) porous film coating for enhanced bioactivity and corrosion behavior of AZ31 Mg alloy for orthopedic applications", *Ceramics International*, 39(1), (2013), p.183-195
- [13] R. Petro and M. Schlesinger, Chapter 1: Applications of Electrochemistry in Medicine, in *Modern Aspects of Electrochemistry Vol:56 - Applications of Electrochemistry in Medicine*, eds. M. Schlesinger, (2013), p.1-32, Springer Science+Business Media New York, 2013, ISBN 978-1-4614-6148-7
- [14] H. H. Elsentriecy and K. Azumi, "Electroless Ni–P Deposition on AZ91 D Magnesium Alloy Prepared by Molybdate Chemical Conversion Coatings", *Journal of The Electrochemical Society*, 156(2), (2009), p.D70-D77
- [15] H.D. Liang, Y.C. Liang, J. A. Gardella Jr., P. He, and B. P. Yatzor, "Potential release of hydrogen fluoride from domestic coal in endemic fluorosis area in Guizhou, China", *Chinese Science Bulletin, Geochemistry*, 56(22), (2011), p.2301-2303
- [16] J.S. Lian, G.Y. Li, L.Y. Niu, C.D. Gu, Z.H. Jiang, Q. Jiang, "Electroless Ni–P deposition plus zinc phosphate coating on AZ91D magnesium alloy", *Surface & Coatings Technology*, 200, (2006), p.5956-5962
- [17] W.X. Zhang, N. Huang, J.G. He, Z.H. Jiang, Q. Jiang, J.S. Lian, "Electroless deposition of Ni–W–P coating on AZ91D magnesium alloy", *Applied Surface Science*, 253, (2007), p.5116-5121
- [18] R. Petro, M. Schlesinger, "Direct Electroless Deposition of Nickel Boron Alloys and Copper on Aluminum Containing Magnesium Alloys", *Electrochemical and Solid-State Letters*, 14(4), (2011), p.D37-D40

- [19] R. Petro, M. Schlesinger, "Direct Electroless Deposition of Low Phosphorous Ni-P Films on AZ91D Mg Alloy", *Journal of The Electrochemical Society*, 159(7), (2012), p.D455-D461
- [20] R. Petro, M. Schlesinger, "Direct Electroless Deposition of Ni-P-Zn Films on AZ91D Mg Alloy", *Journal of The Electrochemical Society*, 160(9), (2013), p.D349-D353
- [21] K. M. Gorbunova, M. V. Ivanov, and V. P. Moiseev, "Electroless Deposition of Nickel-Boron Alloys Mechanism of Process, Structure, and Some Properties of Deposits", *Journal of the Electrochemical Society: Electrochemical Science & Technology*, 120(5), (1973), p.613-618
- [22] J. P. Marton and M. Schlesinger, "The Nucleation, Growth, and Structure of Thin Ni-P Films" *Journal of the Electrochemical Society: Electrochemical Science*, 115(1), (1968), p.16-21
- [23] S. L. Chow, N. E. Hedgecock, and M. Schlesinger, "Electron Microscope Study of the Nucleation and Growth of Electroless Cobalt and Nickel", *Journal of the Electrochemical Society: Electrochemical Science & Technology*, 119(12), (1972), p.1614-1619
- [24] C.-Y. Bai, Y.-H. Chou, C.-L. Chao, S.-J. Lee, M.-D. Ger, "Surface modifications of aluminum alloy 5052 for bipolar plates using an electroless deposition process", *Journal of Power Sources*, 183, (2008) p.174-181
- [25] E. Ghali, *Uhlig's Corrosion Handbook, Second Edition, Chapter 44: Magnesium and Magnesium Alloys*, p.793-830, Edited by R. W. Revie, 2000, John Wiley & Sons Inc
- [26] B. K. W. Baylis, A. Busuttill, N. E. Hedgecock, and M. Schlesinger, "Tin (IV) Chloride Solution as a Sensitizer in Photoselective Metal Deposition", *Journal of the Electrochemical Society: Electrochemical Science & Technology*, 123(3), (1976), p.348-351
- [27] G. L. Song and A. Atrens, "Corrosion Mechanisms of Magnesium Alloys", *Advanced Engineering Materials*, 1(1), (1999), p.11-33
- [28] M. Bouanani, F. Cherkaoui, M. Cherkaoui, S. Belcadi, R. Fratesi, and G. Roventi, "Ni-Zn-P alloy deposition from sulfate bath: inhibitory effect of zinc", *Journal of Applied Electrochemistry*, 29(10), (1999), p.1171-1176
- [29] V. Fournier, P. Marcus, and I. Olefjord, "Oxidation of magnesium", *Surface and Interface Analysis*, 34(1), (2002) p.494-497
- [30] Z.C. Wang, F. Jia, L. Yu, Z.B. Qi, Y. Tang, G.-L. Song, "Direct electroless nickel-boron plating on AZ91D magnesium alloy", *Surface & Coatings Technology*, 206, (2012), p.3676-3685
- [31] M. Schlesinger and D. D. Snyder, *Zinc/Nickel/Phosphorus Coatings and Electroless Coating Method Therefor*, Patent #5,304,403, April 19, 1994.
- [32] M. Schlesinger, X. Meng, D. D. Snyder, "The Microstructure and Electrochemical Properties of Electroless Zinc-Nickel-Phosphorus Alloy", *Journal of the Electrochemical Society*, 138(2), (1991), p.406-410
- [33] M. Schlesinger, X. Meng, D. D. Snyder, "Electroless Ni-Zn-P Films", *Journal of the Electrochemical Society*, 137(6), (1990), p.1858-1859
- [34] A. F. Schmeckenbecher, "Chemical Nickel-Iron Films", *Journal of the Electrochemical Society*, 113(8), (1966), p.778-782

- [35] I. Ohno, Chapter 22: Electroless Deposition of Alloys, in “Modern Electroplating, Fifth Edition”, p.499-506, eds: M. Schlesinger and M. Paunovic, (2010) John Wiley & Sons, Inc., Hoboken, NJ, USA, DOI: 10.1002/9780470602638.ch22
- [36] F. Pearlstein and R. F. Weightman, “Electroless Deposition of Nickel Alloys”, *Electrochemical Technology*, 6, (1968), p.427

Chapter 4: Selective Electroless Deposition on Silicon {Si}	201
4.1 Introduction to Selective Deposition on Silicon {Si}	202
4.2 Silicon Materials and Electronic Applications	202
4.3 Experimental Motivation	209
4.4 Materials and Methods	213
4.5 Experimental Results	214
4.5.1 Electroless Copper {Cu}	216
4.5.2 Electroless Gold {Au}	219
4.5.3 Electroless Nickel {Ni}	222
4.5.4 Role of Ammonium/Ammonia {NH ₄ ⁺ /NH ₃ }	227
4.5.5 Electroless Silver {Ag}	231
4.6 Summary	233
4.7 References	234

4.1 Introduction to Selective Deposition on Silicon {Si}

Silicon {Si}, a tetravalent metalloid whose crystal structure is defined by a cubic unit cell containing four Si atoms in a tetrahedral arrangement, is one of the most important materials in the modern technological age. As a substrate, Si wafers¹ are the literal backbone of transistors, diodes, as well as the foundation of electronics and computer processors, photovoltaic cells, and much more. The selective metallization of Si substrates is essential to the incorporation of Si devices into circuits. Metallization practises and techniques continue to be widely investigated for a number of purposes including conduction tracks on photovoltaic cells [1], and metallic interconnects for memory storage devices and transducers [2].

4.2 Silicon Materials and Electronic Applications

Very pure Si, > 99.9 %, is typically produced by electrodeposition or electrolysis from molten Si compounds [3, 4] but is of little practical use as pure Si due to low conductivity. In order to sufficiently increase conductivity of Si for use as circuit elements within electronic devices, Si wafers are doped with small quantities of other elements. The inclusion of phosphorous {P} or arsenic {As}, pentavalent atoms, as dopants within the Si lattice results in the covalent bonding of four of the valence electrons with the Si atoms with the remaining, fifth, electron left unbound, Figure 4.1. The negative charge of the semiconductor due to the extra electrons provides the naming of n-type Si. The inclusion of boron {B} or gallium {Ga}, trivalent atoms, as dopants within the Si lattice results in the covalent bonding of all valence electrons of the dopant atoms and ‘holes’ within the lattice where the Si electron has no bond, Figure 4.1. The absence of the bond creates an effective positive charge that conducts current by the reconfiguration of the bonds of neighbouring Si atoms, which allows holes to travel across the lattice; hence the naming p-type Si.

¹ Si wafers are typically cut from ingots along the <100> crystal plane for which the Miller indices describe a plane in the yz-plane in Cartesian space.

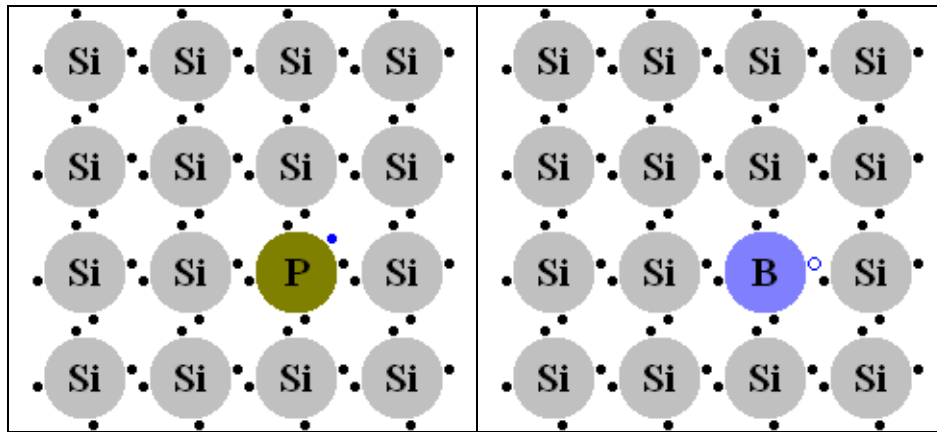


Figure 4.1: Schematic crystal structure of n-type Si (left) with the extra electron shown in blue; and p-type Si (right) with the electron vacancy, or hole, represented by a blue ring.

Both p-type and n-type Si wafers are semi-conducting materials whereas pure, un-doped, Si is closer in nature to an insulator. The abundance of Si and development of ultra-pure Si has largely replaced germanium {Ge} semiconductors which were more prevalent in the early days of electronics [5]. The shift to Si based semiconductors is due to many factors including the relative high price of Ge and the superiority of Si regarding high-power applications [5]. Nevertheless, the shared crystal structure with Si and the ability to dope Ge to form n-type and p-type semiconductors allows for the continued use of Ge-based electronics within a niche market, typically in the form of Si-SiGe alloys for solar cells [6-9]. The continued use of Ge within solar cells is essentially due to its superiority as a photovoltaic material compared to crystalline Si. The superiority of Ge is a result of the wider spectral overlap of Ge with the solar irradiance spectrum [6]. Specifically, Ge covers wavelengths in the range of 300 nm to 1600 nm, compared with 300 nm to 1060 nm for Si, and possesses superior optical absorption coefficients compared to Si in the range of interest [6].

Modification of semiconductor properties from the pure intrinsic semiconductor state, in which the Fermi level is essentially midway between the valence and conduction bands, Figure 4.2, is achieved by doping. The doping of a semiconductor substrate modifies the structure and characteristics of the valence/conduction band-gap by providing a donor energy level below the conduction band, or an acceptor energy level above the valence band depending on the identity of the doping atoms [10, 11]. The presence of the new band provided by the doping atoms shifts the Fermi level of the

semiconductor closer to the conduction band in the case of n-type semiconductors, and closer to the valence band in the case of p-type semiconductors, Figure 4.2.

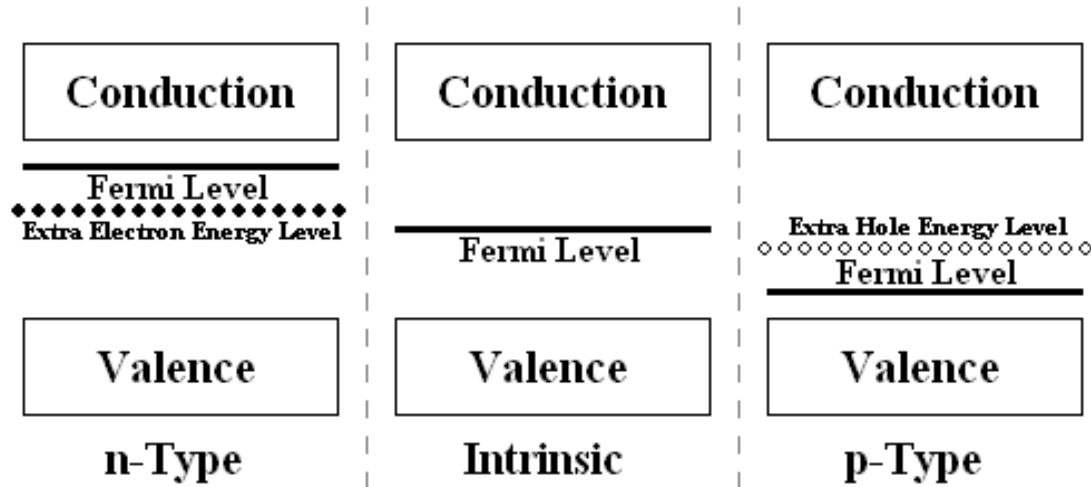


Figure 4.2: Schematics of the band structure of n-type, intrinsic, and p-type semiconductors showing the Fermi level and the energy levels provided by the doping element.

The operational difference between p-type and n-type Si is dependent on the application and is often minimal in the case of both electroless and electroplating experiments; though comparison studies of the metallization behaviour of both substrates remain common. While no substantial difference in plating rate is typically observed between deposition on p-type and n-type Si wafers, it has long been known that p-type and n-type surfaces, when part of a single piece of Si, experience a difference in the plating rate attributed to photovoltages generated at the p-n junction due to the difference in electronegativity between p-type and n-type Si [12]. While the selective deposition experienced on n-type Si under strong illumination is consistent with the generation of a photovoltage, the difference in electronegativity of the materials is exemplified by changes in the deposition based on the chemicals within the solution [12]. Specifically, the difference in plating rate has been found to be dependant on the electrolyte composition. One factor in the composition is the presence of ethylenediaminetetraacetic acid (EDTA) $\{(HO_2CCH_2)_2NCH_2CH_2N(CH_2CO_2H)_2\}$, which forms a Ni-EDTA complex [12]. The presence of the complex elevates the redox potential to such a high value that the difference due to the electronegativity and the photovoltage became negligible [12].

Combining n-type and p-type Si allows for the creation of devices such as diodes, transistors, and photovoltaic cells. Stacking p-type and n-type silicon, most commonly

by growing a layer on the surface of a previous layer, creates a boundary in the central region known as a p-n junction, Figure 4.3. The junction is formed by diffusion of the charge carriers, electrons and holes, between the n-type and p-type layers, respectively. The diffusion at the interface, which may be less than 1 μm thick, forms a depleted region, or depletion zone, where free electrons from the n-type layer fill holes in the p-type layer. The diffusion of the charge carriers produces an electric field within the depletion zone due to the positive charge of the n-type region having positively ionized donors and the negative charge of the p-type region having negatively ionized acceptors [13]. The electric field, which, by convention, points from the n-type layer to the p-type layer, acts as a natural bias discouraging electron motion from the n-type to p-type layers as well as preventing further diffusion of the charge carriers.

The asymmetric conductivity, which is near zero in the reverse direction, of p-n junctions allows their use as diodes for the selective passage, or rectification, of current [14]. The direction of the current is achieved by means of a potential difference applied between the p-type and n-type layers. Application of a more negative potential to the p-type side of the diode compared to the n-type side, known as a reverse bias, increases the effect of the inherent electric field between the n-type and p-type regions of the diode inhibiting electron flow. Reinforcement of the electric field by the reverse bias allows only small, thermal, currents to pass as the applied potential pulls electrons away from the p-n junction towards the contacts [13]. Larger currents are allowed to pass under the forward bias configuration where the potential at the p-type layer is higher than the n-type layer as the electric field of the applied potential counteracts the natural bias of the junction. In alternating current systems, the p-n junction will allow current to flow primarily in one direction [13] given that the p-n junction of a diode will impede, up to a point, any current traveling from the n-type layer to the p-type layer.

Beyond simple diodes, p-n junctions are essential in the construction of junction transistors, invented in 1947 by John Bardeen and Walter Brattain [15], which are produced by adding a third semiconductor layer to a diode forming an additional p-n junction. Application of a small current across the central layer, p-type in an n-p-n junction transistor and n-type in a p-n-p junction transistor, provides control over the passage of current by providing a relative bias between the central layer and each of

the other layers. As in the case of the diode, biasing the layer effectively modifies the band structure of the p-n junction, Figure 4.3, increasing or decreasing the ease with which the electrons may pass from one layer to the next [16].

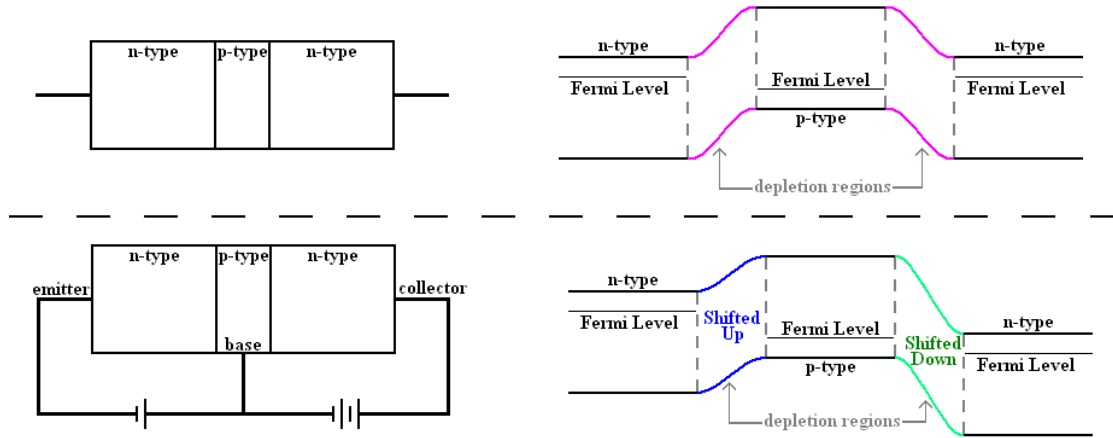


Figure 4.3: Band structure change within a junction transistor after the application of a potential across the transistor. The Fermi Level prior to the application of a potential is effectively the same across the transistor.

The modern version of the junction transistor, the simplest version of the transistor, was described by William Shockley in 1951 [16]. Solid state transistors replaced triode vacuum tubes revolutionizing the electronics industry by allowing for much smaller, more energy efficient amplification and switching of electronic signals. Four basic modes are available for the transistor depending on the forward or reverse bias of each layer and further details as to construction and operation of junction transistors may be found elsewhere [5, 17-23] as the specific metallization of transistors is beyond the scope of the current work.

Another prominent application of the p-n junctions is within photovoltaic cells, commonly known as solar cells, which operate by means of the diode, or asymmetric conduction, properties of p-n junction(s) and the photoelectric properties of the p-type semiconductor layer. The photoelectric effect is the emission of electrons from a material, commonly metal, due to the absorption a photon of appropriate energy by an electron within the material. In terms of the photoelectric effect, the electron is ejected from the material into a vacuum by the absorption of the energy of a photon. The photoelectric properties of p-type semiconductors results in the excitation of valence electrons by photons to the conduction band such that they become free electrons within the material. The promotion of the electrons occurs provided the electrons acquire

sufficient energy, from a photon of appropriate energy, to cross the band gap between the valence and conduction bands. When the p-type semiconductor is part of a p-n junction, the photons pass through the semiconductor layers and some photons are absorbed by valence electrons in the p-type layer and promoted to the conduction band becoming free electrons. Free electrons near the p-n junction are pulled into the n-type layer by the natural bias of the junction which prevents the return flow of the electrons. The resulting charge imbalance between the two layers produces a difference in potential, known as the photovoltaic effect² [24], which can be put to work as a current by providing a path for the electrons to flow back to the p-type layer, namely an outside circuit. Traditionally collection and return of the electrons from the n-type to the p-type layer is achieved by means of conduction tracks on the n-type surface, top, of the photovoltaic cell and a conduction plate on the p-type base of the cell, though other configurations exist [1], Figure 4.4.

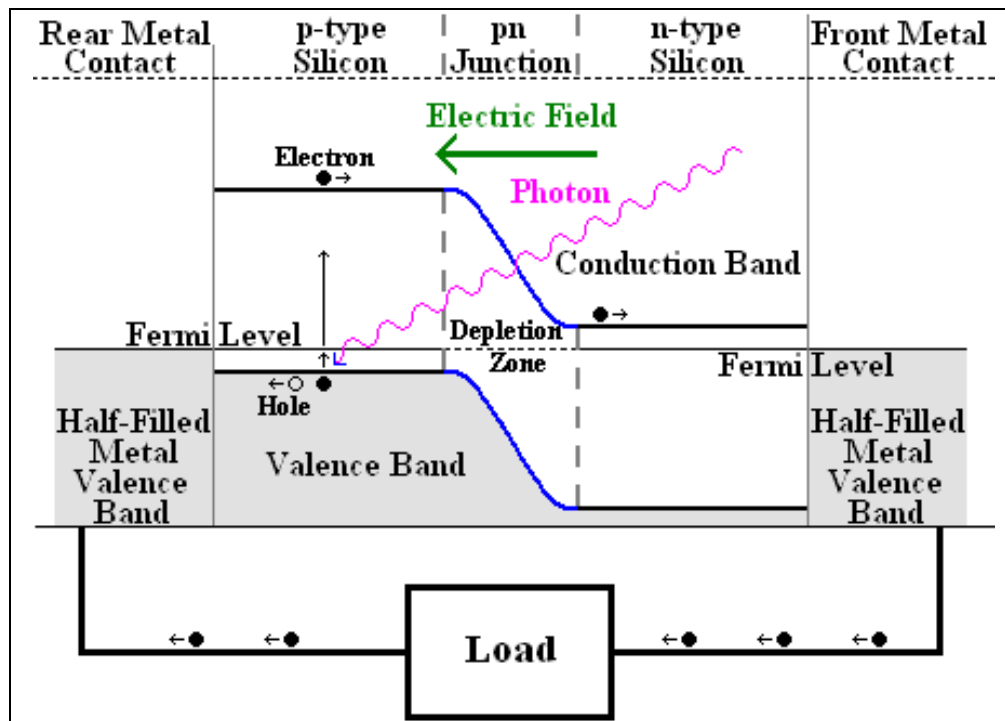


Figure 4.4: Schematic diagram of energy levels and functioning of a solar cell.

² Both the photoelectric and photovoltaic effects are spectrum based. In the case of the photovoltaic effect, the excitation of the electrons is dependent on the energy of the photon and the band gap of the material.

In addition to production of semiconductor devices, it is metallization of the semiconductor elements required in the incorporation of diodes, solar cells, and transistors as elements within a circuit. Failure of metal contacts and the semiconductor material due to electromigration, the migration of ions as a result of the flow of current, of metal along or into the semiconductor is a major factor in eventual lack of functionality. In early electronic devices, interconnections of integrated circuit elements were manufactured out of aluminum {Al} based alloys, such as Al-Si or Al-copper {Al-Cu}, which were prone to electromigration failures. Electromigration failures³ of Al-based interconnections led to the adaptation of Cu as the interconnection material as it possessed improved conductivity and electromigration resistance. The transition to Cu, while reducing electromigration failures, introduced the problem of Cu diffusion into Si, SiO₂, and other dielectrics in addition to the reaction of Cu with Si forming Si containing compounds, silicides [2]. Diffusion of Cu through Si results in poisoning of semiconductor devices while diffusion through SiO₂ leads to degradation of dielectrics [2]. The feasibility of using electroless deposition, specifically of Cu, has been demonstrated for the fabrication of integrated circuits; and fabrication may be achieved on both catalytic and non-catalytic surfaces, where the non-catalytic surfaces require either electrochemical or photochemical activation [2]. While the manufacture and operation specifications of the semiconductor element can mitigate this some of the electromigration effects, the deposition of diffusion resistant materials is by far the best practice. Specifically, work conducted at IBM on the diffusion barrier properties of electroless Ni-P and Co-P alloys determined that only electrolessly deposited metals and alloys, at thicknesses of as little as 1000 Å have barrier properties for Cu diffusion [25]. Additionally, it was determined that Ni-P thin films deposited from nickel sulfamate {Ni(NH₂SO₃)₂} electrolytes provided better diffusion barriers than that those deposited from nickel sulphate {NiSO₄} solutions.

³ Electromigration failures are defined by the time of failure as “the point at which a 50% increase of the resistance due to the electromigration stressing has occurred” [2]

4.3 Experimental Motivation

Within the electronics industry, the method and complexity of Si metallization varies greatly depending on the application for which the metallization is intended. Of the applications, the manufacture of transistors represents the most technically involved process. The complexity of the manufacture of transistors is due to the multi-stepped processes required in order to produce the precision needed to construct properly functioning devices. At the other end of the complexity spectrum, the formation of conduction tracks on Si solar cells is often achieved by baking an Ag-Al paste onto the surface of the Si, a process known as screen-printed metallisation [26, 27]. The metallization of Si typically requires not only high precision and reliability, but also simplicity and affordability for it to displace more complex accepted technologies.

Given the propensity for metals such as Cu and Au to diffuse into Si semiconductors and the propensity of Al for electromigration [2], a great deal of effort has and is currently being put forward in the pursuit of the production of inexpensive metallization techniques for diffusion barriers. Currently, diffusion barrier layers are most often formed by physical vapour deposition (PVD) or chemical vapour deposition (CVD), though diffusion barrier properties of thin electroless Co and Ni films have been demonstrated [2, 25]. Electroless Ni-P plating is a very promising process, especially for the metallization of silicon solar cells, as it is catalytic for the deposition of subsequent Cu or Ag layers while providing good adhesion, a low contact resistance, and preventing diffusion of Cu into the Si [28]. The interest in the semiconductor properties of Si have, since the 1970s, spurred significant investment resulting in a great number of papers and patents for the metallization of Si for both the electronics and solar industries. Established relatively simple electroless techniques include direct deposition from, often alkaline, electrolytes containing ammonium $\{\text{NH}_4^+\}$ and/or fluoride $\{\text{F}^-\}$ ions [29, 30] as well as deposition on scribed surfaces [31]. Deposition both directly and on scribed surfaces are often paired with photochemical techniques, to allow selective deposition. Photochemical techniques, such as the use of photoresists, allow selective deposition by coating the surface in an inert chemical and selectively removing regions where deposits are desired, Chapter 2.2.5.

Early work, in 1968, conducted on the electroless metallization of Si wafers utilized a pre-treatment technique for the purpose of protecting Si surfaces from oxidation and staining [12]. The pre-treatment of the Si wafers consisted of an etched, preservation in methyl alcohol until the deposition, with a 30 second immersion in a 50 % NH_4F solution followed by a rinse methyl alcohol immediately prior to plating in an alkaline solution containing NH_4OH [12]. More recent studies regarding electroless Ni-P deposition on Si continue to use pre-treatments and electrolytes similar to those used as far back as the 1950s [28, 29, 32, 33]. These baths, which contain NH_4^+ ions, have demonstrated that electroless Ni deposition baths of appropriate alkalinity, around pH 8 to 9, and containing a sodium hypophosphite $\{\text{NaH}_2\text{PO}_2\}$ reducing agent allow for displacement deposition of Ni as well as electroless Ni-P growth within a single immersion process [33]. The displacement deposition of Ni, which occurs without the presence of a reducing agent at pH values as low as pH 8, provides the catalytic base layer for the electroless deposition of Ni-P, which requires a higher pH [33]. It is thought the displacement reaction oxidizes the Si substrate in parts while allowing for Ni deposition to a significant degree resulting in coverage greater than typical immersion plating [32]. In contrast to alkaline deposition, pH 8, from a bath containing NH_4F , it has been found that electroless deposition from an acidic solution, pH 2, containing HF does not produce electroless deposits on porous Si, even when the Si substrate has undergone the same pre-treatments as successful alkaline deposits [30]. According to literature, using acidic deposition baths requires the use of activation procedures, most often involving palladium $\{\text{Pd}\}$, to allow for deposition on Si [34, 35]; a process that typically results in lesser adhesion compared to that afforded by alkaline baths using displacement reactions [32]. Another activation method for the acidic, pH 4.2 to 5.0, electroless Ni-P metallization of n-type Si wafer is the electron-beam evaporation deposition of a Fe film on the Si substrate [36]. The production of the Fe film activates the Si surface allowing for the deposition of a homogeneous and nanocrystalline structure of the Ni-P film on the Fe/Si substrate. Increasing the alkalinity of the electrolyte to pH 5.0 was associated with the deposition of a columnar structure nanocrystalline structure compared to the initially amorphous films produced below pH 5 [36]. Cracks in the N-P films formed at pH 5

were attributed to higher internal tensile stress due to a combination of a higher deposition rate and a lower P content [36].

In 2006, around 86 % of all wafer-based Si solar cells were produced using screen printing, a method where a metal paste is baked onto the surface of the cell, to form the Ag front and Al rear contacts with CVD used to grow silicon nitride $\{\text{SiN}_x\}$ as an antireflection coating on the front surface [37, 38]. Ongoing research into electroless deposition alternatives to screen-printed metallization, in connection with the metallization of conduction tracks for solar cell applications; include the selective removal of CVD antireflection coatings using UV ablation and the imbedding of conduction tracks within recessed grooves by mechanical scribing of the semiconductor substrate. Given the use of CVD in the manufacture of solar cells, especially in the deposit of antireflection coatings [28], hybridization of the CVD and electroless deposition has been pursued largely as a means of providing more efficient conduction tracks with lower contact resistivity than screen-printed contacts [28]. The combination of the CVD and electroless deposition processes centers on the selective removal of the antireflection coating on the front surface of the solar cell, a 70 nm silicon nitride layer $\{\text{SiN}_x\text{:H}\}$ produced by plasma-enhanced CVD on p-type textured silicon samples, by a UV laser allowed for subsequent Ni-P deposition only along the ablated lines while leaving the antireflection coating unharmed [28]. The alkaline, pH 8, Ni-P electrolyte used for electroless deposition on the UV scribed Si contained a sodium hypophosphite $\{\text{NaH}_2\text{PO}_2\}$ reducing agent as well as ammonia $\{\text{NH}_3\}$ for pH control and was typical of the electrolytes used for Ni-P metallization of Si [29]. The application of the electroless deposition bath for the UV ablation of the antireflection coating continues the practise of surface contacts established with screen-printed contacts.

Another approach to contact metallization is the imbedding of metal contacts within grooves cut into the semiconductor substrate forming what are known as buried contact solar cells [31, 39-41]. Buried contact solar cells typically have higher conversion efficiency compared to screen printed cells and the metallization of the grooves often incorporates electroless deposition of Ni and Cu [31, 39-41]. The formation of grooves is similar to the method of UV ablation of the antireflection coating; except that the substrate material removed rather than an antireflection coating [39].

Imbedding contacts and conduction tracks of solar cells within grooves formed by mechanical removal of semiconductor material provides the higher conversion efficiency of buried contact solar cells while also providing a lower production cost compared to photolithography/etching or laser scribing [31, 41]. The mechanical scribing of the surface is accomplished either by rotary diamond impregnated dicing blades or diamond point scribers and, like the laser, typically produce grooves that are inherently smooth and require etching for adhesion of deposits [31, 39].

Another important result pertaining to the metallization of silicon includes the enhanced deposition of Ni-P and Cu on porous Si by laser illumination [30, 42]. Effects of enhanced deposition under laser illumination have been widely known as localized heating of the sample can increase the local deposition rate. It has been suggested that enhancement of the alkaline electroless Ni-P deposition rate under laser illumination of porous p-type Si is the result of electron extraction from the conduction band of the Si. The justification of the observation is that the photon energy of the He-Ne laser used as a light source is 1.8 eV which is greater than the band-gap of Si [30]. At this stage several possibilities exist regarding the dependence on the band structure of porous Si difference in connection with the metallization of porous Si under illumination and within dark environments [30, 42]; furthermore, the extent to which localized heating plays a role remains unclear.

The experimental work conducted herein centers upon the selective metallization of Si using techniques based on results achieved with electroless Cu deposition on Mg alloys, see Chapter 3.3. Much like in the case of Mg, Si may be rendered catalytic for electroless deposition baths by means of surface oxide removal. Selective oxide removal, provided the use of appropriate electrolytes, resulted in the formation of selective electroless deposits in regions where the oxide layer had been removed. Existing alkaline electrolytes were investigated for the selective electroless deposition of pure Cu, and pure Au on Si wafers. Most importantly, this work demonstrates a novel application of a long existing acidic electroless Ni-P electrolyte [43], which was found to be successful for selective deposition on Si.

4.4 Materials and Methods

Experimental work was conducted on both n-type <100> and p-type <100> Si wafers supplied by Sigma-Aldrich. Both types of Si wafers possessed a mirrored finish on one side and a micro-textured pattern on the reverse, Figure 4.5.

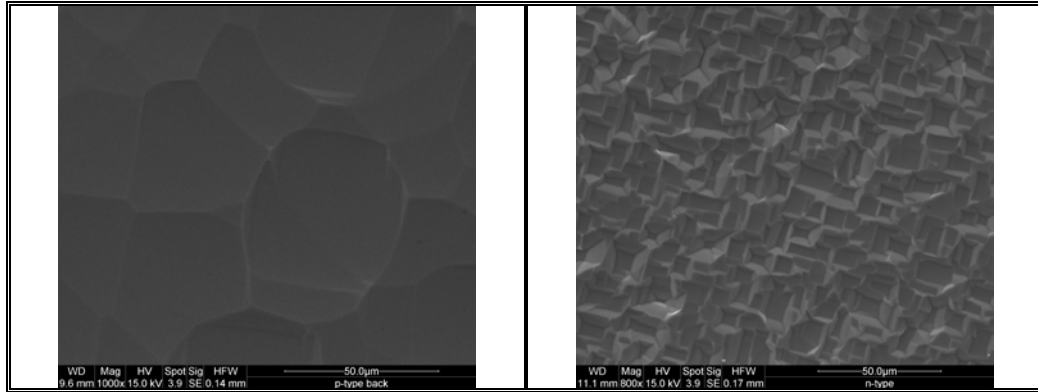


Figure 4.5: SEM images of the micro-textured pattern on p-type (left) and n-type (right) Si wafers used.

The Si samples were fractured from larger Si wafers with an average size of 8 mm – 15 mm × 15 mm – 20 mm × 0.5 mm. Selective oxide removal from the surface of the Si wafer was carried out, on both n-type and p-type, using a diamond tipped scribing utensil. Lines were scribed on the samples at different penetration depths to ensure sufficient layer removal to expose the oxide-free surface. All samples were handled using latex gloves and no pre-cleaning of the sample was performed prior to immersion in the metallization bath. Normal practise was the immediate immersion of samples within the metalizing bath after the scribing procedure was carried out. Additionally, the imperative to immerse the sample within the electrolyte was not present as unlike Mg, the rate of growth for the naturally oxide is claimed in literature to be of the order of $3.5 \pm 0.5 \text{ \AA/decade}$ in ambient air [44].

Metallization of Si wafer samples occurred in beakers with heat provided, where needed, by a SCIOLOGEX MS-H-Pro hotplate. Deposition bath temperatures varied based on the need of the deposition bath and ranged from room temperature to 80 °C. As best as could be achieved, samples were stood against the side of the beaker in cases where both sides were scribed, and laid flat on the bottom of the beaker with the scribed side facing up in instances where only a single side was scribed. Once metallization was completed, the sample was removed from the electrolyte with tweezers and rinsed in a

distilled water bath in order to remove any residue electrolyte from the sample surface. Post-rinse the samples were dried using KIMTECH laboratory clean wipes in order to avert any drying patterns. In some cases adhesion was tested using a scotch tape test, a test where a piece of scotch tape was placed over the sample and removed rapidly. In those instances where the test was carried out, adhesion was found to be good, which is attributed in part to the rough surface provided by the diamond-tipped scribe.

Macroscopic images of the samples were taken using a Hewlett-Packard Scanjet G4010 scanner at a resolution of 600 dpi (dots per inch). Specifically, regarding Si, the reflective nature of the polished side of Si wafers appears black on all scans and magnifies any dust present within the scanner as well as on the sample itself. Microscopic images were acquired using both a Zeiss Axioskop (Model 1) optical microscope with AxioCam high resolution colour (HRc) microscope camera and software AxioVision lite software, as well as an FEI Quanta 200 Environmental Scanning Electron Microscope (SEM) with a Field Emission Gun (FEG). Composition of the deposits was determined using energy-dispersive X-ray spectroscopy (EDS) provided by an EDAX SiLi Detector with Super Ultra Thin Window (SUTW) and EDAX Genesis software as part of the scanning electron microscope (SEM) system. The compositional analysis provided the average concentration of the outer few microns of the deposit weighted toward the outer layers of coating. Beam intensity for SEM and EDS measurements ranged from 10 kV to 20 kV with higher potentials applied for heavier metals, such as Au.

4.5 Experimental Results

Selective deposition of metal on Si surfaces typically requires multi-stepped processes which include many surface treatments. While the case for surface treatments is most often based on the adhesion of the metal film, some pre-treatments are used to catalyze the surface. The fundamental process of electroless deposition on Si requires only removal of surface oxides, to expose the Si surface, to allow for subsequent electroless deposition. Additionally, the selective removal of the surface oxide allows, in cases where the appropriate electrolyte is used for electroless deposition, selective deposition in those regions where the oxide layer has been removed. The method of

oxide removal may be carried out using a number of means including mechanical, chemical, or optical (lithographic) techniques, provided the Si substrate is exposed. In this work, the scribing of the surface using a diamond-tipped scribe ensures greater surface roughness, which results in greater adhesion; smoother surfaces are more prone to low adhesion.

As with electroless deposition at large, the mechanism of electroless deposition of metal on exposed Si is electrolyte dependant and the precise mechanisms involved are, in some cases, topics of ongoing debate. Common mechanisms for electroless deposition include displacement/replacement reactions where a more noble metal displaces a less noble metal, as seen with Cu deposition on Mg, as well as the binding of some ligand or complex on the surface which fosters reduction. In addition to the exposure of the catalytic oxidize-free surface, the deposition of the initial layer can be attributed to any of the traditionally accepted mechanisms as well as some specific to Si. Possible mechanisms in the case of Si may also be related to the bandgap structure of the p-type and n-type Si as well as the presence of exposed/broken bonds on the surface. While the deposition of the initial layer has not been fully investigated, the sustained deposition incurred after the formation of the initial layer, in all cases, was autocatalytic electroless deposition. The principle goal of the work presented herein was the selective metallization of the Si substrate rather than the pursuit of identifying the deposition mechanism. Suggestions as to possible metallization mechanisms were achieved by comparing modifications of the metalizing electrolyte such as the capacity of metallization both with and without the presence of a reducing agent. Proper identification of the deposition mechanism requires electrochemical analysis in the form of the deposition potential and was beyond the scope of the work conducted. Where possible comparisons were made between modified electrolytes in order to determine possible mechanisms for the metallization of the Si substrate; however, the selective metallization was remained the goal rather than the pursuit of the metallization mechanism itself. Metals deposited on Si wafers using the scribing technique included copper {Cu}, gold {Au}, silver {Ag}, as well as nickel phosphorous {Ni_xP_y} alloys and the details of the electrolytes are described in Appendix A. In all cases no measureable difference was observed between the electroless deposition on n-type and p-type Si.

4.5.1 Electroless Copper {Cu}

The electroless Cu electrolyte, modified from the formulation by Schlesinger et al. [45], used for the deposition of electroless Cu on Si wafers, Table 4.1, is identical in composition and operating conditions to that used for the deposition of Cu on Mg alloys, Chapter 3.4.2. The behaviour of the electrolyte was the same as in the case of Mg metallization showing greater stability as the hydroxide concentration decreased. Again, concentrations of NaOH below ~15 g/L appeared most stable with electrolytes containing around 10 g/L NaOH having long term stability while electrolytes containing over ~20 g/L NaOH were only stable for a few hours.

Bath	Chemical Name	Chemical Formula	Composition (g/L)
Bath A	Copper Sulphate Pentahydrate	$\text{CuSO}_4 \cdot 5\text{H}_2\text{O}$	25.0
	Potassium Sodium Tartrate Tetrahydrate (Rochelle's Salt)	$\text{KNaC}_4\text{H}_4\text{O}_6 \cdot 4\text{H}_2\text{O}$	65.0
	Sodium Hydroxide	NaOH	10.0
Bath B	Paraformaldehyde	$\text{HO}(\text{CH}_2\text{O})_n\text{H}$ ($n = 8-100$)	65.0
	Sodium Hydroxide	NaOH	10.0
Operating Temperature: 20 to 25 °C		pH > 12.5	

Table 4.1: Composition of the electroless Cu electrolyte, formulation modified from Schlesinger et al. [45]

Similar to the Mg case, it was determined that electroless deposition of Cu did not occur on surfaces from which the oxide layer was not removed. The lack of deposition on oxide surfaces, as in the case of Mg alloys, is attributed to the stability of the oxide layer in a highly alkaline environment. The highly alkaline nature of the electrolyte allowed for the selective electroless reduction of Cu in only those regions in which the oxide layer had been removed from the n-type Si wafer, Figure 4.6.

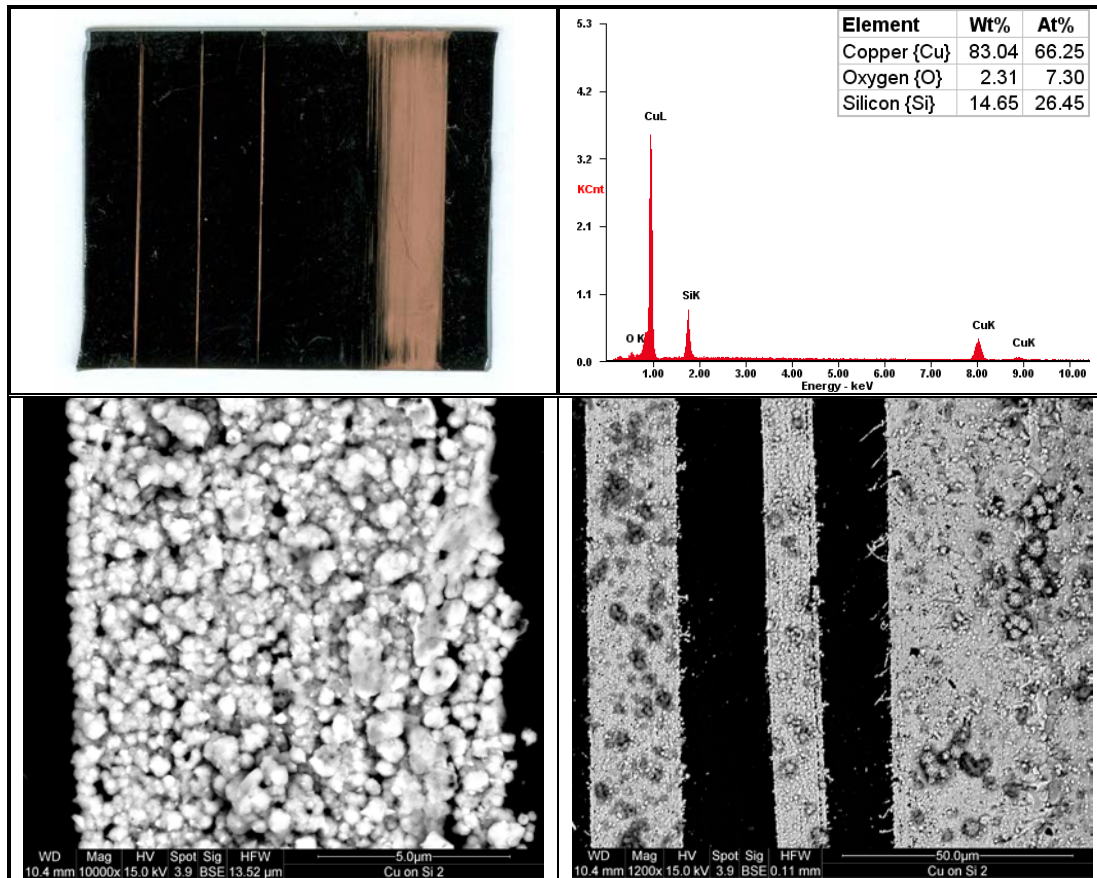


Figure 4.6: Macroscopic image, along with backscatter SEM images, and EDS of selective electroless deposits of Cu [20 min, 25 °C] on a larger than average, approximately 25 mm × 32.5 mm, piece of n-type Si. The large region of electroless Cu is due to surface polishing using 600-grit SiC emery cloth rather than a scribe. The presence of thin, secondary, lines on the SEM image on the right are due to the scribing tool and are part of a single line on the macroscopic image.

The oxygen {O} content within the deposit is attributed to oxidation of the Cu substrate as EDS analysis of the substrate Si indicated the atomic composition to be around 99 % Si with around 0.65 % O and 0.35 % Cu also appearing. The quantities of both Cu and O are considered negligible as no peak other than Si was observed. The lack of O present as background is expected to be a result of the ultra thin oxide layer which does not penetrate into the bulk material and likely measures only a few nanometres in thickness. Furthermore, EDS analysis of both polished and textured sides, as well as reviewing available documentation from the supplier, Sigma-Aldrich, suggested that no coating has been applied to the Si wafer during manufacture. Therefore, the selective electroless deposition on the surface of the Si wafer is concluded to be a result of removal of a thin oxide layer.

In addition to allowing for selective electroless deposition, the presence of the stable oxide layer provides long term stability of the selective deposit as no galvanic couple is formed between the electroless Cu coating and uncoated SiO_x surface of the substrate. The lack of galvanic response, as in the case of Mg alloys, Chapter 3, is observed by a lack of bubbles forming at the interface of the Cu coating and Si surface. Similar selective deposits on Mg alloys are not stable as a galvanic cell quickly develops between the selective Cu coating and exposed Mg substrate.

Unlike the case of Mg, where a reducing agent free electrolyte produces a deposit on the surface, electrolytes not containing the reducing agent are incapable of effectively metalizing the exposed Si substrate, Figure 4.7.

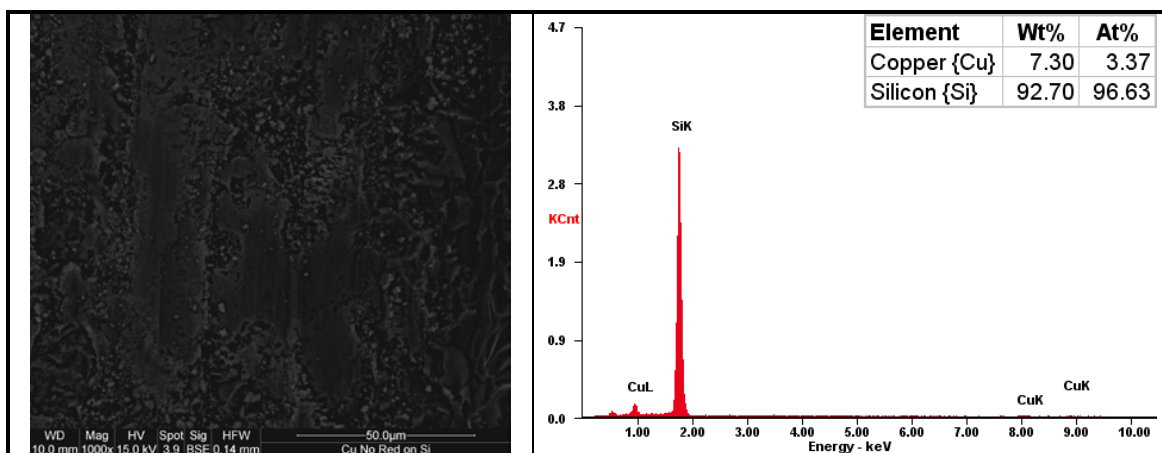


Figure 4.7: Backscatter SEM image and EDS analysis of an attempted electroless deposit of Cu [90 h, 25 °C] on n-type Si from an electrolyte containing no reducing agent.

While no deposit was observed on Si surfaces from electrolytes free of any reducing agent, some Cu was present within the scribed region of the Si wafer. The inconsistent positioning of the small Cu particles may have been the result of an immersion/displacement reaction; though given that precipitation of Cu was observed throughout the electrolyte whether Si was present or not, the Cu particles may have been the result of initial precipitates by virtue of the electrolyte being saturated with Cu²⁺ ions. The lack of deposition without the presence of a reducing agent suggests that exposure of bare Si provides a catalytic surface which allows adsorption of the reducing agent, HO(CH₂O)_nH (n = 8-100), and subsequent electroless deposition.

The role of the textured surface was not explored as the source of any possible enhancement of the catalytic nature of the exposed Si as deposits also occurred on the

smooth side of the sample where the sample was fractured from a larger wafer. Deposits formed on the smooth side edge of the wafer suffered from poor adhesion due to the inability of the deposit to anchor itself into the substrate. Adhesion testing for deposits in scribed regions, using packing tape, was somewhat inconclusive as the excellent adhesion may have been the result of incomplete contact between the deposit and the tape.

4.5.2 Electroless Gold {Au}

The deposition of electroless Au is yet another conductive metal which has applications for Si metallization. The main advantage of Au over other metals is that it does not readily oxidize allowing for good long term conduction. The deposition of electroless Au, as with the electrodeposition of Au, once required cyanide salts [46], though modern formulations have largely done away with the use of cyanide [46-50]. The modern formulation chosen, Table 4.2, does not contain a dedicated reducing agent and instead makes use of a sulphite-thiosulfate $\{SO_3^{2-} - S_2O_3^{2-}\}$ mixed ligand complex with sulphite acting as the main ‘reducing agent’ [49].

Bath	Chemical Name	Chemical Formula	Bath Composition	
			mol/L	g/L
Bath A	Sodium Tetrachloroaurate Dihydrate	$Na(AuCl_4) \cdot 2H_2O$	0.005	1.989
	Boric Acid	H_3BO_3	0.16	9.893
	Sodium Hydroxide*	NaOH	0.01	0.4000
Bath B	Sodium Thiosulphate	$Na_2S_2O_3$	0.065	10.277
	Sodium Sulphite	Na_2SO_3	0.035	4.411
	Boric Acid	H_3BO_3	0.160	9.893
Additives	Sodium Citrate Tribasic Dihydrate	$Na_3C_6H_5O_7 \cdot 2H_2O$	0.25	73.525
Operating Temperature: 60 to 90 °C			pH: 7 to 10	

*Sodium Hydroxide used to adjust pH of ‘Bath A’ to pH 7.

Table 4.2: Electroless Au electrolyte based on the work of Paunovic and C. Sambucetti [49]

Consistent with the work reported in patents by G. Krulik and N. Mandich [51, 52], the electroless Au electrolyte, without the presence of a dedicated reducing agent, provided especially good deposits at more alkaline pH values, $pH > 8$, Figure 4.8. Given that $Na_3C_6H_5O_7$ additives produce a considerable increase in the plating rate by appearing to act as an additional reducing agent [49], $Na_3C_6H_5O_7$ was not added to the electrolytes used to form Au deposits in Figure 4.8.

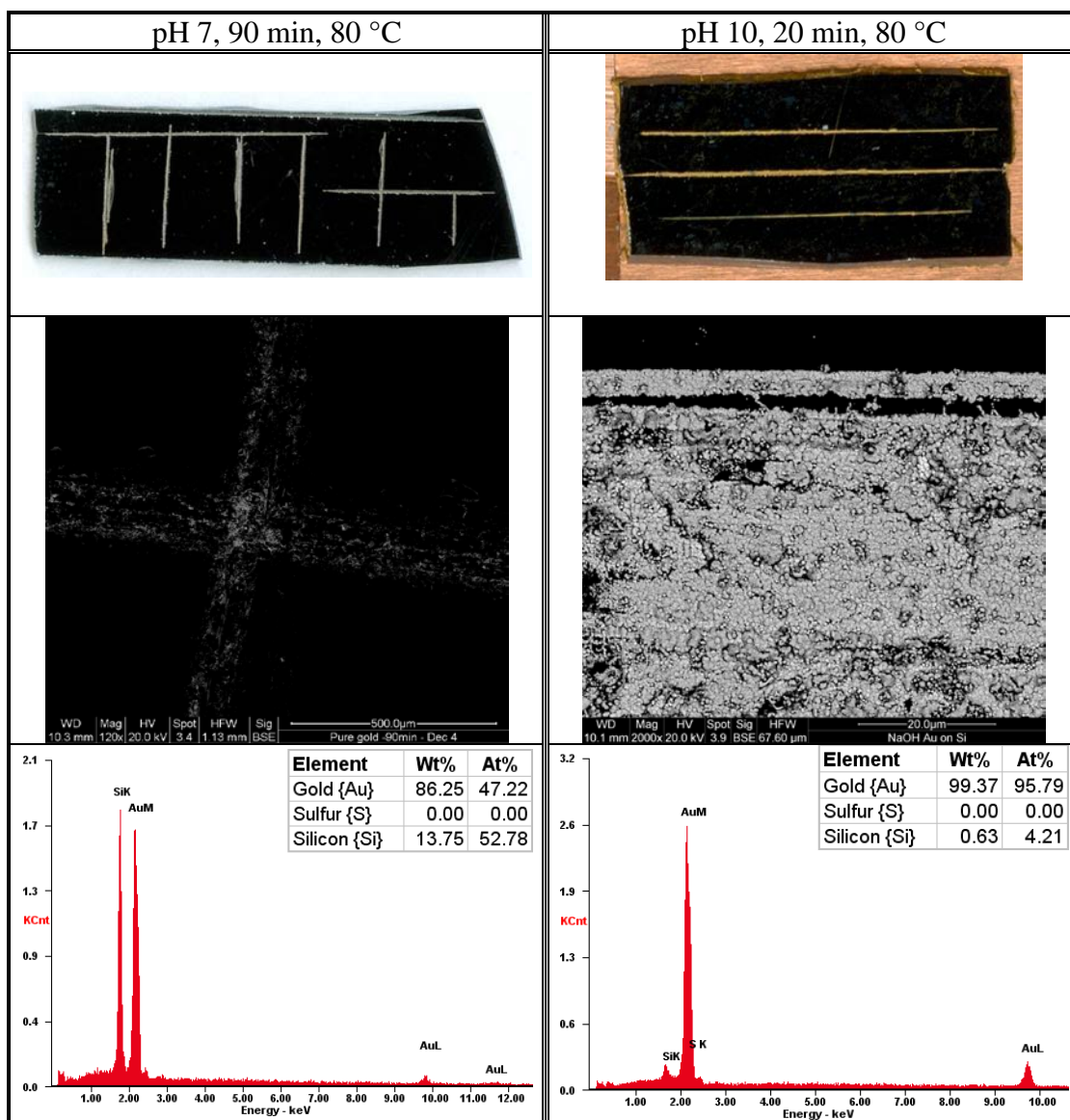


Figure 4.8: Macroscopic, SEM and EDS comparison of electroless Au deposits on n-type silicon formed from pH 7 (left) and pH 10 (right) electrolytes not containing $\text{Na}_3\text{C}_6\text{H}_5\text{O}_7$. The pH of the pH 10 electrolyte was adjusted using NaOH. The EDS analysis on the pH 7 deposit was conducted by targeting the sparse Au particles whereas the analysis of the pH 10 deposit was conducted on the clearly formed deposit.

Concerns using electrolytes of this type center largely on the inclusion of sulphur {S} within the deposit as S based chemicals are used as the reducing agent within this system. While EDS analysis did not detect any S within the Au deposits on Si, S may be co-deposited with the Au under certain conditions and on certain substrates, see Appendix A2, and may have made up a small part of the deposit.

Unlike common electroless Ni-P and Cu electrolytes, in which a dedicated reducing agent is oxidized to provide electrons for the reduction of metal ions, the exact mechanism of electroless Au deposition is the subject of some debate. It is currently

believed that the initial layer deposited from the mixed ligand electrolyte occurs as an immersion, galvanic displacement, layer with subsequent autocatalytic deposition of Au [49]. Results from Osaka et al. argue against the use of the term autocatalytic as they determined that Au deposition from a mixed ligand electrolyte did not occur on an Au sheet and hence the deposition of Au is not autocatalytic [50, 53]. The term substrate-catalyzed deposition is put forward by Osaka et al. to distinguish the Au deposits on Ni-B and Ni-P thin films from typical electroless deposition. The results of their work indicate that the thickness of Au deposits reaches a maximum thickness after approximately 60 minutes at pH 9 and 70 °C [53]. While deposits on Ni support the theory of an immersion deposit, the stable, ordered crystal structure of Si wafers suggest that more may be at work for the electroless plating of scribed Si. One possibility to explain the deposition of Au on Si is oxidation of the Si substrate in parts allowing for a displacement reaction, similar to the mechanism reported for Ni coverage [32]. This possibility is somewhat discounted as EDS results do not show any distinct O peak for electroless Au deposits, though the oxidation may be too small to be determined using EDS.

Another feature of the electrolyte described in Table 4.2 is the naturally alkaline pH provided by the inclusion of the $\text{Na}_3\text{C}_6\text{H}_5\text{O}_7$ additive; which increases the deposition rate atop that provided by the chemical itself. Additional benefits of $\text{Na}_3\text{C}_6\text{H}_5\text{O}_7$ use, beyond providing a pH of around pH 8.5 when dissolved in water⁴, include its well known ability to act as a buffer and stabilizer to Ni and other metals which would normally poison Au electrolytes.

Prolonged deposits of the Au electrolyte within scribed regions of Si, as well as on Ni, have been shown to adopt a well ordered grain structure, Figure 4.9, which is not seen with shorter deposits.

⁴ Experimentally it was determined that $\text{Na}_3\text{C}_6\text{H}_5\text{O}_7$ dissolved in distilled water produced a pH of around 8.7 for $\text{Na}_3\text{C}_6\text{H}_5\text{O}_7$ concentrations between 30.00 g/L and 100.00 g/L.

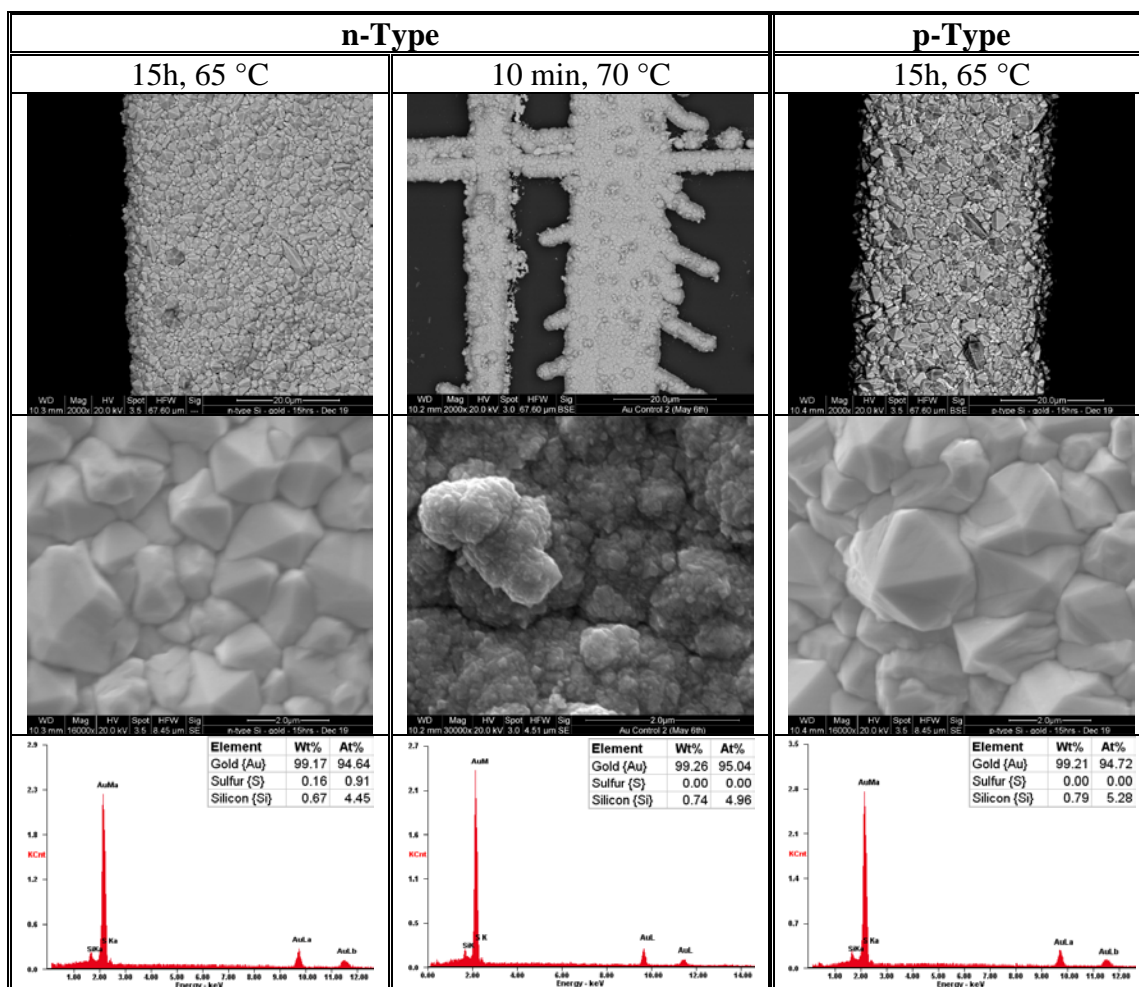


Figure 4.9: (Top) 2000× backscatter and (Middle) secondary emission (16000× for far left and right; 30000× for center) SEM images, with 2 μm scale bars, along with (Bottom) associated EDS of electroless Au deposits on Si using the complete electrolyte shown in Table 4.3. The graphs for the EDS counts show only Au, the largest peak, with a small Si peak to the left from the substrate. Deposition conditions for each deposit are related at the top of each column.

The reason for the well ordered grain structure is at present somewhat unclear. Possible sources of the ordered structure include the temperature of the environment, epitaxial growth, as well as reorganization of the crystallites within the Au rich environment.

4.5.3 Electroless Nickel {Ni}

The most practical metals deposited on Si wafers are the Ni-P alloys as they provide excellent diffusion barriers against the diffusion of Cu and Au into Si, though some diffusion of Ni into the Au/Cu deposit may occur [54]. While most electrolytes

used for Ni-P deposition on Si surfaces are alkaline, acidic and neutral electrolytes, Table 4.3, are also capable of forming deposits by using the scribing technique for Au and Cu.

Chemical Name	Chemical Formula	Composition (g/L)	
		Acidic	Neutral
Nickel Sulphate Hexahydrate	$\text{NiSO}_4 \cdot 6\text{H}_2\text{O}$	29.5	29.5
Sodium Citrate Tribasic Dihydrate	$\text{Na}_3\text{C}_6\text{H}_5\text{O}_7 \cdot 2\text{H}_2\text{O}$	—	23.5
Sodium Succinate	$(\text{NaOOCCH}_2)_2$	15.0	—
Succinic Acid	$\text{C}_4\text{H}_6\text{O}_4$	1.5	—
Sodium Hypophosphite Hydrate	$\text{NaH}_2\text{PO}_2 \cdot \text{H}_2\text{O}$	17.5	17.5
Operating Temperature: 65 °C	pH:	4.7 to 5.3	6.5 to 8.5

Table 4.3: Acidic and neutral electroless Ni-P electrolytes.
 Acidic formulation by J. Marton and M. Schlesinger (1968) [43]
 Neutral formulation modified from M. Schlesinger et al. (1972) [55]

As in the case of electroless Cu and Au electrolytes, both acidic and neutral electroless Ni-P electrolytes were capable of producing good quality deposits within the scribed region. While both deposits appeared exactly as expected of Ni-P, the deposit from the acidic electrolyte contained at most only around 7.5 % P atomically Figure 4.10.

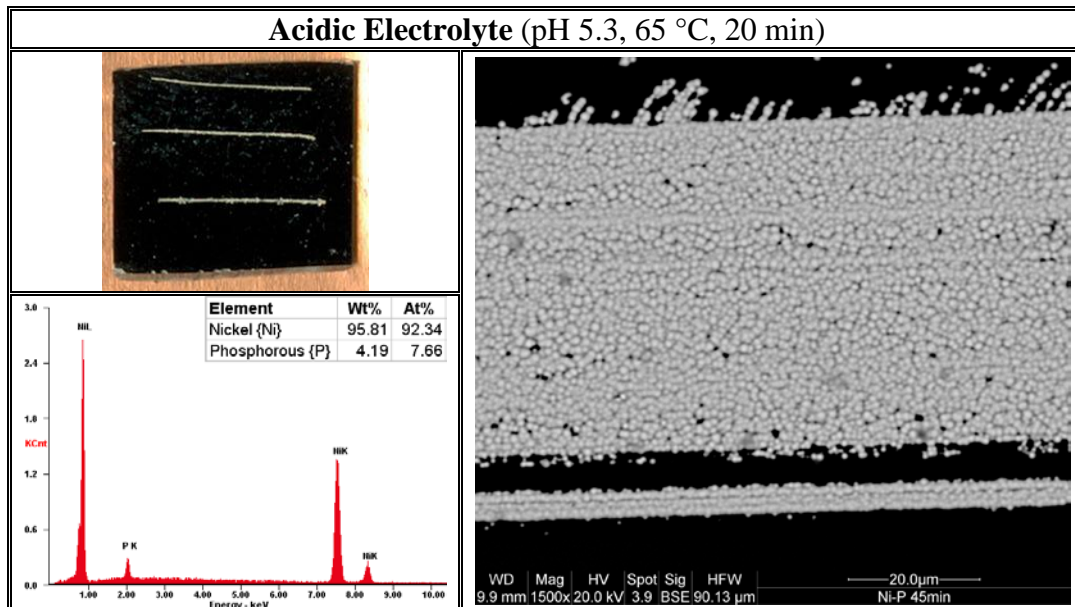


Figure 4.10: Macroscopic image, backscatter SEM image, and EDS analysis of 20 min electroless Ni-P deposits on n-type Si formed within an acidic, pH 5.3, electrolyte.

The low P content within the deposit is a consequence of the alkalinity of the electrolyte as the concentration of P falls within increasing alkalinity. Within acidic electrolytes around pH 4, the P content of electroless Ni-P deposits is expected to be up to 25 % atomically [56]. The atomic ratio of around 7.5 % P within the deposit, Figure

4.10, is consistent with the P content reported for other, similar, acidic electrolytes where the atomic composition of films produced at 85 °C was 84.3 % Ni and 15.7 % P for a pH 4.2 and 89.6 % Ni and 10.4 % P for a pH 5 [36]. As the same conditions on p-type Si produced a deposit of identical P content, the type of Si substrate was found to be inconsequential for the composition of the deposit. Electroless deposition from the electrolyte on Sn/Pd treated glass produced P contents of at least 10 % atomically, which is consistent with expectations of the electrolyte. Finally, immersing a scribed n-type Si sample in the same electrolyte without the NaH_2PO_2 reducing agent produced only a few minor Ni precipitates within the scribed region rather than a full coating.

As the scribing, or oxide removal, technique was adopted from work easily oxidized Mg alloys, Chapter 3.3; an investigation was conducted with respect to the allowable delay in immersing the scribed Si wafer into the Ni-P metalizing electrolyte. The n-type Si wafer samples used were scribed at the same time and immersed within the same electrolyte after < 2 minutes, 45 minutes, 4.5 hours, and 25 hours. Given the extremely slow oxidation rate of Si, it comes as no surprise that deposition occurred within the scribed regions of each of the four samples.

One anomaly present in the case of some deposits on Si was the inability for some scribed regions to form deposits. The inability to form a deposit occurred in cases of both freshly scribed samples as well as the sample exposed to open atmosphere for 25 hours prior to immersion within the acidic electrolyte. The cause of the lack of deposition has been linked to insufficient penetration from the diamond-tipped scribe as well as the catalytic activity and pH of certain electrolytes. Oxidation alone, which may have been a factor in the case of the 25 hour oxidation sample, does not explain the inability to form a deposit on some freshly scribed Si wafer samples. Though no single factor has been confirmed, the issue of deposits not forming appeared most common with electrolytes below pH 7.

In the case of the sample left out for 25 h, no deposit formed initially on the scribed sample and it was removed from the electrolyte. To ensure that the electrolyte was still functional and that scribing of the sample had been appropriately conducted, a small scratch was made in the sample perpendicular to existing scribed regions. Once the sample was placed within the electrolyte a reaction was observed and after 20 minutes the

sample was found to have a deposit within most of the scribed regions. The presence of a reaction upon second immersion appears to support the theory that some exchange of electrons allows deposition by oxidation of the surface [33]. Nevertheless, while a reaction did occur on second immersion, one region remained without any deposit, Figure 4.11. The reasons why Ni-P particles within the scribed region did not act as nucleation sites for further deposition as well as why second scribing of an unrelated part of the surface produced a deposit are presently undetermined.

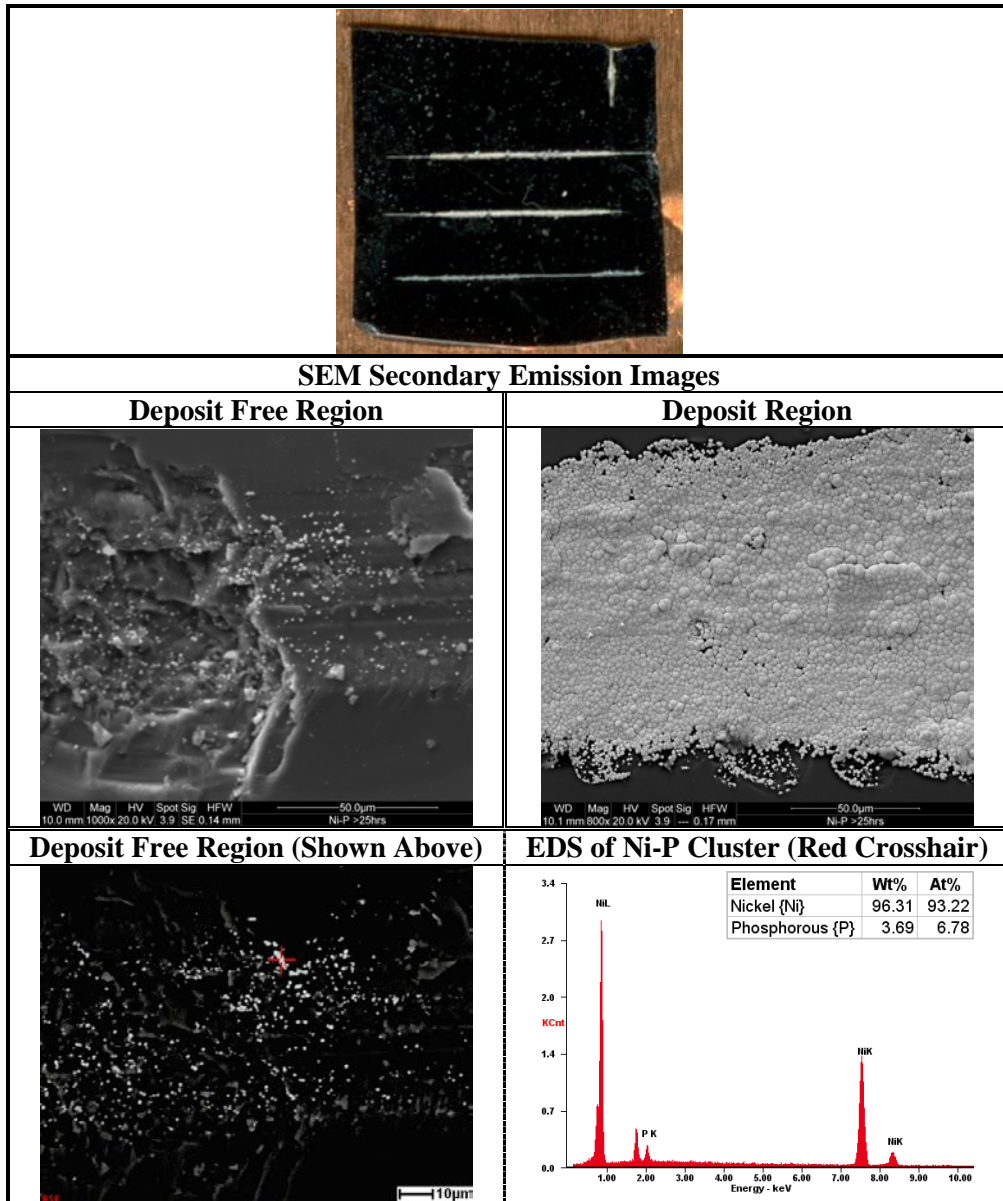


Figure 4.11: (Top) Macroscopic scan, (Top) secondary emission and (Bottom) backscatter SEM images along with EDS analysis of a Ni-P cluster (from backscatter) deposit [20 min, 65 °C] on scribed Si. The EDS analysis clearly shows that the composition of the Ni-P clusters on the surface match the composition of the deposit shown in Figure 4.10.

Deposition from the neutral electrolyte produced Ni-P deposits of similar structure to those produced by the acidic electrolyte. Increasing the pH of the neutral electrolyte beyond pH 7.5 resulted in a deposit that appeared to creep outside of the confines of the scribed regions. Further increasing the pH with sodium hydroxide {NaOH} to pH 10.0 resulted in deposit over the entire surface of the sample as well as within the scribed regions, Figure 4.12. The deposit within the scribed regions appeared to form only slightly prior to the deposit over the surface of the sample.

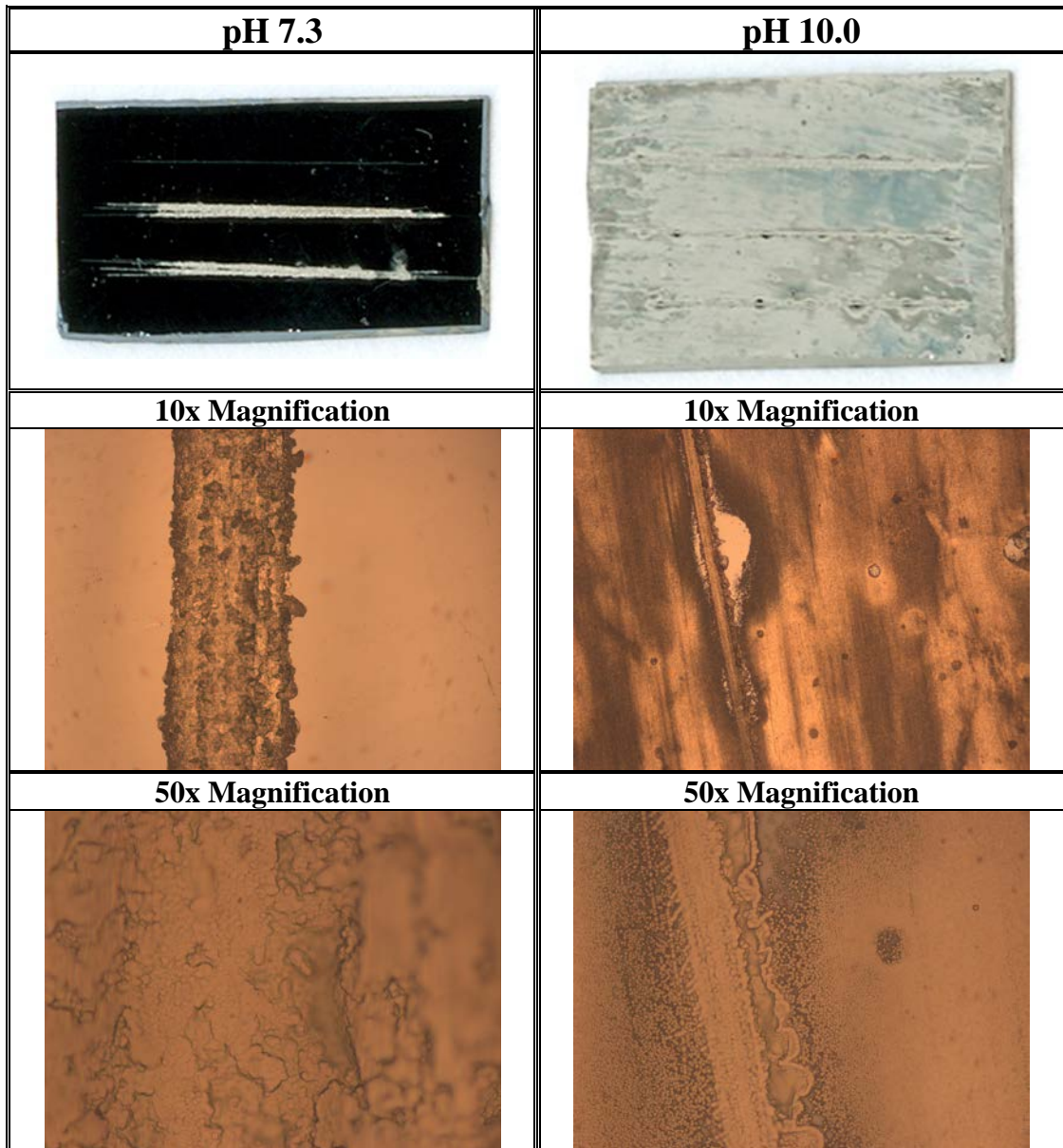


Figure 4.12: Comparison of macroscopic images and microscopic optical images of the Ni-P deposits on scribed n-type Si wafers. Scale bars are not available for optical microscope images; the magnification indicates the power of the used objective.

Rubbing the surface with a laboratory clean wipe to test the adhesion of the deposit indicated bonding of the deposit to the surface does occur. The bonding of the deposit to the mirror smooth surface suggests the formation of the deposit may include etching of the surface in addition to metallization. Additionally, while the electrolyte remained transparent, increasing the pH of the electrolyte beyond pH 12 appeared to result in the electrolyte becoming cloudy and opaque. The change in the appearance of the electrolyte is known to be a consequence of the insolubility of hydrated Ni^{2+} ions within highly alkaline environments. The opaque electrolyte was also found to produce inferior quality deposits than those produced when the electrolyte was transparent.

As mentioned in section 4.3, the electroless deposition of Ni-P alloys on Si typically involves a single alkaline electrolyte. The electrolytes used, which contain NH_4^+ , are capable of forming an initial Ni displacement/immersion layer upon which autocatalytic electroless Ni-P is deposited due to the presence of a reducing agent, typically NaH_2PO_2 . The quality of the Si surfaces prior to deposition in the case of the displacement/immersion electrolytes appears to be oxidized.

4.5.4 Role of Ammonium/Ammonia $\{\text{NH}_4^+/\text{NH}_3\}$

Given that increasing the pH of the neutral electrolyte with NaOH produced a deposit over the entire surface of the sample, the more commonly used pH modifier NH_4OH for Ni electrolytes was also evaluated for its effects on the deposit, Table 4.4.

Chemical Name	Chemical Formula	Composition	
		NaOH	NH_4OH
Nickel Sulphate Hexahydrate	$\text{NiSO}_4 \cdot 6\text{H}_2\text{O}$	29.5 g/L	10.9 g/L
Sodium Citrate Tribasic Dihydrate	$\text{Na}_3\text{C}_6\text{H}_5\text{O}_7 \cdot 2\text{H}_2\text{O}$	23.5 g/L	23.5 g/L
Sodium Hypophosphite Hydrate	$\text{NaH}_2\text{PO}_2 \cdot \text{H}_2\text{O}$	17.5 g/L	17.5 g/L
Sodium Hydroxide	NaOH	8.0 g/L	—
Ammonium Hydroxide	NH_4OH	—	37.5 mL/L
Operating Temperature: 80°C	pH:	10 to 11	

Table 4.4: Electroless Ni-P electrolytes modified from M. Schlesinger et al. (1972) [55]

As with the NaOH containing alkaline electrolyte, the NH_4OH containing electrolyte also produced a deposit over the entire surface of un-scribed Si wafer samples. In order to investigate the role of each element of the electrolyte, electrolytes were produced with a single component left out at each stage. The role of the reducing agent,

NaH₂PO₂, was first isolated with its removal from the electrolyte. At room temperature, the appearance of both electrolytes remained identical to that of electrolytes containing the reducing agent. Both electrolytes appeared capable of forming deposits, though the deposits formed from the NH₄OH electrolyte appeared to be of a superior quality. Increasing the concentration NaOH such that the electrolyte was pushed beyond pH 12 resulted in the electrolyte adopting a gel-like appearance above a temperature of around 60 °C. The gel-like appearance of the electrolyte, which was seen for the complete electrolyte when pushed above pH 12, is a consequence of the insolubility of hydrated Ni²⁺ ions at high pH.

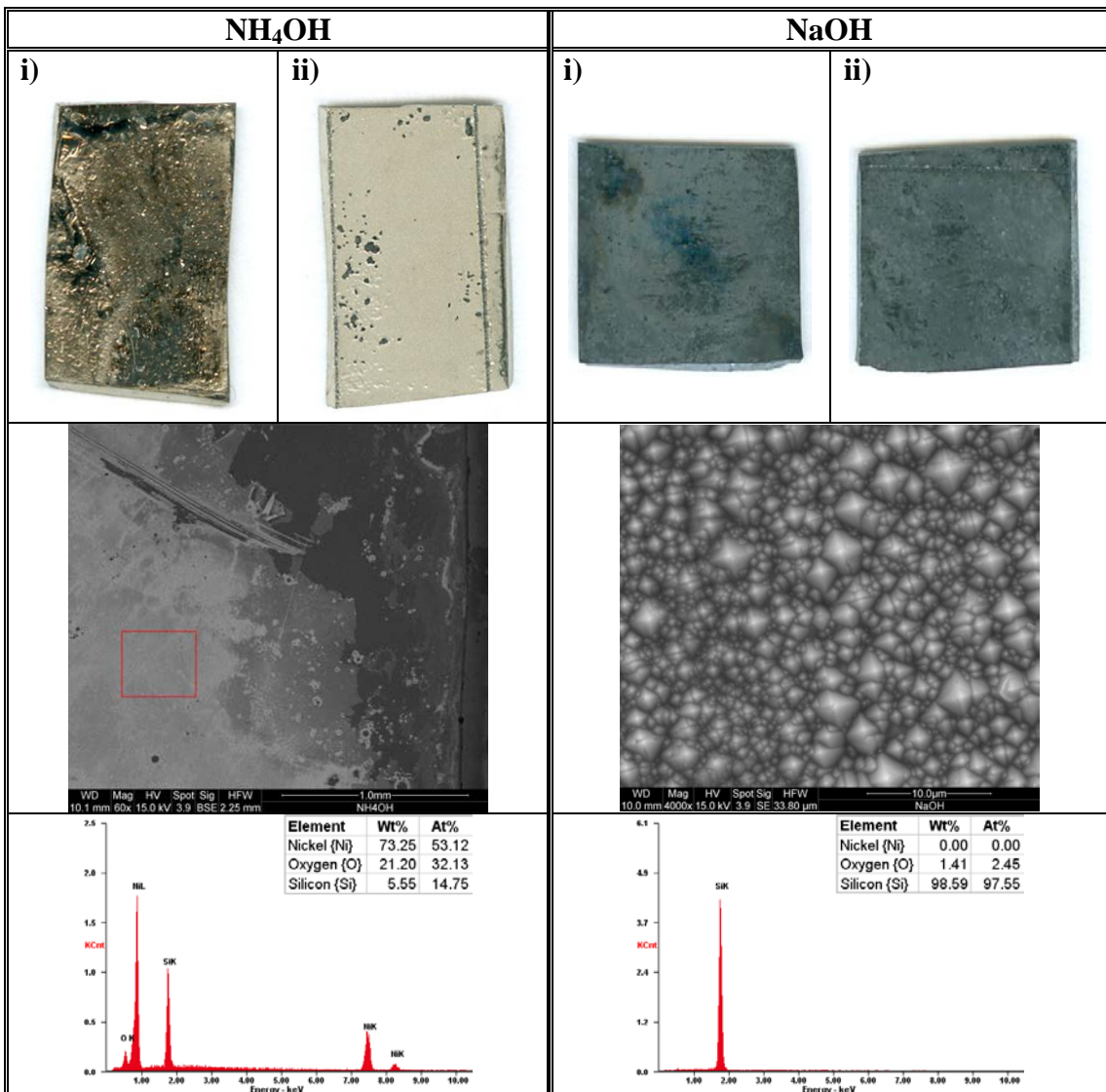


Figure 4.13: (Top) Macroscopic scanned images of (i) polished, (ii) textured sides, along with (Middle) backscatter SEM and (Bottom) associated EDS analysis of n-type Si samples, NH₄OH: 10 mm × 20 mm NaOH: 12 mm × 12 mm, immersed in the reducing agent free electrolytes [20 min, 80 °C] of Table 4.4.

Unlike the NaOH containing electrolyte, the NH₄OH containing electrolyte remained transparent due to the combination of stabilizer and NH₄OH. Immersion of Si wafer sample in both highly alkaline electrolytes resulted in the formation of bubbles on the Si surfaces indicating a reaction was taking place. While macroscopically both samples appeared to have deposits, EDS analysis demonstrated that an Ni deposit was formed only on the Si samples immersed within the NH₄OH electrolyte; with the Si sample immersed in NaOH appearing to have been mostly etched, Figure 4.13. Removal of the Na₃C₆H₅O₇ stabilizer from the both electrolytes resulted in the electrolytes adopting a snow globe-like appearance at room temperature due to the insolubility of hydrated Ni²⁺ ions at high pH. Immersion of un-scribed Si wafer samples within each electrolyte for 40 minutes was associated with a negligible reaction unless the alkalinity of the electrolyte very high, > pH 12, by the addition of NaOH and NH₄OH in excess. The reaction from the highly alkaline environment appeared to again to etch Si if the electrolyte contained on NaOH, and produce a deposit if the electrolyte contained only NH₄OH, Figure 4.14.

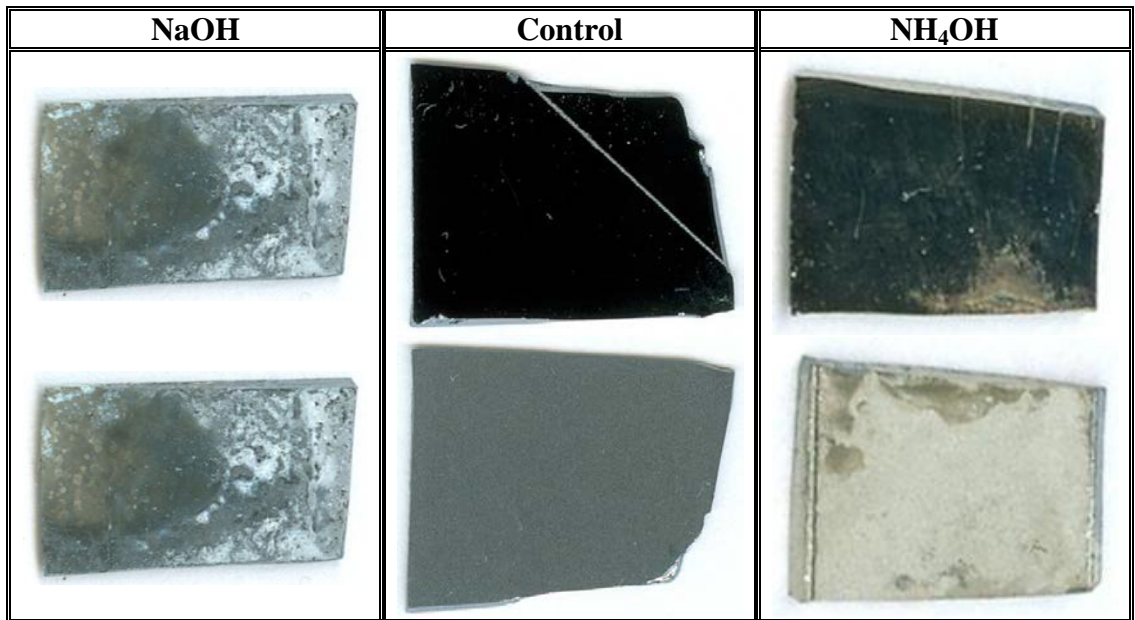


Figure 4.14: Macroscopic scan comparison of the (Top) polished and (Bottom) textured sides of n-type Si wafers after 40 min immersion within electrolytes [70 °C, pH > 12] containing NiSO₄ and (Left) NaOH, (Right) NH₄OH with a (Center) clean control sample for comparison.

The formation of a deposit from the NH₄OH containing electrolyte is explained, in part, by the presence of ammonia {NH₃} within the solution, which coordinates with the Ni²⁺ ions to create nickelhexamine {Ni(NH₃)₆²⁺} complexes. The formation of a Ni

immersion deposit from the NH_4OH containing electrolyte on the un-scribed Si surface suggests that, in addition to the alkaline environment, the $\text{Ni}(\text{NH}_3)_6^{2+}$ complex independently contributes to the formation of the Ni immersion deposit. Conversely, while the etching of the Si surface within the NaOH electrolyte suggests the alkaline environment attacks the SiO_x surface, no evidence of such attack is present from either the Cu or Au electrolytes; the former of which was attempted at pH 14. The role of alkalinity and hydroxide $\{\text{OH}^-\}$ ions in solution may, to a limited extent, render the SiO_x layer soluble and allow deposition. In the case of Ge semiconductors, the oxide layer is soluble in water allowing for immersion deposition of noble metal films such as gold {Au}, palladium {Pd}, and platinum {Pt} in the absence of toxic HF, or any pH adjusters, complexing agents, or reducing agents [57]. The role of NH_4^+ within alkaline Ni electrolytes appears to facilitate the deposition of the immersion layer on Si wafer surfaces and hence appears to, in some way, render the SiO_x layer soluble. The attack of the surface therefore likely has to do with the alkaline NiSO_4 electrolyte rather than the alkaline environment itself. The utility of an etched surface was not explored.

As cobalt {Co} is electrolessly deposited from electrolytes of composition similar to the NH_4OH Ni electrolyte, deposits were attempted on scribed Si from the NH_4OH electrolyte wherein $\text{NiSO}_4 \cdot 6\text{H}_2\text{O}$ was replaced with $\text{CoSO}_4 \cdot 7\text{H}_2\text{O}$. Unlike Ni electrolytes, deposits from the Co electrolyte were produced only within the scribed regions of the Si wafer. Further investigation as to the difference in behaviour was conducted with the creation of a Co electrolyte without the inclusion of a reducing agent. The n-type Si samples, which were not scribed, were placed in the otherwise identical electrolyte for approximately 40 minutes. While the evolution of bubbles from the surface of the Si wafer sample implied the presence of an initial reaction, the evolution of bubbles was not sustained indicating that any reaction was limited. Upon removal from the electrolyte it was apparent that no deposit had formed on the Si surface aside from a few precipitates, Figure 4.15. The lack of Co immersion coating on the Si wafer suggests that there is something unique about the ligand structure of Ni^{2+} ions within alkaline environment which allow the formation of an immersion deposit on Si.

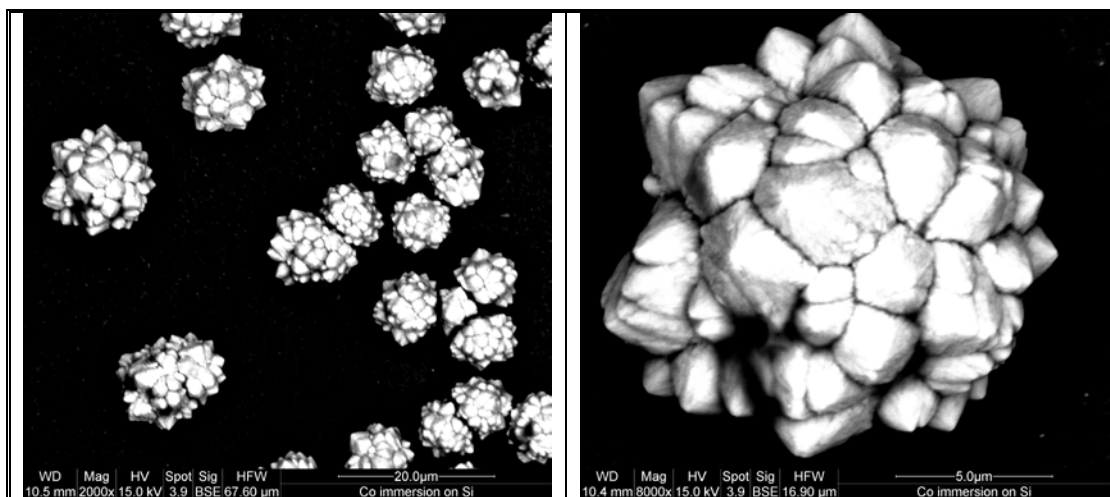
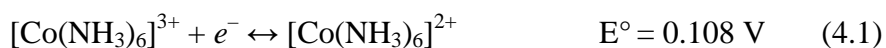


Figure 4.15: Backscatter SEM images of Co precipitates/crystallites formed within 40 minutes on n-type Si from a pH 10, 75 °C electrolyte containing 11.23 g/L $\text{CoSO}_4 \cdot 7\text{H}_2\text{O}$, 23.5 g/L $\text{Na}_3\text{C}_6\text{H}_5\text{O}_7 \cdot 2\text{H}_2\text{O}$, and excess NH_4OH .

Specifically, the inability for the Co electrolyte to form an immersion deposit from the electrolyte containing NH_4OH likely has to do with the relative instability of the hexaminecobalt(II) complex $\{[\text{Co}(\text{NH}_3)_6]^{2+}\}$ compared to the hexaminecobalt(III) complex, Equation 4.1 [58].



Further testing of the role of NH_4OH , and hence NH_3 , within both Cu and Au electrolytes was found to have influence on the deposit. Within electroless Cu deposits the presence of NH_4OH appeared to somewhat limit the deposit as NH_3 attacks Cu. Within Au electrolytes the presence of NH_4OH was found to stabilize and maintain an alkaline pH.

4.5.5 Electroless Ag

Finally, in the interest of direct comparison to the conduction tracks on solar cells, electroless Ag was investigated as another metal to be deposited within the scribed regions of Si wafers. While more expensive than Cu, electroless Ag has the added benefit of often being porous which allows for good solderability. Many common electrolytes exist for the electroless deposition of Ag, and the two chosen were the most simple of the possible electrolytes, Table 4.5.

Bath	Chemical Name	Chemical Formula	Bath Composition	
			mol/L	g/L*
Bath A	Silver Nitrate	AgNO ₃	0.03	5.17
	Ammonium Hydroxide* (28.0 % - 30.0 %)	NH ₄ OH	0.067	4.60
Bath B	Potassium Sodium Tartrate Tetrahydrate (Rochelle's Salt)	KNaC ₄ H ₄ O ₆ · 4H ₂ O	0.096	27.00
	Magnesium Sulphate Heptahydrate	MgSO ₄ · 7H ₂ O	0.008	1.94
Operating Temperature: 25 °C			pH: 10 to 12	

*NH₄OH was measured in mL/L.

Table 4.5: Electroless Ag electrolyte, which is mixed at a 1:1 ratio prior to use [59]

Given that the electrolyte did not contain the commonly used stabilizer, it decomposed during metallization and plating all surfaces, including the beaker, in the process. Therefore, due to the plate out of the electrolyte, it may be possible that reduced Ag particles became mechanically lodged in the rough scribed surface rather than deposited as a result of chemical reduction alone. Nevertheless, the lack of adhesion of the Ag thin film to the SiO_x surface compared to the well adhered scribed regions suggests that electroless deposition within the scribed regions took place. Once the poorly adhered surface film was wiped away, only selective deposition in the scribed regions remained, Figure 4.16.

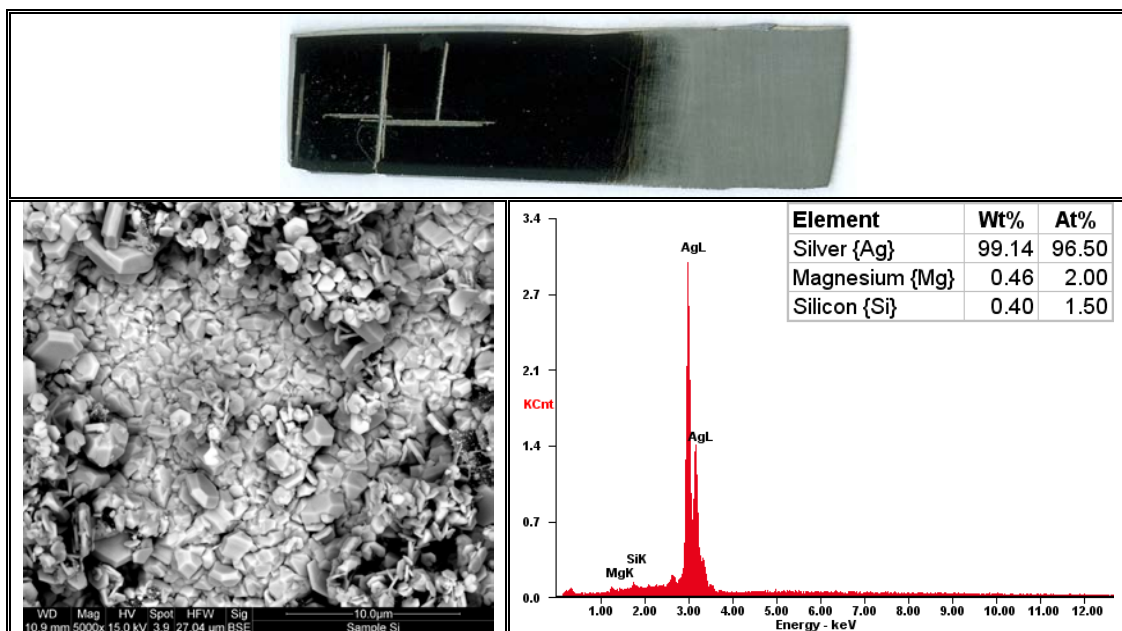


Figure 4.16: Macroscopic image, backscatter SEM image, and EDS analysis of a selective electroless Ag deposit [20 min, 25 °C] on n-type Si.

Given the somewhat porous crystallite structure of the electroless Ag, which provides an easy to solder to the deposit, heat treatment is a likely requirement to produce a more compact deposit. Additionally, selective electroless deposition of this kind appears to provide a producing conductive Ag deposits on n-type and p-type Si surfaces.

4.6 Summary

The electroless deposition of metal, specifically Ni [12] and Cu [60], on exposed, or scribed, Si has been known for some time and is an essential part of the electronics industry, especially buried contact solar cells. Deposition of Ni is typically achieved using alkaline electrolytes which contain NH_4^+ , which has been shown here to produce an immersion deposit on SiO_x surfaces. Additionally, results within this work have demonstrated that removal of the SiO_x layer allows for direct deposition on Si from a host of electrolytes. The most notable of the electrolytes is acidic electroless Ni-P, which had previously been deposited on Si by others using Sn/Pd activation of the surface [34]. While it would be thought that acidic electroless Ni-P would contain P at 25 %, and hence increase the resistance of the deposit, it has been found that P is included only at around 7.5 % making it competitive with alkaline Ni-P electrolytes. The additional selectivity of the acidic Ni-P electrolyte also obviates the need for any masking of the surface which is apparently required for deposition of Ni-P from alkaline electrolytes.

Other results of note within this work include the more general application of scribing for the one step electroless metallization of Si wafers. The capacity of a number of electrolytes to deposit on exposed Si has been shown and expands the possibilities for Si metallization. The selective deposition of Co-P from alkaline electrolytes is reinforced by the lack of immersion deposit formed on SiO_x surfaces and provides another possible diffusion barrier for Si surfaces.

Combined with the appropriate choice of electrolyte, mechanical scribing the surface of Si wafers provided an excellent method of oxide removal and allowed for the selective electroless deposition of metal films only in those regions where the surface was scribed. More generally, oxide removal may be carried out using a number of means including mechanical, chemical, or optical techniques depending what is most

convenient. The role of NH_4^+ , or more specifically NH_3 , within Ni electrolytes was investigated and is understood as an important factor in the formation of immersion Ni deposits on Si wafers. Given the substantial amount of literature pertaining to the metallization of Si, it is possible that similar work to the above has been published elsewhere. Hence, to the best knowledge of the author the above work is novel. The process as laid out within this chapter demonstrates mechanical selectivity for several previously unexplored electrolytes for the metallization of both n-type and p-type Si wafer surfaces in the production of conduction tracks for various electronic purposes. Though previously unexplored for deposition on scribed Si, all electrolytes were previously established for the creation of electroless deposits on other surfaces and previously documented in literature.

4.7 References

- [1] E. Van Kerschaver, and G. Beaucarne, "Back-contact Solar Cells: A Review", *Progress in Photovoltaics: Research and Applications*, 14, (2006), p.107-123, DOI: 10.1002/pip.657
- [2] M. Paunovic, Chapter 17: Electroless Deposition of Copper, in "Modern Electroplating, Fifth Edition", p.433-446, eds: M. Schlesinger and M. Paunovic, (2010), John Wiley & Sons, Inc., Hoboken, NJ, USA, DOI: 10.1002/9780470602638.ch17
- [3] G.M. Rao, "Electrowinning of Silicon from K_2SiF_6 -Molten Fluoride Systems". *Journal of the Electrochemical Society*, 127(9) (1980) p.1940- doi:10.1149/1.2130041
- [4] R. C. De Mattei, "Electrodeposition of Silicon at Temperatures above Its Melting Point". *Journal of the Electrochemical Society*, 128(8) (1981) p.1712-1714, doi:10.1149/1.2127716
- [5] R.D. Middlebrook, Chapter 1: Introduction, in "An Introduction to Junction Transistor Theory", p. 3-21, (1957), John Wiley and Sons, Inc. New York
- [6] G. Sun, F. Chang, and R. A. Soref, "High efficiency thin-film crystalline Si/Ge tandem solar cell" *Optics Express*, 18(4), (2010), p.3746-3753
- [7] Q. H. Fan, C. Chen, X. Liao, X. Xiang, S. Zhang, W. Ingler, N. Adiga, Z. Hu, X.Cao, W. Du, X. Deng, *Solar Energy Materials and Solar Cells*, 94(7), (2010) p.1300-1302
- [8] T. Tayagaki, Y. Hoshi, & Noritaka Usami, "Investigation of the open-circuit voltage in solar cells doped with quantum dots", *Scientific Reports*, 3, Article #2703, DOI: 10.1038/srep02703
- [9] I. Kabacelik, R. Turan, "Germanium solar cells prepared by ion implantation", *Journal of Optoelectronics and Advanced Materials*, 15(7- 8), (2013), p.948-953
- [10] R.D. Middlebrook, Chapter 3: Qualitative Semiconductor Physics, in "An Introduction to Junction Transistor Theory", p. 39-54, (1957), John Wiley and Sons, Inc. New York

- [11] R.D. Middlebrook, Chapter 4: Quantitative Semiconductor Physics, in “An Introduction to Junction Transistor Theory”, p. 55-72, (1957), John Wiley and Sons, Inc. New York
- [12] H. Iwasa, M. Yokozawa, and I. Teramoto, “Electroless Nickel Plating on Silicon”, Journal of the Electrochemical Society: Electrochemical Science, 115(5), (1968), p.485-488
- [13] C. Kittel, Chapter 17: Surface and Interface Physics, in "Introduction to Solid State Physics, Eighth Edition", p.487-514, (2005), John Wiley & Sons, Inc.
- [14] M. G. Raymer, The Silicon Web: Physics for the Internet Age, Chapter 10: Semiconductor Physics: Transistors and Circuits, p. 337-374, CRC Press, 2011
- [15] J. Bardeen, W. H. Brattain “The Transistor, A Semi-Conductor Triode”, Physical Review, 74(2), (1948), p.230 -231
- [16] W. Shockley, M. Sparks, G. K. Teal, “p-n Junction Transistors” Physical Review, 83(1), (1951), p.151-162
- [17] Li.-Q. Xia, M. Chen, Chapter 13: Chemical Vapour Deposition, in “Handbook of Semiconductor Manufacturing Technology, Second Edition”, Eds: R. Doering, Y. Nishi, CRC Press, Taylor and Francis Group, Boca Raton, Florida
- [18] T.E. Seidel, Chapter 14: Atomic Layer Deposition, in “Handbook of Semiconductor Manufacturing Technology, Second Edition”, Eds: R. Doering, Y. Nishi, CRC Press, Taylor and Francis Group, Boca Raton, Florida
- [19] S. M. Rossnagel, Chapter 15: Physical Vapour Deposition, in “Handbook of Semiconductor Manufacturing Technology, Second Edition”, Eds: R. Doering, Y. Nishi, CRC Press, Taylor and Francis Group, Boca Raton, Florida
- [20] J. Reid, Chapter 16: Damascene Copper Electroplating, in “Handbook of Semiconductor Manufacturing Technology, Second Edition”, Eds: R. Doering, Y. Nishi, CRC Press, Taylor and Francis Group, Boca Raton, Florida
- [21] C. H. Ting, M. Paunovic, “Selective Electroless Metal Deposition for Integrated Circuit Fabrication”, Journal of the Electrochemical Society, 136(2), (1989), p.456-462
- [22] C. H. Ting, M. Paunovic, P. L. Pai, and G. Chiu, “Selective Electroless Metal Deposition for Via Hole Filling in VLSI Multilevel Interconnection Structures”, Journal of the Electrochemical Society, 136(2), (1989), p.462-466
- [23] C. H. Ting and M. Paunovic, “Electroless deposition for IC fabrication” U.S. Patent 5,169,680 (1992)
- [24] Martin A. Green, “Photovoltaic Principles”, Physica E, 14, (2002), p.11-17
- [25] M. Paunovic, P. J. Bailey, R. G. Schad, and D. A. Smith, Electrochemically Deposited Diffusion Barriers, Journal of the Electrochemical Society, 141(7), (1994), p.1843-1850
- [26] W. E. Taylor, C. F. Gay and N. Mardesich, “The Impact of Screen Printing on the Cost of Solar Cell Metallization”, Journal of Solar Energy Engineering, 102(1), (1980), p.55-58, doi:10.1115/1.3266122
- [27] K.F. Teng, R.W. Vest, “Metallization of Solar Cells with Ink Jet Printing and Silver Metallo-Organic Inks”, IEEE Transactions on Components, Hybrids, and Manufacturing Technology, 11(3), (1988), p.291-297

- [28] C. Boulord, A. Kaminski, B. Canut, S. Cardinal, and M. Lemitia, “Electrical and Structural Characterization of Electroless Nickel–Phosphorus Contacts for Silicon Solar Cell Metallization”, *Journal of the Electrochemical Society*, 157(7), (2010), p.H742-H745
- [29] M. V. Sullivan, J. H. Eigler, “Electroless Nickel Plating for Making Ohmic Contacts to Silicon”, *Journal of the Electrochemical Society*, 104(4), (1957), p.226-230
- [30] F. A. Harraz, J. Sasano, T. Sakka, and Y. H. Ogata, “Different Behavior in Immersion Plating of Nickel on Porous Silicon from Acidic and Alkaline Fluoride Media”, *Journal of The Electrochemical Society*, 150(5), (2003), p.C277-C284
- [31] A.U. Ebong, M. Taouk, S. Bowden, C. Honsberg, S.R. Wenham, and M.A. Green, “Mechanically Scribed Double Sided Buried Contact Silicon Solar Cells”, *Renewable Energy*, 5(Part I), (1994), p.162-165
- [32] N. Takano, N. Hosoda, T. Yamada, and T. Osaka “Mechanism of the Chemical Deposition of Nickel on Silicon Wafers in Aqueous Solution”, *Journal of The Electrochemical Society*, 146(4), (1999), p.1407-1411
- [33] H. F. Hsu, C. L. Tsai, C. W. Lee, H. Y. Wu, “Mechanism of immersion deposition of Ni–P films on Si(100) in an aqueous alkaline solution containing sodium hypophosphite”, *Thin Solid Films*, 517, (2009), p.4786–4791
- [34] W.L. Liu, S.H. Hsieh, T.K. Tsai, W. J. Chen, S. S. Wu, “Temperature and pH dependence of the electroless Ni–P deposition on silicon”, *Thin Solid Films*, 510, (2006), p.102 – 106
- [35] V. M. Dubin, “Selective Electroless Ni-Cu(P) Deposition for Via Hole Filling and Conductor Pattern Cladding in VLSI Multilevel Interconnection Structures”, *Journal of the Electrochemical Society*, 139(2), (1992), p.633-638
- [36] W. L. Liu, S. H. Hsieh, and W. J. Chen, “Growth Behavior of Ni–P Film on Fe/Si Substrate in an Acid Electroless Plating Bath”, *Journal of The Electrochemical Society*, 157(7), (2010), p.H742-H745
- [37] S. Riegel, F. Mutter, T. Lauermann, B. Terheiden, G. Hahn, “Review on screen printed metallization on p-type silicon”, *Energy Procedia*, 21, (2012), p.14-23
- [38] D.-H. Neuhaus and A. Münzer, “Industrial Silicon Wafer Solar Cells”, *Advances in OptoElectronics*, Article ID: 24521, (2007), p.1-15
- [39] C. M. Chong, S. R. Wenham, and M. A. Green, “High-efficiency, laser grooved, buried contact silicon solar cells” *Applied Physics Letters* 52, (1988) p.407-409, doi: 10.1063/1.99453
- [40] S. R. Wenham, M. A. Green, “Laser Grooved Solar Cell”, United States Patent # 4,626,613, (1986)
- [41] A.U. Ebong, C. Honsberg, S.R. Wenham, and M.A. Green, “Mechanically Grooved, Double Sided, Buried Contact Silicon Solar Cells”, *Renewable Energy*, 11(3), (1997), p.331-340
- [42] M. Jeske, J. W. Schultze, M. Thönissen, and H. Munder, “Electrodeposition of metals into porous silicon” *Thin Solid Films*, 255(1-2), (1995) p.63-65
- [43] J. P. Marton and M. Schlesinger, “The Nucleation, Growth, and Structure of Thin Ni-P Films” *Journal of the Electrochemical Society: Electrochemical Science*, 115(1), (1968), p.16-21

- [44] K. Tsunoda, E. Ohashi, and S. Adachi, "Spectroscopic characterization of naturally and chemically oxidized silicon surfaces" *Journal of Applied Physics*, 94(9), (2003), p.5613-5316
- [45] B. K. W. Baylis, A. Busuttill, N. E. Hedgecock, and M. Schlesinger, "Tin (IV) Chloride Solution as a Sensitizer in Photoselective Metal Deposition", *Journal of the Electrochemical Society: Electrochemical Science & Technology*, 123(3), (1976), p.348-351
- [46] P. A. Kohl, Chapter 4: Electrodeposition of Gold, in "Modern Electroplating, Fifth Edition", p.115-130, eds: M. Schlesinger and M. Paunovic, (2010) John Wiley & Sons, Inc., Hoboken, NJ, USA, DOI: 10.1002/9780470602638.ch4
- [47] Y. Okinaka, "Electroless gold plating baths", US Patent #: US3700469 Original Assignee: Bell Telephone Labor Inc., (1971)
- [48] Y. Okinaka, Masao Hoshino, "Some Recent Topics in Gold Plating for Electronics Applications", *Gold Bulletin*, 31(1), (1998), p.3-13
- [49] Y. Okinaka and M. Kato, Chapter 21: Electroless Deposition of Gold, in "Modern Electroplating, Fifth Edition", p.483-498, eds: M. Schlesinger and M. Paunovic, (2010) John Wiley & Sons, Inc., Hoboken, NJ, USA, DOI: 10.1002/9780470602638.ch21
- [50] T. Osaka, Y. Okinaka, J. Sasano, M. Kato, "Development of new electrolytic and electroless gold plating processes for electronics applications", *Science and Technology of Advanced Materials*, 7, (2006) p.425-437
- [51] G. A. Krulik and N. V. Mandich, U.S. Patent 5,232,492 (1993)
- [52] G. A. Krulik and N. V. Mandich, U.S. Patent, 5,318,621 (1994)
- [53] M. Kato, J. Sato, H. Otani, T. Homma, Y. Okinaka, T. Osaka, O. Yoshioka, "Substrate (Ni)-Catalyzed Electroless Gold Deposition from a Noncyanide Bath Containing Thiosulfate and Sulfite. I. Reaction Mechanism", *Journal of The Electrochemical Society*, 149(3), (2002), p.C164-C167
- [54] A. van Wijngaarden, M. Schlesinger, N. E. Hedgecock, and B. K. W. Baylis, "Interdiffusion Studies of Au/Ni and Au/Ni-P", *Journal of the Electrochemical Society: Solid-State Science and Technology*, 127(5), (1980), p.1124-1128
- [55] S. L. Chow, N. E. Hedgecock, and M. Schlesinger, "Electron Microscope Study of the Nucleation and Growth of Electroless Cobalt and Nickel", *Journal of the Electrochemical Society: Electrochemical Science & Technology*, 119(12), (1972), p.1614-1619
- [56] M. Schlesinger, Chapter 18: Electroless Deposition of Nickel, in "Modern Electroplating, Fifth Edition", p.447-458, eds: M. Schlesinger and M. Paunovic, (2010), John Wiley & Sons, Inc., Hoboken, NJ, USA, DOI: 10.1002/9780470602638.ch18
- [57] L. A. Porter, Jr., H. C. Choi, A. E. Ribbe, and J. M. Buriak, "Controlled Electroless Deposition of Noble Metal Nanoparticle Films on Germanium Surfaces", *Nano Letters*, 2(10), (2002), p.1067-1071
- [58] Petr Vanýsek, Section 8: Analytical Chemistry, Electrochemical Series, in *CRC Handbook of Chemistry and Physics*, Internet Version 2005, p.8-23-8-33, David R. Lide, ed., <<http://www.hbcnpnetbase.com>>, CRC Press, Boca Raton, FL, 2005.

- [59] N. Koura, Chapter 17: Electroless Plating of Silver, in “Electroless Plating: Fundamentals and Applications”, p. 441-462, Edited by G. O. Mallory, J. B. Hajdu, American Electroplaters and Surface Finishers, 1990, Orlando, Florida
- [60] M. Vivar, C. Morilla, I. Antón, J.M. Fernández, G. Sala, “Laser Grooved Buried Contact Cells Optimised for Linear Concentration Systems”, *Solar Energy Materials & Solar Cells*, 94, (2010), p.187–193

Chapter 5: Hybrid Electro-Electroless Deposition	239
5.1 Overview of Electroplating and Electroless Deposition	240
5.2 Theory	242
5.2.1 Multi-layer Deposition	243
5.2.2 Alloy Deposition	246
5.3 Materials and Methodology	246
5.3.1 Electroless Gold {Au} Electrolytes	247
5.3.2 Electrodes and Deposition System	248
5.3.3 Sample Analysis	250
5.4 Ni/Au and Co/Au Results	251
5.5 Application to Coatings on Mg Alloys	259
5.6 Iron Nickel {Fe/Ni} Electrolyte and Ongoing Work	262
5.7 Summary	271
5.8 References	271

5.1 Overview of Electroplating and Electroless Deposition

Electroless deposition was discovered through the electroplating process by Brenner and Riddell [1] with the observation of cathode efficiencies greater than 100 % in the deposition of nickel {Ni} when the additive of sodium hypophosphite {NaH₂PO₂} was present. The discovery of the revolutionary autocatalytic electroless process created an entire field within electrochemistry for the autocatalytic deposition of metals using a reducing agent, such as NaH₂PO₂, rather than an electrical current. The use of reducing agents as additives for electroplating have a number of applications including control over the grain size as well as the inclusion of non-metals. In the case of NaH₂PO₂ use for Ni deposition, phosphorus {P} is the non-metal added as a consequence of the anodic reaction of the reducing agent. The inclusion of non-metals, though possible using the hypophosphite reducing agent [2], occurs more commonly with the addition of acids such as phosphoric acid {H₃PO₄} or phosphorous acid {H₃PO₃} for electroplated Ni-P [3]. Specifically, Ni-P has received significant attention as deposits with greater than 10 % phosphorus are initially amorphous and have an enhanced resistance to corrosion [3]. Differences between Ni-P deposits also exist with electrolessly deposited Ni-P possessing diffusion barrier qualities superior to those afforded by electroplated Ni-P [4].

The separation of electroplating and electroless deposition appears to have come about largely from the desire to establish electroless deposition as its own defined method of deposition. While both electroplating and electroless deposition techniques are often used in concert within industrial plating¹, the processes remain distinct using separate electrolytes for both processes. Recombining electroplating with electroless deposition for the simultaneous deposition of different metals from a single electrolyte does not appear to have been pursued due in part to a perceived lack of applications. However, the combination of electroplating with electroless deposition for the deposition of a single metal has as long been known [2]. Hence, there is a feeling that established deposition techniques, including electroplated multi-layers and alloys, were sufficient and superior to any possible mixed deposition technique. That feeling appears to have acted as a primary deterrent to further mixed electrolyte investigations. Further hampering any pursuit of

¹ Electroless plating is often used to provide a conductive base layer for electroplating.

mixed deposition technique electrolytes was the lack of recognition that electrolytes capable of electroplating and electroless deposition of different metals could be stable and therefore could exist. The hybridized electroless and electroplating process as defined here constitutes both electroplating and electroless deposition of different metals from a single electrolyte; throughout this section the process will be referred to as electro-electroless deposition or equally as hybrid deposition.

Both electro- and electroless deposition have advantages and limitations regarding both the materials and qualities of the deposit. Often cited advantages of electroplating include the ability to deposit pure metals, the resistance of deposition baths to decomposition, good control over the volume of metal deposited, as well as control of deposited materials based on both modification of the deposition potential and electrolyte composition. Electroplating is hindered most by line of sight issues due to the presence of electric field lines. The electric field lines result in uneven deposits over flat surfaces, due to fields at near the edge of the sample, known as the “dog bone effect”, and a total lack of deposits within recessed areas; the only remedy for both is the use of specialized or custom anodes for the substrate. Difficulties in the inclusion of beneficial non-metals into the deposit as well as the need of a conductive surface to allow the electrical reduction of the metal ions from solution also serve to complicate electroplating. The advantages of electroless deposition solve many of the limitations of electroplating with the two deposition techniques exchanging advantages and inadequacies in a complimentary fashion, Table 5.1.

Property	Electroplating	Electroless Plating
Line of Sight Deposition	Yes	No
Even Deposits	Difficult	Simple
Bath Stability	High/Moderate	Moderate/Low
Pure Metal Deposits	Many	Few
Non-Metal Alloyed deposits	Some	Many
Surface for Deposition	Conductive	Catalytic

Table 5.1: Summary of differences between electroplating and electroless plating

Electroless deposition has the advantage of providing even deposits over surfaces and recessed areas with the inclusion of non-metals from most deposition baths achieved by the oxidation of the reducing agent. The chief limitation for electroless deposition, which is remedied by the advantages of electroplating, is the requirement of the deposited

metal to be autocatalytic for ongoing, sustained deposition. This limitation extends to the substrate with the requirement that it also be catalytic for, at minimum, the deposition of a monolayer. Other limitations of electroless deposition include the possibility of spontaneous decomposition of the electrolyte, the sparse availability of deposition baths able to deposit pure metals, and an ongoing deposition process that decreases the precision of layer thickness result in the need for slightly larger tolerances in coating thickness.

5.2 Theory

The combination of the electroless and electroplating techniques for the provision of unique thin film coatings requires the presence of at least two metals; a primary metal to be electrolessly deposited and a secondary metal to be electroplated. The selection of the term primary for the electrolessly deposited metal is due to the requirement that electroless deposition must remain uninhibited by the presence of the secondary metal; that is to say the secondary metal must not poison the electroless deposition such that electroless deposition would not occur. Optimally, to ensure the widest possible application of the hybrid deposition technique, the secondary metal should not be included in the electroless deposit. Due to the mixed potential established within the electrolyte by the primary and secondary metals, unless there is a significant concentration of the less noble metal compared to the more noble metal, it is the more noble of the two metals that will be electrolessly deposited. The electroplating of the secondary metal is achieved in a similar way to traditional electroplating. As demonstrated in the deposition of multi-layers, Chapter 2.2.3, a more noble metal will be included in the electrodeposition of a less noble metal within the same electrolyte. Given that increasing the concentration of the secondary metal will in some instances inhibit electroless deposition, an electroplating potential must be chosen such that a minimal amount of the more noble metal, which is electrolessly deposited, is co-deposited even at a sacrifice to the efficiency of the electroplated deposit.

The complimentary nature of electroplating and electroless deposition techniques suggests that the combination of the deposition techniques within a single electrolyte has the potential to produce many unique thin film coatings. Applications of hybridized

deposition techniques include the deposition of metals of similar standard electrode potential, with the more noble metal being electrolessly deposited, as well as the deposition of binary alloys, where the base is provided by electroless deposition and a second metal is provided by simultaneous electroplating.

5.2.1 Multi-layer Deposition

The deposition of compositionally modulated multi-layers is of significant interest throughout both industry and academia. The many beneficial and practically useful qualities of multi-layers, including enhanced hardness [5], enhanced corrosion [6-9] and wear [10] resistance, and giant magneto-resistance (GMR) properties [11], are the principle reasons for continued investigation. The two main conditions for electroplated, compositionally modulated, multi-layers deposited from a single electrolyte are that both metals are able to be deposited from similar electrolytes and that the metals differ sufficiently in their degree of nobility to prevent alloying. The latter of these restrictions prevent electrodeposition of metal pairs such as iron/nickel, nickel/cobalt, and other metal pairs that are close in nobility, see Chapters 2.2.2, 2.2.3, & 2.4.2. Deposition of compositionally modulated metallic multi-layers of similar nobility is hitherto restricted only to vacuum deposition techniques and techniques utilizing two separate electrolytes.

The idea behind of hybrid electro-electroless compositionally modulated multi-layers is that, unlike electroplating where differing potentials are supplied for reduction/deposition of each metal, only one metal is electroplated while the other is electrolessly deposited by means of a chemical reducing agent. In electroplating terms, the two potentials required for modulated layer deposition within an electro-electroless system are the potential for the reduction of one metal and a zero potential, 0V vs. SHE, for the deposition of the electroless metal. Furthermore, the relative deposition potentials within the system mirror electroplated multi-layers as more noble elements typically require the lower, zero, reduction potential.

For the hybrid deposition of metals having similar reduction potentials, which is not possible using electroplating alone, we have established that a number of critical conditions must be met. The most fundamental, and obvious, condition of electro-electroless deposition is that the electroless deposition is not inhibited by the presence of

the metal to be electroplated. Specifically for multi-layer deposition, the electrolessly deposited metal must not contain the metal to be electroplated. The inclusion of the metal to be electroplated within the electroless deposit is a genuine concern as some metals are readily co-deposited as part of electroless deposition. One example is the co-deposition of Fe as part of electroless Ni-P deposition within appropriate deposition baths, Table 5.2.

Chemical Name	Chemical Formula	Electrolyte Composition	
		mM/L	g/L*
Nickel Sulphate Hexahydrate	$\text{NiSO}_4 \cdot 6\text{H}_2\text{O}$	56	14.7
Sodium Potassium Tartrate Tetrahydrate	$\text{KNa}_2\text{C}_4\text{H}_4\text{O}_6 \cdot 4\text{H}_2\text{O}$	100-350	39.2-137.2
Sodium Hypophosphite Hydrate	$\text{NaH}_2\text{PO}_2 \cdot \text{H}_2\text{O}$	94	10.0
Ammonium Hydroxide	NH_4OH	3600	140
Ferrous Ammonium Sulphate Hexahydrate	$\text{Fe}(\text{NH}_4)_2(\text{SO}_4)_2 \cdot 6\text{H}_2\text{O}$	20	7.8
Operating Conditions		Deposit Content wt. %	
Temperature	75 °C	25 % Fe	
pH	11.2	0.5% to 1.0 % P	

* NH_4OH is measured in mL/L and not g/L

Table 5.2: Example electrolyte for electroless Ni-Fe-P alloy [12]

To overcome possible inclusion of the electroplated metal within the electroless deposit, it is best to provide an electrolyte which is not capable of depositing the electroplated metal as an alloy. The most convenient method of preventing electroless co-deposition is altering the pH of the electrolyte as the deposition of most electroless alloys is pH dependent.

The second concern in the hybrid deposition technique is the simultaneous deposition of the electrolessly deposited metal during the electroplating step. Given that electroless deposition is based on the net oxidation and reduction potentials of the reducing agent and metal complex, respectively, it is likely that applying a deposition potential for electroplating will disturb the electroless deposition process. It is expected that in those cases where the electroless deposition portion of the hybrid deposit is disturbed by the applied potential a temporary minimization or cessation of electroless deposition will occur. In cases where the deposition rate of the electroless deposition step is not altered by the electroplating step, a shortened electroplating step would allow for minimal inclusion of the electrolessly deposited metal.

Along with the concern of simultaneous electroless deposition in the electroplating step, the possibility of co-deposition of the normally electrolessly deposited metal by the applied electroplating potential is also an issue for maintaining compositionally pure modulated multi-layers. The issue of co-deposition exists for electroplated compositionally pure multi-layers and is overcome by increasing the concentration of the less noble metal relative to the more noble metal. The relative increase in the concentration of the less noble metal ensures that the rate of reduction of metal the less noble metal is high and the rate of reduction of the more noble metal is slow and controlled by diffusion [13]. As increasing the concentration of the less noble metal may inhibit electroless deposition, applying a more negative potential than is required for the reduction of the electroplated metal can mitigate the inclusion and co-deposition of the electrolessly deposited metal. Lowering the potential below the optimum for the reduction of the electroplated metal provides a more pure deposit at the cost of efficiency, though other issues regarding the grain size and overall morphology of the deposit may arise.

It is understood that the compositionally modulated multi-layers produced by electro-electroless deposition often results in alloys deposited in the electroless plating step. The alloys deposited are produced as a result of the anodic reaction of the reducing agent and result in the inclusion of non-metals. The electroless deposition of alloys within multi-layers has been explored largely for metal/metal alloys such as permalloy, Fe₂₀Ni₈₀, and other multi-metal combinations rather than metal/non-metal alloys such as Fe/Ni-P [14]. Possible benefits of Ni-P layers arise from the superior diffusion barrier properties of electrolessly deposited Ni-P [4]. While such benefits have been established using other metallization techniques, such as electroplating alone, hitherto the concept of hybrid electro-electroless deposition (HEED) for the purpose of reducing two separate and distinct metals has not been explored. Furthermore, the deposit of similar metals, previously not possible from an aqueous electrolyte, was restricted to vacuum deposition.

5.2.2 Alloy Deposition

In addition to the deposition of multi-layers, careful control over the electroplating portion of the process allows for the possibility of customized high precision alloying. Alloying using the hybrid technique can afford more flexibility than either electroplating or electroless deposition alone. The electroplating of alloys is dependent mostly on the concentration of the metal ions in solution and the applied reduction potential. The inclusion of non-metals within the electroplated film, to improve film qualities such as corrosion resistance, occurs with the addition of organic acids, such as H_3PO_4 for the inclusion of P. The electroless deposition of alloys is limited largely by the composition and concentration of the solution which results in the deposition of only select alloys. Similar to electroplating, the ratio of two metal salts within the electrolyte will influence the ratio of the metals deposited within the coating, though without the added control of the applied external reduction potential. The composition of electroless alloys further determined by the pH of the electrolyte, as the pH typically controls the concentration of non-metal included within the deposit. The presence of non-metal, which is a consequence of the anodic, oxidation, of the reducing agent, is included within the deposit as anodic and cathodic reactions occur on the same surface rather than separate surfaces as in electroplating.

Alloying by means of hybrid deposition affords control based on the reduction potential similar to electroplating while also allowing for control of non-metal inclusion from electroless deposition with control over the pH of the electrolyte. Hybrid alloying, rather than being limited by the composition of the solution as in electroless plating, gains an added and more prominent dependence on the electroplating step of the electro-electroless deposition process. The deposition of alloyed deposits relaxes the restriction that the secondary metal not be co-deposited with primary electrolessly deposited metal.

5.3 Materials and Methodology

The most critical requirement of electro-electroless electrolytes is the preservation of the electroless deposition process. The potential at which electroless deposition occurs is based on the coming together of the oxidation potential of the reducing agent and the reduction potential of the metal salt. Incorporation of other metals within the electrolyte

can easily disturb the equilibrium and balance necessary for successful electroless deposition. Therefore, development of electro-electroless electrolytes within this work was based on common electroless plating electrolytes with additional metal salts added for electroplating.

5.3.1 Electroless Gold {Au} Electrolytes

Initial experimental results for hybrid deposition were obtained in studying Ni/Au multi-layer systems. Due to the large difference in nobility between Ni and Au half-reactions, $+1.498 \text{ V}_{\text{Au}^{3+}}$ vs. SHE and $-0.257 \text{ V}_{\text{Ni}^{2+}}$ vs. SHE, respectively, the Ni/Au system provides an excellent standard for the exploration of hybrid deposition. While other systems such as Ni/Cu are more commonly studied for multi-layer deposition [15], electroless deposition of Cu from an electrolyte containing Ni often results in the co-deposition of a small amount of Ni [16]. The amount of Ni included within the deposit is dependent on the concentration of Ni^{2+} in the electrolyte. The concentration of Ni within the deposit is approximately 2 % atomic for an 8:1 ratio of Cu to Ni with increasing Ni concentration resulting in increased Ni inclusion within the deposit [17]. Most importantly, to ensure greatest purity of the Ni layer, the concentration of Ni within the electrolyte would have to be greater than the Cu concentration so as to prevent significant co deposition of Cu in the electroplating step. The concentration dependent co-deposition of Ni within the electroless of Cu along as well as inclusion of Cu on within electroplated Ni deposits makes Ni/Cu deposition baths ill suited for studying electro-electroless processes.

In order to study electro-electroless deposition the more noble metal must be electrolessly deposited as compositionally pure similar to electroplated multi-layers. Aside from co-deposition, hindering auto-catalytic electroless decomposition or the stability of the electrolyte are common concerns. While electroless Au electrolytes are typically rendered unstable by the presence of ions such as Ni^{2+} or Co^{2+} [18], the electrolyte chosen for this work, Table 5.3, demonstrated exceptional stability in the presence of NiSO_4 or CoSO_4 . Specifically, the Au electrolyte remained stable with the addition of Ni^{2+} , or Co^{2+} , ions at over 30 times the concentration of Au within the electrolyte.

Bath	Chemical Name	Chemical Formula	Bath Composition	
			mol/L	g/L
Bath A	Sodium Tetrachloroaurate Dihydrate	$\text{Na}(\text{AuCl}_4) \cdot 2\text{H}_2\text{O}$	0.005	1.989
	Boric Acid	H_3BO_3	0.160	9.893
	Sodium Hydroxide*	NaOH	0.010	0.4000
Bath B	Sodium Thiosulphate	$\text{Na}_2\text{S}_2\text{O}_3$	0.065	10.277
	Sodium Sulphite	Na_2SO_3	0.035	4.411
	Boric Acid	H_3BO_3	0.160	9.893
Additives	Sodium Citrate Tribasic Dihydrate	$\text{Na}_3\text{C}_6\text{H}_5\text{O}_7 \cdot 2\text{H}_2\text{O}$	0.250	73.525
Ni Additives	Nickel Sulphate Hexahydrate	$\text{NiSO}_4 \cdot 6\text{H}_2\text{O}$	0.076	20.000
Co Additives	Cobalt Sulphate Heptahydrate	$\text{CoSO}_4 \cdot 7\text{H}_2\text{O}$	0.076	21.333
Operating Temperature: 80-90 °C		pH: 7 to 10 (Adjusted with NaOH)		

*Sodium Hydroxide used to adjust pH of 'Bath A' to pH 7.

Table 5.3: Electroless Au/Ni and Au/Co electrolytes for electro-electroless deposition

Note: Complete electrolyte contains half the total amount of each component in bath A and Bath B as they are mixed at a 1:1 ratio.

The electro-electroless plating bath was assembled with Baths A and B mixed at a 1:1 ratio and let sit for 24 hours to ensure formation of Au complexes within the electrolyte were complete. After the 24 hour period, $\text{Na}_3\text{C}_6\text{H}_5\text{O}_7$ was added to the electrolyte. Once dissolved a line was marked on the beaker indicating the volume of the solution to be maintained throughout the lifetime of use. A solution containing the metal salt to be electroplated, either NiSO_4 or CoSO_4 , was then added to the electrolyte in a volume no more than 5 % of the total volume of the original electrolyte. It should be noted that the 1:1 ratio of Bath A to Bath B produces an electrolyte with half the molar concentration of Au within the final electrolyte; hence, the molar ratio of the Ni, or Co, to Au is twice that obtained from Table 5.3. Additionally, similar to electrolytes for the electroplating of Ni/Cu multi-layers, the less noble metal is in excess [15], though the ratio of mass is only 10:1 for Ni/Au rather than 7600:1 used for Ni/Cu and Co/Cu [11].

5.3.2 Electrodes and Deposition System

The substrates used within this work consisted of commercially available 99.99 % pure nickel {Ni}, 99.99 % pure Cu, and 99.99 % pure cobalt {Co}, Table 5.4, metal plates.

Alloy	Balance	C	Cu	Fe	Mn	Si	Other						
Ni	Ni	0.08 % max	0.25 % max	0.4 % max	0.35 % max	0.35 % max	0.01 % max						
Cu	Cu	None	None	None	None	None	None						
Alloy	Balance	Ag	Al	Bi	Ca	Cr	Cu	Fe	Mg	Mn	Ni	Si	Sn
Co	Co	2	1	<1	1	<1	3	3	1	<1	2	5	1

Table 5.4: Nominal composition of the Ni, Cu, and Co electrodes in wt% (Ni, Cu) and ppm (Co), respectively²

The metal plates, 1 mm to 2 mm thick, were machined to have a width between 1.0 cm and 4.0 cm and cut to a length of between 5 cm and 9 cm. The metal plates were wet polished using a LECO SS200 grinder/polisher, most often using 240-grit SiC emery paper, to ensure a uniform surface and remove any potential surface contaminants. After polishing, the samples were wiped clean with laboratory clean wipes and attached as cathodes within the electroplating circuit, Figure 5.1.

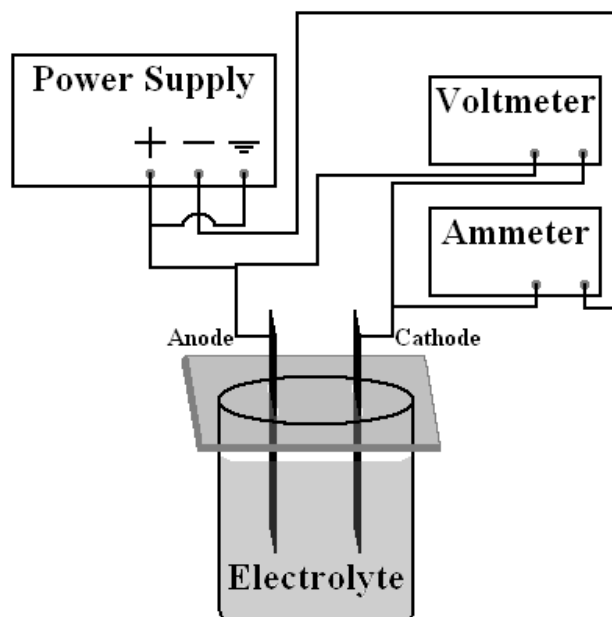


Figure 5.1: Schematic diagram of the electro-electroless plating system.

The prepared Ni and Co plates initially used as anodes within the system for Ni/Au and Ni/Co electrolytes, respectively, were later replaced by a platinum {Pt} plate measuring 25 mm × 25 mm × 1.0 mm. As shown in the diagram, the system was composed of a power supply, a Keithly 2200-20-5 Programmable Power Supply 20V 5A,

² “Ultra Corrosion-Resistant Nickel Alloy 200/201” and “Super-Conductive 101 Cu” purchased from McMaster-Carr, www.mcmaster.com; 99.99+% Cobalt purchased from Goodfellow Corporation, www.goodfellow.com.

and two multimeters, Keithly 2100 6½ Digit Multimeter, with one measuring the voltage and the other the current. No standard electrode was used within the work due to complications arising from using high temperature electrolytes. Records of the applied current and voltage were obtained using Keithly Instruments Tool Version 2.02 software. An acrylic plate with two slits, through which the electrodes were inserted into the electrolyte, shown in Figure 5.1, helped protect the electrolyte from evaporation during prolonged deposits. The deposition procedure, potentials applied, and electrolytes used, beyond sample preparation, varied based on the goal of the investigation.

5.3.3 Sample Analysis

Sample analysis was consistent with the processes and basic procedures outlined within Chapters 3 and 4. Macroscopic images of the samples were taken using a Hewlett-Packard Scanjet G4010 scanner at a resolution of 600 dpi (dots per inch). Scanning electron microscope (SEM) images were taken using an FEI Quanta 200 Environmental SEM with a Field Emission Gun (FEG). Compositional analysis of the claddings was obtained using energy-dispersive X-ray spectroscopy (EDS) as part of the SEM system. Acquisition of the EDS data occurred using an EDAX SiLi Detector with Super Ultra Thin Window (SUTW) and EDAX Genesis software.

The use of EDS provided the average composition of the outer few microns of the deposit weighted toward the outer layers of coating. Typical beam strength/potential for both EDS and SEM measurements was 20 kV; this was especially the case for Au so as to acquire good EDS data. The selection of beam strength for EDS measurements was a compromise between higher beam strengths, which provided better resolution of Au within the thin films and more rapid EDS data acquisition but deeper x-ray penetration into the coating; and lower beam strengths, which resulted in slower data acquisition but provided for less penetration into the coating thereby producing a better compositional analysis of the surface. As before, common feature of backscatter SEM images is darker regions surrounding larger grains which are due to shadowing from elevation differences. Other dark regions between grains are most often the cause of minor divots in the coating due to H₂ bubbles from the anodic reaction combined with a lack of agitation of the solution.

5.4 Ni/Au and Co/Au Results

Initial experiments using the Ni/Au and Co/Au electrolytes were focused on verifying the capacity to obtain both electroplating and electroless deposits from a single electrolyte. Due to the impossibility of determining the presence of a Ni deposit on Ni substrates using EDS, Ni/Au electrolytes were used in connection with deposits on Co substrates while Co/Au electrolytes were used for deposits on Ni substrates. As a matter of practicality, the first layer formed on the substrates was electroless Au as the deposition began immediately with immersion of the substrate within the electrolyte. Additionally, the choice of substrate was also made based on the positive reaction of the substrate to the electrolyte compared to other substrates, such as Cu, which provided inferior electroless coatings. Details as to the Au electrolyte and reactions with substrates are found in Section A2 of Appendix A.

Qualitative verification of the capacity to form electroplated deposits on the Au coated substrate was achieved by raising the sample several millimetres within the electrolyte between each electroless plating and electroplating step, Figure 5.2. Due to the difficulty associated with using a standard electrode with the heated electrolyte, the electroplating potential was set such that the color of the deposit qualitatively showed little Au inclusion. The substrate for each deposit was kept identical so that setting identical potentials over several experiments would produce nearly identical results.

Notable features of the individual layers include discontinuities in the first Au layer as well as a considerable amount of S in localized region on the electroplated Co layer. The discontinuities present within the initial Au layer are the result of the short electroless deposition time. Regions, literally spots, high in S as part of the Co layer may be a result of the ligand structure around Co^{2+} ions, or other reduction processes associated with S containing chemicals. The spots appear as granules on the surface of the coating, as determined by secondary emission SEM, and contain Co and S at an atomic ratio of around 73.5 % Co to 26.5 % S, the same as the rest of the coating. Most importantly, while the electro layer does contain S, the electroless layers appear to remain free of S contamination indicating the Au layer was deposited as compositionally pure. Inclusion of sulphur in the electroplating layer does not come as a surprise using the

mixed ligand electrolyte as the co-deposition of sulphur has previously been established for electroplating of Au from a similar electrolyte [19].

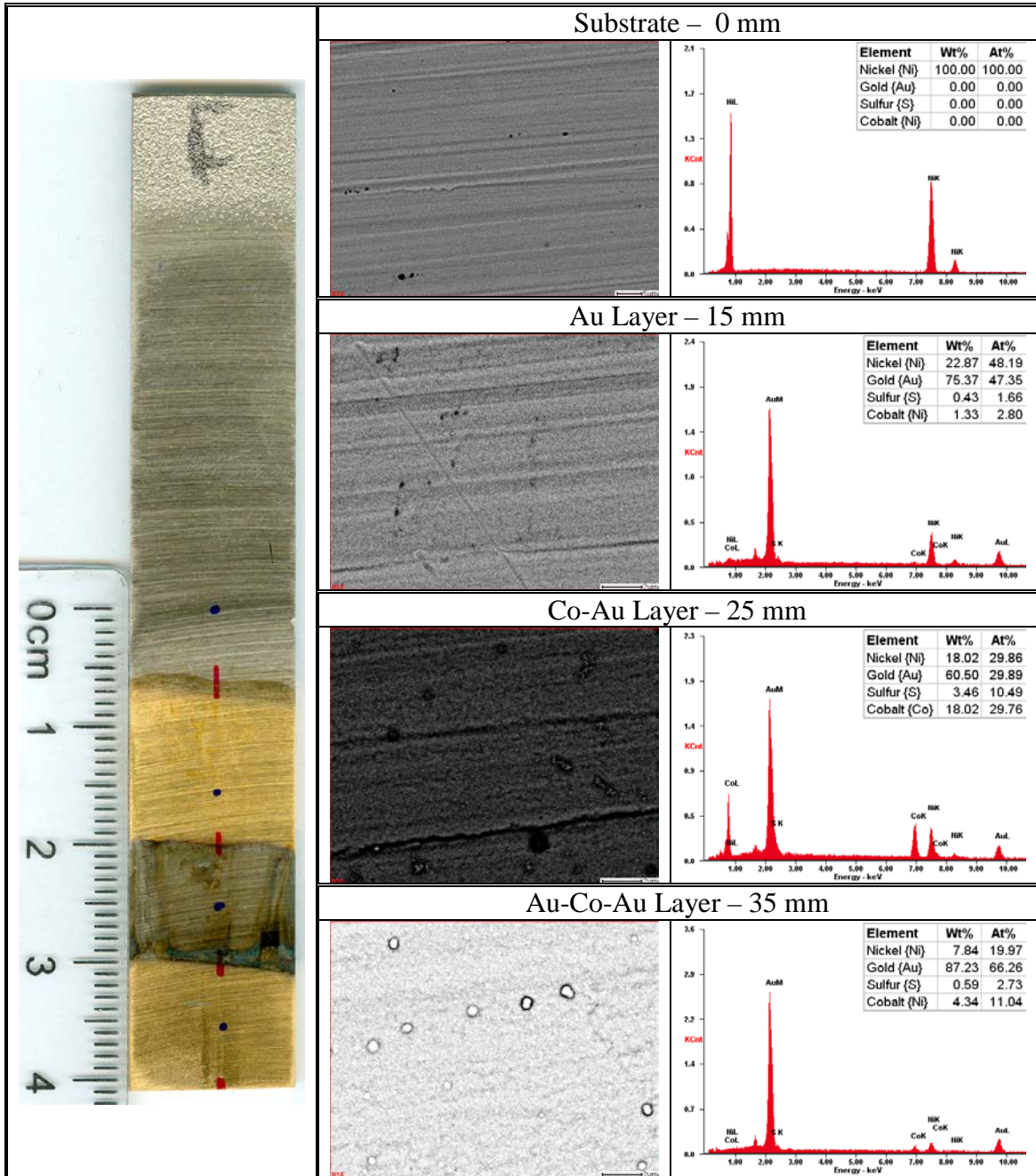


Figure 5.2: (Left) Macroscopic image of electroless/electro/electroless tri-layer Au/Ni/Au deposit on a Ni plate along with sequential (Middle) backscatter SEM images, and (Left) associated EDS analysis provided for regions noted by Blue Spots on the macroscopic image. The deposit consisted of 20 min electroless, 60 s [2 V, 0.4 A] electro, 20 min electroless deposits. Electrolyte conditions of pH 7, 80 °C, with Pt anode. Scale bars for SEM images: 5 μ m for ‘Substrate’, 2 μ m for ‘Au’, ‘Co-Au’, and ‘Au-Co-Au’ layers.

Incremental analysis EDS of the deposit determined an apparent falling concentration of the substrate, as would be expected for layers of increasing thickness.

More frequent EDS of the coating provides a trend for the layers that more clearly demonstrates compositional modulations of the layers in the tri-layer configuration, Figure 5.3.

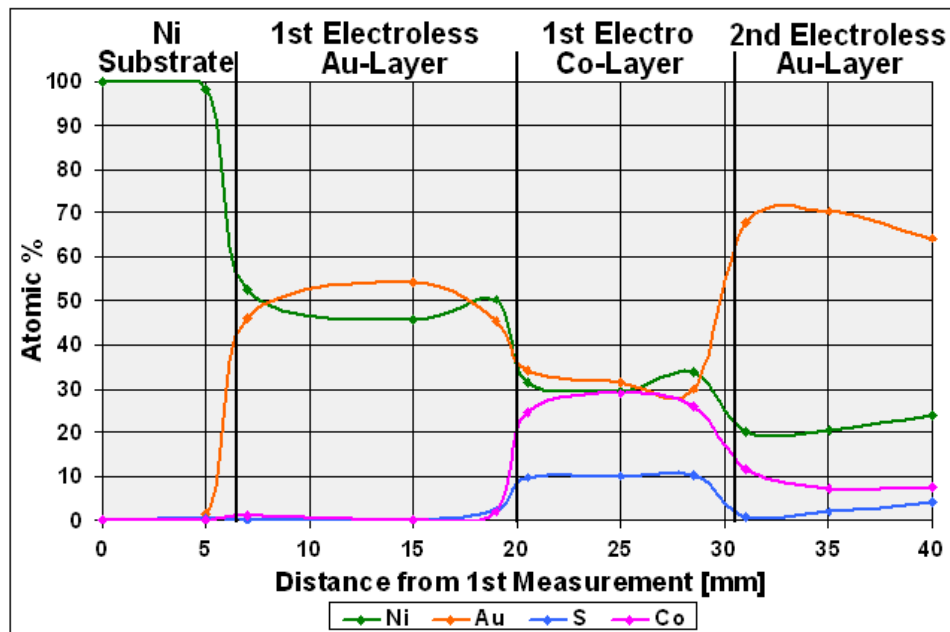


Figure 5.3: Graph of EDS results to the right of the Blue and Red Spots on the macroscopic sample in Figure 5.2. EDS results presented in the graph were obtained using 16000x magnification of the sample in regions with fewest aberrations such as granules on the surface.

As expected of the deposit, the signal from the Ni substrate decreases over the length of the sample indicating shielding of the substrate by the increasing layer thickness. The increasing atomic percentage of the Ni substrate about the interfaces is attributed to reactions present at the air/electrolyte interface affecting the coating. Similarly, the trend of increasing Ni content towards the end, 40mm, of the sample is due to the small size of the Pt anode relative to the Ni cathode. The relative peaks of each element are associated with the electro and electroless deposition phases with S apparently co-deposited with the electroplating of Co. These results echo previous results obtained using a Ni/Au electrolyte on a Co substrate, Appendix B.

Unlike electroless Au electrolytes, increasing the alkalinity of the electrolyte from pH 7 to pH 10 did not produce a more rapid electroless Au deposit in the case of the Ni/Au and Co/Au electrolytes. The comparative determination of the deposition rate was achieved by raising the pH of the pH 7 electrolyte to 10 and immersing a Ni substrate within the electrolyte for the same duration as was previously done in the pH 7 electrolyte. Comparing EDS analysis of the coating, the quantification of the Ni signal

for the pH 10 deposit remained around the same value as for the pH 7 deposit indicating the Au layer was of roughly the same thickness, Figure 5.4.

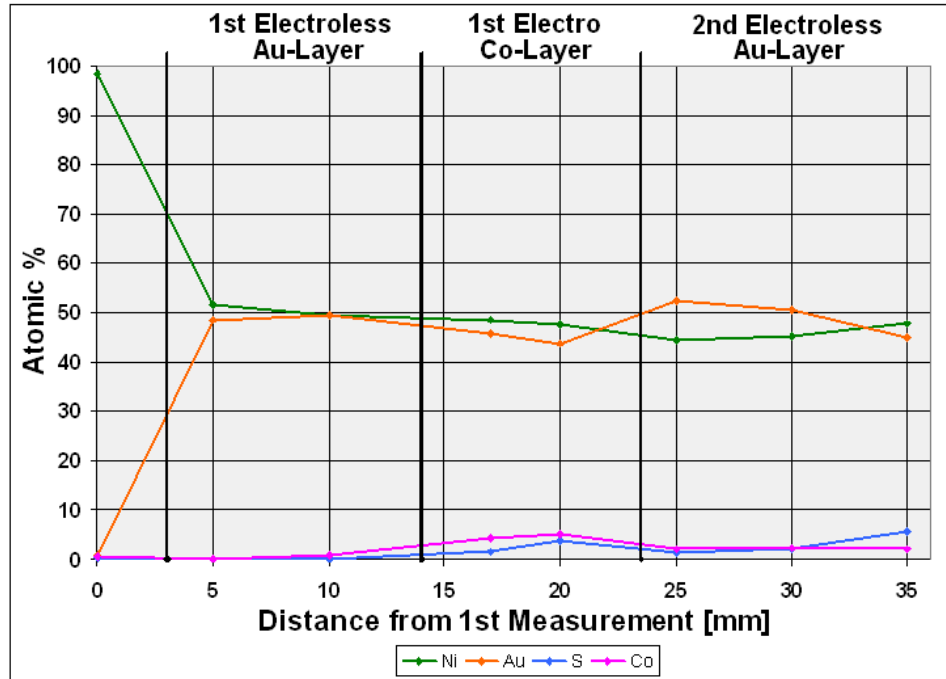


Figure 5.4: Graph of EDS results of an Au-Co-Au tri-layer deposit from a pH 10 electrolyte using a Co anode. Quantitative EDS analysis was obtained for the layers at 16000x magnification in regions having least aberrations, such as granules, on the surface.

The lack of pH dependent response is attributed, in part, by the presence of $\text{Na}_3\text{C}_6\text{H}_5\text{O}_7$ within both the pH 7 and pH 10 Ni/Au and Co/Au electrolytes. In the case of the electroless Au electrolyte alone, increasing the pH of the electrolyte above pH 7 results in a greater deposition rate whether NaOH or $\text{Na}_3\text{C}_6\text{H}_5\text{O}_7$ are used alone or in combination. In the case of electro-electroless Ni/Au and Co/Au electrolytes, $\text{Na}_3\text{C}_6\text{H}_5\text{O}_7$ is used as a stabilizer to allow the inclusion of Ni and Co ions but also increases the plating rate according to Paunovic and C. Sambucetti [20, 21]. Hence the inclusion of $\text{C}_6\text{H}_5\text{O}_7^{3-}$ within the electrolyte appears to maximize the deposition rate without having to increase the pH. Additionally, while depletion of the electrolyte may have contributed to the decrease in deposition rate; previous deposits for durations longer than the combined 41 minutes electro-electroless have been conducted with little change to the deposition rate of the Ni/Au and Co/Au electrolytes.

The lack of defined Co layer within the pH 10 electrolyte is attributed to the use of a larger Co anode rather than the small Pt anode, used in the deposit shown in Figure 5.2.

While the larger Co anode provided a similar potential difference between the electrodes as well as the current supplied, around 2.00 V and 40 mA, a significantly inferior electro-Co deposit was obtained. The inferior quality deposit of the Co anode compared to that provided by the Pt anode was associated with a darkening of the electrolyte. The darkening, which did not occur with use of the Pt anode, was associated with the production of precipitates and was attributed to the anodic reaction on the Co anode. Analysis of the particulates indicated that they were high in Au but also contained Co and S and were likely the cause for what appears to be a largely displacement layer formation of the final electroless Au step.

Given absence of a reducing agent within the electrolyte, it would be reasonable to assume that the deposit is of a hybrid electro-immersion deposit (HEID) coating rather than a hybrid electro-electroless deposit (HEED) coating. While this may be convenient to assume, the electrolyte is similar to that used and patented by G. Krulik and N. Mandich [22] in which autocatalytic deposition was observed without the presence of a ‘dedicated’ reducing agent. The authors of the patent believe that the sulphite–thiosulphate mixed ligand complex acts as a reducing agent, with sulphite acting as the main reducing agent [20], providing conditions for autocatalytic deposition³. Further determination of the autocatalytic tendency of the initial electroless Au layer is obtained by comparing the results of the initial 20 minute electroless Au layer of Figure 5.2 with an initial 5 minute electroless Au layer, Figure 5.5. As is clearly seen, the 20 minute electroless Au deposit provided greater shielding of the substrate than the 5 minute electroless Au layer⁴. Additionally, the shape of the 5 minute deposit is characteristic of autocatalytic electroless deposition further supporting the formation of a HEED coating.

To better understand the composition of the Co/Au tri-layer HEED coatings a quantitative verification of the Au within the electroplated deposit was carried out by electroplating Co on Ni from the Co/Au electrolyte at a variety of potentials. The results, Figure 5.6, which do not provide a definitive result as to the source of any co-deposited Au, be it electro- or electrolessly plated, does provide some indications as to the composition of the layer formed during the electroplating step.

³ Further details regarding the Au electrolyte may be found in Section A2 of Appendix A.

⁴ To ensure a proper comparison, EDS was carried out at a maximum magnification to ensure that the beam was targeted on the coating.

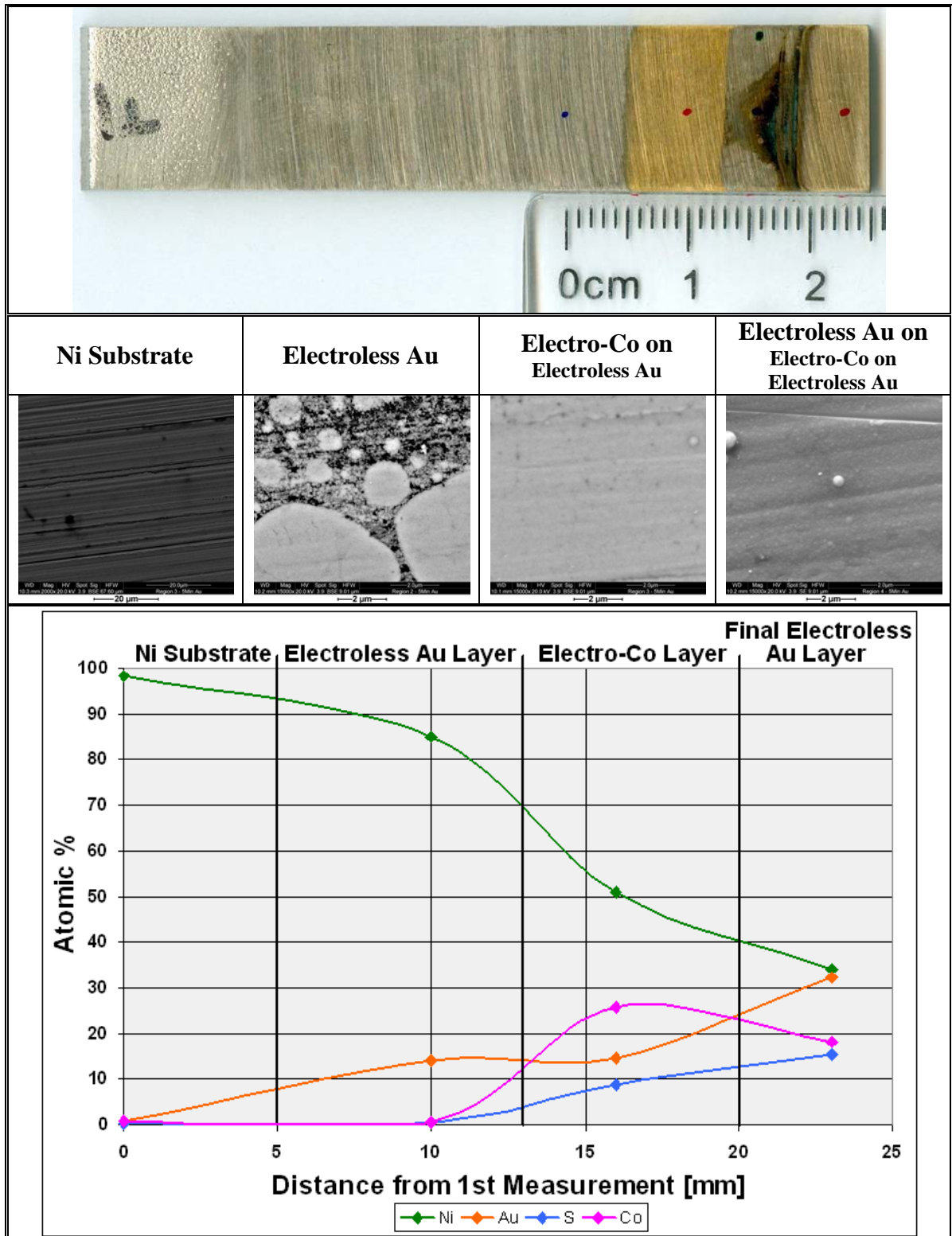


Figure 5.5: Macroscopic image along with backscatter SEM images of regions of a Co/Au HEED coating [5 min electroless, 60 s electro, 5 min electroless] on a Ni substrate. Quantitative EDS analysis was obtained for the layers at 60000x magnification in regions with fewest aberrations such as holes or granules on the surface. Scale bars for SEM images: 20 μm for 'Substrate', 2 μm for 'Au', 'Co on Au', and 'Au on Co on Au' layers.

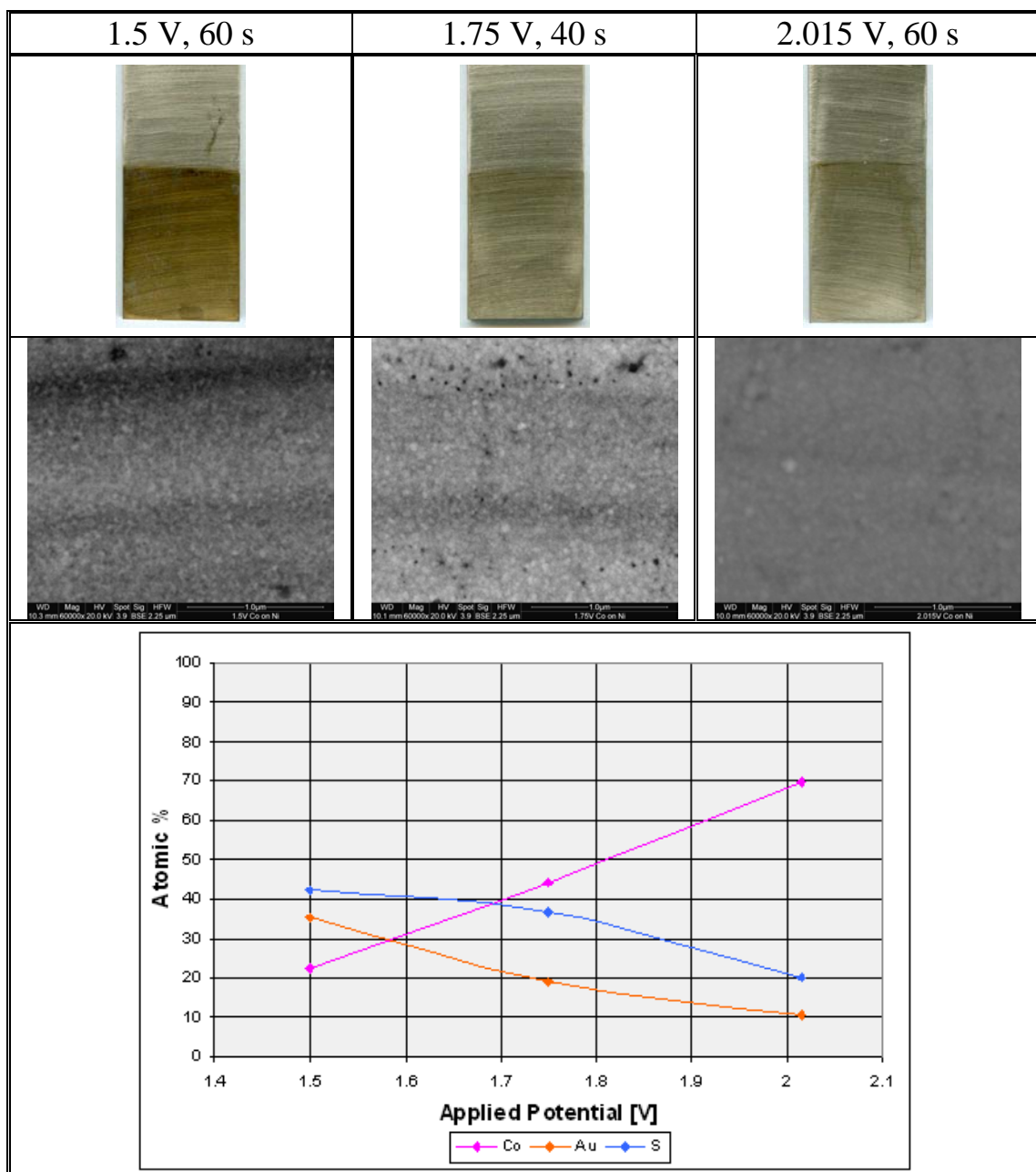


Figure 5.6: Macroscopic images, with 1 μm scale bars, backscatter SEM images, and a graph EDS analysis of electrodeposited Co on Ni from an 80 °C Co/Au HEED electrolyte for three different applied potentials.

While it may be convenient to suggest the S inclusion within the deposit is a result of electroless Au deposition, electroless Au deposits on Ni substrates from the same electrolyte contained little S, Figure 5.2. Additionally, results from the 5 minute electroless Au deposit did reveal some high S within pores indicating that the source of S within Au deposits is likely from adsorbed on the Ni substrate surface. The adsorption of S initially on the substrate is consistent with initial electroless reduction. Coatings formed

over an extended period have shown no S content further supporting initial nucleation and reduction as the source of S within the deposit. In addition to the decreasing S for the Co/Au electrolyte, electrodeposits carried out from a Ni/Au electrolyte on Co demonstrated a trend of decreasing S content, Figure 5.7. The trends associated with S content are likely the result of ligand structures within the electrolyte and play an important role in determining the properties of multi-layered deposits.

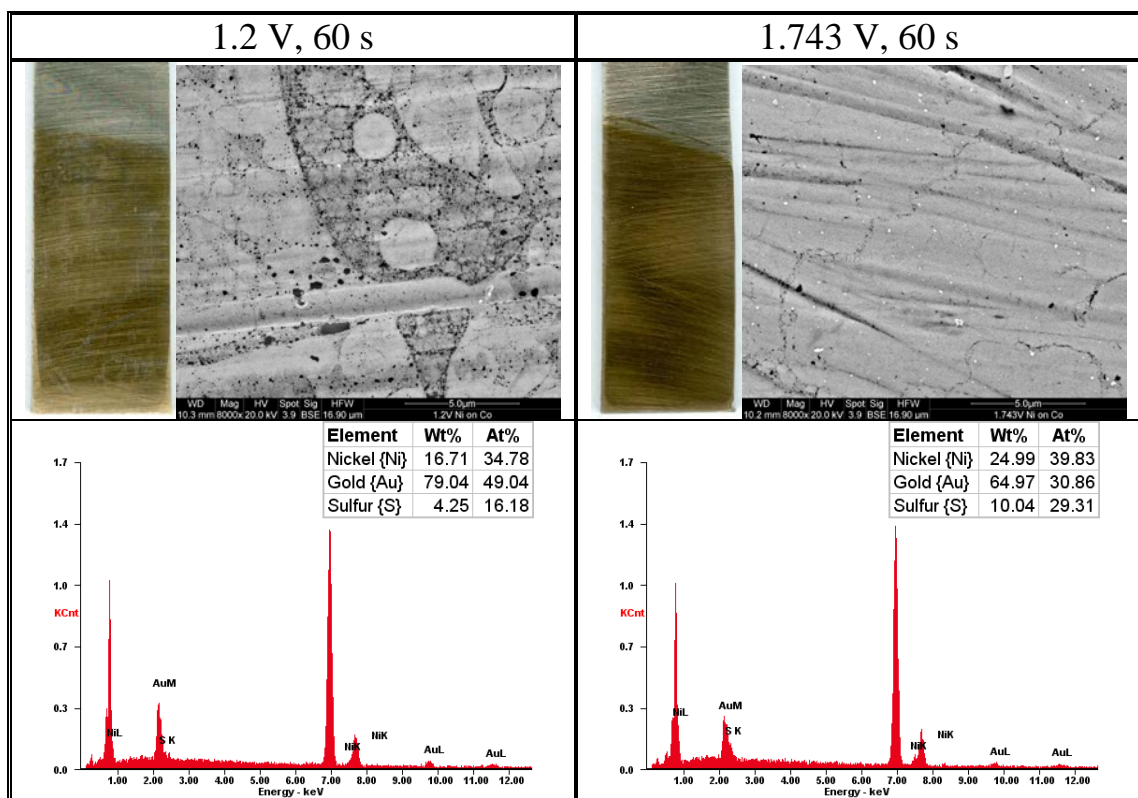


Figure 5.7: Macroscopic images, backscatter SEM images, and EDS analysis for electroplated Ni on Co from an 80 °C Ni/Au HEED electrolyte for two different applied potentials.

In cases of both Co/Au and Ni/Au electrolytes, while it is undetermined whether the Au is included within the deposit by electroplating or by simultaneous, parallel, electroless plating, it is apparent that increasing the deposition potential decreases the concentration of co-deposited Au. The results shown in Figures 5.6 and 5.7 suggest that the co-deposition of Au could be due to both electroless deposition as well as electroplating but that increasing the potential limits the inclusion regardless of the source. The minimum amount of Au within the electroplated deposit is yet to be determined; however, the trend provided in literature suggests a highly pure Co, or Ni, layer is possible given the excess of Co^{2+} , or Ni^{2+} , ions.

As a final measure of the plating conditions for the Co/Au electrolyte, voltammograms were produced by sweeping the potential in the system and measuring the current. Due to the use of a power supply and multimeters in place of a potentiostat/galvanostat and the lack of standard electrode within the system, the voltammograms were termed a “poor-man (PM) voltammogram” as a matter of distinction. The electrodes were the same as for the electro-electroless deposits, namely a Pt anode and Ni cathode, Figure 5.8.

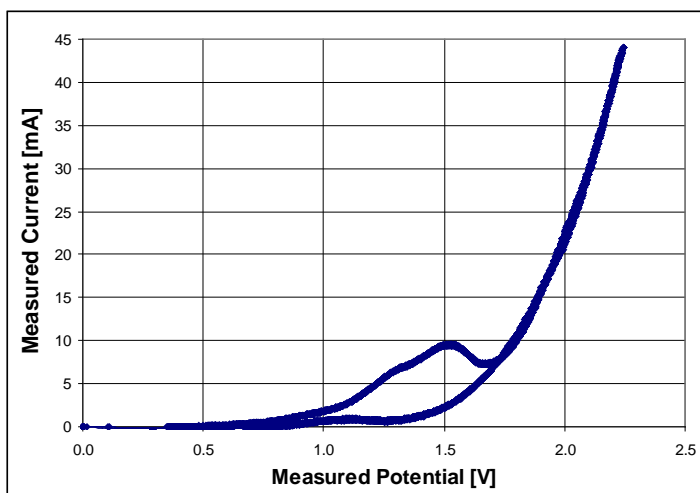


Figure 5.8: PM Voltammogram for the alkaline, pH 10, 80 °C Co/Au electrolyte.

As can be seen in the PM Voltammogram, a peak is present around 1.5 V indicating the efficient reduction of some chemical species from within the electrolyte. Comparing with the electroplating tests conducted within Figure 5.7, it appears that the reduced chemical species is high in S. Finally, though somewhat unsophisticated, the PM Voltammogram provides accurate information of the electroplating cell provided the same materials are used for the electrode pair.

5.5 Application to Coatings on Mg Alloys

An immediate application of hybrid electro-electroless deposit (HEED) coatings is the improvement of corrosion resistant properties of Ni-Zn-P coatings on Mg alloys. Application of an electroplating step after initial coating formation allows for the deposition of Ni or Zn rich layers atop Ni-Zn-P layers. Initial electroless deposition provides a continuous coating over the surface accessing recesses areas. The coating of recessed areas, which is difficult using standard electroplating, prevents the formation of a

galvanic cell between coated and uncoated regions of a part. Secondary, or pulsed, electroplating then provides a reinforcement of outer layers of the cladding. The electroplated reinforcements allow for greater corrosion protection, and in the case of multi-layers, greater wear protection of the substrate.

Specific to Ni-Zn-P coatings and multi-layers produced therein, Zn enrichment of the coatings provides a more anodic layer relative to the remainder of the coating. The arrangement of such layers produces a sacrificial multi-layer structure which protects the coating from corrosion by forcing corrosion to propagate along the coating surface rather than through the coating to the substrate. The formation of sacrificial multi-layer coatings [7] has previously been established for Ni/Zn layers; though hitherto, layers were deposited from separate electrolytes [6, 8]. Electroplating from the hybrid electro-electroless electrolyte, this work, in place of a two bath system produces some alloying of the Zn layer [9] as is expected when depositing the less noble metal of a binary multi-layer electrolyte. While it may be more practical to form such deposits using electroplating alone [9], the expected corrosion resistance offered by the inclusion of P has not been quantitatively evaluated. Additionally, the inclusion of P may be impractical using electro-multilayer deposits.

Applying electro-electroless conditions to increase the Zn content deposited from a Ni-Zn-P electrolyte, Table 5.5, on Mg alloys, a deposit darker in color than the typical Ni-Zn-P coating was obtained. Analysis of the composition using EDS determined that while electroless Ni-Zn-P struggles to obtain Zn content within the coating above 24 % wt., or 20 % at., see Chapter 3.4.4, Zn content within the final, electro-, layer was around 37 % wt., or 32 % at., within the HEED coating, Figure 5.9.

Chemical Name	Chemical Formula	Composition (g/L)
Nickel Sulphate Hexahydrate	$\text{NiSO}_4 \cdot 6\text{H}_2\text{O}$	6.5715
Zinc Sulphate Heptahydrate	$\text{ZnSO}_4 \cdot 7\text{H}_2\text{O}$	7.1885
Sodium Citrate Tribasic Dihydrate	$\text{Na}_3\text{C}_6\text{H}_5\text{O}_7 \cdot 2\text{H}_2\text{O}$	23.50
Sodium Hypophosphite Hydrate	$\text{NaPH}_2\text{O}_2 \cdot \text{H}_2\text{O}$	17.50
Ammonium Hydroxide*	NH_4OH	25.0
Operating Temperature: 80 °C	pH before use (20 °C): 11	

* NH_4OH is measured in mL/L and not g/L

Table 5.5: Electroless Ni-Zn-P electrolyte, similar to Table 3.21, for electro-electroless deposit formation on Mg alloys.

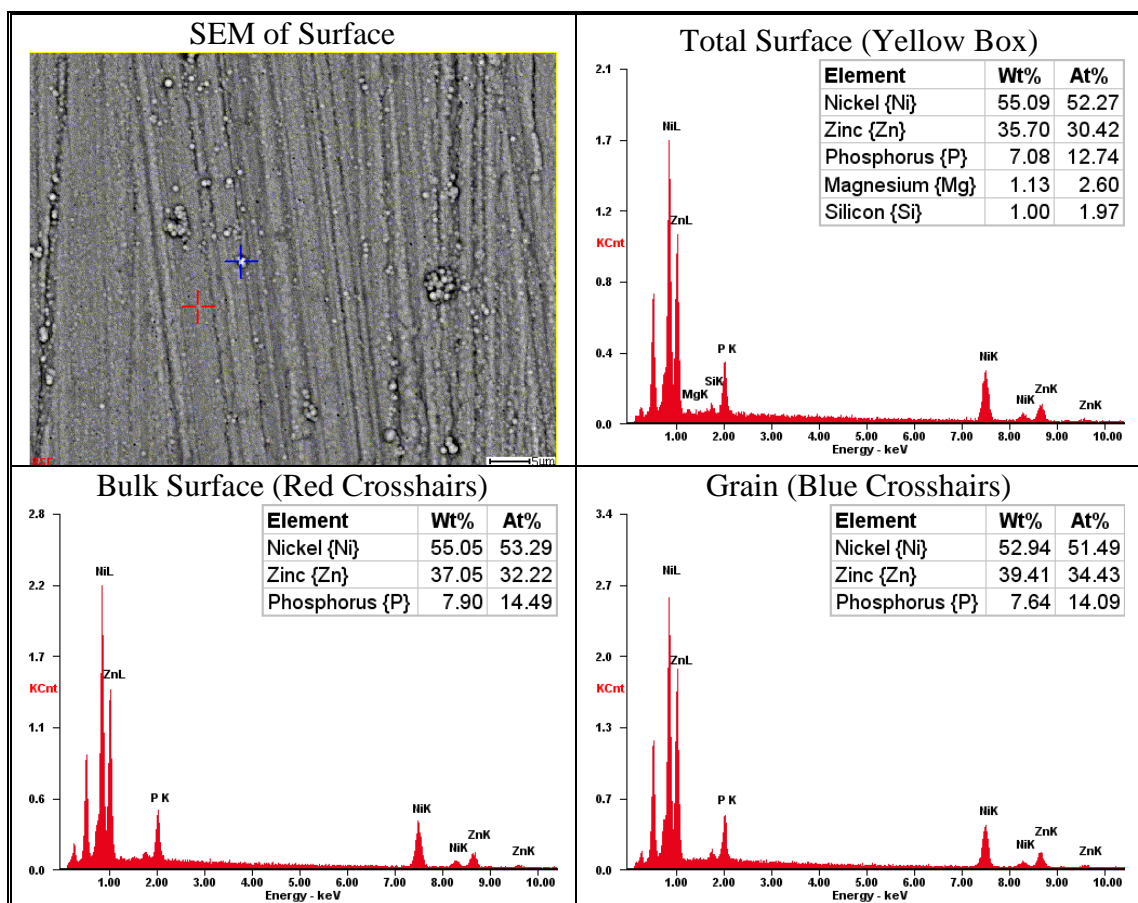


Figure 5.9: Backscatter SEM image and associated EDS analysis of a Ni-Zn-P/Ni-Zn HEED coating [1st Layer: electroless, 75 °C, 45 min; 2nd Layer: electro, 75 °C, 2.15 V (54.7 mA), 15 min] on an AZ91D Mg alloy.

Given penetration of the electron beam within the Ni-Zn-P coating, EDS analysis implies that Zn content within the electrodeposited layer is likely higher than that measured in Figure 5.9. As seen from results in Chapter 3.4.4 as well as the previous section, the shielding of the Mg substrate is due to the thicker electroless Ni-Zn-P deposit rather than the final electroplated layer. The 2 % atomic Mg and Si within the deposit are attributed to non-catalytic silicon carbide {SiC} imbedded within the substrate during sample preparation, specifically polishing, resulting in thin spots within the deposit.

The application of HEED coatings to the Ni-Zn-P electrolyte for coatings on Mg alloys is only a singular representation of the possibilities available using hybridized plating. Application of the technique to existing and commonly used electrolytes, such as other Ni-P electrolytes, offers the possibility of creating specifically alloyed layers independent of the electroless deposit.

5.6 Iron Nickel {Fe/Ni} Electrolyte and Ongoing Work

The success of hybrid electro-electroless deposition may be expanded to other metal pairs such as Fe/Ni and Co/Ni. The restriction of electroless deposition of Co and co-deposition of Fe to alkaline environments presents a means of limiting the inclusion of metals within the electroless step. Further, the ability to both electroplate Fe and Co as well as electrolessly deposit Ni in acidic environments allows electroless Ni deposits to remain compositionally ‘pure⁵’.

Initial modifications of typical electroless Ni-P electrolytes have shown promise in allowing the formation of electroless Ni-P deposits on Sn/Pd treated glass despite the presence of another metal, such as Fe or Co, within the electrolyte. The presence of a secondary metal often reduces electroless deposition rates due to a shift in the cathodic potential of the electrolyte. As a matter of practicality, electroless deposition of Ni-P from electrolytes containing other metals allows a qualitative determination of the concentration at which a reasonable deposition rate for an electroless coating is no longer possible. This consideration was not required for the Ni/Au and Co/Au electrolytes as the specific Au electrolyte was unaffected by the inclusion of either Ni or Co.

The composition of the electro-electroless Fe/Ni was kept simple using only the metal salts, stabilizer/complexing agent, and reducing agent, Table 5.6. The electrolyte, which was a variant of the alkaline Ni-P electrolytes used in the cladding of Mg alloys, Chapter 3.4.3 & 3.4.4, used sodium citrate which also acts as a buffer in the neutral regime, Table 2.3.

Chemical Name	Chemical Formula	Composition (g/L)
Nickel Sulphate Hexahydrate	$\text{NiSO}_4 \cdot 6\text{H}_2\text{O}$	15.0
Sodium Citrate Tribasic Dihydrate	$\text{Na}_3\text{C}_6\text{H}_5\text{O}_7 \cdot 2\text{H}_2\text{O}$	15.0
Sodium Hypophosphite Hydrate	$\text{NaH}_2\text{PO}_2 \cdot \text{H}_2\text{O}$	12.5
Ferrous Ammonium Sulphate Hexahydrate	$\text{Fe}(\text{NH}_4)_2(\text{SO}_4)_2 \cdot 6\text{H}_2\text{O}$	7.5
Operating Temperature: 75 °C		pH: 4.5 to 5.5

Table 5.6: Hybrid electro-electroless electrolyte for Fe/Ni deposition; Ni:Fe ratio is 3:1.

⁵ Compositionally pure in the case of electroless Ni deposition accounts for the inclusion of an anodic byproduct such as P or B forming Ni-P or Ni-B alloys.

The Ni:Fe ratio within the electrolyte was set at a molar ratio of 3:1 as it allowed for electroless deposition of pure Ni-P on Sn/Pd treated glass, Figure 5.10, while still containing a significant amount of Fe within the electrolyte.

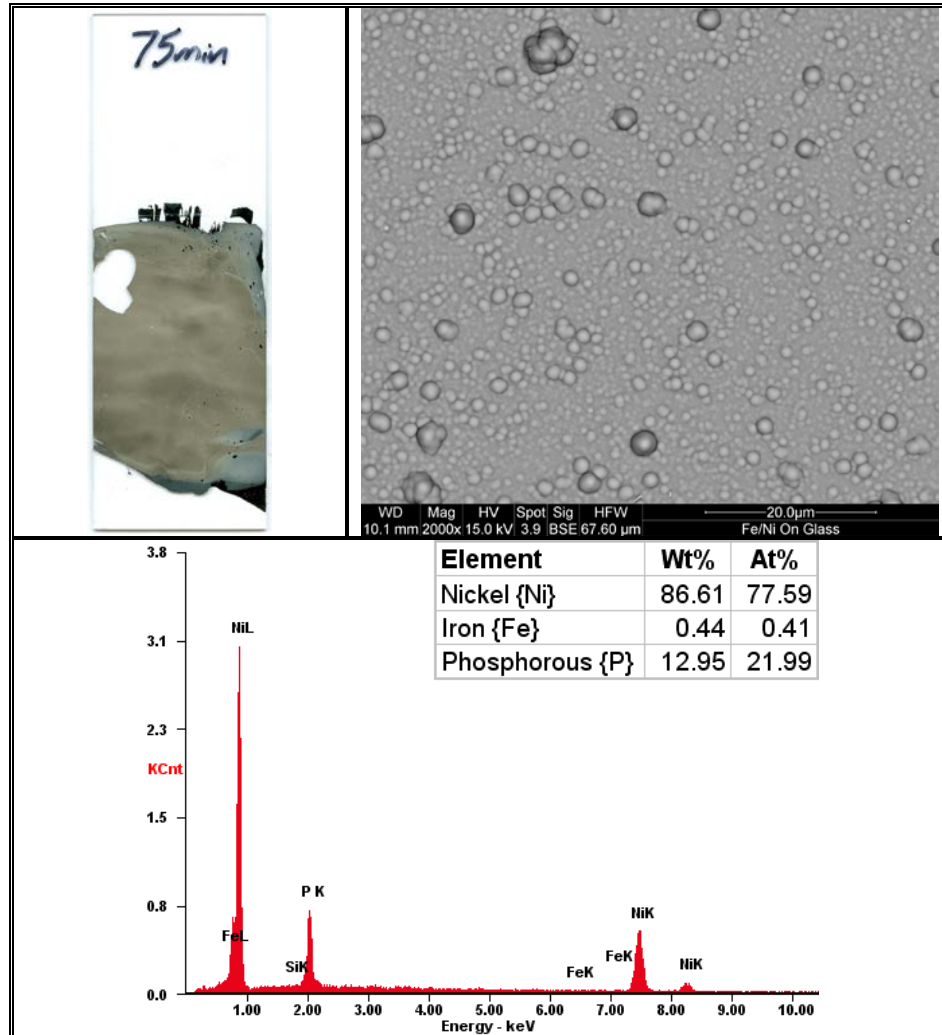


Figure 5.10: Macroscopic image, backscatter SEM image and EDS analysis of an electroless Ni-P deposit [75 min, 70 °C] from a 3:1 Ni:Fe electrolyte on Sn/Pd treated glass; treated region 45 mm × 25 mm.

The inability of the electrolyte to form electroless deposits on Cu substrates provided a substrate upon which to measure the composition of the electroplated deposit against several applied potentials, Table 5.7, without concern of initial electroless plating. Electroplating was carried out at 70 °C, the minimum operating temperature for electroless deposition, with Cu substrates used as the cathode and a Ni plate used as the anode. While the electroless deposition was not initially present, some electroless reduction cannot be entirely ruled out during the electroplating step.

Applied Voltage [V]	Stable Average / (Median)		Duration (Stability) [s]	Atomic % (Weight %)		
	Voltage [V]	Current [A]		Ni	Fe	P
2.0	1.954 (1.948)	0.0077 (0.0087)	152.46 (143.26)	N/A	N/A	N/A
2.5	2.393 (2.387)	0.0180 (0.0191)	147.04 (137.03)	41.51 (44.07)	51.49 (52.01)	7.00 (3.92)
3.0	2.660 (2.655)	0.0573 (0.0580)	145.12 (140.75)	59.92 (64.17)	29.06 (29.59)	11.04 (6.24)
3.5	2.943 (2.937)	0.0938 (0.0949)	149.61 (142.01)	61.10 (66.03)	25.75 (26.47)	13.15 (7.50)
4.0	3.801 (3.802)	0.2110 (0.2103)	149.45 (144.7)	60.05 (64.76)	27.40 (28.10)	12.55 (7.14)
4.5	4.179 (4.181)	0.3375 (0.3355)	170.01 (146.89)	66.46 (72.07)	19.04 (19.64)	14.50 (8.29)
5.0	4.659 (4.663)	0.3733 (0.3686)	155.05	69.56 (75.20)	16.24 (16.70)	14.20 (8.10)
6.0	5.365 (5.424)	0.5388 (0.5546)	44.49	69.02 (74.59)	16.92 (17.39)	14.06 (8.02)

Table 5.7: Measured voltage, current, and duration of electroplated Fe/Ni deposits including the atomic % and weight % of EDS results for deposits at various applied voltages.

Notes: To maintain Fe within the electrolyte, multiple solutions were produced from a single electrolyte and each solution was run no more than 5 times. The deposit for 2.0 V applied was too thin.

The duration of stability represents the region in which the potential varied least. Since the applied potential was held constant, it was the measured current that varied most, whereas deposits at constant current would have produced a varying potential. The amount of variation in the current during electroplating was largest for lower potentials as polarization of the electrolyte required more time, Figure 5.11.

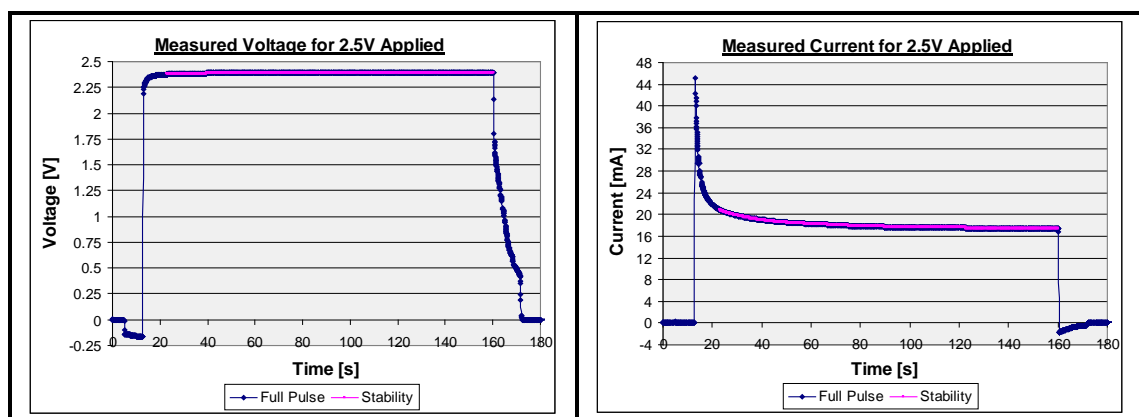


Figure 5.11: Plot of the measured voltage and current for an applied deposition potential of 2.5 V for the deposition of Fe from a 3:1 Ni:Fe electrolyte. The region in pink is an example of what was considered the region of stability.

The presence of a charging region for low applied potentials, observed under 5 V, is likely related to the formation of electrical double layer as well as the lack of standard

electrode used within the electroplating configuration. At, and above, 5 V the measured current and potential were stable suggesting that the applied potential was sufficient to overcome the formation of any double layer. Inclusion of a standard electrode within the system is likely to have produced a more even pulse, though the charging characteristics would remain.

Plotting the atomic concentration of Ni, Fe, and P against the applied potential, Figure 5.12, reveals a general trend for the inclusion of Fe within the deposit.

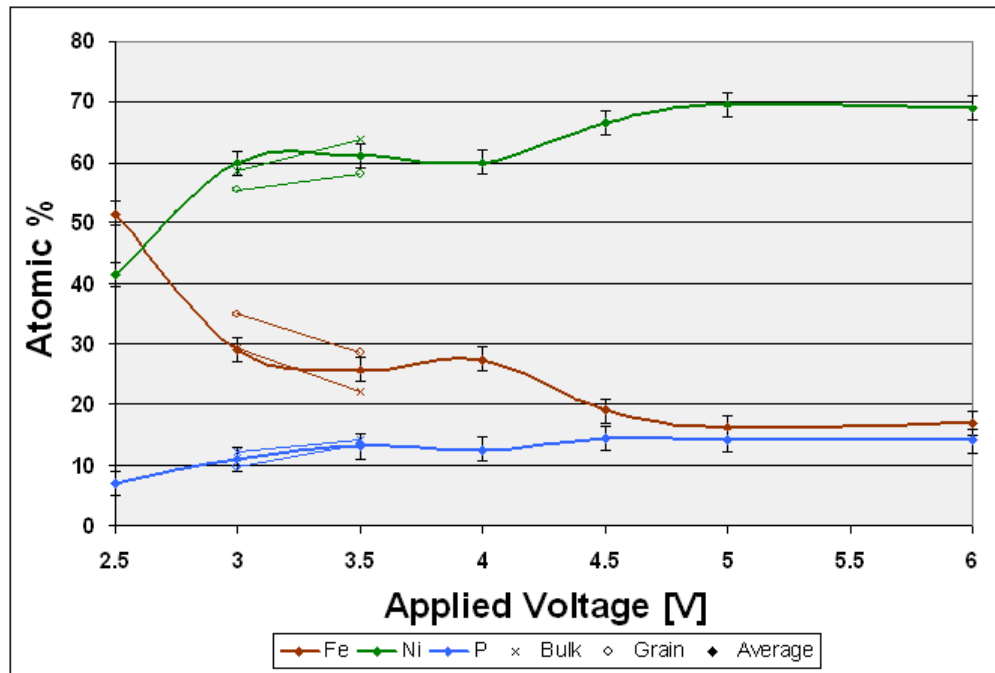


Figure 5.12: Plot of the atomic % of Ni, Fe, and P within the electroplated coatings presented in Table 5.7. Analyses of grains are included for those coatings upon which they were clearly visible.

At low applied potentials a greater amount of Fe is present within the deposit, around 50 %, and at higher potentials the concentration of Fe drops to around 20 % atomic. At higher applied potential the ratio of Ni to Fe is similar to that of permalloy, which contains 80 % Ni and 20 % Fe; with inclusion of P remaining roughly constant at around 13 % atomic for applied potentials above 3.5 V.

The trend depicted in Figure 5.12 is for Fe/Ni HEED electrolytes that have been heated for approximately one hour prior to use. Additionally, the electrolyte was observed to undergo a slight change in color when brought to operating temperature. The change in color was seen to persist, though to a lesser extent, after the electrolyte was cooled, suggesting some reaction within the electrolyte was taking place. Electroplated

deposits at 5 V applied, around 4.65 V measured, between the electrodes produced deposits of differing composition depending on how quickly the electrolyte was used after being assembled. The highest Fe content within a deposit to date was measured by EDS to be atomically around 70 %, with Ni and P content around 22 % and 7 %, respectively. Electrolytes utilized immediately after assembly included higher Fe, Figures 5.13 & 5.14, than those used after over an hour at operating temperature, Figure 5.15.

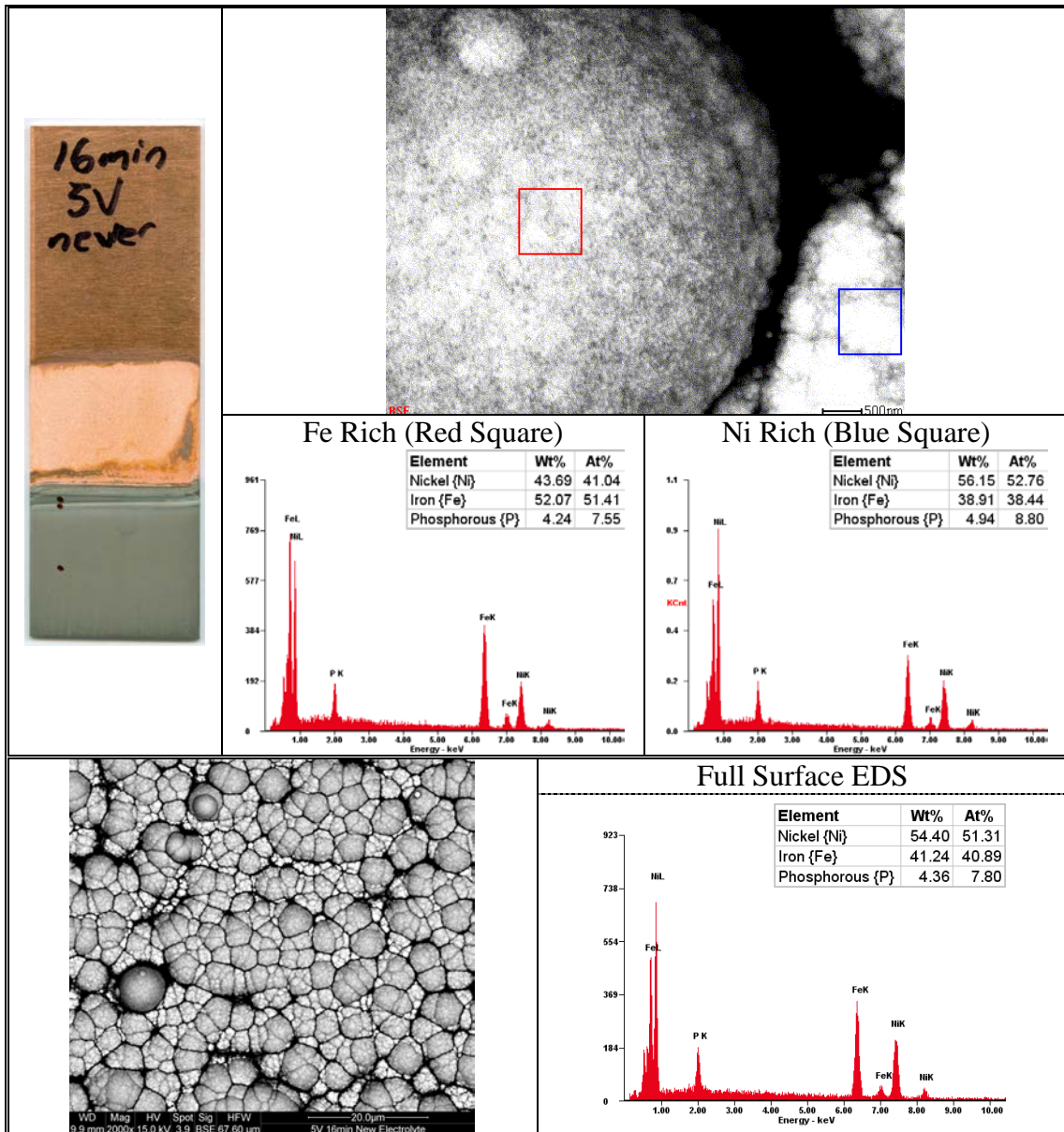


Figure 5.13: Macroscopic scan, backscatter SEM images, scale bars: (Top) 500 μm, (Bottom) 20 μm, and associated EDS analyses for an electroplated deposit [16 min, 80 °C, 5 V applied, Full Pulse: 4.6742 V, 0.4542 A, Median: 4.6677 V, 0.4754 A] on an 80 mm × 25 mm × 1mm Cu substrate from a newer Fe/Ni electrolyte. Note: All EDS and SEM data collected near the lower spot on the sample.

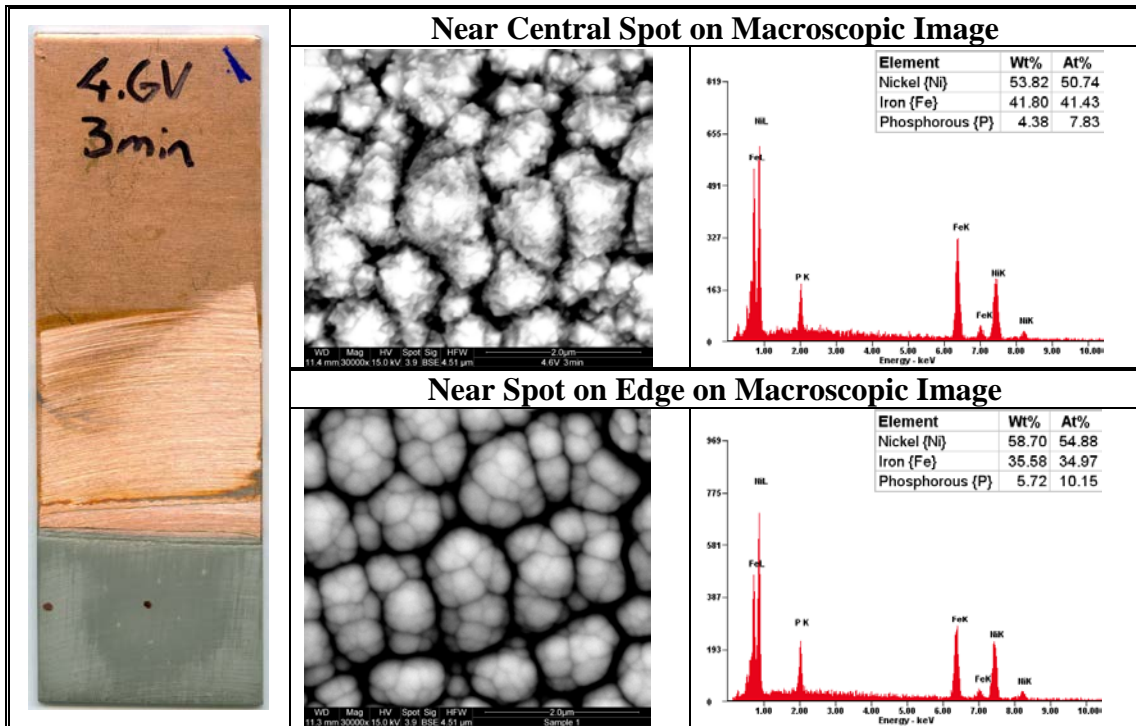


Figure 5.14: Macroscopic scan, backscatter SEM images, 2 μm scale bars, and associated EDS analyses for an electroplated deposit [3 min, 80 °C, 4.6 V applied] on an 80 mm × 27 mm × 1mm Cu substrate from a newer Fe/Ni electrolyte.

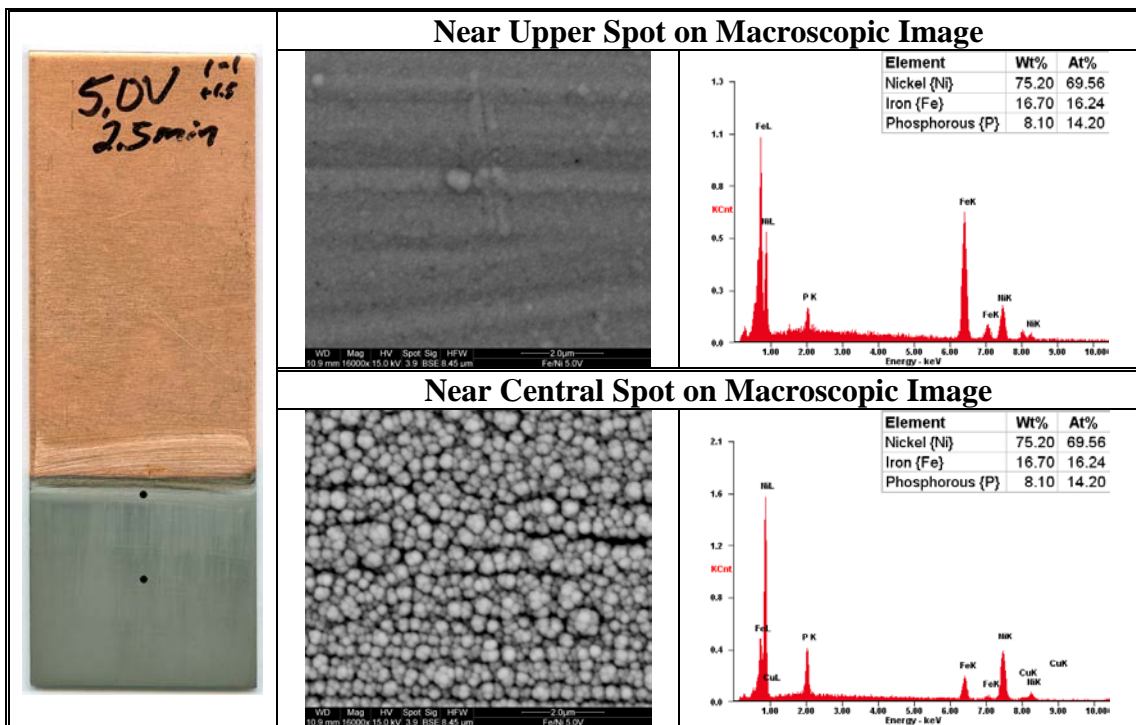


Figure 5.15: Macroscopic scan, backscatter SEM images, 2 μm scale bars, and associated EDS analyses for an electroplated deposit [2.5 min, 80 °C, 5 V applied, Full Pulse: 4.6588 V, 0.3733 A, Median: 4.6626 V, 0.3686 A] on an 80 mm × 27 mm × 1mm Cu substrate from an older Fe/Ni electrolyte. Note: The signal from the substrate in the upper area was atomically around 9 % Cu while the lower area showed a Cu content of around 4.5 %; the difference is a reflection of a thicker deposit lower on the substrate.

The difference between the newer, Figures 5.13 & 5.14, and older, Figure 5.15, electrolytes is attributed to a dynamic ionic, and possibly ligand, structure within the electrolyte. The initial form of the Fe ions within the solution is the divalent form, Fe^{2+} , provided by the Fe salt. As the electrolyte is heated a color change, towards a more yellow green, and a drop in pH, from around 5.5 to around 4.5, suggests the presence of a reaction. Additionally, deposits at higher applied potentials have a more jagged structure, Figure 5.14, when the electrolyte is fresh compared to when the electrolyte has been heated for some time, around one hour. Given the observations, the change in deposit contents, as well as the standard electrode potential series; it assumed that Fe^{2+} is oxidizing and forming Fe^{3+} , which is nobler than Ni^{2+} , Table 5.8, and hence explains the decreasing Fe content measured for electrolytes which have been heated for over an hour prior to use, such as in Table 5.7.

Half-Reaction	E° (V)
$\text{Fe}^{3+} + 3e^- \leftrightarrow \text{Fe}_{(s)}$	-0.037
$\text{Ni}^{2+} + 2e^- \leftrightarrow \text{Ni}_{(s)}$	-0.257
$\text{Fe}^{2+} + 2e^- \leftrightarrow \text{Fe}_{(s)}$	-0.447

Table 5.8: Standard electrode potentials for Ni and Fe metals

In addition to affecting the electroplated deposit, the change in the electrolyte also significantly influences the formation of electroless deposits. Electroless deposits formed within aging electrolytes have been seen to be dissolved back into the solution. This is thought to occur due to an oxidation reaction of the Ni forming Ni^{2+} and a reduction of the Fe^{3+} in solution as the electrolyte ages. Regarding electroplating, the use of fresher electrolytes allows for electroplating at lower potentials as older electrolytes are unable to form deposits of any thickness or quality at potentials under 2 V.

The transient environment of the Fe/Ni electrolyte requires significant more study. The addition of $\text{Fe}(\text{NH}_4)_2(\text{SO}_4)_2 \cdot 6\text{H}_2\text{O}$ as an aqueous solution to the electrolyte rather than as a solid does appear to improve the stability of the electrolyte. In addition to the inconsistent behaviour of the electrolyte itself, electroplated deposits were found to vary in composition over the length of the sample. Variation of the composition over the length of the sample was most clearly observed in the case of higher applied potentials, around 5 V, Figure 5.15, though it appears to have been present on most samples.

In order to verify the capacity of the electrolyte to lend itself to the formation of hybrid electro-electroless deposits a bi-layer structure was attempted on a Cu substrate. The attempt was made independent of the composition of the initial electroplated layer, with the goal of showing the inclusion of Fe within one layer and the purity of the electrolessly plated layer. For the electroplated layer, the applied potential was held at 1.406 V for 3 min followed by a second shorter applied potential of 1.879 V for 30 s to ensure a complete deposit. The sample was raised and an electroless deposit was allowed to form on the sample over the course of 4 hours, Figure 5.16.

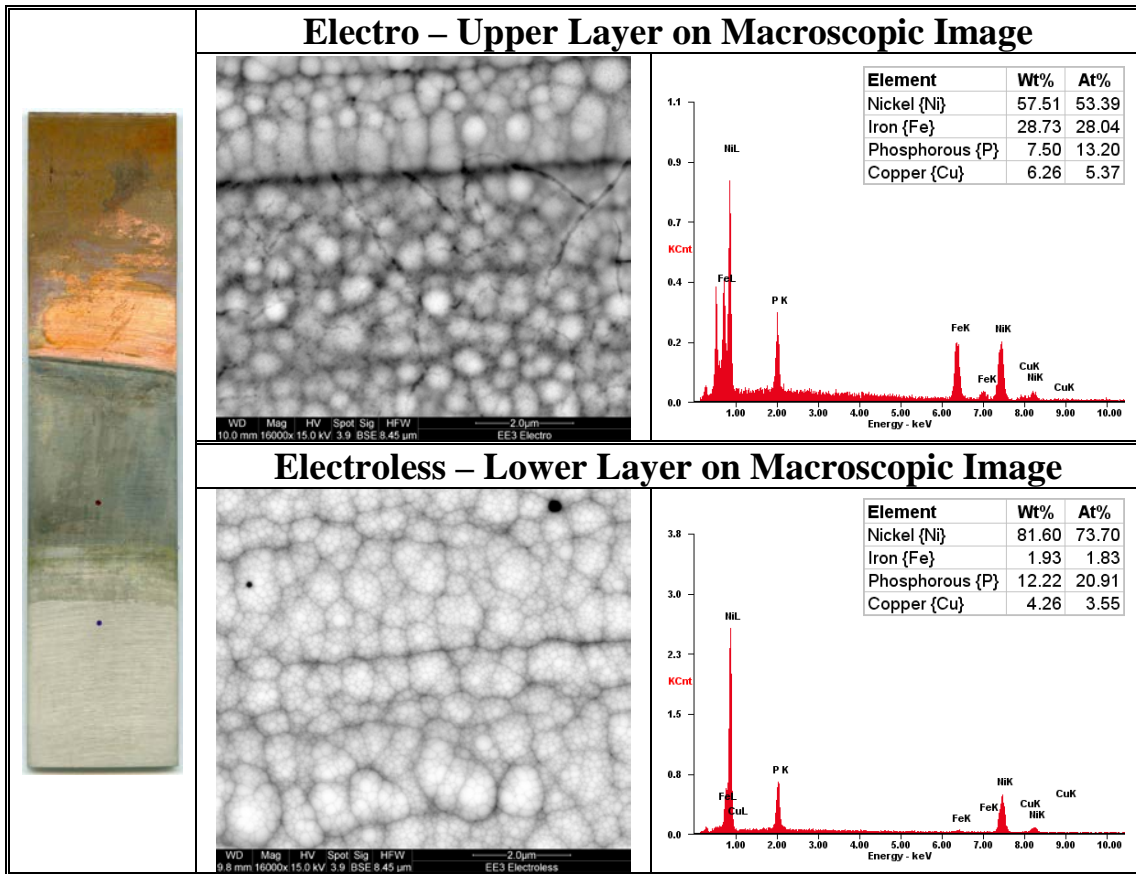


Figure 5.16: Macroscopic scan, backscatter SEM images, with 2 μm scale bars, and associated EDS analysis of a Fe/Ni HEED bi-layer deposit [75 $^{\circ}\text{C}$, Electro: 3 min, 1.406 V, 0.377 A; 30 s, 1.879 V, 0.53 A; Electroless: 4 h] from a newer Fe/Ni electrolyte on an 80 mm \times 20 mm \times 1mm Cu sample. Note: Due to prolonged, 4hrs, electroless deposition, some of the electrolyte evaporated leaving a transition layer.

Combining both the electroplated layer along with an electrolessly plated layer is able to reduce Fe content of the surface layer. Though some dissolution of P of the initial electroplated layer may be taking place, Fe remains present according to EDS measurements. Furthermore, EDS analysis of pores in the Ni-P coating suggests that the Ni/Fe deposit remains intact as Fe is more prominent atomically; 74.87 % Ni, 12.87 % Fe,

7.31 % P, 4.95 % Cu. The transient behaviour of the Fe/Ni electrolyte for single electrodeposited layer also extends to the formation of the bi-layer deposit as electrolytes which had undergone multiple uses dissolved the electrodeposited Ni-Fe deposit at the air electrolyte interface, Figure 5.17. It should be noted that while dissolution is supported by the electroless deposition observations on glass, the cause of the dissolution may have been, in part, due to a galvanic reaction between the Cu substrate and incomplete Ni/Fe coating. Utilizing newer electrolytes was seen to overcome the issue of interface dissolution.

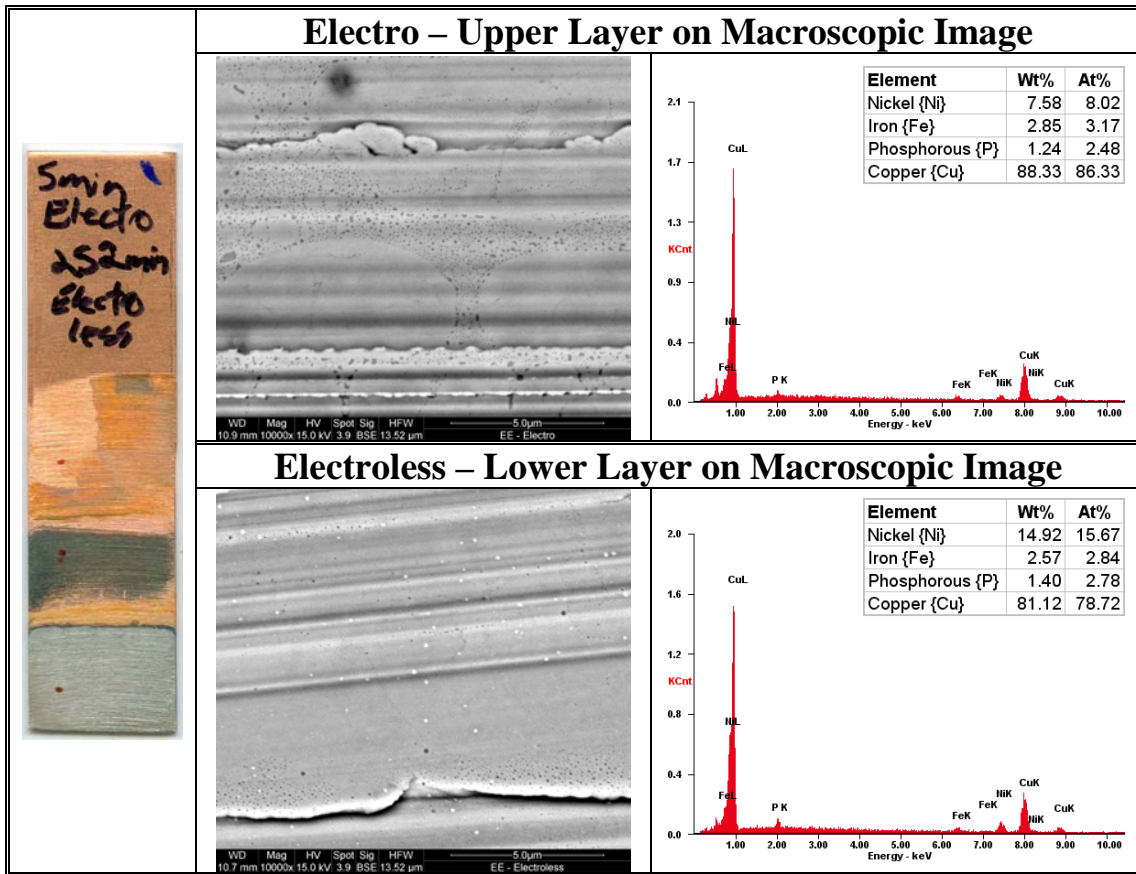


Figure 5.17: Macroscopic scan, backscatter SEM images, with 5 µm scale bars, and associated EDS analysis of a Fe/Ni HEED bi-layer deposit [80 °C, Electro: 5 min, 2.25 V applied, 2.12 V & 22.9 mA measured; Electroless: 4 h 12 min] from an older Fe/Ni electrolyte on an 80 mm × 20 mm × 1mm Cu sample. Note: A 2 min electroplating layer under the same conditions was applied to the reverse side prior to the electro deposit on the side shown. The 2 min deposit was to prevent potential galvanic cell reaction between the Cu substrate and Ni/Fe coating.

The success of electro-electroless methods may be expanded to other magnetic metal pairs such as Ni and Co. The restriction to alkaline environments for the electroless deposition of Co along with the ability to both electroplate Co and electrolessly deposit Ni in acidic environments allows for the possibility of such deposits. Ongoing work has

shown promise for the deposition of Co/Ni HEED multi-layers, though establishing good electroless coatings from the electrolyte remain the first priority. Additionally, experiments regarding enhanced electroless alloying of electroplated metals are ongoing with focus on transitional multi-layer structures. Importantly the rate of electroless deposition both outside and during electroplating must be formally established in order to produce desired and replicable deposits.

5.7 Summary

Hybrid electro-electroless deposit (HEED) coatings provide an effective and flexible means of producing deposits not previously obtainable by other deposition techniques. The capacity to deposit multi-layered, alloyed, or composite coatings from a single electrolyte provides allows the production of materials with unique mechanical and electrical properties. While few electrolytes have been identified for this novel and emerging method of deposition; further study and understanding of common electrolytes will serve to broaden the applications of HEED coatings. Additionally, though alloyed multi-layers, and well as multi-layers with transitional degrees of alloying, have long existed, HEED coatings allow for easy incorporation of non-metals, such as phosphorous {P}, in an easy to control manner. The deposition of HEED coatings is at present only in the infancy of development and further study and electrolyte development will only broaden the applications for which such coatings are suited.

5.8 References

- [1] A. Brenner and G. Riddell, "Nickel Plating on Steel by Chemical Reduction", J. Res. Nat. Bur. Std., 37(1), (1946), p.31-34, DOI: <http://dx.doi.org/10.6028/jres.037.019>
- [2] A. L. Peach, "Electro-electroless plating method", US Patent #3303111, (1963)
- [3] G.A. Di Bari; Chapter 3: Electrodeposition of Nickel, in "Modern Electroplating, Fifth Edition", p.79-114, eds: M. Schlesinger and M. Paunovic, (2010) John Wiley & Sons, Inc., Hoboken, NJ, USA, DOI: 10.1002/9780470602638.ch3
- [4] M. Paunovic, M. Schlesinger; Chapter 8: Electroless Deposition, Fundamentals of Electrochemical Deposition, Second Edition, p.139-168, (2006), John Wiley & Sons, Inc.
- [5] D. Simunovich, M. Schlesinger, and D.D. Snyder, "Electrochemically Layered Copper - Nickel Nanocomposites with Enhanced Hardness", Journal of the Electrochemical Society, 141(1), (1994), L10-L11

- [6] J.-y. Fei, G.D. Wilcox, “Electrodeposition of zinc–nickel compositionally modulated multilayer coatings and their corrosion behaviours”, *Surface & Coatings Technology*, 200, (2006), p.3533– 3539
- [7] C Turk, Texas Instruments Inc, US 3847560 A “Corrosion resistant metallic multilayer structure” Filed: Jul 30, 1969; Publication: Nov 12, 1974
- [8] M. Rahsepar and M. E. Bahrololoom, “Corrosion resistance of Ni/Zn–Fe/Zn and Ni/Zn/Zn–Fe compositionally modulated multilayer coatings” *Corrosion Engineering, Science and Technology*, 46(1), (2011), p.70-75
- [9] V. R. Rao and A. Chitharanjan Hegde, “Nanofabricated Multilayer Coatings of Zn-Ni Alloy for Better Corrosion Protection”, *Protection of Metals and Physical Chemistry of Surfaces*, 49(6), (2013), p.693–698.
- [10] W. Zhang, Q. Xue, “Tribological properties of nickel-copper multilayer film on beryllium bronze substrate”, *Thin Solid Films*, 305(1-2), (1997), p.292-296
- [11] K. D. Bird and M. Schlesinger, “Giant Magnetoresistance in Electrodeposited Ni/Cu and Co/Cu Multilayers”, *J. Electrochem. Soc.*, 142(4), (1995), p.L65-L66
- [12] A. F. Schmeckenbecher, “Chemical Nickel-Iron Films”, *Journal of the Electrochemical Society*, 113(8), (1966), p.778-782
- [13] M. Paunovic, M. Schlesinger, and D.D. Snyder; Chapter 1: Fundamental Considerations, in “Modern Electroplating, Fifth Edition”, p.1-32, eds: M. Schlesinger and M. Paunovic, (2010) John Wiley & Sons, Inc., Hoboken, NJ, USA, DOI: 10.1002/9780470602638.ch1
- [14] M. AlHajDarwish, H. Kurt, S. Urazhdin, A. Fert, R. Loloee, W. P. Pratt, Jr., and J. Bass, “Controlled Normal and Inverse Current-Induced Magnetization Switching and Magnetoresistance in Magnetic Nanopillars”, *Physical Review Letters*, 93(15), (2004) Article #157203, DOI: 10.1103/PhysRevLett.93.157203
- [15] J. Yahalom and O. Zadok, Formation of composition-modulated alloys by electrodeposition, *Journal of Material Science*, 22(2), (1987), p.499-503
- [16] A. Hung, K. -M. Chen, “Mechanism of Hypophosphite-Reduced Electroless Copper Plating”, *Journal of the Electrochemical Society*, 136(1), (1989), p.72-75
- [17] J. Li and P. A. Kohl, “The Deposition Characteristics of Accelerated Nonformaldehyde Electroless Copper Plating”, *Journal of The Electrochemical Society*, 150(8), (2003), p.C558-C562
- [18] P. A. Kohl; Chapter 4: Electrodeposition of Gold, in “Modern Electroplating, Fifth Edition”, p.115-130, eds: M. Schlesinger and M. Paunovic, (2010) John Wiley & Sons, Inc., Hoboken, NJ, USA, DOI: 10.1002/9780470602638.ch4
- [19] T. Osaka, M. Kato, J. Sato, K. Yoshizawa, T. Homma, Y. Okinaka, and O. Yoshioka, “Mechanism of Sulfur Inclusion in Soft Gold Electrodeposited from the Thiosulfate-Sulfite Bath”, *Journal of The Electrochemical Society*, 148(10), (2001), p.C659-C662
- [20] Y. Okinaka, M. Kato, Chapter 21: Electroless Deposition of Gold, in “Modern Electroplating, Fifth Edition”, p.483-498, eds: M. Schlesinger and M. Paunovic, (2010) John Wiley & Sons, Inc., Hoboken, NJ, USA, DOI:10.1002/9780470602638.ch21
- [21] M. Paunovic and C. Sambucetti, in *Proc. Symp. on Electrochemically Deposited Thin Films*, Vol. 31, M. Paunovic, Ed., Electrochemical Society, Pennington, NJ, (1994), p. 34.
- [22] G. A. Krulik and N. V. Mandich, U.S. Patent 5,232,492 (1993)

Chapter 6: Summary	273
6.1 Overview of Summary	274
6.2 Magnesium {Mg}	274
6.3 Silicon {Si}	275
6.4 Hybrid Electro-Electroless Deposit (HEED) Coatings	276

6.1 Overview of Summary

Applications of the work contained within this dissertation span across several industries and demonstrate several novel methods of electroless thin film formation on a variety of surfaces. Specifically, the breadth spanned by the work contained within this dissertation includes applications of electroless deposition within the automotive, electronics, and other sectors. The following summary sets out the achievements contained within this dissertation in the development and understanding of coatings in for a variety of applications within those sectors.

6.2 Magnesium {Mg}

Magnesium {Mg} alloys, while possessing many industrially advantageous properties, have seen limited use due to the high reactivity of Mg which results in corrosion. The electroless cladding of Mg alloys was previously conducted as part of a complex, multi-stepped process using relatively hazardous chemicals, such as hexavalent chromium {Cr⁶⁺} and more recently hydrofluoric acid {HF}, see Chapter 3.2. As part of work within this dissertation, the novel and relatively simple process of oxide removal prior to immersion within an alkaline electrolyte was established as a means of coating Mg alloys. Specifically, the immersion of dry polished Mg alloy surfaces within alkaline, pH > 12.5; electroless copper {Cu} electrolytes, Chapter 3.4.2, produced stable deposits on the Mg alloy surface. The autocatalytic electroless Cu deposit, which was determined to have an immersion deposition component, was formed on Mg alloys in around 15 to 20 minutes within room temperature electrolytes. The porosity of Cu deposits was found to create an active galvanic couple between the Cu cladding and Mg alloy substrate which was visible when the sample was immersed in distilled water. The immersion technique for detecting the formation of a galvanic cell was found to apply also to the formation of other coatings on Mg alloys.

The autocatalytic deposition of electroless nickel-phosphorous {Ni-P} thin films on Mg alloys, Chapter 3.4.3, used conventional, pre-existing, electrolytes and was found capable of forming deposits on both polished and oxidized Mg alloy surfaces. Most of the electrolyte formulations shared a common stabilizer mixture comprised of citrate {C₆H₅O₇³⁻} and ammonium {NH₄⁺} ions, with a few electrolytes using tartrate

$\{C_4H_4O_6^{2-}\}$ ions in place of citrate $\{C_6H_5O_7^{3-}\}$. Details of the process, established within this work, include the elimination of corrosion promoting ions, such as the chloride anion $\{Cl^-\}$ as well as the use of an alkaline environment to mitigate galvanic corrosion during initial nucleation of the coating. Extensions of the results obtained within this work for Ni-P allowed the formation of other good quality coatings on Mg alloys including cobalt-phosphorous $\{Co-P\}$ and nickel-boron $\{Ni-B\}$, as well as several ternary alloys of Ni-P, Chapter 3.4.4, including nickel-cobalt-phosphorous $\{Ni-Co-P\}$, nickel-zinc-phosphorous $\{Ni-Zn-P\}$, nickel-iron-phosphorous $\{Ni-Fe-P\}$, and nickel-rhenium-phosphorous $\{Ni-Re-P\}$ coatings.

The coatings produced provide a first level of protection of Mg alloys against corrosion and allow other thin film deposition to further increase the corrosion and wear resistance of the underlying Mg substrate. The development and modification of the commonly used electrolytes, especially the removal of the most aggressive corrosion promoting ions, as well as maintaining a clean surface is central to the ability to deposit metal thin films on Mg alloys.

6.3 Silicon {Si}

The intense amount of research conducted in connection with solar cells and electronics industries would seem to leave little room for novel applications. While the technique of simple oxide removal and immersion within an electrolyte, first established here for Mg alloy substrates, has not been applied to Si wafers in the same way as within this work, similar techniques were previously established for buried-contact solar cells, Chapter 4.3. The novel work conducted in connection with Si substrates included, among other aspects, an investigation into the role of ammonium ions $\{NH_4^+\}$ within Ni-P electrolytes traditionally used for the metallization Si, Chapter 4.5.4. The presence of NH_4^+ ions and ammonia $\{NH_3\}$ molecule within Ni electrolytes was determined to be a significant factor in the formation of Ni immersion deposits on silicon oxide $\{SiO_x\}$ surfaces. The presence of NH_4^+/NH_3 within the electrolyte appears to provide a ligand structure to the Ni^{2+} ions that uniquely affects SiO_x surface and allows deposition on the underlying Si layer.

More generally, this work demonstrates that selective deposition can be achieved by selective oxide removal and metallization within common electrolytes. Specifically it was shown that aside from alkaline electroless nickel phosphorous {Ni-P} electrolytes, which form immersion deposits on Si independent of the inclusion of $\text{NH}_4^+/\text{NH}_3$, selective electroless deposition can be achieved from a large number of electrolytes. Electrolytes capable of selective electroless deposition include those for alkaline electroless copper {Cu}, Chapter 4.5.1, alkaline electroless gold {Au}, Chapter 4.5.2, alkaline electroless silver {Ag}, Chapter 4.5.5, alkaline electroless cobalt phosphorous {Co-P}, Chapter 4.5.4, as well as acidic nickel phosphorous {Ni-P}, Chapter 4.5.3.

The most notable result regarding selective deposition on Si wafers is the formation of the Ni-P coating on Si from an acidic electrolyte, Chapter 4.5.3. The metallization of Si from acidic electrolytes had previously only been obtained by using tin/palladium {Sn/Pd} activation of the Si surface. Additionally, while it was expected that acidic electroless Ni-P would contain phosphorous {P} at 25 %, which would increase the resistance of the deposit, it was been found that P is included only at around 7.5 %. The apparent lesser inclusion of P effectively allows acidic Ni-P coatings to form low P deposits on Si, which were previously known only to alkaline electrolytes. Finally, though mechanical scribing is established in literature, Chapter 4.2, the removal of the oxide layer for selective deposition does not appear to be explicitly provided in literature and potentially allows the inexpensive manufacture of conduction tracks for solar cells.

6.4 Hybrid Electro-Electroless Deposit (HEED) Coatings

Since the discovery of electroless deposition within the electroplating process, the utilization of some electroless deposition within electroplating has been used as a means of improving cathode efficiencies and including non-metals. The development of hybrid electro-electroless deposition (HEED) within this work is quite different in that the metal targeted for electroplating is not the same metal targeted for electroless deposition, Chapter 5.2. The combination of electroplating and electroless deposition allows for added flexibility in the composition of the deposit compared to either electroplating, or electroless deposition, alone. Under ideal conditions, this novel technique can be made to deposit multi-layers with electroless deposition of the more noble metal and separate

electroplating of the less noble metal each as compositionally pure layers from a single electrolyte. Additionally, the HEED coatings have the capacity to produce unique alloys due to an ongoing electroless process, including the transitional alloying of electroplated layers. Most notable concerning HEED coatings is the capacity to deposit alternating layers of metals of similar nobility. Electroplated multi-layers of metals of similar nobility can, at best, only produce two distinct alloys. Conversely, the ability to deposit electrolessly allows for, at the minimum, a compositionally pure electroless layer to be produced along with an alloyed electroplated layer.

The capacity of HEED to provide a compositionally pure electroless layer in addition to an alloyed electroplated layer was established within this work for nickel/gold {Ni/Au}, cobalt/gold {Co/Au}, Chapter 5.4, and iron/nickel {Fe/Ni}, Chapter 5.6, electrolytes. While the formation of compositionally pure Au layers and Ni/Au alloy layers can, due to the difference in nobility of the metals, be achieved using electroplating; the deposition of compositionally pure Ni layers and alloyed Ni/Fe layers is, in this dissertation, made trivial despite the closer nobility of the metals.

Of greatest benefit in the near term is the application of HEED coatings to nickel-zinc-phosphorous {Ni-Zn-P} thin film deposits on Mg alloy substrates, Chapter 5.5. The increased Zn content obtainable using electroplating, 32 % Zn atomically, compared to conventional electroless plating, 20 % Zn atomically, allows for the production of a sacrificial layer on Mg alloys. Additionally, as Ni content can also be increased within electroplating, multi-layers depleted of Zn and rich in Ni can be produced to provide a highly corrosion resistant, sacrificial layer structure.

Chapter 7: Future Work	278
7.1 Introduction of Future Work	279
7.2 Cladding of Magnesium {Mg} Alloys	279
7.3 Electroless Metallization of Silicon {Si}	280
7.4 Hybrid Electro-Electroless Deposition (HEED) Coatings	281
7.5 Ionic Liquids (ILs)	281

7.1 Introduction of Future Work

The work presented within this dissertation represents completed studies on the electroless thin film coating of magnesium {Mg} alloys, electroless deposition on silicon {Si}, as well as the fundamental requirements to produce hybrid electro-electroless deposit (HEED) coatings. The results presented herein satisfy the initial goals of those studies and several interesting avenues of investigation for future work became possible. This section serves to elaborate on some of the directions that may be taken up as future work.

7.2 Cladding of Magnesium {Mg} Alloys

The coating produced within this work for the protection of Mg alloys from galvanic corrosion provides a crucial step in the direction of wider industrial use of Mg alloys. Protection from galvanic corrosion is paramount for further cladding of Mg alloy substrates which is needed to provide robust mechanically and long term corrosion resistance to Mg alloys.

The most direct manner in which to further improve the qualities of the coating and provide more robust mechanical and general corrosion protection is the coating of the established layer with secondary/additional deposits. For example, one of the most commercially viable is the deposition of nickel-zinc-phosphorous {Ni-Zn-P}. Combining the deposit with the application of multi-layer HEED coatings with alternating layers rich in Zn and Ni provides a sacrificial layer arrangement to the coating and may easily be produced from the electroless electrolyte itself.

The issue of some sparse pinholes/micro-pores within electroless copper {Cu} coatings persist to an extent and may inhibit secondary deposition other than by certain, alkaline, electrolytes. Elimination of the pin holes, which was attempted by altering the bath chemistry, appears to require an additive in the electrolyte to increase the deposition rate. Furthermore, the typical more crystalline Cu deposits also play an important role in supporting pinhole formation compared to the more amorphous Ni-P deposits.

Nickel boron {Ni-B} deposition is yet another process with significant potential. The well known smoothness and hardness of Ni-B coatings make them ideal for industrial applications. One limiting factor in Ni-B deposition is the short lived nature of

the electrolyte explored within this dissertation. Exploring other highly alkaline, $\text{pH} > 13.5$, Ni-B electrolytes, as well as adjusting the formulation of the electrolyte cited within this dissertation seem to be the two best methods of improving Ni-B coatings on Mg alloys. Given the results concerning Ni-B and the hindering effect of chloride ions $\{\text{Cl}^-\}$, the replacement of nickel chloride $\{\text{NiCl}_2\}$ with nickel sulphate $\{\text{NiSO}_4\}$ or nickel acetate $\{\text{Ni}(\text{CH}_3\text{COO})_2\}$ provides an easy first step in improving Ni-B coatings. Further incorporating ammonium hydroxide $\{\text{NH}_4\text{OH}\}$ in place of, or along with, sodium hydroxide $\{\text{NaOH}\}$ is also expected to be beneficial.

More generally, metallization conditions, including pH, temperature, and electrolyte composition, must be refined in order to minimize stress and fractures in Ni-P and Ni-Me-P (Me – metal) coating. The exploration heat treatment also provides a possible means of alleviating some of the issues surrounding pinhole/micro-pores as well as stress within the coating. The pursuit of a better understanding of both when and how immersion, and displacement, coatings will form may also improve the deposition of existing, and yet undiscovered, coatings on Mg alloys. The presence of immersion coatings typically enhances adhesion by providing a good intermetallic bond between metal thin films and Mg substrates.

7.3 Electroless Metallization of Silicon {Si}

The electroless deposition of a variety of metals, including gold $\{\text{Au}\}$, silver $\{\text{Ag}\}$, copper $\{\text{Cu}\}$, and most importantly nickel phosphorous $\{\text{Ni-P}\}$ alloys, within scribed regions of an Si surface provide many significant benefits for low cost electronics. In addition to determinations of the conductivity of deposits, further exploration of the oxide removal and direct deposition of metals within scribed regions provide an initial avenue of exploration. Additionally, better understanding of the role of ammonium ions $\{\text{NH}_4^+\}$ and ammonia $\{\text{NH}_3\}$ molecules within electrolytes would be beneficial. A comparison of the adhesion provided by mechanically scribed surfaces with other scribe and oxide removal techniques, such as laser ablation or rotary blade scribing, might also be of interest to determine the effect of the rough scribed surface on adhesion.

7.4 Hybrid Electro-Electroless Deposition (HEED) Coatings

The establishment of HEED coatings within this work provides one of the most interesting and industrially important results within this work. Aside from the application of providing further mechanical strength and corrosion resistance to magnesium {Mg} alloys, practical applications of hybrid deposition include the production of previously unobtainable alloys and multi-layers using wet chemistry techniques. The capacity to deposit at least one compositionally pure layer from electrolytes containing metal ions of similar nobility was previously restricted to vacuum deposition techniques but was shown possible within this work. Applications of HEED coatings include electroforming in which a deposit produced subsequently detached from the substrate as a stand alone part.

The further development of HEED coatings might be through systematic investigation of the capacity of a given electrolyte to electrolessly deposit one metal in the presence of another without the occurrence of electroless co-deposition. Electrochemical techniques such as accurate voltammograms are essential for further development of both multi-layered and alloyed HEED coatings. Lastly, understanding of the dynamics within the mixed purpose electrolyte is required for the expected high precision alloyed deposits produced by HEED.

Generally speaking, the goal of HEED coatings is the formation of multi-layer deposits with unique magnetic and mechanical properties. Regarding mechanical properties, HEED coatings composed of Fe/Ni-P multi-layers provide the potential for high hardness thin films which are not brittle, which is an issue with pure Fe. The enhanced, layer dependent, hardness of electroplated Ni/Cu multi-layers, Chapter 2.4.3, which renders the multi-layer structure harder than either component metal suggests that the same effect may be produced with a harder metal pair, such as Fe/Ni-P. Metal pairs possible for such multi-layers include Co/Ni-P, Fe/Ni-P, and Fe/Ni-W-P among others.

7.5 Ionic Liquids (ILs)

Though relatively little was said directly concerning ionic liquids (ILs), the unique electrolytes were at one point pursued as a means of electrolessly depositing aluminum {Al} and zinc {Zn} on Mg alloys. Since HEED has only begun to be explored in the context of aqueous electrolytes, there exists great potential in the adaptation of

hybrid deposition to IL electrolytes, which may be more accommodating to the process. Specifically, the non-aqueous environment provided by ILs is, at least in theory, ideal for the development of HEED coatings that cannot be obtained using aqueous electrolytes. A specific example of an IL electrolyte which may be suitable for the formation of HEED coatings is the mixture of the zinc chloride-1-ethyl-3-methylimidazolium chloride ($\text{ZnCl}_2\text{-EMIC}$) and aluminum chloride-1-ethyl-3-methylimidazolium chloride ($\text{AlCl}_3\text{-EMIC}$) ILs. The $\text{ZnCl}_2\text{-EMIC}$ and $\text{AlCl}_3\text{-EMIC}$, which were both considered for deposition on Mg alloys and share a common organic salt, have the potential to provide new coatings for Mg and other surfaces. Additionally, beyond the combination of Al and Zn ILs, estimates place the number of possible ILs in the order of 10^{18} which effectively provide endless possibilities for electrolyte composition.

Appendix A: Summary of Electroless Electrolytes

A.1 Electroless Silver {Ag}

Bath	Chemical Name	Chemical Formula	Bath Composition			
			Bath 1		Bath 2	
			mol/L	g/L	mol/L	g/L
Bath A	Silver Nitrate	AgNO ₃	0.03	5.17	0.14	2.375
	Ammonium Hydroxide* (28.0 % - 30.0 %)	NH ₄ OH	0.067	4.60	0.036	2.50
Bath B	Potassium Sodium Tartrate Tetrahydrate (Rochelle's Salt)	KNaC ₄ H ₄ O ₆ · 4H ₂ O	0.096	27.00	0.0175	4.935
	Magnesium Sulphate Heptahydrate	MgSO ₄ · 7H ₂ O	0.008	1.94	—	—
	Ethylenediamine*	C ₂ H ₄ (NH ₂) ₂	—	—	0.0936	6.25
Operating Temperature: 25 °C			pH: 10 to 12		pH: 10 to 12	

*NH₄OH and C₂H₄(NH₂)₂ are measured in mL/L and not g/L

Table A1: Electroless Ag electrolytes [A1]

Electrolytes for the deposition of electroless Ag typically require stabilizers as the electrolytes are prone to uncontrolled reduction/decomposition. Electrolytes containing lower concentrations of Ag⁺ ions are found to often be more stable. Increased stability due to lower Ag⁺ ion concentration typically results in slower deposition rates, with reduction occurring primarily on the intended, activated, surface rather than all surfaces in contact with the electrolyte. The deposition rates of electroless Ag electrolytes are strongly temperature dependant [A1] with increased temperature increasing the deposition rate while also decreasing the stability of the electrolytes. Using stabilizers such as 3-iodotyrosine {C₉H₁₀INO₃} or 3,5-diiodotyrosine {C₉H₉I₂NO₃} increase the effective lifetime of the electrolyte [A1]. The stability of the electrolyte is also greatly affected by the pH; pairing stabilizer use with pH control can increase the lifetime of the electrolyte to approximately 1 week [A1].

The formulation, 'Bath 2', Table A1, is modified from a similar formulation which contains 0.003 M (0.51 g/L) AgNO₃; 0.035 M (9.87 g/L) KNaC₄H₄O₆ · 4H₂O; 0.018 M (1.2 mL/L) C₂H₄(NH₂)₂; and 0.00004 M (0.017 g/L) 3,5-diiodotyrosine as the stabilizer [A1]. The formulation for 'Bath 2' presented in literature is constituted in a single bath form rather than in a binary fashion and NH₄OH is not included at any stage. Electroless film deposition and formation using both Ag electrolyte formulations

presented in Table A1 was observed to progress as decomposition reactions of the electrolyte. The role of NH_4OH within the electrolyte for 'Bath 2' was as additional pH control and as a stabilizer for the electrolyte. While stability of the 'Bath 2' electrolyte increased slightly with the inclusion of NH_4OH , it is possible that it was at the cost of an associated decrease in the deposition rate. The deposition rates of electrolytes were not compared and it is possible positive net effect was produced by the inclusion of NH_4OH .

A.2 Electroless Gold {Au}

Bath	Chemical Name	Chemical Formula	Bath Composition			
			Bath 1		Bath 2	
			mol/L	g/L	mol/L	g/L
Bath A	Sodium Tetrachloroaurate Dihydrate	$\text{Na}(\text{AuCl}_4) \cdot 2\text{H}_2\text{O}$	0.005	1.989	0.005	1.989
	Boric Acid	H_3BO_3	0.16	9.893	0.16	9.893
	Sodium Hydroxide*	NaOH	0.01	0.400	0.01	0.4000
Bath B	Sodium Thiosulphate	$\text{Na}_2\text{S}_2\text{O}_3$	0.10	15.811	0.065	10.277
	Sodium Sulphite	Na_2SO_3	0.10	12.604	0.035	4.411
	Boric Acid	H_3BO_3	0.16	9.893	0.160	9.893
Additives	Sodium Citrate Tribasic Dihydrate	$\text{Na}_3\text{C}_6\text{H}_5\text{O}_7 \cdot 2\text{H}_2\text{O}$	0.50	147.05	0.25	73.525
	Sodium Hypophosphite Hydrate	$\text{NaPH}_2\text{O}_2 \cdot \text{H}_2\text{O}$	0.075	6.599	—	—
Operating Temperature: 80 to 90 °C			pH: 7 to 10			

*Sodium Hydroxide used to adjust pH of 'Bath A' to pH 7.

Table A2: Electroless Au electrolyte based on the work of Paunovic and C. Sambucetti [A2, A3]

The electroless Au electrolyte is made up of two separate electrolytes which are slowly added together to allow proper ligand formation and produce the clear coloured working electrolyte. Given the clear colour of the final electrolyte is clear and the yellow and clear colours of 'Bath A' and 'Bath B', respectively, the mixture of both components should be sufficiently slow as to produce as minimal a color change in the mixture as possible. The mixture is let sit for 24 hours to ensure the proper ligand formation before the addition of additives and actual use. The formulations are one of a number of non-cyanide containing baths and contain both sulphite $\{\text{SO}_3^-\}$ and thiosulphate $\{(\text{S}_2\text{O}_3)^{2-}\}$ as complexing agents [A2]. Of the commonly used ligands for electroless Au deposition, the Au(I) cyanide $\{(\text{Au}(\text{CN})_2)^-\}$ complex is most stable having a stability constant of 10^{39} while the $(\text{Au}(\text{S}_2\text{O}_3)_2)^{3-}$ complex has a stability constant of 10^{26} and the $(\text{Au}(\text{SO}_3)_2)^{3-}$ complex has a stability constant of 10^{10} [A2]. The use of both $\text{S}_2\text{O}_3^{2-}$ and SO_3^- as complexing agents within the electrolyte forms a mixed ligand complex of $\text{Au}(\text{S}_2\text{O}_3)(\text{SO}_3)^{3-}$ rather than the individual Au(I) sulphite $\{(\text{Au}(\text{SO}_3)_2)^{3-}\}$ and Au(I) thiosulfate $\{(\text{Au}(\text{S}_2\text{O}_3)_2)^{3-}\}$ complexes which have been used in other Au electrolytes [A2]. The mixed ligand structure provides a greater stability to the electrolyte compared to those electrolytes containing SO_3^- alone, though the stability is less than those

electrolytes containing only $(\text{S}_2\text{O}_3)^{2-}$ as the complexing agent. Electrolytes containing only SO_3^- as the complexing agent require stabilizers as the $(\text{Au}(\text{SO}_3)_2)^{3-}$ complex spontaneously decomposes into Au(III) and Au metal. Conversely, due to the high stability of the $(\text{Au}(\text{S}_2\text{O}_3)_2)^{3-}$ complex few reducing agents are able to provide a practical deposition rate. Additionally, the accumulation of free $(\text{S}_2\text{O}_3)^{2-}$ known to decelerate Au deposition [A2] and increased concentration of $(\text{S}_2\text{O}_3)^{2-}$ has been linked to dramatic increases in the porosity of Au deposits; hence lower concentrations of $(\text{S}_2\text{O}_3)^{2-}$, around 0.01 M, are preferred [A4].

The formulation of 'Bath 1' in Table A2 is identical to the one put forward by M. Paunovic and C. Sambucetti [A3] as well as M. Schlesinger. Similar formulations to 'Bath 1' with different constituent concentrations have been since used by others including T. Osaka [A4-A6]. The addition of 0.5 M citrate $\{\text{C}_6\text{H}_5\text{O}_7^{3-}\}$ within 'Bath 1', as proposed by Paunovic and Sambucetti, produces a considerable increase in the plating rate by appearing to act as an additional reducing agent; the plating rate achieved at pH 7.5 and 70 °C was $0.9 \mu\text{m}\cdot\text{h}^{-1}$ [A2]. The electrolyte reported by Paunovic and Sambucetti ultimately was stable for only about 10 h, but could be extended for much longer periods with the addition of a stabilizer such as thiocyanate $\{\text{SCN}^-\}$ [A2]. The formulation 'Bath 2' in Table A2 is a variant of 'Bath 1' in the same table and contains no additives as well as a modified ratio of $\text{Na}_2\text{S}_2\text{O}_3$ to Na_2SO_3 . The decrease of the concentration in $\text{Na}_2\text{S}_2\text{O}_3$ is aimed at controlling the potential porosity of the deposit while the relative increase of $\text{Na}_2\text{S}_2\text{O}_3$ compared to Na_2SO_3 was aimed at increasing the stability of the electrolyte. Just as with 'Bath 1' without any additives, 'Bath 2' undergoes reduction and deposits on catalytic surfaces; including Cu, Ni, Co and Fe; without the use of any standard reducing agent, such as thiourea, ascorbic acid, hypophosphite, hydrazine, erythorbic acid, or polyphenol [A2].

The phenomenon of ongoing autocatalytic reduction without the use of a dedicated reducing agent has been reported in patents by G. Krulik and N. Mandich [A7, A8]. The electrolyte composition put forward in those patents [A7, A8] have the same general composition and contain disodium ethylenediaminetetraacetic acid (Na_2 -EDTA) $\{\text{Na}_2\text{C}_{10}\text{H}_{16}\text{N}_2\text{O}_8\}$ in place of H_3BO_3 . The plating rate of the patented electrolytes directly on electroless Ni deposited on Cu-clad epoxy glass laminated printed

circuit boards vary depending on deposition conditions, such as pH, temperature, and additives. The embodiments of the electrolytes within the patent have the capacity to plate 0.03 to 0.3 μm thick Au layers in 15 min from electrolytes of pH from 6.5 to 10.0 at temperatures from 55 to 90 $^{\circ}\text{C}$ [A2]. The highest deposition rate presented within the embodiments of the patent deposited Au at a thickness of 12 millionths of an inch, 0.3 μm , in 15 minutes using a pH 10 electrolyte heated to 90 $^{\circ}\text{C}$ consisting of 30 g/L $\text{Na}_2\text{S}_2\text{O}_3$, 20 g/L Na_2SO_3 , 0.1 g/L $\text{Na}_2\text{-EDTA}$, and 1 g/L of Au as a Au(I) complex [A7].

In the case of Au deposition from electrolytes containing no dedicated reducing agent on electroless Ni surfaces [A7], the initial layer is deposited as an immersion, galvanic displacement, layer with subsequent autocatalytic deposition of Au [A2]. In contrast, it has been shown that deposition from similar electrolytes on Ni-B progress due to a substrate-catalyzed reaction with only a minor contribution of the galvanic displacement reaction [A5]. The mechanism behind autocatalytic Au deposition without a dedicated reducing agent has been suggested by the inventors of the patent [A7] to be due to the sulphite–thiosulphate acting as a reducing agent with sulphite acting as the main reducing agent [A2]. According to the authors of the patent [A7], the proposed role of the sulphite requires the inclusion of strong complexing agent, such as ethylenediaminetetraacetic acid (EDTA) $\{\text{C}_2\text{H}_4(\text{N}(\text{CH}_2\text{CO}_2\text{H})_2)_2\}$ or nitrilotriacetic acid (NTA) $\{\text{N}(\text{CH}_2\text{CO}_2\text{H})_3\}$, as sulphite is oxidized by air and the oxidation catalyzed by impurities such as Cu^{2+} and Ni^{2+} ions liberated into solution during the formation of the immersion layer [A2]. According to the authors, the bath is completely stable for more than 10 replenishment cycles over the period of many months [A2]. Additionally, further work by patented by G. Krulik and N. Mandich demonstrated that the electroless deposition from a sulfite-thiosulfate mixed ligand electrolyte can be increased by adding an amino acid such as glycine, alanine, glutamine, leucine, lysine, and valine [A2, A8]. Deposits of 0.39 to 1.0 μm thick Au were obtained in 10 minutes using baths containing one of the amino acids, or mixtures of two or more of those compounds [A2].

Concerning the formulations presented in Table A2, it has been observed, as part of experiments within this work, that electroless deposition of Au from mixed ligand electrolytes is somewhat substrate dependent. One example of substrate dependence is deposition on Cu substrates wherein the Au electrolyte produces bluish silver deposits.

According to EDS, the blue-silver deposits contain non-trivial or even fair amounts of sulphur, Figure A1. Though the work of others includes deposition on Cu substrates with no issue [A2, A7], given that the formulation used within this work was not the same as those used within the patents, the slight differences in electrolyte composition may be the reason for the discrepancy between the work of others and the work presented herein.

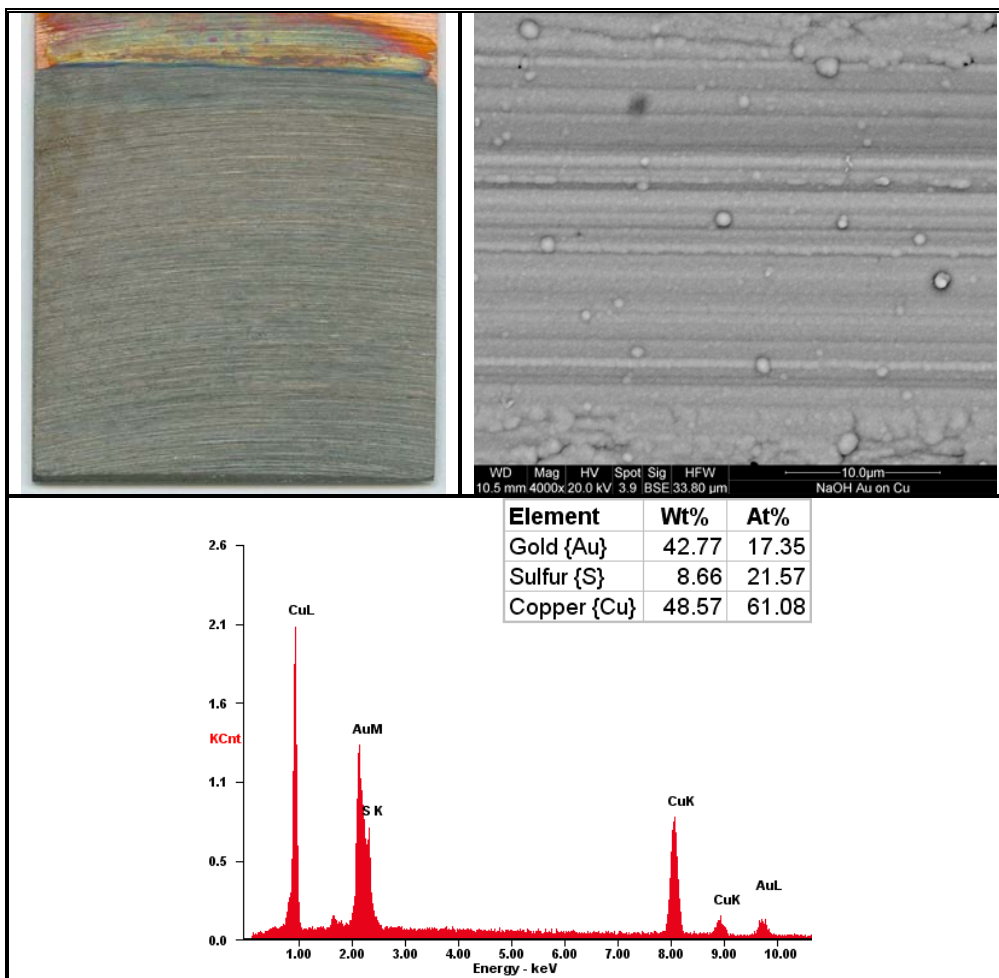


Figure A1: Macroscopic scanned image, backscatter SEM image, and EDS analysis of an Au deposit [20 min, 80 °C] on a Cu substrate. The Au deposit contains a significant amount of S compared to those deposits on n-type silicon {Si} wafers.

The overall poor quality of the deposit was attributed in part to dissolution of the Cu substrate by the electrolyte along with a simple displacement reaction for the initial layer of the Au film; both of which led to the inclusion of Cu in the deposit. Verification of the inclusion of Cu was achieved by subsequent deposits from the electrolyte on Ni after having been used for deposits on Cu substrates as those deposits contained trace amounts of Cu, Figure A2.

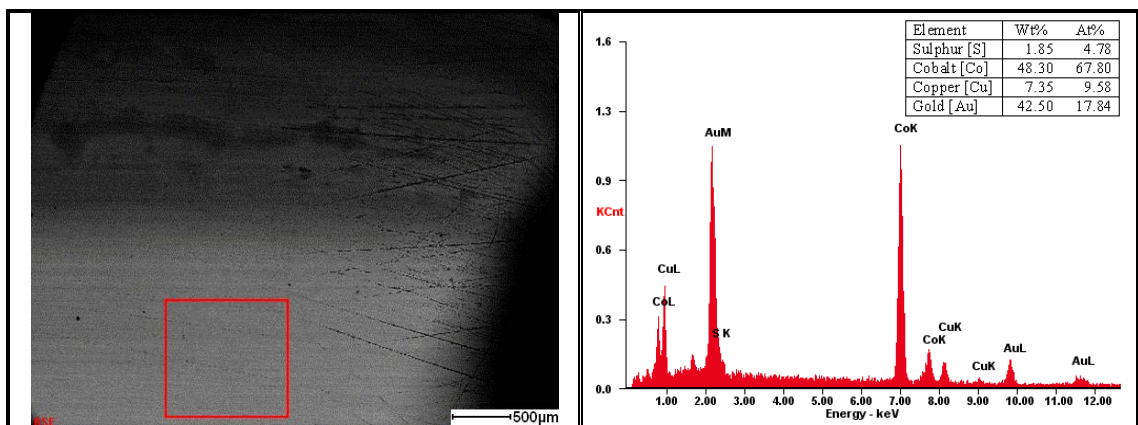


Figure A2: Backscatter SEM image, with a 500 μm scale, along with EDS of an electroless Au deposit [40 min, 65 $^{\circ}\text{C}$] on a Co substrate. Area of the red box is approximately 800 μm \times 800 μm . The deposit contains Cu due to previous use of the Au electrolyte on a Cu substrate.

Immersion of Co substrates within the room temperature pH 7 Au electrolyte produced a dark sulphur rich Au deposit on the surface of the substrate and also imparted a rose color to the normally white/clear electrolyte. Given the results of alkaline electroless Au on Cu substrates, the change in color of the electrolyte is thought to result from displacement of the Co substrate in an immersion type reaction. The deposition of Au from a heated, > 70 $^{\circ}\text{C}$, electrolyte produces a proper Au coloured deposit. The speed of the deposit formation along with the shorter immersion time appears to limit any dissolution of the Co substrate. Subsequent electroless Au deposits from electrolytes used to deposit on Co substrates have shown no Co content when evaluated using EDS.

Other intricacies of the electrolyte include the pH dependence of the electrolyte for Au deposits on Ni and Co. At pH 7 the Au electrolyte, heated to 80 $^{\circ}\text{C}$, deposits formed slowly and possessed macroscopic discontinuities. Increasing the pH, by using chemicals such as NaOH or NH_4OH , increases the deposition rate in accordance with the observation of others [A2, A7]. Immersion of the Ni or Co substrates within pH 10 Au electrolytes, heated to 80 $^{\circ}\text{C}$, produces excellent quality deposits for samples immersed for the same amount of time as those in the pH 7 electrolyte. Other methods of increasing the pH include the addition of $\text{Na}_3\text{C}_6\text{H}_5\text{O}_7$ which produces a pH of around 8 when added at 0.25 mol/L. The pH 8 electrolyte also produces good quality deposits on Ni and Co substrates as is expected of the more alkaline pH electrolyte. Interestingly, while it may be convenient to suggest the superior deposition is solely the result of increased pH of the electrolyte, it has been found that the addition of $\text{Na}_3\text{C}_6\text{H}_5\text{O}_7$ along

with the inclusion of either NiSO_4 or CoSO_4 within the electrolyte produces a pH 7 electrolyte capable of forming excellent quality deposits. These observations for Ni and Co substrates have also been made for the formation of electroless Au deposits on silicon {Si} substrates. On Si, as on Co and Ni, the pH 7 electrolyte does not form continuous deposits. Best results for electroless Au deposition on Si appear to require the electrolyte at pH 10, with or without the presence of additives. The requirement of increased alkalinity for increased deposition rate is consistent with the results reported in the initial patent by G. Krulik and N. Mandich [A7].

While good quality deposits are typically achieved on Co, Ni, and Si; the Au electrolyte a dependency on the substrate upon which deposition occurs was also observed for Fe substrates, specifically cold-rolled, or 'low carbon', steel. Deposits on cold-rolled steel substrates at pH 7 were of poor quality deposit and immediately shed within the electrolyte causing contamination. Increasing the pH to pH 10, whether by using NH_4OH or NaOH , does not improve the quality of the deposit or prevent the reactions which cause shedding. Only deposition from electrolytes containing $\text{Na}_3\text{C}_6\text{H}_5\text{O}_7$ appeared to allow deposition on Fe surfaces further indicating that the presence of $\text{Na}_3\text{C}_6\text{H}_5\text{O}_7$ is a significant factor in the behaviour of the electrolyte.

Finally, the remarkable stability of the electrolyte in the presence of Ni^{2+} and Co^{2+} ions, which allows for electro-electroless deposition, see Chapter 5, is likely the result of the $\text{Na}_3\text{C}_6\text{H}_5\text{O}_7$ additive within the electrolyte. In addition to increasing the deposition rate [A2], the presence of $\text{Na}_3\text{C}_6\text{H}_5\text{O}_7$, a commonly used buffering and complexing agent for Ni and Co electrolytes, appears to prevent degradation of the Au electrolyte. The likely sequestration of the Ni^{2+} and Co^{2+} ions within citrate $\{\text{C}_6\text{H}_5\text{O}_7^{3-}\}$ complexes is speculated to be the reason for the lack of inclusion of either Ni or Co within subsequent deposits, such as on Si substrates. Similarly, it is believed the co-deposition of Cu with Au is a result of similar, high, nobility of Cu and Au metals and may be the result of Cu and Au having a shared ligand structure. Even with contaminants within the electrolyte, the Au electrolytes produced appeared to have long term stability over several months of cyclical inactivity and use.

A.3 Electroless Copper {Cu}

Bath	Chemical Name	Chemical Formula	Bath Composition (g/L)		
			Bath 1*	Bath 2	Bath 3
Bath A	Copper Sulphate Pentahydrate	$\text{CuSO}_4 \cdot 5\text{H}_2\text{O}$	40.0	25.0	—
	Copper Hydroxide	$\text{Cu}(\text{OH})_2$	—	—	13.9
	Potassium Sodium Tartrate Tetrahydrate (Rochelle's Salt)	$\text{KNaC}_4\text{H}_4\text{O}_6 \cdot 4\text{H}_2\text{O}$	100.0	65.0	65.0
	Sodium Hydroxide	NaOH	25.0	10.0	10.0
Bath B	Paraformaldehyde	$\text{HO}(\text{CH}_2\text{O})_n\text{H}$ ($n = 8-100$)	65.0	65.0	65.0
	Sodium Hydroxide	NaOH	40.0	10.0	10.0
Operating Temperature: 20 to 25 °C			pH: ≥ 12.5		

Table A3: Electroless Cu thin film electrolytes

*Formulation by Schlesinger et al. (1976) [A9]

The stability of the electroless Cu electrolyte has been found to be dependant largely on the hydroxide $\{\text{OH}^-\}$ concentration within the electrolyte. When the Cu electrolyte has a total OH^- concentration of around 10 g/L, the electrolyte remains stable for several weeks, though the deposition rate is reduced compared to more alkaline version of the electrolyte. Increasing the OH^- concentration to about 15 g/L reduces the stability of the electrolyte with decomposition often occurring within a day. Electrolytes with OH^- concentrations above 20 g/L are stable for only a few hours and eventually begin to precipitate Cu with deposition occurring on those precipitates; the precipitated Cu is often fluffy and non-compact. Heating the electrolyte increases the deposition rate but often also produces a yellowish dust-like Cu containing precipitate which deposits on Sn/Pd catalyzed surfaces in place of a metallic Cu deposit. Heating electrolytes containing more than 20 g/L of NaOH increases the rate decomposition and provides poor quality deposits due to the precipitation of Cu metal.

Replacing CuSO_4 with $\text{Cu}(\text{OH})_2$ requires additional mixing for 'Bath A' in order to dissociate and complex the Cu within the electrolyte. Commercially available $\text{Cu}(\text{OH})_2$, which is used in the above table, is listed having Cu(II) content of 56 to 57 % as determined by EDTA titration¹. The employ of $\text{Cu}(\text{OH})_2$ comes at the risk of the formation of some copper(II) oxide $\{\text{CuO}\}$, a black oxide which does not easily

¹ EDTA titration is a standardized process that allows the determination of metal ions present by the formation of metal-EDTA complexes.

dissociate and forms when $\text{Cu}(\text{OH})_2$ is exposed to moisture or elevated temperatures, $> 185\text{ }^\circ\text{C}$. Inclusion of NH_4OH within the electrolyte has the positive effect of forming a Cu complex which includes NH_3 as a ligand as well as the negative effect of liberating NH_3 gas which dissolves Cu. The inclusion of NH_4OH within the electrolyte prevents deposition on either Si or Sn/Pd catalyzed surfaces.

A.4 Electroless Nickel Boron {Ni-B} Alloys

Bath	Chemical Name	Chemical Formula	Bath Composition
Bath A	Nickel Chloride Hexahydrate	NiCl ₂ · 6H ₂ O	30.0 g/L
Bath B	Sodium Hydroxide	NaOH	40.0 g/L
	Ethelenediamine (> 99.5 %)	H ₂ NCH ₂ CH ₂ NH ₂	60.0 mL/L
	Sodium Borohydride	NaBH ₄	1.0 g/L
Operating Temperature: 80 to 90 °C			

Table A4: Electroless Ni-B electrolyte
Formulation modified from Gorbunova et al. (1973) [A10]

The pH of ‘Bath A’ is acidic around pH 5 and the pH of ‘Bath B’ is around pH 14; when combined the electrolyte is alkaline at about pH 14. The assembly of the Ni-B electrolyte requires the careful addition of ‘Bath A’ to ‘Bath B’ such that precipitates do not form. The slow mixing of the baths is needed as borohydride {BH₄⁻} ions rapidly oxidize in acidic and neutral aqueous environments; hence the dissolution of NaOH and C₂H₄(NH₂)₂ must be the first steps in the creation of ‘Bath B’. Adding ‘Bath B’ to ‘Bath A’ results in the rapid oxidation of BH₄⁻ in the environment established by the NiCl₂ of ‘Bath A’ which vigorously reduces the Ni²⁺ ions producing black nickel boride {Ni₂B} precipitates, effectively destroy the electroless Ni-B electrolyte. The deposition rate for this formulation of Ni-B electrolyte is frequently slow compared to other electrolytes and adequate electrolyte temperature is essential. Increasing the amount of NaBH₄ by up to a factor of 10 appeared to have some effect on increase the time before the electrolyte would become ineffective and appeared slightly improve the deposition rate. The above formulation, which was used for deposition on glass and Mg, does not include any stabilizers, such as thallium nitrate {TlNO₃} or lead chloride {PbCl₂} together with 2-mercaptobenzothiazole {C₇H₅NS₂} [A10] and is prone to only a few cycles before either becoming ineffective or succumbing to uncontrolled reduction/precipitation.

A.5 Electroless Nickel Phosphorus {Ni-P} Alloys

Chemical Name	Chemical Formula	Composition (g/L)
Nickel Sulphate Hexahydrate	$\text{NiSO}_4 \cdot 6\text{H}_2\text{O}$	29.5
Sodium Hypophosphite Hydrate	$\text{NaPH}_2\text{O}_2 \cdot \text{H}_2\text{O}$	17.5
Sodium Succinate	$(\text{NaOOCCH}_2)_2$	15.0
Succinic Acid	$\text{C}_4\text{H}_6\text{O}_4$	1.5
Operating Temperature: 65°C		pH: 4.7 to 5.3

Table A5.1: Acidic electroless Ni-P electrolyte
Formulation by J. Marton and M. Schlesinger (1968) [A11]

Chemical Name	Chemical Formula	Composition (g/L)
Nickel Sulphate Hexahydrate	$\text{NiSO}_4 \cdot 6\text{H}_2\text{O}$	10.0 - 20.0
Sodium Citrate Tribasic Dihydrate	$\text{Na}_3\text{C}_6\text{H}_5\text{O}_7 \cdot 2\text{H}_2\text{O}$	23.5
Sodium Hypophosphite Hydrate	$\text{NaPH}_2\text{O}_2 \cdot \text{H}_2\text{O}$	17.5
Ammonium Hydroxide* (28.0 % - 30.0 %)	NH_4OH	0.0 - 50.0
Operating Temperature: 70 to 90 °C		pH: 7 to 12

* NH_4OH is measured in mL/L and not g/L

Table A5.2: Alkaline electroless Ni-P electrolyte
Formulation modified from M. Schlesinger et al. (1972) [A12]

Electroless Ni-P can be deposited from both acidic, Table A5.1, and alkaline, Table A5.2, electrolytes. The difference between acidic and alkaline electrolytes exists in the alloy deposited. Acidic electroless Ni-P produces a Ni_3P alloy containing approximately 25 % P, whereas alkaline electrolytes produce alloys which range from 25 % P to as little as 2 % P [A12-A15]. The acidic electrolyte provided is direct from literature whereas the alkaline electrolytes are modified from one which contained NaOH and ammonium chloride $\{\text{NH}_4\text{Cl}\}$ in place of NH_4OH [A15]. The replacement of Cl^- ions allows for greater stability of the electrolyte for electroless deposition on Mg alloys.

A.6 Electroless Nickel Zinc Phosphorus {Ni-Zn-P} Alloys

Chemical Name	Chemical Formula	Bath Composition (g/L)			
		25%Zn	35%Zn	50%Zn1	50%Zn2
Nickel Sulphate Hexahydrate	$\text{NiSO}_4 \cdot 6\text{H}_2\text{O}$	7.87425	6.82435	5.2495	6.82435
Zinc Sulphate Heptahydrate	$\text{ZnSO}_4 \cdot 7\text{H}_2\text{O}$	2.87125	4.01975	5.7425	7.46525
Sodium Citrate Tribasic Dihydrate	$\text{Na}_3\text{C}_6\text{H}_5\text{O}_7 \cdot 2\text{H}_2\text{O}$	23.500	23.500	23.500	23.500
Sodium Hypophosphite Hydrate	$\text{NaPH}_2\text{O}_2 \cdot \text{H}_2\text{O}$	17.500	17.500	17.500	17.500
Ammonium Hydroxide* (28.0 % - 30.0 %)	NH_4OH	37.5	37.5	62.5	50.0
Average pH before use (20 °C)		11.61	11.63	11.96	11.63
Operating Temperature: 85 °C					

* NH_4OH is measured in mL/L and not g/L

Table A6: Electroless Ni-Zn-P electrolytes
Formulations modified from Schlesinger et al. (1991) [A13, A14]

Similar to the alkaline electroless Ni-P electrolyte, the above Ni-Zn-P electrolyte was created by modifying a previously existing [A13, A14] electrolyte. The modification of the electrolyte consisted of replacing $\text{NiCl}_2 \cdot 6\text{H}_2\text{O}$ with $\text{NiSO}_4 \cdot 6\text{H}_2\text{O}$, ZnCl_2 with $\text{ZnSO}_4 \cdot 7\text{H}_2\text{O}$, and NaOH and NH_4Cl with NH_4OH . The modified electrolytes behaved similar to those found in the literature with the P content of the deposit decreasing, and Zn content increasing, with increasing alkalinity. The 50%Zn2 electrolyte contains 25 % more metal ions compared to the other 25 %, 35 %, and 50 % Zn electrolytes.

A.7 Electroless Cobalt Phosphorus {Co-P} Alloys

Chemical Name	Chemical Formula	Bath Composition (g/L)	
		Co-P	Ni-Co-P
Cobalt Sulphate Heptahydrate	$\text{CoSO}_4 \cdot 7\text{H}_2\text{O}$	11.2	0.0-11.2
Nickel Sulphate Hexahydrate	$\text{NiSO}_4 \cdot 6\text{H}_2\text{O}$	—	0.0-10.5
Sodium Citrate Tribasic Dihydrate	$\text{Na}_3\text{C}_6\text{H}_5\text{O}_7 \cdot 2\text{H}_2\text{O}$	23.5	23.5
Sodium Hypophosphite Hydrate	$\text{NaPH}_2\text{O}_2 \cdot \text{H}_2\text{O}$	17.5	17.5
Ammonium Hydroxide*	NH_4OH	37.5	37.5
Approximate pH		11 to 12	
Operating Temperature (°C)		70 to 90 °C	

* NH_4OH is measured in mL/L and not g/L

Table A7: Electroless Co-P and Ni-Co-P electrolytes

Unlike electroless Ni-P, which can be deposited from both acidic and alkaline electrolytes, Co-P requires an alkaline environment for electroless deposition. The Co-P electrolytes, Table A7, are variants of the alkaline Ni-P electrolytes, Tables B5 & B6, and are consistent with other alkaline Co-P electrolytes found in literature [A16]. The ratio of Ni to Co within Ni-Co-P alloy deposits is dependent on the ratio of Ni to Co within the electrolyte. As with Ni-P, the P content within the alloy is dependent on the alkalinity of the electrolyte, with greater alkalinity reducing the content of P within the deposit. Though the alkalinity of the electrolyte in Table A7 is between pH 11 and 12, deposition will occur at lower pH values even around pH 7. The employ chemicals free of Cl^- ions again provides greater stability of the electrolyte for electroless deposition on Mg alloys.

A.8 Other Electroless Nickel Metal Phosphorus {Ni-Me-P} Alloys

Chemical Name	Chemical Formula	Bath Composition (g/L)			
		Ni-Fe-P	Ni-Re-P	Ni-W-P	Ni-Mo-P
Nickel Sulphate Hexahydrate	$\text{NiSO}_4 \cdot 6\text{H}_2\text{O}$	14.7	3.5	7.0	26.3
Potassium Sodium Tartrate Tetrahydrate (Rochelle's Salt)	$\text{KNaC}_4\text{H}_4\text{O}_6 \cdot 4\text{H}_2\text{O}$	65.0	—	—	—
Sodium Citrate Tribasic Dihydrate	$\text{Na}_3\text{C}_6\text{H}_5\text{O}_7 \cdot 2\text{H}_2\text{O}$	—	8.5	40.0	88.2
Ammonium Iron(II) Sulphate Hexahydrate	$\text{Fe}(\text{NH}_4)_2(\text{SO}_4)_2 \cdot 6\text{H}_2\text{O}$	20.0	—	—	—
Potassium Perrhenate	KReO_4	—	0.2	—	—
Sodium Tungstate Dihydrate	$\text{Na}_2\text{WO}_4 \cdot 2\text{H}_2\text{O}$	—	—	3.5	—
Sodium Molybdate Dihydrate	$\text{NaMoO}_4 \cdot 2\text{H}_2\text{O}$	—	—	—	24.6
Sodium Hypophosphite Hydrate	$\text{NaPH}_2\text{O}_2 \cdot \text{H}_2\text{O}$	10.0	10.0	10.0	12.1
Ammonium Hydroxide *	NH_4OH	3.6	50.0	50.0	—
Approximate pH		11.2	8.8 to 9.2	8.2	9.0
Operating Temperature (°C)		75 to 85	85 to 95	85 to 95	85 to 95

* NH_4OH is measured in mL/L and not g/L

Table A8: Electroless Ni-Me-P electrolytes; Me: Fe, Re, W, Mo
Formulations modified from Chapter 22 of Modern Electroplating, 5th Edition, Edited by M. Schlesinger and M. Paunovic [A16]

Some of the above electrolytes were attempted only on Mg alloy substrates and, as a control, on Sn/Pd treated glass. The effectiveness of these electrolytes on Mg alloy substrates may be found in Chapter 3.4.4. The formulation for Ni-Fe-P, while calling for pH 11.2 was successfully attempted on Mg alloys at pH 9.2, see Chapter 3.4.4. The pH of the electrolytes is typically adjusted using NaOH, though in applications attempted pH adjustments were carried out using NH_4OH as better results were achieved on Mg alloys.

A.9 References

- [A1] N. Koura, Chapter 17: Electroless Plating of Silver, in “Electroless Plating: Fundamentals and Applications”, p. 441-462, Edited by G. O. Mallory, J. B. Hajdu, American Electroplaters and Surface Finishers, 1990, Orlando, Florida
- [A2] Y. Okinaka and M. Kato, Chapter 21: Electroless Deposition of Gold, in “Modern Electroplating, Fifth Edition”, p.483-498, eds: M. Schlesinger and M. Paunovic, (2010) John Wiley & Sons, Inc., Hoboken, NJ, USA, DOI: 10.1002/9780470602638.ch21
- [A3] M. Paunovic and C. Sambucetti, in Proc. Symp. on Electrochemically Deposited Thin Films, Vol. 31, M. Paunovic, Ed., Electrochemical Society, Pennington, NJ, 1994, p. 34.
- [A4] T. Osaka, Y. Okinaka, J. Sasano, M. Kato, “Development of new electrolytic and electroless gold plating processes for electronics applications”, Science and Technology of Advanced Materials, 7, (2006) p.425–437
- [A5] M. Kato, J. Sato, H. Otani, T. Homma, Y. Okinaka, T. Osaka, O. Yoshioka, “Substrate (Ni)-Catalyzed Electroless Gold Deposition from a Noncyanide Bath Containing Thiosulfate and Sulfite, I. Reaction Mechanism”, Journal of The Electrochemical Society, 149(3), (2002), p.C164-C167
- [A6] J. Sato, M. Kato, H. Otani, T. Homma, Y. Okinaka, T. Osaka, O. Yoshioka, “Substrate (Ni)-Catalyzed Electroless Gold Deposition from a Noncyanide Bath Containing Thiosulfate and Sulfite, II. Deposit Characteristics and Substrate Effects” Journal of The Electrochemical Society, 149(3), (2002), p.C168-C172
- [A7] G. A. Krulik and N. V. Mandich, U.S. Patent 5,232,492 (1993)
- [A8] G. A. Krulik and N. V. Mandich, U.S. Patent, 5,318,621 (1994)
- [A9] B. K. W. Baylis, A. Busuttill, N. E. Hedgecock, and M. Schlesinger, “Tin (IV) Chloride Solution as a Sensitizer in Photoselective Metal Deposition”, Journal of the Electrochemical Society: Electrochemical Science & Technology, 123(3), (1976), p.348-351
- [A10] K. M. Gorbunova, M. V. Ivanov, and V. P. Moiseev, “Electroless Deposition of Nickel-Boron Alloys Mechanism of Process, Structure, and Some Properties of Deposits”, Journal of the Electrochemical Society: Electrochemical Science & Technology, 120(5), (1973), p.613-618
- [A11] J. P. Marton and M. Schlesinger, “The Nucleation, Growth, and Structure of Thin Ni-P Films” Journal of the Electrochemical Society: Electrochemical Science, 115(1), (1968), p.16-21
- [A12] S. L. Chow, N. E. Hedgecock, and M. Schlesinger, “Electron Microscope Study of the Nucleation and Growth of Electroless Cobalt and Nickel”, Journal of the Electrochemical Society: Electrochemical Science & Technology, 119(12), (1972), p.1614-1619
- [A13] M. Schlesinger, X. Meng, D. D. Snyder, “Electroless Ni-Zn-P Films”, Journal of the Electrochemical Society, 137(6), (1990), p.1858-1859
- [A14] M. Schlesinger, X. Meng, D. D. Snyder, “The Microstructure and Electrochemical Properties of Electroless Zinc-Nickel-Phosphorus Alloy”, Journal of the Electrochemical Society, 138(2), (1991), p.406-410

- [A15] M. Schlesinger, Chapter 18: Electroless Deposition of Nickel, in “Modern Electroplating, Fifth Edition”, p.447-458, eds: M. Schlesinger and M. Paunovic, (2010) John Wiley & Sons, Inc., Hoboken, NJ, USA, DOI: 10.1002/9780470602638.ch18
- [A16] I. Ohno, Chapter 22: Electroless Deposition of Alloys, in “Modern Electroplating, Fifth Edition”, p.499-506, eds: M. Schlesinger and M. Paunovic, (2010) John Wiley & Sons, Inc., Hoboken, NJ, USA, DOI: 10.1002/9780470602638.ch22

Appendix B: Nickel/Gold {Ni/Au} Electro-Electroless Layers on a Cobalt {Co} Substrate

In this appendix, an example of a nickel/gold {Ni/Au} hybrid electro-electroless deposit (HEED) tri-layer coating, produced on a cobalt {Co} substrate, is presented. The copper {Cu} inclusion within the deposit, as seen by its rose colour, is a consequence of prior use of the electrolyte for deposition of an HEED coating on a Cu substrate. As mentioned in Appendix A2, the electroless deposition of Au from the electrolyte was found to dissolve Cu and include it in other deposits on other substrates.

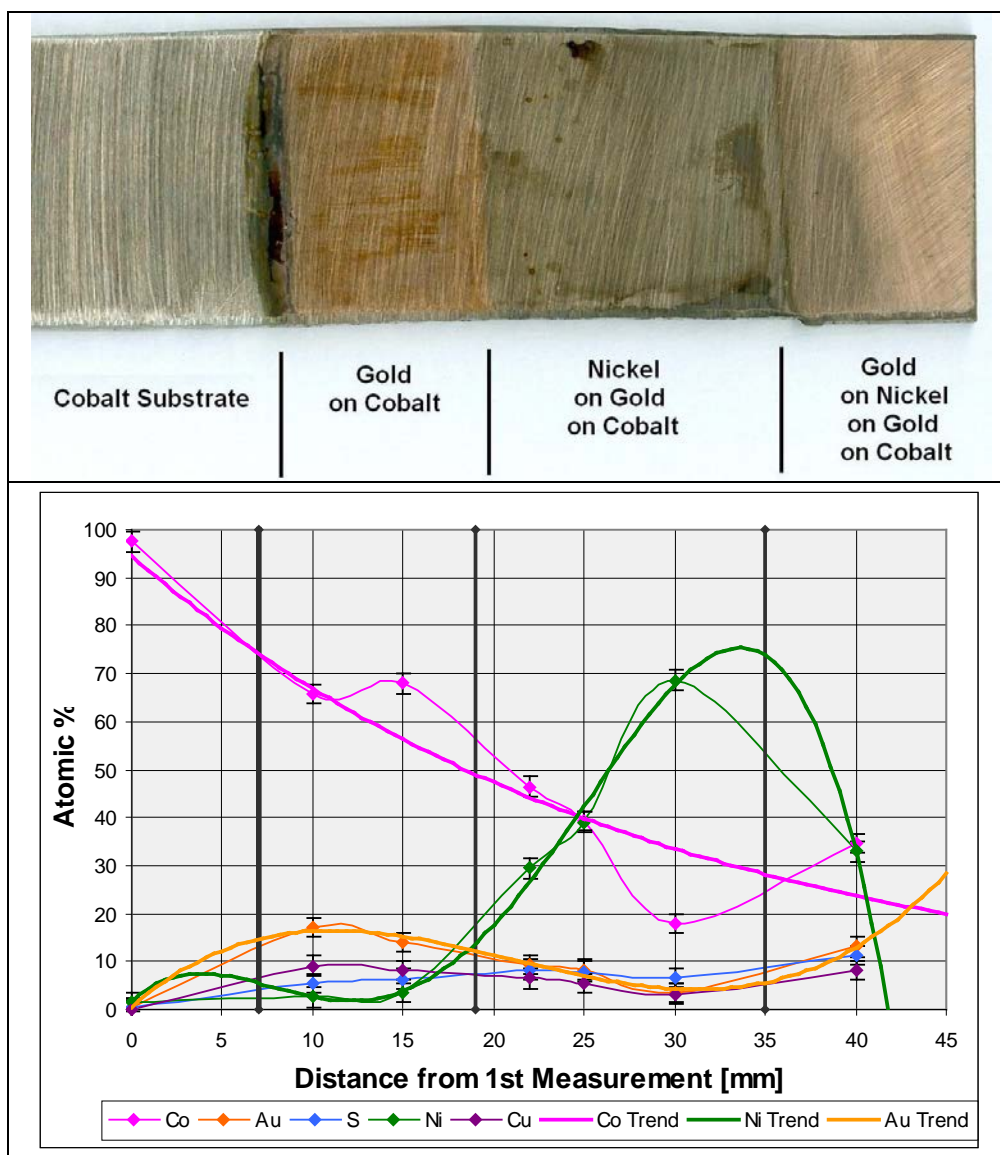


Figure B1: Macroscopic image along with a graph of EDS results for a Ni/Au HEED coating [40 min electroless, 90 s electro, 40 min electroless; 65 °C] on a Co substrate.

Vita Auctoris

NAME: Robert Petro

PLACE OF BIRTH: Windsor, Ontario, Canada

YEAR OF BIRTH: 1985

EDUCATION: École Secondaire L'Essor,
St Clair Beach, Ontario, Canada
1999-2003

University of Windsor,
Windsor, Ontario, Canada
2003-2007 B.Sc.

University of Windsor,
Windsor, Ontario, Canada
2008-2014 Ph.D.